

**„A profile through the Central American Landbridge in western
Panama: 115 Ma Interplay between the Galápagos Hotspot and
the Central American Subduction Zone“**

Dissertation

zur Erlangung des Doktorgrades
der Mathematisch-Naturwissenschaftlichen Fakultät
der Christian-Albrechts-Universität
zu Kiel

vorgelegt von

Britta Lissinna

Kiel

2005

Referent: Prof. Dr. Kaj Hoernle

Korreferent:.....

Tag der Disputation.....

zum Druck genehmigt Kiel, den

Danksagung

Für die Vergabe dieser Doktorarbeit, den kritischen Diskussionen und der Durchsicht meiner Manuskripte danke ich Prof. Kaj Hoernle. Seine Anregungen hinsichtlich der Darstellung und Publikationen von Ergebnissen haben entscheidend zum Gelingen dieser Arbeit beigetragen. Für die Betreuung während der Geländearbeit und den aufgrund meiner Schwangerschaft ohne mich durchgeführten Geländearbeiten, möchte ich Kaj Hoernle, Paul van den Boggard und Reinhard Werner danken. Unserem Kooperationspartner in Panama Juan de Dios Villa möchte ich für seine logistische Unterstützung danken. Zusätzlich möchte ich insbesondere Reinhard Werner für die Ausarbeitung des DFG Projektantrages HO-1833/6-1 & 2 Panama Terranes danken. Colin Devey danke ich dafür, dass er sich für eine weitere finanzielle Unterstützung für mich eingesetzt hat, ohne diese wäre die Arbeit wahrscheinlich nicht zustande gekommen.

Weiterer Dank gebührt, Folkmar Hauff und Silke Hauff für die Durchführung der Sr-Nd-Pb Isotopenanalytik, Paul van den Boggard und Jan Stiklus für die $^{40}\text{Ar}/^{39}\text{Ar}$ Datierungen, sowie Dagmar Rau für die RFA-Analytik. Ein besonderer Dank für die freundliche Aufnahme und Hilfestellung bei der chemischen Aufbereitung von ICP-MS Analysen geht an Heidi Blaschek, Dieter Garbe-Schönberg, die bedauerlicherweise verstorbene Sonja Klauke und Ulrike Westernstroehrer (Institut für Geologie und Paläontologie an der Universität Kiel). Für die kritischen Diskussionen und Unterstützung möchte ich meinen Kollegen von Gebäude 12 Jörg Geldmacher, Maxime Portnyagin und Seth Sedofsky danken.

Für die Vergabe eines Graduiertenstipendiums sowie die Förderung des Projektes HO-1833/6-1 & 2 Panama Terranes, möchte ich der Deutschen Forschungsgemeinschaft (DFG) danken. Für das große Interesse und die positive Wertung der Forschungsergebnisse möchte ich Guillermo Alverado und David Scholl danken.

Einen besonders großen Dank geht an meine Familie insbesondere meinen Mann Ralf Ahrens für die lange moralische und praktische Unterstützung, meinen Schwiegereltern für die Unterstützung und tolle Betreuung von Johanna und an Johanna einfach nur dafür das sie da ist.

Zusammenfassung

Die Zielsetzung dieser Arbeit ist zum einen die Rekonstruktion der Entwicklungsgeschichte des Galápagos-Hotspots anhand der Untersuchung von 17–115 Mill. J. alten vulkanischen Gesteinen im südlichen Mittelamerika. Dabei sollen die tektonischen Auswirkungen beim Auftreffen von Galápagos-Hotspotspuren auf die zentralamerikanische Landbrücke sowie der „Input“ in die Subduktionszone untersucht werden. Desweiteren soll durch die Analyse der tertiären bis quartären Inselbogengesteine entlang der panamaischen Subduktionszone die Bildungsgeschichte, Paläotektonik sowie die geochemische Entwicklung des panamaischen Inselbogens untersucht werden.

Der erste Focus des ersten Kapitels dieser Arbeit liegt auf der Untersuchung aufgehobener Plateaukruste der Karibischen Platte, welche auf den Halbinseln Soná und Azuero und entlang der pazifischen Küste von Ostpanama aufgeschlossen ist. Laser- $^{40}\text{Ar}/^{39}\text{Ar}$ -Datierungen dieser Komplexe reichen von 71 bis 115 Mill. J..

Ein zweite Schwerpunkt liegt auf der Rekonstruktion der bereits subduzierten Geschichte des Galápagos-Hotspots (68-15 Mill. J.), die anhand von akkretierten magmatischen Komplexen entlang der pazifischen Küste Panamas untersucht wurde. Es wurden räumliche Variationen der Geochemie akkretierter magmatischer Komplexe untersucht, um eine mögliche paläozäne bis miozäne Zonierung des Galápagos-Hotspots zu überprüfen, wie Sie während der letzten 20 Mill. J. zu beobachten war. Die Geochemie der magmatischen Komplexe zeigt Affinität zu Ozeaninselbasalten (OIB) und reicht von tholeiitischer bis alkaliner Zusammensetzung. Nur selten treten mittelozeanische Rückenbasalte (N-MORB) auf. Laser- $^{40}\text{Ar}/^{39}\text{Ar}$ -Datierungen der Gesteine reichen von 17 bis 66 Mill. J.. Die magmatischen Komplexe bestehen aus akkretierten Ozeaninseln, Seamounts, aseismischen Rückenstrukturen und ozeanische Kruste. Die Spurenelement- und Sr-Nd-Pb-Isotopen-Signaturen zeigen, dass sich die für den Galápagos-Hotspot typischen vier Mantelkomponenten (nördliche, südliche, zentrale und östliche Komponente) schon in den paläozänen bis eozänen Hotspotspuren (66–50 Mill. J.) nachweisen läßt. Die isotopische Zonierung und die räumliche Anordnung der akkretierten magmatischen Komplexe ist vergleichbar mit der heutigen Zonierung des Galápagos-Archipels: Isotopen-Signaturen mit Affinität zur nördlichen Galápagos-Mantelkomponente wurden nordwestlich von Panama in magmatischen Gesteinen der Halbinsel Quepos (Costa Rica) bestimmt. Von Osa bis Coiba treten Laven mit Affinität zur östlichen Galápagos-Mantelkomponente und auf der südwestlich davon gelegenen Halbinsel Azuero magmatische Gesteine mit südlicher und östlicher Galápagos Mantelkomponente auf.

Die Akkretion der Paläo-Galápagos-Hotspotspuren an den pazifischen Plattenrand der karibischen Platte erfolgte im wesentlichen zwischen dem Frühen Paläozän und dem

Mittleren Eozäns (~60–45 Mill. J.). Dieser Akkretionsgürtel erstreckt sich von Quepos (Costa Rica) bis Azuero. Spätere Akkretion von Hotspotspuren vom Frühen Miozän bis zum Quartär (<23 Mill. J.) erfolgte nur sporadisch. Akkretierte magmatische Komplexe des Späten Eozäns bis Miozäns sind im südlichen Teil der Halbinsel Azuero und an der westlichen Küste von Coiba aufgeschlossen. Dies weist darauf hin, dass eine Paläo-Galápagos-Hotspotspur vor ca. 20–30 Mill. J. und eine weitere während der letzten 5 Mill. J. unter dem westlichen Panama subduzierte. Anhand unserer Untersuchungen können wir schlussfolgern, dass Paläo-Galápagos-Hotspotspuren fast während des gesamten Tertiärs entlang der pazifischen Küste Panamas akkretierten.

Das zweite Kapitel behandelt die geochemische Entwicklung des Inselbogen-vulkanismus‘ Panamas, dessen Auftreten sich über das gesamte Känozoikum erstreckt. Es wurden vulkanologische Studien, Laser- $^{40}\text{Ar}/^{39}\text{Ar}$ Datierungen, Haupt- und Spurenelement-sowie Sr-Nd-Pb-Isotopen-Analysen an Proben des Inselbogens durchgeführt, um neben der magmatischen die tektonische Entwicklungsgeschichte des panamaischen Inselbogens zu untersuchen. Neue Laser- $^{40}\text{Ar}/^{39}\text{Ar}$ -Datierungen an tholeiitischen bis calc-alkalinen Proben liegen zwischen 60.9 ± 0.5 Mill. J. und 7.4 ± 0.7 Mill. J.. Isotopen-Signaturen von paläozänen Inselbogenvulkaniten bestätigen den Einflußbereich einer nahe gelegenen suduzierenden Paläo-Galápagos-Hotspotspur. Zwischen ca. 50–30 Mill. J. migrierte das westpanamaische Inselbogensegment nach Nordwesten. Es wird angenommen, dass die bisher vorherrschende tektonische Akkretion während dieses Zeitraumes von tektonischen Erosionsprozessen abgelöst wurde. Die Rate der tektonischen Erosion zwischen ca. 50–30 Mill. J. liegt bei $84\text{--}96 \text{ km}^3 \text{ Ma}^{-1} \text{ km}^{-1}$, vergleichbar mit den Raten des heutigen Costa Ricas

Angereicherte Pb-Isotopen-Signaturen (Galápagos Signatur) in Inselbogenvulkaniten von Azuero (~45 Mill. J.) und dem östlichen Panama (12–22 Mill. J.) deuten auf eine ostwärts Verlagerung der subduzierenden Hotspotspur relativ zum Inselbogen hin. Das ostpanamaische Inselbogensegment ist entlang einer linkslateralen Verschiebung entlang der Panamakanal-Störungszone nach Norden relativ zum westpanamaischen Inselbogensegment verschoben. Der überlagernde jüngere, miozäne Inselbogen erstreckt sich jedoch in einem zusammenhängenden Stück von West- bis Ostpanama. Daraus schliessen wir das die Verschiebung des paläozänen bis späteozänen Inselbogensegments zwischen dem Späten Eozän und dem Frühen Miozän (40–20 Mill. J.) erfolgte. Der Inselbogenvulkanismus in Ostpanama endete ca. vor 12 Mill. J., zeitgleich mit der Kollision von Ostpanama mit Südamerika. Vom Pliozän bis zum Holozän (4.5 ± 0.17 to 0.1 ± 0.08 Mill. J.) nahm die vulkanische Aktivität signifikant ab und war auf kleinvolumige Eruptionen von Adakiten und Alkalibasalten in Westpanama beschränkt. Eine mögliche Erklärung dafür ist, dass die Subduktion von Coiba-und Cocos-Rücken zur Bildung eines „slab windows“ geführt hat.

Entlang der exponierten Enden der subduzierenden Lithosphärenplatte können dabei adakitische Schmelzen entstehen. Die Alkalibasalte könnten durch die Metasomatisierung des Mantelkeils mit den adakitischen Schmelzen oder durch die Aufschmelzung von aufsteigender Asthenosphäre gebildet worden sein.

Die beobachteten geochemischen Variationen der untersuchten Inselbogenvulkanite lassen sich durch Interaktion von Galápagos-Hotspotsuren mit der Panama vorgelagerten Subduktionszone erklären. Der Galápagos-Hotspot stellt damit auch einen signifikanten Faktor für die tektonische Entwicklung Panamas dar.

Summary

The purpose of this study was to investigate volcanic rocks in Panama (17-115 Ma) to understand the long-term evolution of the Galápagos hotspot, the input into the Panamanian subduction zone and the tectonic interplay with the Central American landbridge. The second focus of this study was the subduction output along the Panamanian subduction zone over the last 65 Ma. Furthermore the growth, paleotectonic and geochemical evolution of the Panamanian island arc.

The first chapter focuses on uplifted parts of the Caribbean oceanic plateau and accreted magmatic igneous complexes outcropping along the Pacific coast of Panama and north to Volcan Barú. One of the major goals of this study was to identify additional portions of the Caribbean basement in Panama and to determine their age range and geochemical composition. Ages of the Caribbean large igneous basalts, determined by $^{40}\text{Ar}/^{39}\text{Ar}$ step-heating range from 71-115 Ma.

A second major goal of this study was to understand the intermediate history of the Galápagos hotspot and to evaluate spatial variations in the geochemistry of accreted terranes providing possible evidence for earlier zonation of the Galápagos hotspot as has been proposed for the < 20 Ma history of the Galápagos hotspot. Magmatic complexes with ocean island basalt-type geochemical signatures and rarely mid-ocean ridge basalt-type signatures form the southern part of the Azuero and Soná peninsulas and islands off the Pacific coast of western Panama yielded ages of 17-66 Ma. These complexes represent accreted islands, seamounts, aseismic ridge volcanic complexes and oceanic crust. Geochemical composition of the accreted igneous complexes range from tholeiitic to alkalic. Trace element and Sr-Nd-Pb isotope compositions show that the four mantle components observed at the Galápagos hotspot (Northern, Southern, Central and Eastern domains) were present at the major paleo-Galápagos track which formed from 66-50 M. Isotopic zonation and geometry of the accreted igneous complexes confirm that the zonation found at the present Galápagos archipelago was similar 66-50 Ma ago. Northern domain composition outcrop at Quepos (Costa Rica), Eastern domain composition extends from Osa to Coiba and Southern and Central domain compositions were found at Azuero. The paleo-Galápagos hotspot tracks were primarily accreted during the Early Paleocene to Middle Eocene (~ 60–45 Ma) extending from Quepos (Costa Rica) to Azuero. Thereafter accretion of paleo hotspot tracks is rare and sporadic and extends at least from the Early Miocene to Quaternary (<23 Ma). Late Eocene to Miocene accreted complexes have been found in southern Azuero and the western coast of Coiba Island, indicating that the hotspot track was being subducted off western Panama ca. 20-30 Ma ago and over the last 5 Ma. Based on our results we confirm that paleo-Galápagos hotspot

tracks were accreted to the Panamanian Pacific coast during most of the Tertiary. The third focus was to constrain the input into the Panamanian subduction system through time.

The second article/chapter focuses on arc magmatism in Panama covering the entire Cenozoic, providing a unique opportunity to assess compositional changes in arc volcanism through time. In order to constrain the tectonic evolution of the southern central American landbridge we have carried out a regional geochronologic and geochemical (major and trace element and Sr-Nd-Pb isotope) study of arc volcanism in Panama since the inception of subduction at the western edge of the Caribbean large igneous province to the present. New Ar^{40}/Ar^{39} ages of tholeiitic to calc-alkaline island arc magmatism occurring throughout Panama range from 60.9 ± 0.5 to 7.4 ± 0.7 Ma.

A paleo-Galápagos hotspot track was subducted beneath central and southern Costa Rica and western Panama from about 60-45 Ma ago, leaving a belt of accreted ocean island and seamount volcanoes and fragments of submarine aseismic ridges extending from Quepos (Costa Rica) to the Azuero Peninsula (Panama). Isotopic composition of Paleocene subduction-related rocks from the Azuero Peninsula confirm the nearby subduction of a hotspot track. Northern migration of the Western Panamanian arc is documented from ca. 50–30 Ma indicating that tectonic erosion may have been more prominent than accretion. Tectonic erosion was probably induced by the subduction of a paleo-Galápagos hotspot track comparable to the present situation offshore Costa Rica. Tectonic erosion rates of $84\text{--}96 \text{ km}^3 \text{ Ma}^{-1} \text{ km}^{-1}$ for the Panamanian arc between 50-30 Ma were calculated. These rates are in the range of the recent Costa Rican tectonic erosion rates. Elevated Pb isotope ratios (increased Galápagos-type geochemical signature) in arc rocks on Azuero in the Middle Eocene (~45 Ma) and in eastern Panama in the Early Miocene (~20 Ma) suggest eastern migration of the subducting hotspot track. The Paleocene to late Eocene arc is offset to the north in eastern Panama as compared to western Panama; however, the Miocene arc is contiguous from western to eastern Panama, suggesting left-lateral displacement between the Late Eocene and Early Miocene (40-22 Ma) in the Panama canal region. The shift of the subducting hotspot track from Azuero to the east may have induced the left-lateral displacement. Volcanism in eastern Panama ceased around 12 Ma coeval to the collision of eastern Panama with South America. In the Pliocene through Holocene (4.5 ± 0.17 to 0.1 ± 0.08 Ma) volcanism was restricted to low volume eruptions of alkaline and adakitic magmatism in western Panama primarily in the forearc region of the Miocene arc (south of the Cordillera Central). The subduction of the Coiba and Cocos Ridges may have allowed a slab window to open, leading to melting of the exposed slab edges and subsequent formation of adakites. Melting of mantle, which had been metasomatized by adakitic melts, could produce alkali basalts. Another possible source of the alkali basalts found in Panama is melting of Galápagos-type mantle

upwelling through the slab window. In conclusion, the interplay between the Galápagos hotspot track and the Panamanian subduction zone can explain variations in the geochemistry of arc rocks through time and has a significant impact in the tectonic evolution of Panama.

Table of Contents

Zusammenfassung	I
Summary	IV
Danksagung	VII

Article (Chapter) 1: Subduction Input

Ocean Island Basalt-type volcanic rocks in Panama (17 - 115 Ma): Long-term Evolution of the Galápagos Hotspot and Input into the Panamanian Subduction Zone

Abstract	1
1 Introduction	2
2 General Geology	3
2.1 Tectonic Setting of Panama	3
2.2 Caribbean large igneous province & Galápagos hotspot tracks	5
3 Analytical Procedures	7
4 Results	9
4.1 Field Observations & Petrography	9
4.2 Geochronology	12
4.3 Major and Trace Elements	13
4.4 Sr-Nd-Pb Isotope Ratios	16
5 Discussion	20
5.1 Mafic igneous complexes outcropping along the Pacific coast of Panama and near Changuinola	20
5.2 Detailed discussion of the origin of the individual Panamanian igneous complexes	22
5.3 Zonation and temporal evolution of the paleo-Galápagos hotspot track	27
6 Conclusion	32
7 Acknowledgements	33
8 References	33
9 Tables	39

Article (Chapter) 2: Subduction Output

65 Ma of Arc Magmatism in Western Panama: A Case Study of the Growth of the Central American Landbridge

	Abstract	47
1	Introduction	48
	1.1 Geological Background	49
	1.2 Tectonic overview	52
2	Analytical Procedures	53
3	Results	55
	3.1 Geochronological results	55
	3.2 Petrography	59
	3.3 Classification	61
	3.4 Major and trace elements	61
	3.5 Isotopes	66
4	Discussion	71
	4.1 Forming of an island arc	71
	4.2 Northern migration of the arc	77
5	Evolution of the Central American Landbridge at Panama: Interaction of the Galápagos hotspot with the Panamanian subduction zone	79
6	Conclusions/Summary	84
7	Acknowledgements	85
8	References	85
9	Tables	92

Article (Chapter) 1: Subduction Input

Ocean Island Basalt-type volcanic rocks in Panama (17 - 115 Ma): Long-term Evolution of the Galápagos Hotspot and Input into the Panamanian Subduction Zone

Lissinna, B., Hoernle, K., Hauff, F., van den Bogaard, P.

Leibniz-Institute for marine sciences IFM-GEOMAR, Wischhofstrasse 1-3, 24148 Kiel

Abstract

This study focuses on igneous rocks in the accretionary complexes located along the western coast of Panama in order to reconstruct the subducted history of the Galápagos hotspot in more detail and to constrain the input into the Panamanian subduction system during the Cenozoic. Uplifted parts of the Caribbean oceanic plateau along the Pacific coast of Eastern Panama and on the Azuero and Soná Peninsulas yielded an $^{40}\text{Ar}/^{39}\text{Ar}$ step-heating age range from 71-115 Ma. Magmatic complexes with ocean island basalt-type geochemical signatures and rarely N-MORB-type signatures form the southern part of the Azuero and Soná Peninsulas and islands off the Pacific coast of western Panama ranging in age from 17-66 Ma. These complexes represent accreted ocean islands, seamounts, aseismic ridge volcanic complexes and ocean crust. Geochemical composition of the accreted igneous complexes range from tholeiitic to alkalic. Trace element and Sr-Nd-Pb isotope compositions show that the four mantle components observed at the Galápagos hotspot (Northern, Southern, Central and Eastern domain) were present in the paleo-Galápagos hotspot track formed 66-50 Ma ago. Isotopic zonation and geometry of the accreted igneous complexes (66-50 Ma) confirm that the zonation found at the present Galápagos archipelago was similar 66-50 Ma ago. Northern domain composition outcrop at Quepos (Costa Rica), Eastern domain composition extends from Osa to Coiba and Southern and Central domain compositions were found at Azuero. The paleo-Galápagos hotspot tracks were primarily accreted during the Early Paleocene to Middle Eocene (~60–45 Ma) extending from Quepos (Costa Rica) to Azuero about a maximal distance of 400 km. Thereafter accretion of paleo hotspot tracks is rare and sporadic and extends at least from the Early Miocene to Quaternary (< 23 Ma). Northern migration of the Western Panamanian arc is documented from ca. 50–40 Ma indicating that tectonic erosion may have been more prominent than accretion. Late Eocene to Miocene accreted complexes have been found in southern Azuero and the western coast of Coiba Island, indicating that the hotspot track was being subducted off western Panama ca. 20-30 Ma ago and over the last 5 Ma.

1 Introduction

The Caribbean Plate consists of thickened oceanic crust (up to 20 km), believed to result from intraplate magmatism related to the Cretaceous Galápagos hotspot or mantle plume [Duncan and Hargraves, 1984; Hauff et al., 1997, 2000a,b; Sinton et al., 1998; Kerr et al., 1996; Hoernle et al., 2002, 2004]. The Caribbean oceanic plateau large igneous province (CLIP) formed in the Pacific above the Galápagos hotspot during several magmatic episodes between ca. 70-140 Ma [Hoernle et al., 2004]. The resulting plateaus were accumulated at the Greater Antilles subduction zone to form the Caribbean Plate. Subduction on the western margin of the Caribbean began ~70 Ma ago [Kesler et al., 1977] It has been previously inferred that the Panamanian Pacific coast is partly formed of Caribbean basement [Donnelly et al., 1990; Sinton et al., 1998; Hauff et al., 2000a,b; Hoernle et al., 2002]. A pillow sequence from Soná Peninsula was interpreted by Hoernle et al. [2002] as part of the Caribbean igneous province. One of the major goals of this study was to identify additional portions of the Caribbean basement in Panama and to determine their age range.

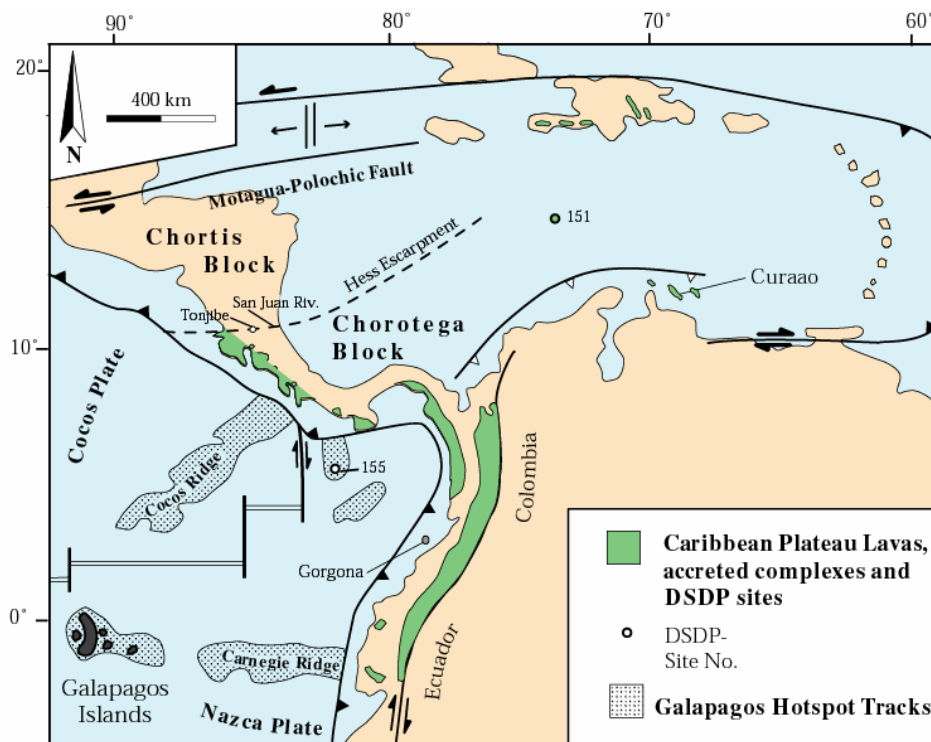


Fig.1: Overview map of Central America, the Caribbean and northwestern South America. Igneous complexes in Panama, Costa Rica, Colombia, uplifted circum Caribbean basement, DSPD drill sites and the present Galápagos archipelago and adjacent hotspot tracks is shown modified after Kerr et al. [1997] and Hauff et al. [2000a].

Accreted parts of the paleo-Galápagos hotspot tracks (21-66 Ma) have been identified in the accretionary complex of the Panamanian subduction zone, the southern part of the Central American subduction system. These remnants of subducted Galápagos ocean islands,

seamounts and aseismic ridges connect the CLIP with the Galápagos hotspot tracks on the Pacific seafloor [Hoernle *et al.*, 2002]. Accreted paleo Galápagos hotspot tracks in Costa Rica range in age from 55-65 Ma [Hauff *et al.*, 2000a] and from 52-66 and 21-38 Ma in Panama [Hoernle *et al.*, 2002]. For the Costa Rican accreted Galápagos terranes at Quepos and Osa, Middle Eocene (49-41Ma) accretion has been inferred [Hauff *et al.*, 2000a]. A second major goal of this study was to fill in additional gaps in the intermediate history of the Galápagos hotspot and to evaluate spatial variations in the geochemistry of the accreted terranes providing possible evidence for earlier zonation of the Galápagos hotspot as has been proposed for the < 20 Ma history of the Galápagos hotspot [Hoernle *et al.*, 2000; Geldmacher *et al.*, 2003; Werner *et al.*, 2003]. The third major goal was to constrain the input into the Panamanian subduction system for the last ca. 70 Ma. Using Ar⁴⁰/Ar³⁹ laser dating and geochemical investigations, we confirm that the western Panamanian basement consists of uplifted and/or accreted Caribbean plateau basalts. We also confirm that paleo-Galápagos hotspot tracks were accreted to the Panamanian Pacific coast during most of the Tertiary.

2 General Geology

2.1 Tectonic Setting of Panama

Panama is situated at the junction of 5 plates: the North American, Caribbean, Cocos, Nazca and South American Plates. The Panama-Costa Rica microplate is moving northward at a rate of 7-11 mm/year relative to the stable Caribbean Plate, forming the North Panama Deformed Belt (NPDB) where the Panama-Costa Rica microplate overrides the Caribbean Plate [Adamek *et al.*, 1988; Silver *et al.*, 1990; Kellog *et al.*, 1995]. Additionally Panama moves eastward at a rate of 10-20 mm/yr colliding with northern South America [Kellog *et al.*, 1995]. The Cocos Plate subducts beneath southern Costa Rica and western Panama at a rate of 72 mm/year [Kellog *et al.*, 1995]. Three seismically active N-S-trending, right-lateral strike-slip fracture zones (Panama, Balboa and Coiba form a 70-km-wide right-lateral transform boundary between Cocos and Nazca Plate [Adamek *et al.*, 1988; Kolarsky and Mann, 1995]. The fracture zones intersect the South Panama Deformed Belt (SPDB), an accretionary prism complex developed along the continental slope. Magnetic anomalies on the Nazca Plate constrain a northwestward jump in the Cocos-Nazca Plate boundary at 11 to 8 Ma [Lonsdale and Klitgord, 1978]. Prior to ~ 2 Ma the Coiba fracture zone may have been the active plate boundary between Nazca and Cocos Plates [Lonsdale and Klitgord, 1978; McMillan *et al.*, 2004]. The exact kinematic evolution of the Panama and Coiba fracture zones is still unsolved.

In a seismic study of western Panama, a decrease in seismicity was documented towards the east reflecting a lateral change in stress associated with the geometry of the Nazca Plate beneath the region [Cowan *et al.*, 1995]. Deep seismic events (70-115 km) between the Gulf of Chiriquí and the Cordillera Central define a NE-dipping zone, providing evidence for lithosphere subducting beneath Panama [Cowan *et al.*, 1995]. Additionally high heat flow

along the isthmus (comparable with the Galápagos ridge system and 4 times higher than the Caribbean [*de Boer et al.*, 1991]) and Recent volcanism at Volcan Barú and the LaYeguada volcanic complex (western Panama) [*Defant et al.*, 1991] are consistent with Holocene oblique subduction beneath western Panama [*Moore and Sender*, 1995; *Westbrook et al.*, 1995]. Active deformation along the SPDB extends eastward to at least longitude 80°30' (S Azuero) [*Moore and Sender*, 1995].

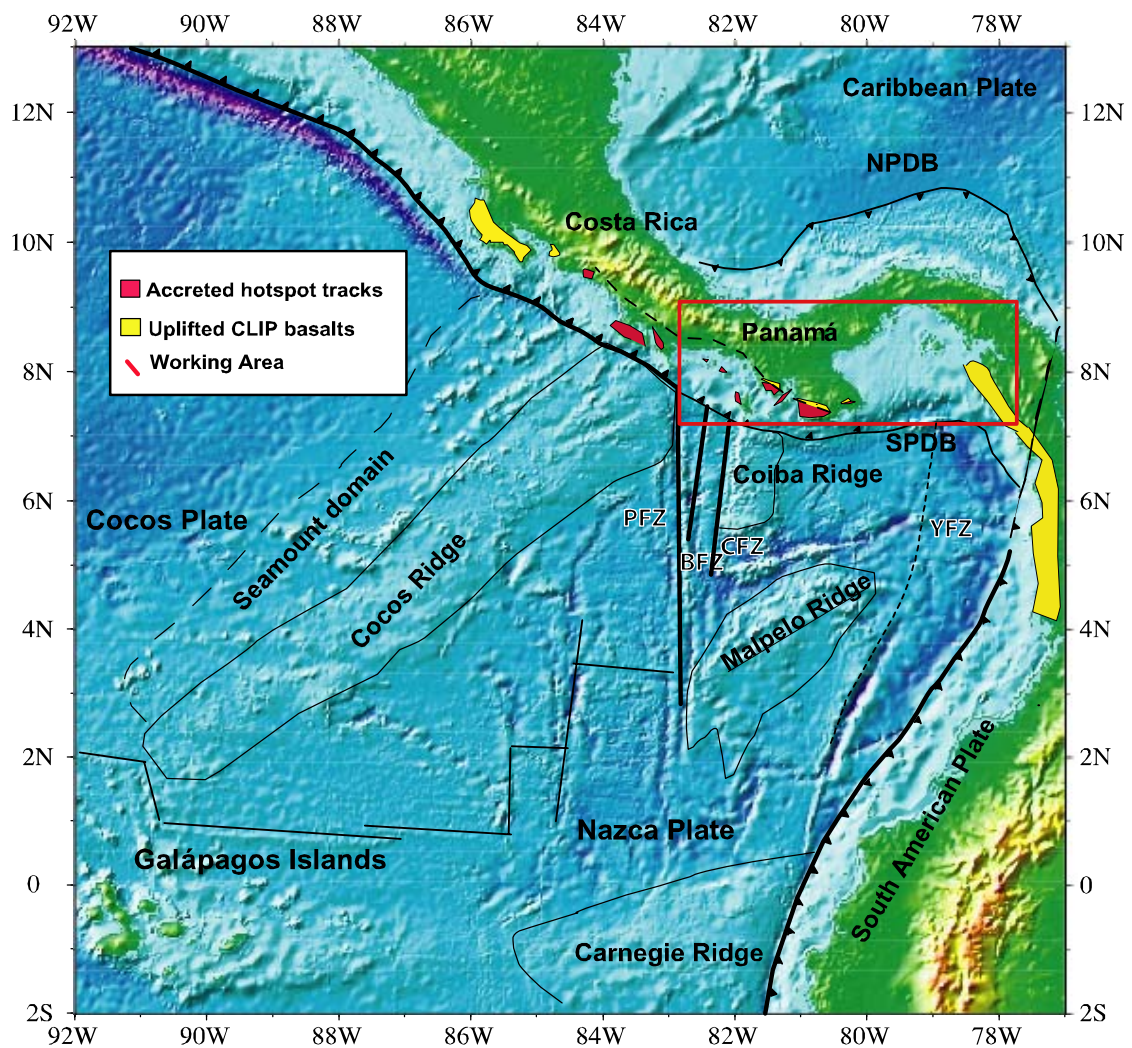


Fig.2: Tectonic map of Southern Central America including the Galápagos Islands and hotspot tracks. The South Panama Deformed Belt (SPDB) represents an active accretionary prism extending from at least 80°W to 83° W [*Kolarsky and Mann*, 1995]. North Panama Deformed Belt (NPDB) is a broad belt of deformation north of the Panamanian Isthmus [*Bowland and Rosencrantz*, 1988]. The Panama Fracture Zone (PFZ), Balboa Fracture Zone (BFZ) and the Coiba Fracture Zone (CFZ), Yaquina Fracture Zone (YFZ) recently active fracture zones and precursors forming the Cocos Nazca boundary.

The dip of the subducting slab is inferred to be between 3° and 6° to the northeast [MacKay and Moore, 1990; Kolarsky and Mann, 1995]. A broad 30-km-wide accretionary wedge is formed in which sedimentary rocks of the subducting Nazca Plate appear to underplate the overriding Panama-Costa Rica microplate [Kolarsky and Mann, 1995].

The Panama-Choco arc terrane (including NW Colombia) collided with South America about 6-12 Ma ago, an important step in the eventual formation of the Pliocene landbridge between North and South America [Keigwin, 1982; Keller, 1989; Duque-Caro, 1990]. A Coiba Ridge like ridge is assumed to have subducted beneath Panama adjacent to the Yaquina fracture zone since at least 9 Ma [McMillan *et al.*, 2004]. The Coiba fracture zone is interpreted to represent the Cocos-Nazca boundary since ~3 Ma ago [McMillan *et al.*, 2004]. Collision of the Cocos and Coiba Ridges with southwestern Costa Rica and western Panama and its northeast convergence may be responsible for the origin of left-lateral strike-slip faults [Vergara Muñoz, 1988]. Left-lateral, strike-slip faulting of WNW-ESE-trending faults extend from Azuero to southern Costa Rica [e.g. Okaya and Ben-Avraham, 1987; Kolarsky and Mann, 1995]. The Azuero-Soná fault system appears to be continuous with the Ballena-Celmira fault zone of southern Costa Rica, a strike slip fault or oblique-slip fault separating two distinct basement blocks of the Costa Rican forearc [Corrigan *et al.*, 1990]. Additionally major rifting and subsidence in the Gulf of Chiriquí in the Early Pliocene is associated with left-lateral strike-slip faulting along the western Panamanian Pacific coast [Kolarsky and Mann, 1995]. Structural arches in the fore-arc basement are inferred to be produced by the recent subduction of the Coiba Ridge [Kolarsky and Mann, 1995]. Initial subduction of the Cocos Ridge beneath Costa Rica ranges from 8 to 1 Ma depending on the proposed model [Lonsdale and Klitgord, 1978; Collins *et al.*, 1995; de Boer *et al.*, 1995; Abratis and Wörner, 2001; McMillan *et al.*, 2004]. Pliocene (~5-3.5 Ma) changes in sedimentation rates and deepening of the outer fore-arc basin, angular unconformities of the arc and cessation of calc-alkaline volcanism in Costa Rica may have been initiated by the subduction of the Coiba Ridge and by the passage of the Cocos-Nazca-Caribbean triple junction [MacMillan *et al.*, 2004]. Ensuing subduction of the Cocos Ridge (3-2 Ma) may have continued this process [MacMillan *et al.*, 2004].

2.2 Caribbean large igneous province & Galápagos hotspot tracks

Ages of igneous rocks from the Caribbean large igneous province (CLIP) in Central America (Nicoya, Herradura, Golfito Peninsulas in Costa Rica and Sona Peninsula in Panama), DSPD sites in the Caribbean, northwestern Colombia, Ecuador, Curaçao and the Greater Antilles range from 139 to 69 Ma [Hauff *et al.*, 1997, 2000a, 2000b; Sinton *et al.*, 1997, 1998; Kerr *et al.*, 1997, 2002; Révillon *et al.*, 2000; Lapierre *et al.*, 2000; Hoernle *et al.*, 2002, 2004;] [Fig.9]. Volcanism in these magmatic provinces has been interpreted as being formed by the starting plume head of the Galápagos hotspot [e.g. Duncan and Hargraves, 1984; Sinton *et al.*, 1998; Hauff *et al.*, 2000a], but recently it has been inferred

that a pulsing Galápagos hotspot may have formed multiple intraplate igneous plateaus and other volcanic structures since ~139 Ma [Hoernle *et al.*, 2004]. It can still be assumed that the most voluminous pulse of flood basalt volcanism extended from ~95-83 Ma, with additional pulses possibly having occurred from ~139-133 Ma, ~118-111 Ma and 81-69 Ma [Hauff *et al.*, 2000a; Hoernle *et al.*, 2002, 2004; Kerr *et al.*, 1997; Sinton *et al.*, 1997, 1998]. After the formation of the multiple volcanic structures over the Galápagos hotspot, they drifted northeastward during the Cretaceous until they reached the Greater Antilles subduction zone located between the Americas [e.g. Duncan and Hargraves, 1984; Hauff *et al.*, 2000a; Hoernle *et al.*, 2002, 2004]. The older (~139-133 Ma and ~118-111 Ma) plateaus or other volcanic structures were accreted along the western margin of the Greater Antilles subduction zone [Hoernle and Hauff, 2005]. The largest plateau (~83-95 Ma) may have jammed the east-dipping subduction, causing a polarity reversal in subduction beneath the Greater Antilles at ~70-75 Ma [e.g. Hoernle *et al.*, 2002; Hoernle and Hauff, 2005].

East dipping subduction on the western edge of the CLIP began at ~70 Ma, leading to the formation of the Late Cretaceous to Tertiary Central American Arc. Geochemical data of igneous complexes (20.8-66.0 Ma) along the Pacific margin of Costa Rica and Panama are consistent with being accreted portions of ocean island and seamount volcanoes and aseismic ridges, derived from the Galápagos hotspot.

The Nazca and the Cocos Plate were formed by the breakup of the Farallon Plate at ~23 Ma due to migration of a preexisting fracture zone over the Galápagos hotspot [Handschuhmacher, 1976]. During the last 20 Ma, the geometry between the Galápagos hotspot and Galápagos or Cocos-Nazca spreading center (CNS) changed several times, leading to the formation of Galápagos hotspot tracks on the Cocos and Nazca Plates with varying volume and pattern of geochemical zonation.

Four main portions of the Galápagos hotspot tracks are exposed on the seafloor, Cocos Ridge and NW seamount province, Carnegie Ridge, Malpelo Ridge and Coiba Ridge [Fig. 1, 2]. The most prominent ridges are the Cocos Ridge on the Cocos Plate subducting beneath Costa Rica and the Carnegie Ridge on the Nazca Plate subducting beneath Ecuador. The Cocos track is built up of two main morphological and geochemical domains 1) the Cocos Ridge, up to 300 km broad and more than 1000 km long, extends from the CNS to the trench off the coast of Costa Rica, and 2) the Costa Rica and Cocos Island seamount provinces northwest of the Cocos Ridge. The ridges are mainly tholeiitic whereas the seamount provinces are primarily alkalic. The oldest preserved part of the Cocos track adjacent to the Costa Rican trench forms a now-drowned 13.0-14.5 Ma paleo-Galápagos Archipelago [Werner *et al.*, 1999; Hoernle *et al.*, 2000].

The Coiba Ridge, is presently located south of the Azuero Peninsula and Coiba Island, adjacent to the Coiba fracture zone (CFZ). It is a ~100 km wide by ~150 km long ridge. The geometry of the Coiba Ridge is extraordinary among the Galápagos hotspot tracks being

highest in the west and sloping down to the east. It has been inferred that it represents a part of uplifted crust adjacent to a triple junction [Lonsdale and Klitgord, 1978; McMillan *et al.*, 2004]. Geochemistry of drilled (DSDP Site 155) and dredged rocks however suggest that it may represent part of a Galápagos hotspot track [Hauff *et al.*, 2000a; Werner *et al.*, 2003]. Alternatively the Galápagos-type geochemistry of Coiba Ridge may have resulted from plume-ridge interaction. The overlying sediments have been dated paleontologically giving a minimum age of 15 Ma for the igneous portion of the Coiba Ridge [van Andel *et al.*, 1973]. Based on paleomagnetic data, the oldest crust beneath the Coiba Ridge formed during the initial opening of the Cocos-Nazca spreading center (CNS) between 22.7-21.0 Ma giving a maximum age for its formation [Werner *et al.*, 2003]. The Coiba Ridge may be an extension of the Cocos Ridge which was offset to the south along the Panama fracture zone, representing a paleo-transform fault [Hoernle *et al.*, 2002].

The Malpelo Ridge is situated to the south on the Nazca Plate. Malpelo Island on the Malpelo Ridge yielded $^{40}\text{Ar}/^{39}\text{Ar}$ ages of 15.8-17.3 Ma, indicating a minimum age of 17.3 Ma for the Malpelo Ridge [Hoernle *et al.*, 2002; Werner *et al.*, 2003]. Based on the interpretation of magnetic anomalies, the Malpelo and the Carnegie Ridges were once attached and separated by seafloor spreading between 14.5-9.5 Ma [Werner *et al.*, 2003].

3 Analytical Procedures

Major and trace elements are reported in Table 1 and isotope data in Table 2 in section 9. Rock powders were prepared by 1) crushing the samples to 0.5 - 1.0 cm chips, and then 2) picking of rock chips free of obvious signs of alteration and the presence of xenolithic material under the binocular microscope. Chips were ground to a flour in an agate mill. Major and trace elements (SiO_2 , Al_2O_3 , MgO , Fe_2O_3 , CaO , Na_2O , K_2O , TiO_2 , MnO , P_2O_5 and Ba, Cr, Ni, Sr, Zr) were analyzed with a Phillips X'Unique PW1480 X-ray fluorescence spectrometer (XRF) at the Leibniz Institute for Marine Sciences (IFM-GEOMAR). Volatile content was measured on a Fisher-Rosemount CWA 5003 infrared photometer and is reported in section 9 Table 1. Major elements in all plots are normalized on a volatile free basis. Ca content was corrected assuming that CO_2 comes from CaCO_3 . International reference standards JB-2, JB-3 (basalts), JA-2 (andesites), JR-1 (rhyolites) were measured with the samples and results are reported in Table 1 in section 9.

Additional trace elements (Rb, Y, Nb, Hf, Ta, Pb, Th, U, and REE) were analyzed by inductively coupled plasma-mass spectrometry at the institute of Geosciences, University of Kiel using a VG Plasmaquad PQ1 and a Agilent 7500c ORS quadrupole plasma mass spectrometer. Samples were cooked in a multi-stage acid pressure dissolution with HF-aqua regia- HClO_4 . Details of the analytical procedures are reported in Garbe-Schönberg [1993]. Reproducibility estimated from duplicate sample preparation and replicate measurements was better than 1.5% RSD for all analyzed elements. International standards JB-2, BIR-1, BHVO-

1 and blanks were analyzed with the samples in order to accuracy of the measurements [Tab 1B, section 9].

Sr-Nd-Pb analysis were carried out on whole rock powders and chips that were leached in hot (130°C, 1h) 6N HCl for Sr and 2N HCl (70°C, 1h) for Pb in order to minimize the effects of alteration and sample handling. Chemical separation procedures are described in *Hoernle and Tilton* [1991]. Sr, Nd isotopic ratios were analyzed on a TRITON thermal ionization mass spectrometer (TIMS) and Pb isotopic ratios were analyzed on a Finnigan MAT 262 RPQ²⁺ TIMS at the Leibniz Institute for Marine Sciences. Both instruments operate in static multicollection. Sr and Nd isotopic ratios are normalized within run to $^{86}\text{Sr}/^{88}\text{Sr}=0.1194$ and $^{146}\text{Nd}/^{144}\text{Nd}=0.7219$ respectively and all errors throughout the manuscript are reported as 2σ . Over the course of the study NBS987 gave $^{87}\text{Sr}/^{86}\text{Sr}=0.710258 \pm 0.000008$ (N=51), La Jolla $^{143}\text{Nd}/^{144}\text{Nd}=0.511846 \pm 0.000005$ (N=49) and our inhouse Nd-monitor SPEX $^{143}\text{Nd}/^{144}\text{Nd}=0.511711 \pm 0.000006$ (N=39). Sr-Nd replicate analyses (separate digests) were within the external errors of the standards. NBS981 (n=70) gave $^{206}\text{Pb}/^{204}\text{Pb}=16.900 \pm 0.007$, $^{207}\text{Pb}/^{204}\text{Pb}=15.438 \pm 0.009$ and $^{208}\text{Pb}/^{204}\text{Pb}=36.528 \pm 0.030$ and are corrected to the NBS 981 values given in *Todt et al.* [1996]. Pb replicate analyses (separate digests) of 14 samples were within 0.021%/amu. Finally, Sr, Nd and Pb total chemistry blanks were <100 pg and thus considered negligible.

To compare isotopic signatures of CLIP basalts and the paleo-Galápagos hotspot track to present day Galápagos composition, all data were age corrected and then the isotopic composition was projected from time of formation until today assuming source parent/daughter ratios of $^{87}\text{Rb}/^{86}\text{Sr}=0.048$, $^{147}\text{Sm}/^{144}\text{Nd}=0.15$, $^{238}\text{U}/^{204}\text{Pb}=10$, $^{235}\text{U}/^{204}\text{Pb}=0.07$ and $^{232}\text{Th}/^{204}\text{Pb}=40$.

$^{40}\text{Ar}/^{39}\text{Ar}$ ages for 9 igneous rocks are reported in Table 3 and Fig. 3 and 10. Matrix separates were analyzed. Total fusion of matrix (mx) separates using a 25 W Spectraphysics Argon Ion laser connected to a MAP 216 noble gas mass spectrometer was carried out at the Geochronology Laboratory at IFM-GEOMAR. All samples were irradiated for 144 hours in the 5-MW reactor at the GKSS Research Center in Geesthacht (Germany). For vertical and lateral control of the neutron flux gradient, Taylor Creek rhyolite (TCR) sanidine (Batch 85G003, 27.92 Ma [*Duffield and Dalrymple*, 1990]) was used as monitor crystals.

Mean apparent ages (WMA) were calculated when two step-heating ages of one sample were analyzed separately. $^{40}\text{Ar}/^{39}\text{Ar}$ isochron ages represent the closing age if the $^{40}\text{Ar}/^{36}\text{Ar}$ intercept lies within 2σ error standard deviation (95% confidence level) of the atmospheric value ($^{40}\text{Ar}/^{36}\text{Ar}=295.5$). If $^{40}\text{Ar}/^{36}\text{Ar}$ initial ratios deviate by more than 2σ standard deviation from the atmospheric value, a mean apparent age is calculated.

Laser step-heating analyses were conducted on the basaltic matrix (mx). Step-heating plateaus comprise three or more contiguous steps and $X \geq 50\%$ of total ^{39}Ar released. Plateaus

with <50% of the total ^{39}Ar released need to be treated with caution, and ages are only accepted if consistent with other geological age criteria. Probability-of-fit of the weighted-mean age of the steps is greater than 5%. Slope of the error-weighted line through the plateau ages is not different from zero at 5% confidence. The geological timescale of *Palmer and Geissman* [1999] is used throughout the paper.

4 Results

4.1 Field Observations & Petrography

Samples presented in this study come from the Pacific coast regions of western (Soná and Azuero Peninsulas and Bolaños, Icaico, Ladrones, Secas, Coiba, Santa Catalina and Cébaco Islands) and eastern (Bahia Piña) Panama and from Piedra Blanca north of Volcano Barú [Fig.3 A,B, C]. The rocks can be divided into two major groups based on petrography, occurrence and age. Petrographically the sampled rocks can be divided into two main groups: 1) aphyric rocks, 2) porphyritic rocks. The aphyric rocks have tholeiitic compositions and contain plagioclase, clinopyroxene, ilmenite and magnetite in the groundmass. The porphyritic rocks contain phenocrysts of plagioclase, clinopyroxene (partly titanaugite), olivine (often altered to iddingsite), titanomagnetite and ilmenite. Alteration products and secondary phases are serpentine, chlorite, pyrite and epidote. Picrites have been found on southern Azuero and Bolaños Island. Phenocrysts are large idiomorph olivine crystals (25-30%), plagioclase (2-10%), clinopyroxene (~3%) and titanomagnetite (2%).

Sequences of aphyric tholeiitic pillow basalts and sheet flows, commonly associated with Late Cretaceous radiolarian cherts, are exposed in southern Azuero and southern Soná near to the ASFZ and along the Pacific coast of Darien. On Azuero near Torio, sheet flows lie on and surround blocks of Coniacian radiolarian cherts [*Kolarsky et al.*, 1995]. Along the Darien coast south of the Gulf of An Miguel, pillow basalts sometimes overlie and are sometimes conformably overlain by radiolarian cherts indicating an abyssal origin. In eastern Panama near Bahia Piña, aphyric basaltic sills and dikes are common in the chert sequences. Pillow basalts and diabases overlain by deformed cherts were also sampled around the Gulf of San Miguel (eastern Panama). These sequences were interpreted in the field to reflect uplifted portions of the Caribbean basement.

Accreted porphyritic tholeiitic to alkalic basaltic igneous rocks from western Panama (Azuero Peninsula and Bolaños, Icaico, Ladrones, Secas, Coiba, Santa Catalina and Cébaco Islands) occur as 1) dikes/sills, 2) pillow basalts/sheet flows, indicative of subaqueous eruptive conditions, and 3) agglutinates and lava flows which are partly columnar and associated with basis/top breccias, providing evidence for subaerial volcanism. These sequences are interpreted to reflect portions of accreted ocean island and seamount volcanoes and aseismic volcanic ridges, belonging to a paleo-hotspot track [*Hoernle et al.*, 2002].

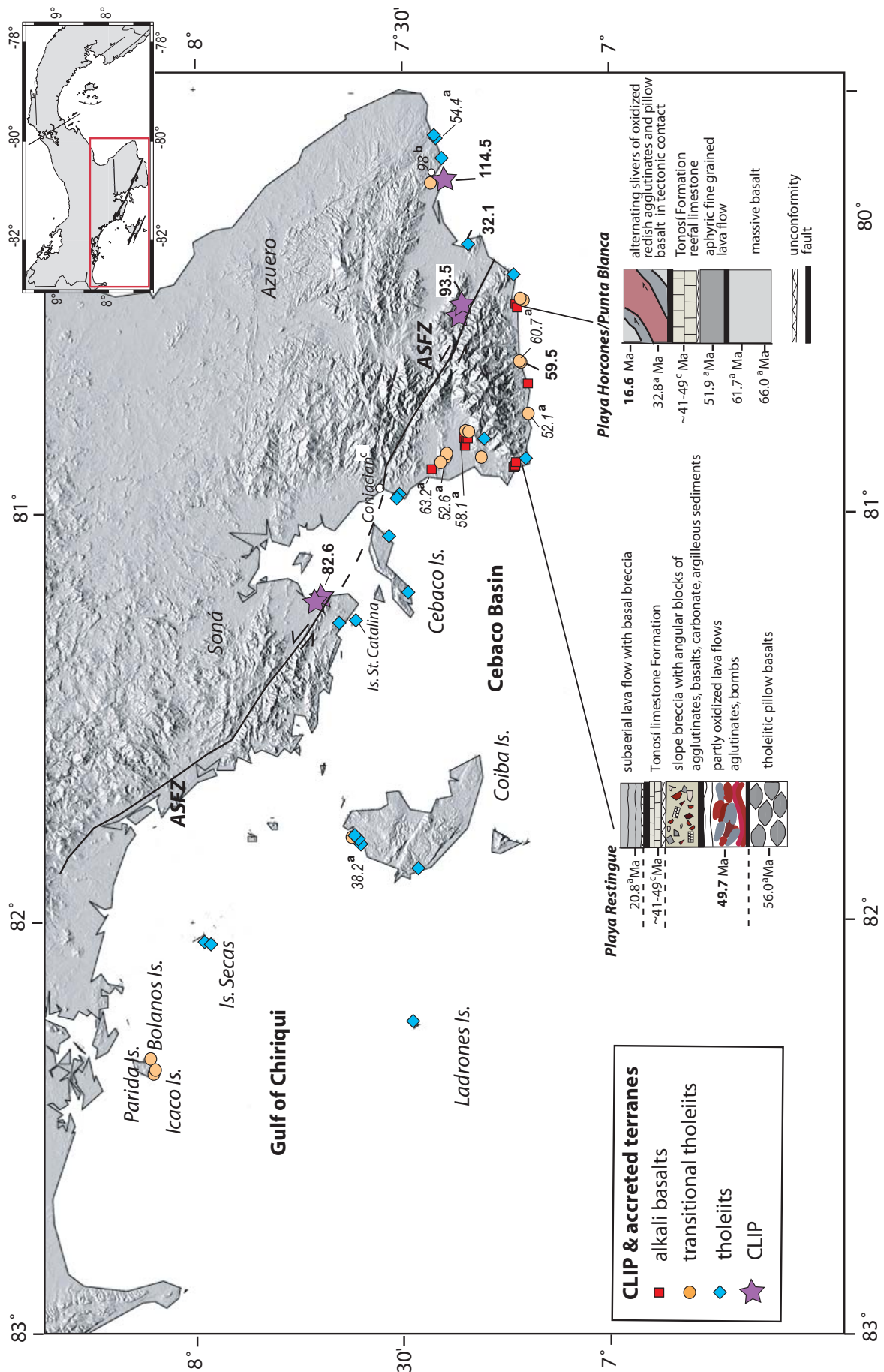


Fig. 3: A) Map of western Panama showing the Azuero and Sona Peninsulas and offshore islands. Sample locations are shown for Caribbean Large Igneous Province (CLIP) and younger accreted oceanic igneous terranes, as well as lithostratigraphic columns for selected outcrops. $^{40}\text{Ar}/^{39}\text{Ar}$ ages from this study are shown in bold. Superscripts denote sources of additional ages: (a) $^{40}\text{Ar}/^{39}\text{Ar}$ ages from *Hoernle et al.* [2002], (b) K/Ar age from *Bourgeois et al.* [1982], (c) Fossil ages for the Tonosí Formation and a radiolarian chert *Kolarsky et al.* [1995].

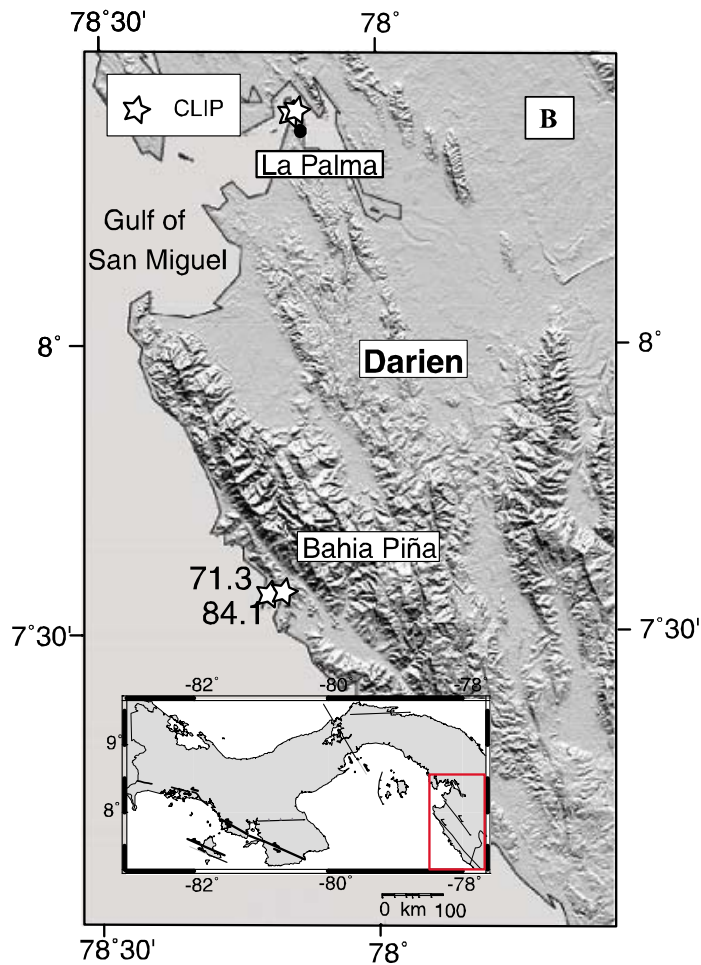
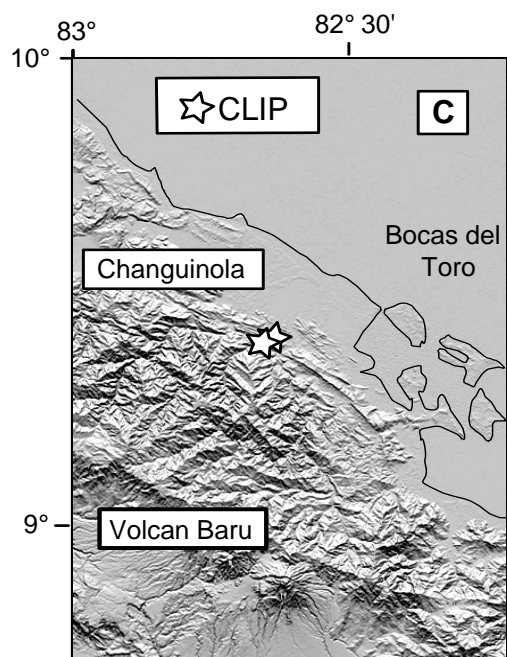


Fig. 3 B: Map of eastern Panama, Pacific coast of Darien. Sample location for CLIP samples and new $^{40}\text{Ar}/^{39}\text{Ar}$ laser ages.

Alkali basalts were only found on southern Azuero Peninsula and in general appear to have been erupted under subaerial conditions, consistent with their reflecting late-stage volcanism on an ocean island volcano. Two representative lithostratigraphic sections of the accreted complexes are described below. At Playa Horcones near Punta Blanca (central southern coast of Azuero) [Fig. 3A], massive aphyric basalts are unconformably overlain by reefal limestone. At the western part of the beach at Punta Blanca, alternating slivers of pillow basalts (erupted under submarine conditions) and heavily oxidized, reddish, aphyric agglutinates (erupted under subaerial conditions) are in tectonic contact. At Playa Restingue (SW Azuero), non vesicular, clinopyroxene, plagioclase-bearing pillow basalts (erupted under submarine conditions) [Fig. 3A] are in fault contact with highly vesicular, oxidized (reddish), clinopyroxene-, olivine- and plagioclase-phyric lava flows with top/bottom breccias, agglutinates and bombs.

A reefal limestone above the beach, overlying the aforementioned units, contains the Eocene foraminifera *Lepidocyclina*. A volcanic breccia at Playa Restingue contains angular blocks of tholeiitic to alkaline basaltic igneous rocks, some of which are fragments of highly



oxidized, reddish agglutinates. It also contains carbonates and argillaceous sediment clasts, possibly reflecting an ocean island slope breccia belonging to the volcanic apron facies. At the eastern end of Playa Restingue, an olivine, plagioclase alkaline lava flow with a basal breccia was sampled. These sections will be discussed in more detail below.

Fig. 3 C: Map of northwestern Panama. Sample location of CLIP samples from the Campanian to Maastrichtian (84-65 Ma) Changuinola Formation along the Changuinola river.

4.2 Geochronology

The oldest rocks of Panama are found in the southern part of Azuero and in Darien. A pillow basalt at Playa Venado yielded a $^{40}\text{Ar}/^{39}\text{Ar}$ matrix stepheat plateau age of 108.9 (± 2.8 , all errors given as 1σ) Ma with 61% plateau and 120.6 (± 2.9) Ma with 71% plateau [Tab.3]. Since the ages are within error at the 95% confidence level (2σ), the error weighted mean age for these samples was calculated and is 114.5 (± 2.0) Ma.

Tab. 3: New $\text{Ar}^{40}/\text{Ar}^{39}$ step-heating plateau ages from basaltic matrix of Panama.

Sample	Age [Ma]	\pm	1σ	Rock typ	Location	Type of data	% ^{39}Ar in plateau	MSWD
CLIP								
Az-38-1	108.9	± 2.8		pillow basalt	S Azuero	Matrix STH PLA	61%	1.5
	120.6	± 2.9				Matrix STH PLA	71%	1.7
	114.5	± 2.0				Matrix STH MAA		
Az-26-1	93.5	± 5.3		massive basalt	S Azuero	Matrix STH PLA	61%	0.99
M202bKH	84.1	± 1.0		basalt	E. Panama/ Bahia Pina	Matrix STH PLA	97%	0.8
M200bKH	68.8	± 3.1		pillow basalt	E. Panama/ Bahia Pina	Matrix STH PLA	55%	1.6
	73.9	± 3.2				Matrix STH PLA	47%	1.4
	71.3	± 2.2				Matrix STH MAA		
G54	82.6	± 3.2		massive basalt	SE Soná	Matrix STH PLA	79%	3.2
accreted Galapagos hotspot track								
M21KH	59.9	± 2.30		basalt	S Azuero	Matrix STH PLA	63%	1.0
M108b	49.7	± 0.40		basalt	SW Azuero	Matrix STH PLA	55%	1.2
G39	32.1	± 2.6		pillow basalt	S Azuero	Matrix STH PLA	40%	1.70
G30	16.6	± 0.3		pillow basalt	S Azuero	Matrix STH PLA	43%	

STH = Laser step-heating analysis

PLA = Plateau age

MAA = Mean apparent age (inverse-variance-weighted)

Bourgeois et al. [1982] reported a K/Ar age of 98 Ma (with no error being given) for an igneous rock from Playa Venado. An aphyric basaltic rock near the village of Jobero on southern Azuero, yielded an $^{40}\text{Ar}/^{39}\text{Ar}$ plateau age of 93.5 (± 5.3) Ma. On the eastern coast of the Soná Peninsula at Punta Hicaco south of the ASFZ, a tholeiitic pillow sequence yielded an $^{40}\text{Ar}/^{39}\text{Ar}$ plateau age of 82.6 (± 3.2) Ma. The plateau age of 82.6 Ma agrees well with the Coniacian maximum age (89-85) for the tholeiitic pillow sequence near the Rio Torio on the west coast of Azuero [*Kolarsky et al.*, 1995; *Hoernle and Hauff*, in press]. Tholeiitic pillow basalts at two different localities from Bahia Piña (Darién) produced $^{40}\text{Ar}/^{39}\text{Ar}$ matrix plateau ages of 84.1 (± 1.0) Ma and an error weighted mean age of 71.3 (± 4.4) for two stepheat analyses of the same sample [Tab.3].

The stepheat matrix $^{40}\text{Ar}/^{39}\text{Ar}$ plateau age of Portobello (southern Azuero) from this study yielded an age of 59.9 (± 2.3) Ma [Tab.3], confirming a $^{40}\text{Ar}/^{39}\text{Ar}$ total fusion age of 60.7 (± 1.1) from *Hoernle et al.* [2002]. At Playa Restingue, a basaltic lava flow yielded a matrix stepheat $^{40}\text{Ar}/^{39}\text{Ar}$ plateau age of 49.7 (± 0.4) Ma [Tab.3]. An olivine-bearing basalt found at Punta Bucaró yielded a stepheat matrix $^{40}\text{Ar}/^{39}\text{Ar}$ plateau age of 32.1 (± 2.6) Ma with 40% plateau [Tab.3]. The youngest accreted rocks found in Panama were sampled at Punta Blanca. An aphyric basalt provides an $^{40}\text{Ar}/^{39}\text{Ar}$ age of 16.6 (± 0.3) with a 43% plateau [Tab.3]. Due to the small plateaus for the last two ages, these ages should be treated with caution. Nevertheless, we note that similar ages have been reported from Punta Blanca, southern Azuero by *Hoernle et al.* [2002].

4.3 Major and Trace Elements

The sampled volcanic rocks range from tholeiites to alkali basalts in composition with MgO of 4.28-9.38 wt. %, SiO₂ of 47.13-51.55 wt. %, Al₂O₃ of 11.30 to 16.76 wt. % and CaO of 7.11 to 13.02 wt. % in samples normalized to 100 % on a volatile-free basis. H₂O content for most samples ranges between 1.0-2.7 wt. % (84 % of samples) and 1.0-5.23 wt. % (all samples); CO₂ ranges between 0.1-3.49 wt. %. On binary diagrams with MgO on the x-axis SiO₂, CaO, Ni and Cr form positive trends, whereas FeO_t, TiO₂, K₂O, P₂O₅ and most incompatible trace elements (e.g. Nb, Zr, Ba, Sr, Th, La) form crude negative trends [Fig. 4,5].

The large variability in Rb, Ba, K, Sr compared to more immobile elements, combined with evidence for alteration from thin sections, indicates that these elements have been effected by secondary processes and therefore are excluded from further discussion as well as in the incompatible element (spider) diagram. Fluid mobile elements Rb, Ba and K are probably secondary enriched due to seawater alteration [*Krolikowska-Ciaglo et al.*, 2005].

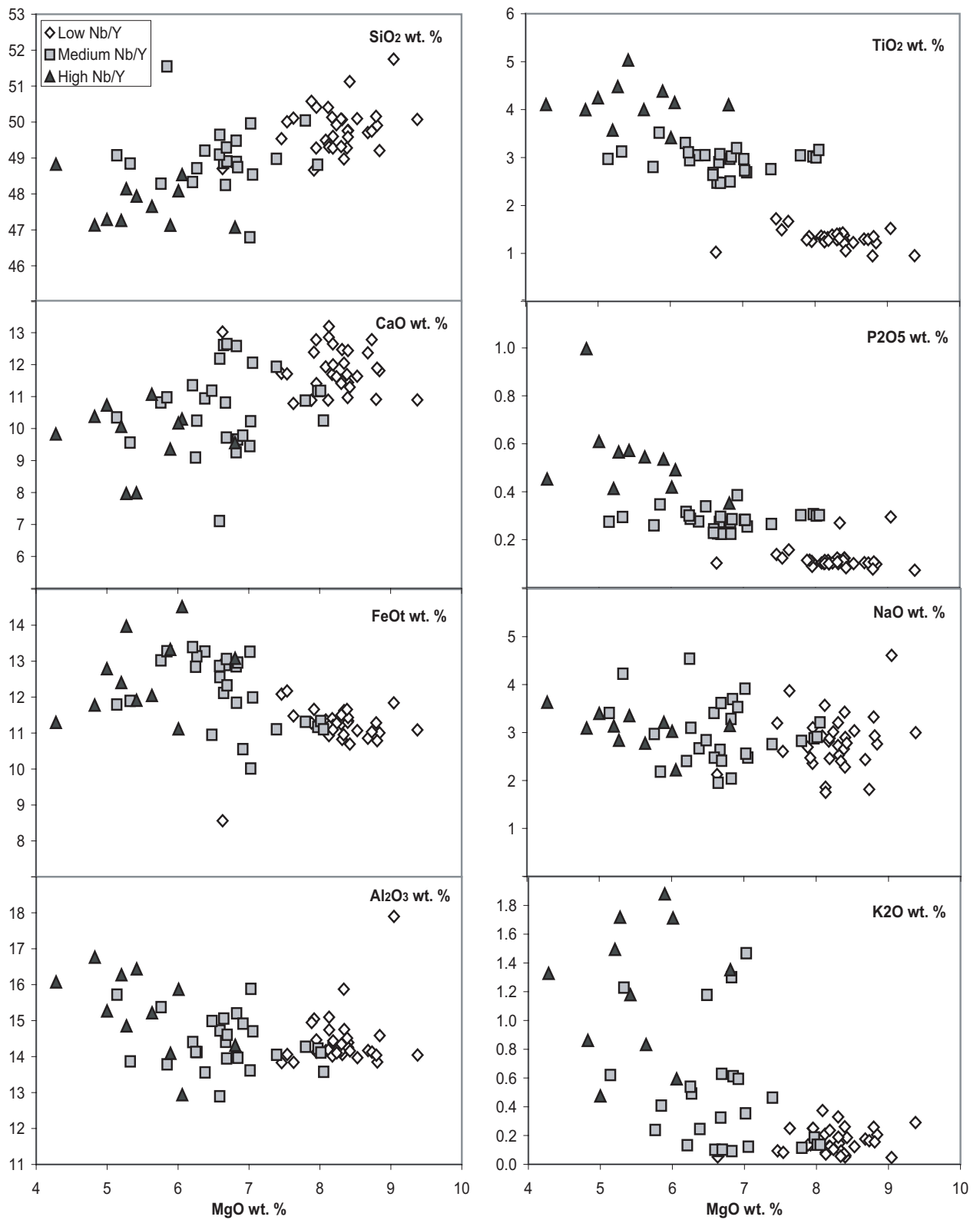


Fig. 4: MgO versus selected major and compatible trace elements, samples are grouped in high Nb/Y, medium Nb/Y and low Nb/Y.

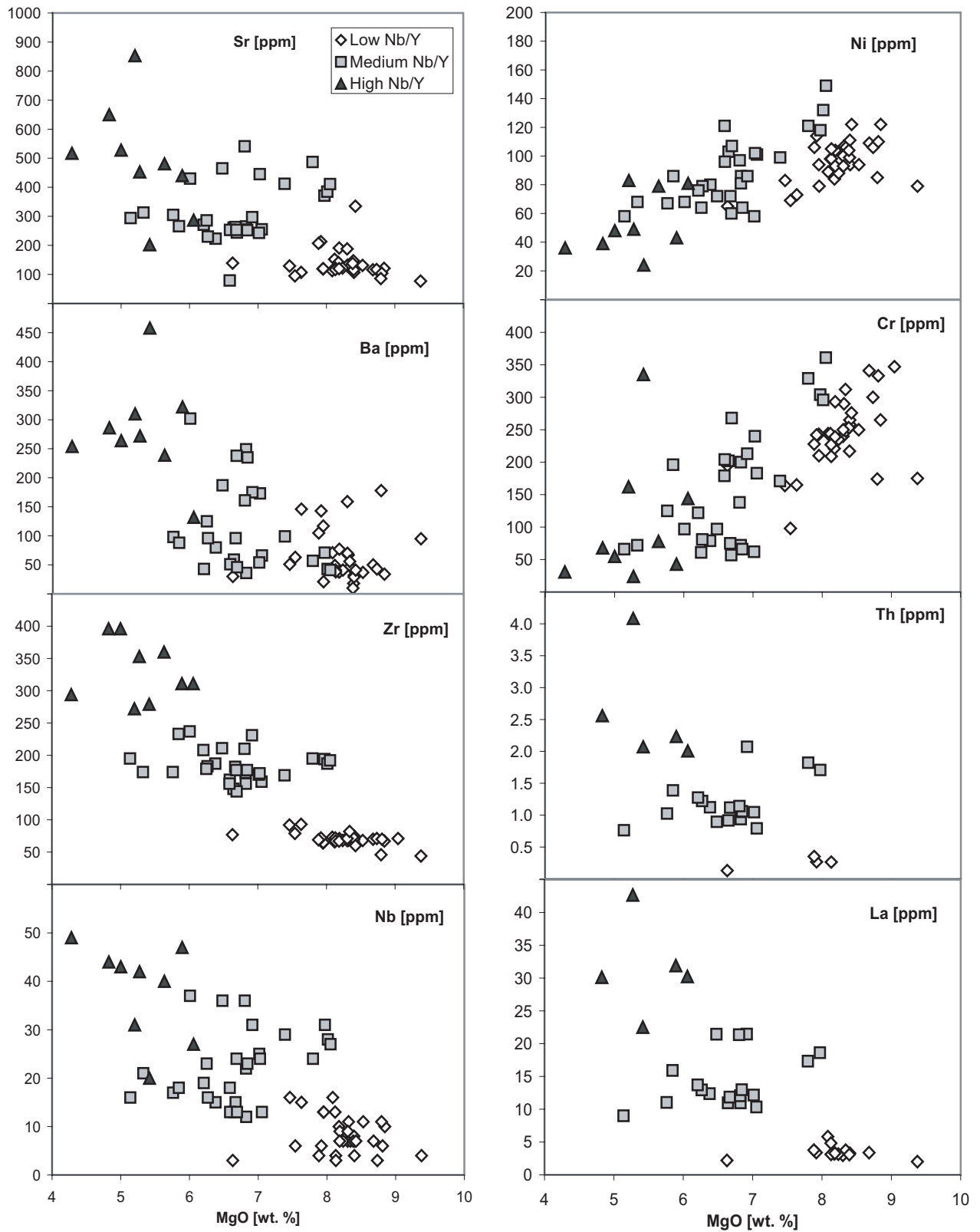


Fig. 5: MgO versus trace elements, samples are subdivided into high Nb/Y, medium Nb/Y and low Nb/Y.

On the incompatible-element diagram the samples show distinct patterns [Fig. 6A]. Based on relatively immobile trace element ratios samples has been divided into a high $(La/Sm)_N = 1.35-2.16$, a medium $(La/Sm)_N = 1.16-1.32$ and a low $(La/Sm)_N = 0.69-0.90$ group. The high $(La/Sm)_N$ group consists primarily of alkali basalts whereas the medium and low $(La/Sm)_N$ groups consists of tholeiitic rocks. The concentration of highly and moderately incompatible elements increases with increasing La/Sm, such that each La/Sm group forms a distinct field on the incompatible element diagram. Ratios of Nb/Zr, Nb/Y and La/Yb also correlate positively with La/Sm.

The high and medium $(La/Sm)_N$ group have convex-up patterns with a peak for Nb and Ta, trough for Pb, and a positive HREE slope on the incompatible element diagram. Such incompatible element patterns are distinct from subduction zone (or arc) basalts [e.g. *Elliott et al.*, 1997], which are characterized by relative Nb depletion (i.e. $(La/Nb)_N < 1$) and relative Pb enrichment (i.e. $(Ce/Pb)_N \ll 20$). The incompatible element characteristics of the studied rocks (with $(La/Nb)_N = 1.20 \pm 0.11$ and $(Ce/Pb)_N = 5.22 \pm 1.27$, $N=34$) are to the contrary characteristic of ocean island basalts (OIB) [Fig. 6B]. The middle Nb/Y group [Fig. 4,5] and the middle $(La/Sm)_N$ group are very similar showing affinities to tholeiitic OIB's whereas the high $(La/Sm)_N$ and Nb/Y group are similar to alkalic OIB's. High $(La/Sm)_N$ rocks have the highest concentrations of moderately to highly incompatible elements (e.g. Th, Nb, Ta and the LREE), yet have HREE patterns overlapping with the medium $(La/Sm)_N$ group, suggesting derivation of both groups of rocks from a similar source through different degrees of melting.

The low $(La/Sm)_N$ group is characterized through positive sloping incompatible element patterns [Fig. 6A]. Pb shows a pronounced trough and the REE patterns are flat and do not show an Eu-anomaly [Fig. 6A]. The low $(La/Sm)_N$ group is similar to the low Nb/Y group [Fig. 4,5] group. Patterns of the incompatible element diagram are with one exception (Az-59-4) more enriched in incompatible compositions than N-MORB of *Sun and McDonough*, [1989] but less enriched than the E-MORB patterns of *Sun and McDonough*, [1989]. Az-59-4 shows N-MORB composition for all incompatible elements, consistent with it being derived from oceanic crust.

4.4 Sr-Nd-Pb Isotope Ratios

The measured, initial and initial projected to the present (assuming source parent/daughter ratios) Sr-Nd-Pb isotope data are presented in Table 2 of the Appendix. Two samples (Az-26-1 and M108bKH) have extremely high $^{87}Rb/^{86}Sr$ ratios, placing their initial values in question, considering the mobility of both Rb and Sr in marine settings. Nd and Pb isotopic compositions are less susceptible to seawater alteration [e.g. *Hauff et al.*, 2000b]. Initial Nd-Pb isotope variations for distinct ages of the paleo-Galápagos hotspot tracks (17-38 Ma, 50-66 Ma, 71-95 Ma, 110-125 Ma), show that the source developed to more radiogenic Pb and Nd isotopic compositions with time [Fig. 7]. The younger samples (17-38 Ma) are the most radiogenic.

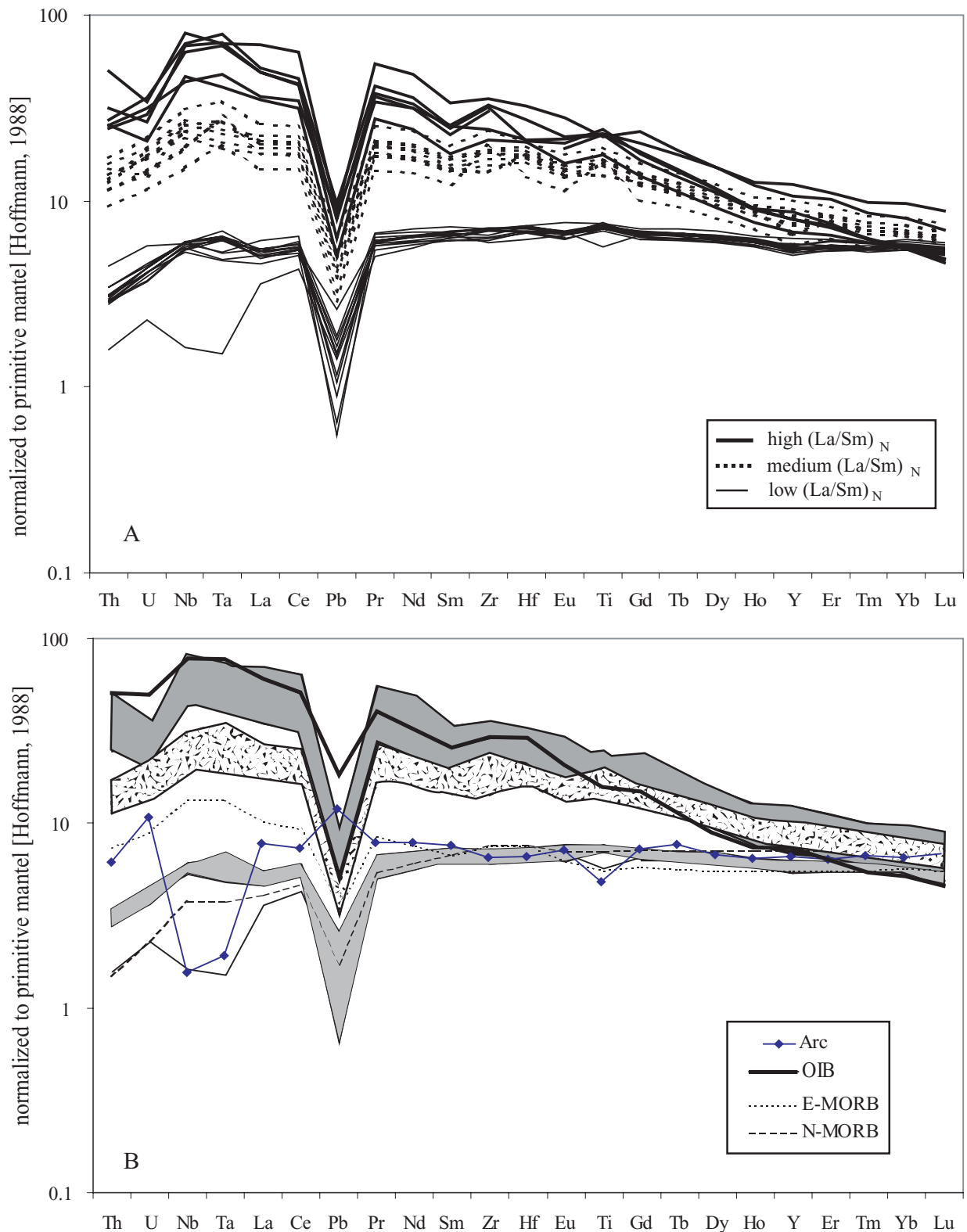


Fig. 6: Incompatible element diagrams A) Samples are divided based on relatively immobile trace element ratios into a high $(La/Sm)_N=1.35-2.16$, a medium $(La/Sm)_N=1.16-1.32$ and a low $(La/Sm)_N=0.69-0.90$ group; B) representative arc [Eliot et al., 1997], OIB, E-MORB and N-MORB [Sun and McDonough, 1989] patterns show that the investigated rocks are not subduction but hotspot related. Az-59-4 displays the most depleted trace element patterns and also isotope ratios [Fig. 7] is interpreted as N-MORB oceanic crust.

Overlap of the CLIP and paleo-tracks with the calculated Galápagos hotspot field is demonstrated [Fig. 7]. Older CLIP (110-125 Ma) and the younger paleo-hotspot track (17-33Ma) are distinct from the younger CLIP (71-95 Ma) and the old paleo-hotspot track (50-66 Ma), which overlap with one another.

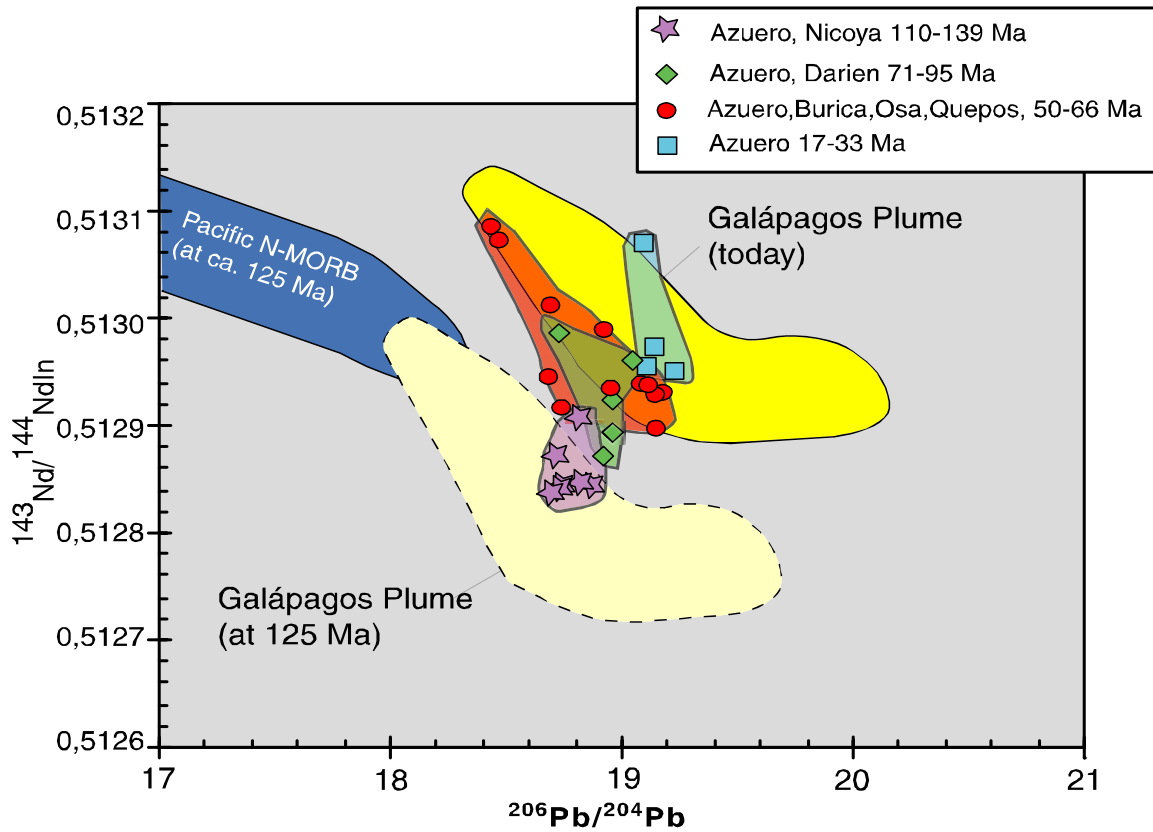


Fig. 7: Initial isotopes of CLIP and paleo-hotspot tracks found in Panama and Costa Rica compared to source variations of the Galápagos hotspot fields 120 Ma, 80 Ma 60 Ma ago composed of initial values of the $^{206}\text{Pb}/^{204}\text{Pb}$ and $^{143}\text{Nd}/^{144}\text{Nd}$ isotopes and the recent field. Dated samples from Nicoya, Quepos, Osa and Burica are shown for comparison [Hauff *et al.*, 2000a, Hoernle *et al.*, 2004]

When the initial isotopic compositions of the accreted terranes are projected to the present (see fig. 8 caption for assumed parent/daughter ratios for the source), all analyzed samples with one exception (Az-59-4 from SW Azuero) have higher Sr and Pb and lower Nd isotope compositions compared to E-MORB of the Galápagos Spreading Center 86.4°W-87.4°W longitudes. Sr-Nd-Pb isotope compositions of all analyzed rocks plot within the four geochemical domains defined by Sr-Nd-Pb isotopic composition of the present Galápagos hotspot referred to as Northern, Southern, Eastern and Central domains based on their relative geographic position [Hoernle *et al.*, 2000] [Fig. 8]. The majority of the analyzed rocks plot in the field of the Central and Eastern Galápagos domain [Fig. 8]. Sample M108b shows the highest Pb and Sr and low Nd isotope compositions that overlap with those of the southern

Galápagos domain. Az-104-1 from the southern coast of Azuero plots near the Southern domain field.

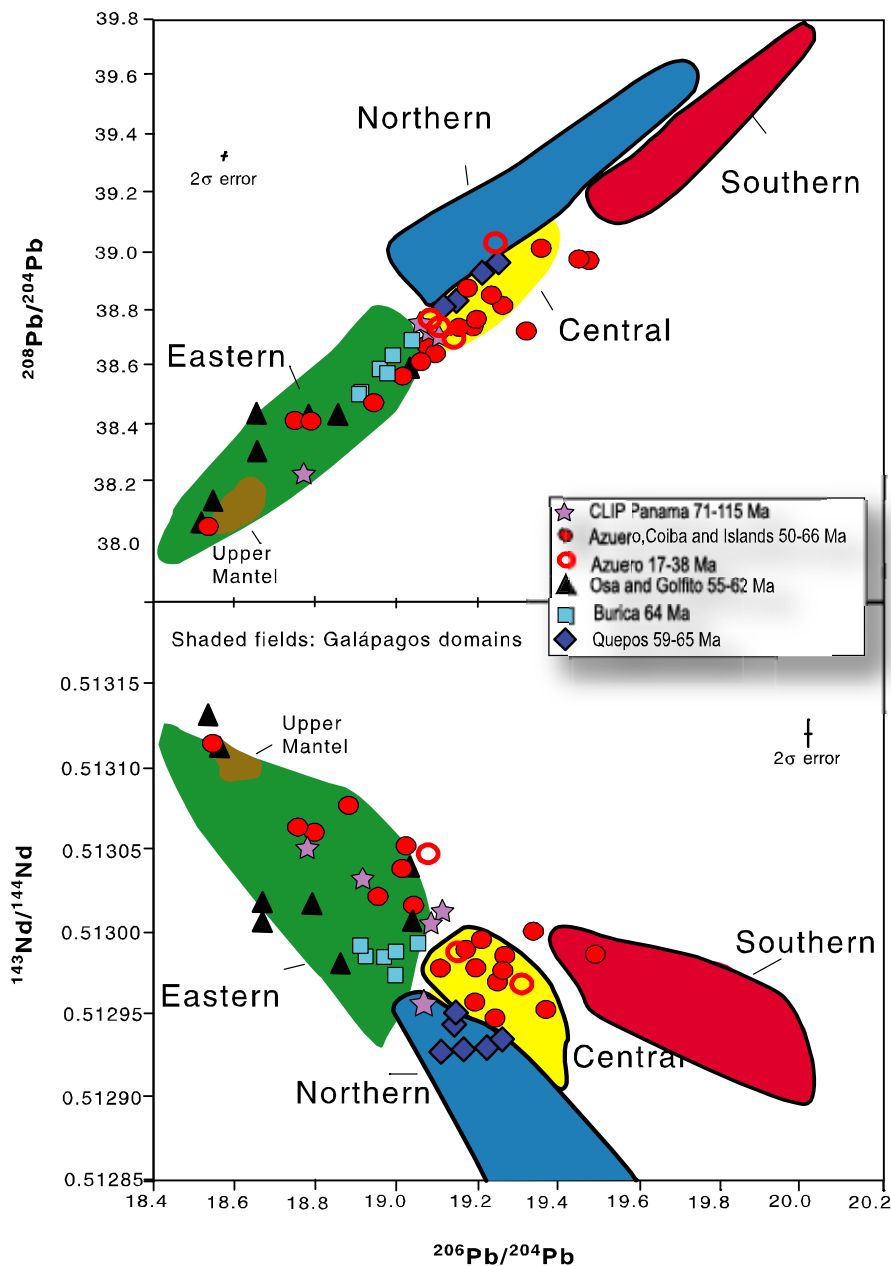


Fig. 8: $^{206}\text{Pb}/^{204}\text{Pb}$ versus $^{208}\text{Pb}/^{204}\text{Pb}$ and $^{206}\text{Pb}/^{204}\text{Pb}$ versus $^{143}\text{Nd}/^{144}\text{Nd}$ isotope correlations diagrams illustrate that analyzed samples from Panama and Costa Rica have isotopic composition similar to those of Central, Northern and Eastern Galapagos Domains (shaded fields according to *Hoernle et al.* [2000]; *Werner et al.* [2003]). Samples from Panama are from this study and *Hoernle et al.* [2002] and Costa Rican samples are from *Hauff et al.* [2000a]. Upper mantle values are from *Hauff* [unpublished data]. For all samples, initial values were calculated and then were projected to the present assuming the following parent/daughter ratios for the source $^{147}\text{Sm}/^{144}\text{Nd}=0.15$, $^{238}\text{U}/^{204}\text{Pb}=10$, $^{235}\text{U}/^{204}\text{Pb}=0.07$ and $^{232}\text{Th}/^{204}\text{Pb}=40$.

5 Discussion

5.1 Mafic igneous complexes outcropping along the Pacific coast of Panama and near Changuinola

The studied mafic igneous rocks do not show typical subduction-zone trace element characteristics, for example they do not have Nb and Ta troughs on multi-element diagrams and have a well-defined trough for Pb [Fig.6 A,B]. These geochemical characteristics are not consistent with derivation in a subduction zone but rather are consistent with derivation in an oceanic setting, either at a mid-ocean ridge or an intraplate or ocean island setting. Higher Th to Ce content of all samples compared to N-MORB and higher Sr and Pb and lower Nd isotope ratios in the analyzed rocks suggest a more enriched source than N-MORB (with the exception of sample Az-59-4). Trace element and Sr, Nd, Pb isotopic compositions of the samples plot within the range of lavas from the CLIP, the Galápagos Islands and hotspot tracks on the Cocos and Nazca Plates, and the Galápagos or Cocos-Nazca Spreading center, where plume-ridge interaction takes place [Fig. 7, 8, 9].

$^{40}\text{Ar}/^{39}\text{Ar}$ plateau ages of the igneous complexes studied in Panama range from 17-115 Ma. A large-scale episode of volcanism took place in the central Caribbean and Columbia between ~72-78 Ma [Kerr *et al.*, 1996; Sinton *et al.*, 1998]), which is believed to reflect a major episode of CLIP volcanism [Sinton *et al.*, 1998; Hoernle *et al.*, 2002, 2004]. The oldest rocks with arc affinities in Central America crop out in eastern Panama and on Azuero and reach an age of 66 Ma (K/Ar age), leading to the suggestion that subduction may have begun around 70 Ma on the western margin of the CLIP [Kesler *et al.*, 1977]. Campanian to Maastrichtian volcanic rocks near Piedra Blanca in the Changuinola region were interpreted to be the oldest arc rocks in Central America [Fisher and Pessagno, 1965]. Our geochemical data for samples from this area however do not confirm arc affinities but instead show that these rocks have compositions similar to CLIP, consistent with the volcanic succession associated with the thick sequence of Campanian to Maastrichtian limestones to be uplifted Caribbean basement. Samples that are >70 Ma from Azuero, Sona and Darien come from sheet flows, pillow lavas and dikes/sills that are generally associated with radiolarian cherts, indicating deposition/intrusion in a deep marine environment. Therefore we interpret all samples >70 Ma to be derived from uplifted portions of CLIP basement.

Mafic igneous complexes with ages of 17-66 Ma occur in fault blocks several meters to several kilometers across. In southwestern Azuero, mafic igneous complexes younger than 70 Ma in age primarily outcrop south of the Azuero-Sona Fault Zone (ASFZ). We interpret this area to reflect an accretionary complex. These younger samples are geochemically similar to rocks from the Galápagos Islands and hotspot tracks and from the Galápagos Spreading Center, where it has interacted with the Galápagos Hotspot. Similar rocks in Costa Rica (Quepos, Osa, Golfito and Burica) and western Panama (Azuero and Coiba Island) have

previously been interpreted as accreted portions of the paleo-Galápagos hotspot tracks [Hauff *et al.*, 1997, 2000a; Hoernle *et al.*, 2002; Hoernle and Hauff, in press].

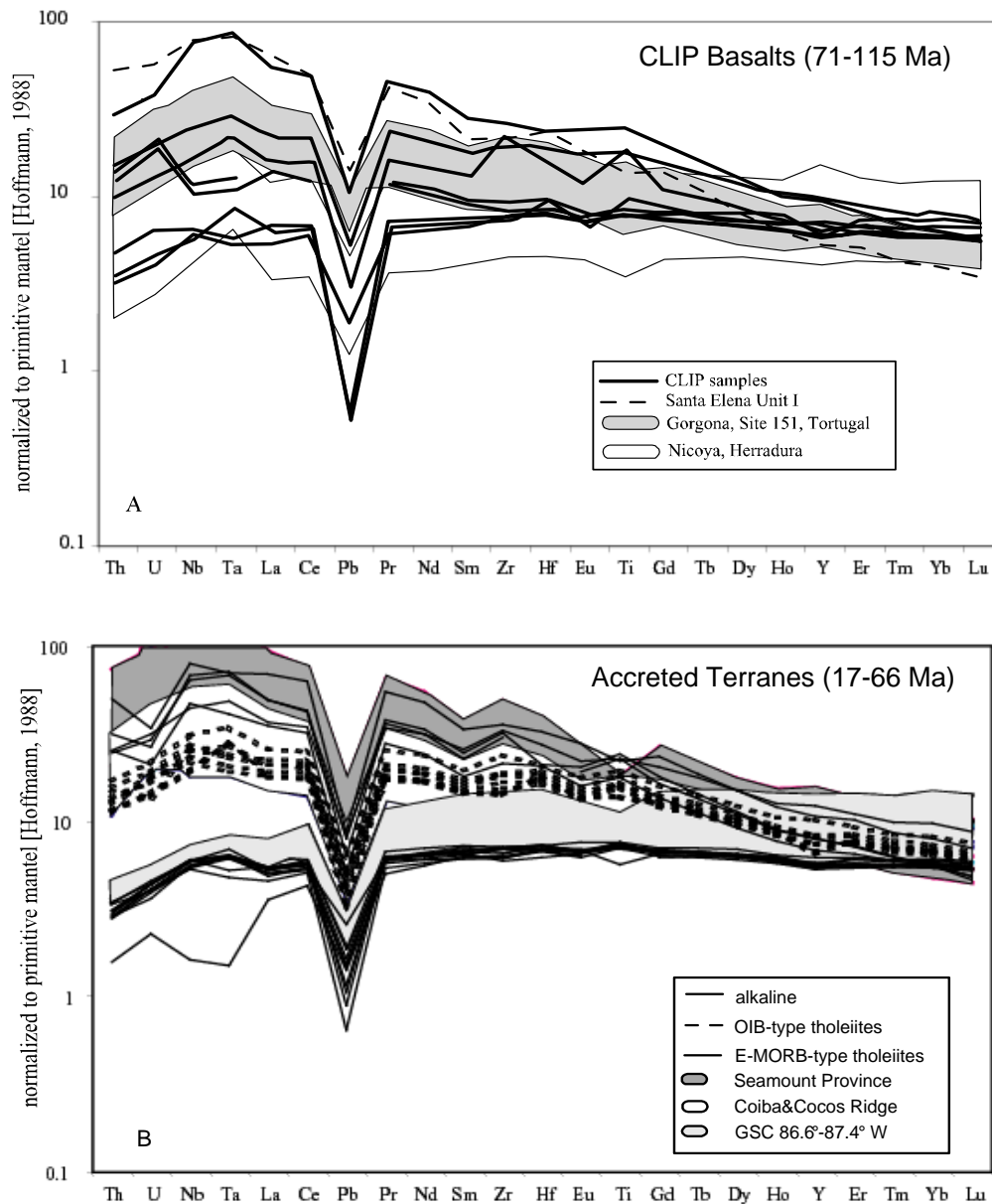


Fig. 9 A: Samples > 70 Ma have incompatible trace element characteristics similar to CLIP rocks. Santa Elena Unit 1, Nicoya, Herradura and Tortugal (Costa Rica) fields are from Hauff *et al.* [2000a] and Hoernle *et al.* [2004], Caribbean DSPD Site 151 from Hauff *et al.* [2000b] and Gorgona Island field from Kerr *et al.* [1996].

B: Accreted mafic igneous terranes < 70 Ma old have incompatible element characteristics similar to the Galápagos Islands and hotspot tracks: 1) Galápagos Spreading Center lavas between 86.6° and 87.4°W that have been affected by the Galapagos Hotspot, 2) Cocos and Coiba Ridges, 3) Seamount Province of the Galapagos hotspot track NW of the Cocos Ridge [Hauff *et al.*, 2000 a; Hoernle *et al.*, 2000, 2002; Christie *et al.*, 2005; Harpp *et al.*, 2005]

In conclusion, we interpret the 17-66 Ma mafic igneous complexes with geochemical affinities to the Galápagos Hotspot to be accreted portions of paleo-Galápagos hotspot tracks (ocean island and seamount volcanoes and aseismic ridges similar to the Cocos and Carnegie Ridges) and in rare cases fragments of ocean crust.

5.2 Detailed discussion of the origin of the individual Panamanian igneous complexes

5.2.1 CLIP (>70 Ma)

The Caribbean large igneous province formed in the Pacific above the Galápagos hotspot [Hoernle *et al.*, 2004], exceptionally showing large tectonically uplifted areas, which are subaerial exposed. The province is built up of thickened oceanic crust (up to 20 km) belonging to the flood-basalt sequences along the margin of South America and to the Caribbean Plate. Uplifted or accreted Caribbean plateau lavas have been described for Costa Rica, Colombia, Ecuador, Curaçao and were drilled in the Central Caribbean DSPD sites 150-153 [Hauff *et al.* 1997, 2000a, 2000b; Sinton *et al.*, 1997,1998; Kerr *et al.*, 1997, 2002,; Révillon *et al.*, 2000; Lapierre *et al.* 2000; Hoernle *et al.*, 2002, 2004;]. The range of published $^{40}\text{Ar}/^{39}\text{Ar}$ ages from throughout the province extends from 69 to 139 Ma [Fig.10, Hoernle *et al.*, 2004]. First pulses of flood basalt volcanism may have occurred from ~ 133 to 139 Ma and from ~ 118 to 111 Ma [Hoernle *et al.*, 2004]. The main pulse of flood basalt magmatism range from about 95 to 83 Ma, followed by a second pulse ranging from 81 to 69 Ma [Hauff *et al.* 1997, 2000a, 2000b; Sinton *et al.*, 1997, 1998; Kerr *et al.*, 1997, 2002,; Révillon *et al.*, 2000; Lapierre *et al.* 2000; Hoernle *et al.*, 2002, 2004;]. The majority of Caribbean flood basalts displays E-MORB multi element patterns (i.e Nicoya and Herradura (Costa Rica), Colombia, Curaçao) [i.e. Hauff *et al.*, 2000a,b]. Extremely depleted geochemical compositions shows the komatiites from Gorgona Island (Colombia) whereas alkalic HIMU-OIB-type compositions are shown by lavas from Santa Elena, Tortugal (Costa Rica), Gorgona Island and DSPD site 151 (Caribbean Plate) [Kerr *et al.*, 1996; Hauff *et al.*, 2000a,b; Hoernle *et al.*, 2004]. Hoernle and Hauff [in press] are the first to point out that the rocks from Santa Elena, Tortugal (Costa Rica), Gorgona Island and DSPD site 151 (Caribbean Plate) show similar enriched geochemical signatures. These enriched signatures may be attributed to an enriched component in the CLIP similar to the northern Galápagos component [Alvarado *et al.*, 1997; Kerr *et al.*, 2004; Hoernle and Hauff, in press].

$\text{Ar}^{40}/\text{Ar}^{39}$ stepheat plateau ages of the Panamanian igneous complexes ranging from 71 to 115 Ma are situated on Soná and Azuero Peninsula near to the ASFZ and in Darien along the Pacific coast (Eastern Panama). A 114.5 ± 2.0 Ma old tholeiite were sampled in southeastern Azuero (Playa Venado) with E-MORB signature [Tab. 3]. On Azuero north of the ASFZ massive basalts yielded an age of 93.5 Ma. Ages from Soná and western Azuero at the Rio Torio section range from 82.6 Ma to post Coniacian (89-85 Ma) [Kolarsky *et al.*, 1995]. Tholeiitic pillow basalts found at Bahia Piña yielded an $^{40}\text{Ar}/^{39}\text{Ar}$ ages of 84.1 ± 1.0

Ma and 71.3 ± 2.2 Ma [Tab. 3], consistent with the Coniacian to Campanian (89–71 Ma) age determined from associated sedimentary units for eastern Panama [Case, 1974]. Ages of these Panamanian igneous complexes are comparable to complexes found in Costa Rica, Colombia, Curaçao, Haiti and DSPD-Leg 15 [Hauff *et al.*, 2000a; Hoernle *et al.*, 2002, 2004; Kerr *et al.*, 1997, 2002; Sinton *et al.*, 1997, 1998] [Fig. 10]. These rocks are coeval with the main pulse of flood basalt volcanism of the Galápagos hotspot extending from 83-95 Ma and to the latest pulse of flood basalt volcanism extending from 81-69 Ma [Hauff *et al.*, 2000a; Hoernle *et al.*, 2002, 2004; Kerr *et al.*, 1997; Sinton *et al.*, 1997, 1998]. Accordingly paleontological dating of radiolaria and foraminifera of the sedimentary rocks associated with the pillow basalts around the Gulf of San Miguel (Eastern Panama) infer a Late Cretaceous probably Early Campanian age (~ 80 Ma) [Bandy and Casey, 1973].

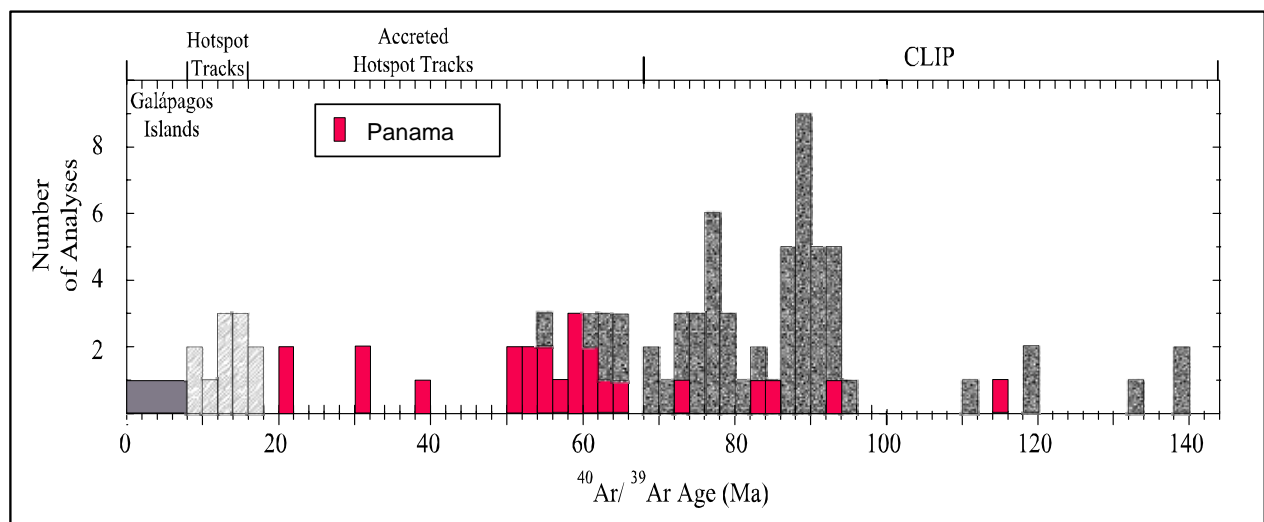


Fig. 10: Histogram of published and new $\text{Ar}^{40}/\text{Ar}^{39}$ age data from Galápagos islands, hotspot tracks, accreted paleo-hotspot tracks and the Caribbean large igneous province (CLIP) [Christie *et al.*, 1992; Kerr *et al.*, 1997, 2002; Sinton *et al.*, 1997, 1998; Werner *et al.*, 1999; Révillon *et al.*, 2000; Hauff *et al.*, 2000a,b; Hoernle *et al.*, 2002, 2004].

The CLIP samples from Panama range from tholeiites to alkali basalts. They cover the whole range in incompatible element compositions that have been observed previously throughout the CLIP, ranging from low to high $(\text{La}/\text{Sm})_{\text{N}}$ rocks (0.77 - 2.04 N=7). The oldest rocks situated on Azuero (115 Ma) and the youngest CLIP from Darien (71 Ma) are the most depleted in incompatible elements. Their incompatible element abundances are similar to Nicoya and Herradura lavas [Fig. 9A]. The 83-84 Ma old rocks from Sona and Darien have intermediate $(\text{La}/\text{Sm})_{\text{N}}$, $(\text{Gd}/\text{Yb})_{\text{N}}$ and highly and moderately incompatible element abundances. Their composition is similar to the enriched alkali basalts from Gorgona Island, LREE-enriched DSPD Site 151 samples and alkali basalts from Tortugal (Costa Rica) igneous rocks [Fig.5B & 8A] The second oldest CLIP sample from Azuero (94 Ma) is the most

alkaline and most enriched in highly incompatible elements (e.g. LREE) and has a similar composition to alkali basalts from Santa Elena Unit I (northwestern Costa Rica). Santa Elena Unit I and Tortugal samples have Sr, Nd, Pb isotopes similar to the alkali basalt from Azuero overlapping with the northern Galápagos domain [Hoernle and Hauff, in press]. The trace element and isotopic composition of this Azuero sample provides additional evidence that this enriched composition is a part of the CLIP [Hoernle and Hauff, in press].

Geochronological and geochemical data from pillows and sheet flows from Nicoya and Herradura were interpreted to represent fragments of several plateaus formed by a pulsing Galápagos hotspot [Hoernle et al., 2004]. Accordingly we infer that the mafic Cretaceous rocks with oceanic geochemical affinities from Azuero, Soná and Darien were part of an oceanic plateau which may have formed from the Galápagos hotspot. Accretionary processes related to Late Cretaceous and Cenozoic subduction could have caused the uplift of this former oceanic plateau [Case, 1974; Hauff et al., 2000a]. The 115 Ma old tholeiite from Playa Venado may represent the basement (oceanic crust) on which the 84–94 Ma plateau formed. The N-MORB to E-MORB type composition could reflect interaction of the Galápagos plume with the spreading center at which this crust was formed. Contemporaneous lavas 111–118 Ma from Nicoya give evidence that the Galápagos hotspot was active at this time. The 93.5–84 Ma unit from Azuero and Darien were presumably formed during the main plateau phase. Whereas the later 83–71 Ma volcanism could have formed when the western edge of the 89 ± 6 Ma plateau passed over the plume tail. Along the Colombian and Panamanian border samples with large quantities of Campanian radiolarians and Maastrichtian foraminifera were observed and emphasize the correlation between the Darien basement (Serranía del Sapo) with the Colombian Serranía de Baudó. The Serranía de Baudó represents a north-south trending oceanic terrane of western Colombia. Volcanic rocks of the Serranía de Baudó were dated by $^{40}\text{Ar}/^{39}\text{Ar}$ laser dating at a range from 72–78 Ma [Kerr et al., 2002; Kerr et al., 1996]. The eastern Panamanian CLIP lavas are assumed to form the prolongation of the Colombian Serranía de Baudó to the north representing an accreted Galápagos terrane. Positive gravity anomalies are continuous over the Serranía del Sapo (Darien) to the Western Colombian Cordilleras confirming a unique Panama-NW Colombian terrane [Case, 1974; Kellog et al., 1995].

5.2.2 Accreted paleo-hotspot tracks

Most studied mafic accreted igneous complexes occur on the southern end of the Azuero Peninsula. South of the ASFZ, no subduction related magmatic rocks were found [Fig. 3A], only basalts with ocean island basalt type trace element signatures [Fig. 6B, 9B]. The complex history of this area is mirrored at Playa Horcones near Punta Blanca. The oldest magmatic unit [66.0 (± 0.7) Ma, $^{40}\text{Ar}/^{39}\text{Ar}$ age] is an accreted aphyric, tholeiitic basalt with ocean-island basalt type trace element geochemistry [Hoernle et al., 2002]. This basalt is unconformably overlain by reefal limestone of the Middle Eocene (49–41) unit of the Tonosí

Formation [Kolarsky *et al.*, 1995]. The limestone has been deposited after the basalt was accreted to the Pacific margin of Panama thus providing a minimum age for its accretion. A similar fossiliferous limestone has been observed as a fault sliver at Playa Restingue [Kolarsky *et al.*, 1995]. A tholeiitic basaltic pebble at Playa Horcones also yielded an Early Paleocene age of 61.7 ± 0.6 Ma [Hoernle *et al.*, 2002]. Above the beach, an aphyric fine-grained massive flow of tholeiitic composition was dated at 51.9 ± 0.8 Ma [Hoernle *et al.*, 2002]. At the western part of the beach at Punta Blanca, fault slivers of alkaline pillow basalt and heavily oxidized, reddish, aphyric agglutinates are exposed representing submarine and subaerial eruptive conditions respectively. The pillow basalts yielded ages of 15.6 ± 0.3 [Tab. 3] and 32.8 ± 0.4 Ma [Hoernle *et al.*, 2002]. Tholeiitic pillows were found to the east at Punta Bucaró producing a stepheat matrix $^{40}\text{Ar}/^{39}\text{Ar}$ plateau age of 32.1 ± 2.6 Ma [Tab. 3].

The complex history south of the ASFZ is also revealed at Playa Restingue. Pillow basalts erupted under submarine conditions at Playa Restingue with ocean island basalt-type geochemical compositions yielded a stepheat matrix $^{40}\text{Ar}/^{39}\text{Ar}$ plateau age of 56.0 ± 1.7 Ma [Hoernle *et al.*, 2002]. A tholeiitic lava flow with basal/top breccia yielded a $^{40}\text{Ar}/^{39}\text{Ar}$ plateau age of 49.7 ± 0.4 Ma [Tab. 3]. The oxidized reddish color and high vesicularity of agglutinates and lavas, as well as basal and/or top breccias of the lava flows provide evidence for subaerial volcanism. The dated rocks may represent the submarine (pillow basalts) and subaerial (agglutinates and lava flows) parts of an ocean island volcano. A reefal limestone above the beach belonging probably to the Tonosi Formation contains the Eocene foraminifera *Lepidocyclina*. The lithostratigraphic section implies a seamount stage for the Restingue volcano from 56.0 to maximum of 50 Ma, followed by a phase of subaerial volcanism (~50 Ma). A very heterolithologic slope breccia at Playa Restingue containing tholeiitic and alkaline basaltic magmatic rocks, some of which are fragments of oxidized, reddish, agglutinates, but also contains carbonates and argillaceous sediments represents the erosional deposits of the ocean island volcano. The overlying transgressional reefal limestone is part of the Middle Eocene Tonosi Formation (49-41 Ma) [Kolarsky *et al.*, 1995] also providing a minimum accretionary age for this ocean island volcanic complex. The radiometric ages indicate that the volcano was active for at least 6.5 Ma. Later accreted subaerial sequences crop out at the eastern end of Playa Restingue. An alkaline lava flow with a basal breccia yielded an $^{40}\text{Ar}/^{39}\text{Ar}$ plagioclase stepheat age of 20.8 ± 1.8 Ma [Hoernle *et al.*, 2002].

East of Playa Restingue on the southern coast of Azuero, columnar-jointed, alkaline basaltic lava flows with basal breccias occur at Punta Piro and Portobello indicating subaerial eruptions. Pillow basalts and hyaloclastites found in Portobello also point to submarine eruptive conditions. Igneous rocks of the Portobello complex yielded $^{40}\text{Ar}/^{39}\text{Ar}$ ages of 59.9 ± 2.3 Ma [Tab. 3] and 60.7 ± 1.1 Ma [Hoernle *et al.*, 2002], within error of each other. We interpret the Portobello outcrop as an accreted part of an ocean island volcano similar but older than the Restingue ocean island complex.

At western central Azuero, alkaline basalts at Rio Quebro were dated radiometrically yielding an $^{40}\text{Ar}/^{39}\text{Ar}$ age of 63.2 ± 0.6 Ma [Hoernle *et al.*, 2002]. Vesicular tholeiitic pillow basalts with hyaloclastites and an aphyric lava flow outcrop near Loma del Los Monos. The contact between these units is not exposed. The lava flow yielded a $^{40}\text{Ar}/^{39}\text{Ar}$ age of 52.6 ± 0.6 Ma [Hoernle *et al.*, 2002]. River pebbles of the Rio Pavo and Rio Playita near to the village of Flores range from tholeiitic to alkaline, reflecting the compositional range of the mountain chain predominating in southwestern Azuero. An $^{40}\text{Ar}/^{39}\text{Ar}$ age of 58.1 ± 0.3 Ma was determined on a tholeiitic basalt [Hoernle *et al.*, 2002]. In southeastern Azuero aphyric tholeiitic pillow lavas crop out along the coast. These pillow basalts with E-MORB-type trace element signatures were sampled at the bay of Circuelo and to the west near the village of Venado. The Circuelo sample yielded an $^{40}\text{Ar}/^{39}\text{Ar}$ matrix stepheat laser age of 54.4 ± 1.5 Ma [Hoernle *et al.*, 2002]. The southern coast of Soná is composed of tholeiitic pillow basalts displaying an E-MORB-type geochemical signature. The area is interpreted as an accreted part of an aseismic ridge similar to the Cocos or Carnegie Ridges.

The northeastern coast of Coiba Island consists of tholeiitic pillow basalts. A tholeiite from Punta Baltizar yielded a total fusion $^{40}\text{Ar}/^{39}\text{Ar}$ age of $38.2 (\pm 2.4)$ Ma [Hoernle *et al.*, 2002]. At Playa Hermosa on central eastern Coiba Island, basalts, lava flows with top and bottom breccias and agglutinates point to deposition under subaerial conditions. Heavily tectonized pillow lavas associated with cherts were found at Punta Hermosa, representing the tectonic contact of the hotspot-related and subduction-related rocks forming the eastern and southern part of the island. The subduction related rocks are of Paleocene age [Lissinna *et al.*, in prep.] and are overlain by Middle Eocene limestone of the Tonosí Formation [Kolarsky *et al.*, 1995]. The southern coast of Cébaco Island between the Soná and Azuero Peninsulas consists of tectonized aphyric, vesicular, E-MORB-type tholeiitic pillow basalts which were sampled at Punta Guaraja and at the Punta Rancho di Paja. Islands in the Gulf of Chiriquí Ladrones, Secas, Icaco and Bolaños also show ocean island geochemical affinities. The Ladrones and Secas Island are characterized by aphyric, E-MORB-type tholeiitic pillow basalts and columnar jointed trachybasalt. Massive columnar-jointed basaltic lava flows and pillow basalts on Icaco and Bolaños Islands have OIB-type tholeiitic compositions. Picrites outcrop on the Bolaños Islands.

Summary

Accretionary complexes containing portions of the paleo-Galápagos hotspot track occur on the western Panamanian Islands Ladrones, Secas, Icaco, Bolaños, Coiba, Santa Catalina and Cébaco Islands and on southern Soná and Azuero Peninsulas. OIB-type tholeiites occur on the Islands of Bolaños and Icaco and in southern Azuero, E-MORB-type tholeiites outcrop on Coiba, Secas, Ladrones and Cébaco Islands and the southern coast of Soná and Azuero. OIB-type alkaline basalts have only been found on SW Azuero, south of

the ASFZ thus far. Whereas the E-MORB and tholeiitic OIB-type basalts generally occur as pillow lavas and sheet flows, indicating submarine deposition, the OIB-type alkaline basalts show evidence for shallow water or subaerial deposition, suggesting late stage volcanism on ocean island volcanoes. The volcanological observations from Playa Restingue provide clear evidence for emergence of a submarine volcanic edifice above sea level and the formation of an ocean island which probably subsequently drowned, as is reflected by the presence of reefal clasts in the slope breccia. The accreted Restingue terrane is comparable to the Quepos terrane in Costa Rica described by *Hauff et al.* [1997, 2000a]. The E-MORB and OIB-type tholeiites, most likely represent accreted aseismic ridges and seamount (or shield) stage volcanism of hotspot volcanoes. We conclude on the basis of field, geochemical and geochronological observations that the igneous rocks along the Pacific coast of Panama represent accreted pieces of paleo-Galápagos hotspot tracks.

Our study also shows that subaerial volcanism can be extended beyond 17 Ma [*Werner et al.*, 2003] extending the period of time for speciation of the unique Galápagos flora and fauna. Accordingly to *Christie et al.*, [1992] and *Werner et al.*, [2003] continuous subaerial volcanism of the Galápagos archipelago may have existed for the last 66 Ma taking ages of accreted Restingue, Portobello and Quepos ocean islands into account.

5.3 Zonation and temporal evolution of the paleo Galápagos hotspot track

The Galápagos hotspot displays a horseshoe-shaped geochemical zonation of enriched plume material in its outer and depleted in its inner part [Fig. 11, *White and Hofmann*, 1978]. All four isotopically defined mantle components of the Galápagos hotspot currently observed at Galápagos [*Hoernle et al.*, 2000] existed for the last 85 Ma (Northern, Central, Eastern and Southern Domain) [*Geldmacher et al.*, 2003]. CLIP lavas from Costa Rica, Curaçao, Western Colombia and central Caribbean DSPD sites show that the Central Galápagos (Fernandina-like) component was the dominant component of the early plume head stage [*Geldmacher et al.*, 2003].

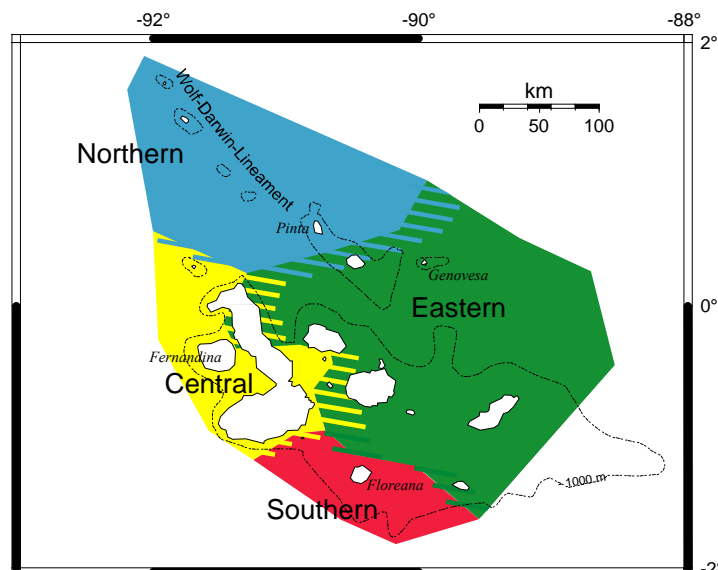


Fig. 11: The Galápagos archipelago with the four isotopically and geographically defined domains [modified from *Hoernle et al.*, 2000, *Harpp and White*, 2001, *Geldmacher et al.*, 2003].

Hoernle et al., [2000] and *Werner et al.*, [2003] described the unique zonation observed at the Galápagos archipelago and which could be extended to ~20 Ma. Miocene to Late Eocene accreted hotspot tracks (17–38 Ma) were used to assess whether the zonation can be extended to the Late Eocene.

Younger accreted igneous rocks (17-38 Ma) of southern Azuero consists of OIB-type and E-MORB-type tholeiites displaying Eastern and Central Galápagos domain isotope ratios consistent with the zonation of the central part of an Galápagos hotspot track [Fig. 12 A]. The northern and southern part/domains of the hotspot track could not be found. Thus we tried to assess whether the zonation observed at the Galápagos Islands and hotspot tracks [*Hoernle et al.*, 2000; *Geldmacher et al.*, 2003; *Werner et al.*, 2003] can be observed in the Paleocene accreted igneous complexes.

Accreted Galápagos terranes ranging in age from 50-65 Ma have been identified extending from Quepos (Costa Rica) to Osa, Golfito, Burica, Islands in the Gulf of Chiriquí to Azuero Peninsula going from NW to SE along the Pacific coast of central America. Starting in the NW at Quepos (59–65 Ma), the $^{206}\text{Pb}/^{204}\text{Pb}$ versus $^{143}\text{Nd}/^{144}\text{Nd}$ data plot within the northern Galápagos domain compositional field and the $^{206}\text{Pb}/^{204}\text{Pb}$ versus $^{208}\text{Pb}/^{204}\text{Pb}$ data lie on the border between the Central and Northern Galápagos domain compositional fields [Fig. 8]. The Nd-Hf system is known as highly resistant to alteration. Nd-Hf isotope ratios for the Quepos lavas (59-65 Ma) are similar to central and northern Galápagos domain [*Geldmacher et al.*, 2003]. Osa and Golfito (55–62 Ma) and Burica (64 Ma) lavas have Pb, Nd, Sr isotope ratios comparable to Eastern Galápagos domain composition. Sr-Nd-Pb isotope ratio of the western Panamanian Secas, Icaço, Ladrones, Bolaños and Coiba Islands (38 Ma) are consistent with Eastern Galápagos domain composition. Whereas lavas from Azuero are consistent with Southern and Central domain compositions [Fig. 8, 12]. Restingue is inferred to represent a seamount/ocean island complex providing a minimum age-range from 56.0-49.7 Ma. Accreted lavas represent endmember composition. Az-59-4 (56 Ma) is the most unradiogenic rock found in Panama consistent with the most depleted end of the eastern Galápagos domain or with oceanic crust/Upper Mantle composition [Fig. 8]. On the other hand M108b (49.7 Ma) is consistent with southern Galápagos domain composition representing the most enriched Pb and low Nd isotope ratios [Fig. 8]. We deduce that the oceanic crust basement was together accreted with the upper ocean island complex. Oceanic crust is very rarely found accreted along the coast of southern Central America. An exception forms a gabbro depleted in isotopic composition similar to Eastern Galápagos domain composition, which was found at the Quepos igneous complex, representing probably a part of the oceanic basement of the ocean island. One further sample from southwestern Azuero plot on the southern domain field (M104-1, 60.7 Ma). All other subaerial and submarine accreted complexes of southwestern Azuero (52-66 Ma) fall in the range of Central Galápagos domain composition. Only one sample at the eastern edge of Azuero (Az-39-1; 54.4 Ma) is consistent with the Eastern Galápagos domain. In conclusion, in the 58 ± 8 Ma time slice of

accreted terranes along the Pacific coast of Costa Rica and Panama, a similar geochemical zonation as is present in the Galápagos islands and the Cocos hotspot track going from NW to SE, i.e. going from Northern to Eastern, to Central and to Southern Galápagos domain composition is observed. The Eastern domain which is formed downstream or in the direction of plate motion (i.e. to the northeast) can overlie the three enriched domains formed at the leading edge of the plume, explaining the presence of eastern domain compositions along the entire belt of accreted terranes.

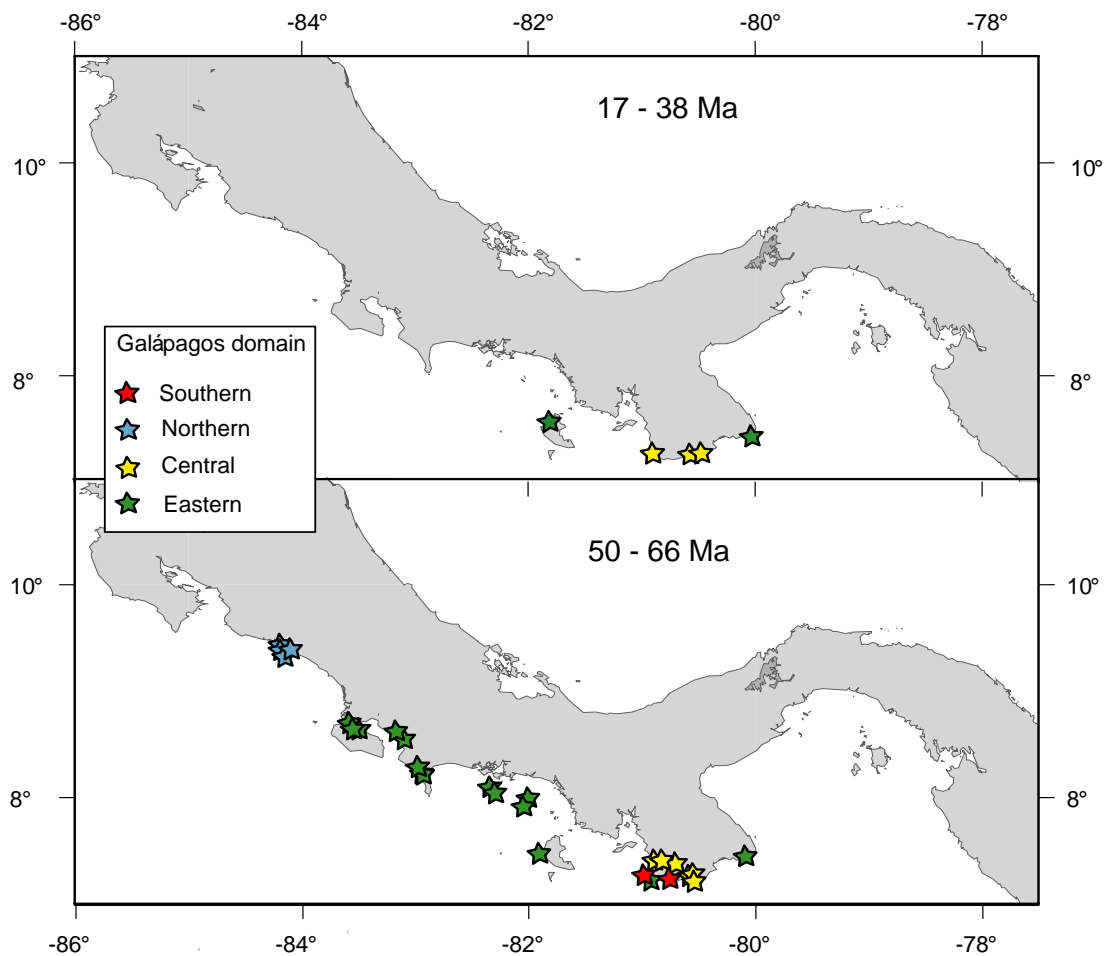


Fig. 12: Overview map illustrating the affiliation of the accreted Galapagos hotspot track igneous complexes to the Galapagos domains and their distribution along the Costa Rican and Panamanian Pacific coast; A) Young Panamanian accreted complexes are consistent with Central and Eastern Galapagos domain; B) 50-66 Ma Galapagos miniplateau accreted from Quepos to southeastern Azuero yielding Northern, Eastern, Central and Southern Galapagos isotope domains.

The isotope ratios of the CLIP volcanic rocks found in Panama overlap for the most part within the compositional fields of the Eastern Galapagos domain [Fig. 8]. CLIP rocks from Soná and Darien 71 to 84 Ma and the oldest CLIP (114.5 Ma) from Azuero fall within the Eastern Galapagos domain compositional field. Northern domain composition is only

displayed for the 93.5 Ma old CLIP from Azuero. Curaçao and Colombian CLIP lavas show southern domain-like signatures in their Hf and Nd isotopic compositions [Geldmacher *et al.*, 2003].

5.4 Tectonic Model

It has been proposed that the Caribbean plateau formed through accumulation of several oceanic plateaus and other volcanic structures which range in age from 139 to 69 Ma [Hoernle *et al.*, 2004]. These plateaus drifted westward with the Farallon Plate from the Galápagos hotspot to the present day Antilles Arc [Hoernle *et al.*, 2002]. The 94 and 115 Ma old CLIP lavas found in southern Azuero are inferred to be formed as part of this early oceanic plateaus. It has been shown that Early Cretaceous (111-139 Ma) igneous rock found in Nicoya have chemical compositions consistent with their origin from the Galápagos hotspot [Sinton *et al.*, 1997; Hauff *et al.*, 1997, 2000a, Hoernle *et al.*, 2004]. They may reflect accreted parts of several oceanic plateaus [Hoernle *et al.*, 2004], comparable to the accreted terranes forming the Central, Western and Pacific Cordillera in Ecuador and Columbia [Kerr *et al.*, 1997]. These South American accreted complexes range in age from 72.5 to 123 Ma [Kerr *et al.*, 1997, 2002, Lapierre *et al.*, 2000]. Nicoya and Colombian CLIP lavas are inferred to represent accreted complexes on the northern and southern edges of the gateway between the Americas to the proto-Caribbean [Hoernle *et al.*, 2004]. As western Panama is situated in the middle of this gateway, it is difficult to envisage how 115 Ma rocks can be accreted to the western side of the 89 ± 6 Ma plateau. Another possibility is that the 115 Ma rocks of southern Azuero form part of the oceanic crust upon which the plateau was emplaced. The slight enrichment of incompatible elements and Sr-Nd-Pb isotopes relative to N-MORB can be explained by a hotspot, possibly even the Galápagos hotspot, with a nearby spreading center. It has been shown that the Galápagos hotspot or an other hotspot with similar chemical composition was active between 111-118 Ma [Hoernle *et al.*, 2004]. The oceanic crust formed at 115 Ma subsequently drifted eastwards. 94 Ma old parts of an oceanic plateau formed on this crust. CLIP samples of this period were found at southern Azuero. Di Marco *et al.* [1995] present paleomagnetic data showing an equatorial paleolatitude for Late Cretaceous rocks from Azuero, consistent with derivation from the paleo-Galápagos hotspot. The Campanian (84 – 71 Ma) to Maastrichtian Piedra Blanca CLIP probably have been formed as a part of the youngest Clip phase. Their position north to the Volcan Barú and northeast to the older terranes found on Azuero infers that these lavas may have been erupted on the western margin of the 89 ± 6 Ma oceanic plateau.

The Serranía del Sapo basaltic complex in eastern Panama (Darién) continues into western Columbia where it forms the Serranía de Baudo complex. Both the Serranía del Sapo and Serranía de Baudo complexes are associated with cherts and other sediments having Campanian to Maastrichtian fossils (radiolarian and foraminifera respectively) [Bandy and

Casey, 1973]. $\text{Ar}^{40}/\text{Ar}^{39}$ age dating of the basaltic rocks have also produced Late Cretaceous ages (72 – 78 Ma) for the Serranía de Baudo [Kerr *et al.*, 1996; Kerr *et al.*, 2002] and 71 - 84 Ma for the Serranía del Sapo (this study). Positive gravity anomalies are continuous over the Serranía del Sapo to the Serranía de Baudo providing additional evidence for a contiguous Panama-NW Colombian terrane [Case, 1974; Kellog *et al.*, 1995]. For the origin of the Serranía de Baudo igneous complex two different models have been proposed 1) it represents an accreted terrane [i.e. Kerr *et al.*, 1996] or 2) it has been formed by volcanism on the western edge of the 89 ± 6 Ma Caribbean plateau [Sinton *et al.*, 1998]. In order for a combined the Serranía del Sapo/Serranía de Baudo complex to be an accreted terrane implies that the 89 ± 6 Ma plateau had already completely drifted over the Galápagos hotspot such that the Serranía del Sapo/Serranía de Baudo complex formed to the west. With the initiation of subduction at ~ 65 -70 Ma, this complex/terrane then collided with the western margin of the 89 ± 6 Ma oceanic plateau. The 84 Ma old CLIP lavas of Darien are contradictory to the terrane model such as lying in the age range for the 89 ± 6 Ma oceanic plateau. Thus we propose that the last pulse of flood basalt volcanism was somewhat larger ranging from 69 - 84 Ma partly overlapping with the first pulse, erupting lavas on the western margin of the 89 ± 6 Ma CLIP plateau. The Soná CLIP lavas (82.6 Ma) and the Campanian to Maastrichtian pillow lavas and sheet flows on western Azuero near Rio Torio probably belong also to this last CLIP phase and were accreted to Central America before the forming of the Central American trench.

Accreted igneous rocks along the Pacific border of Costa Rica range in age from 65-54 Ma (N=6) [Sinton *et al.*, 1997; Hauff *et al.* 2000a, Hoernle *et al.*, 2002]. In Panama accreted rocks of the Galápagos paleo-hotspot track range from 66 to 50 Ma (N=12) and from 38 to 16 Ma (N=6) [Hoernle *et al.*, 2002 & this paper]. The 66 – 50 Ma (N=18) terranes extending from Quepos (central Costa Rican Pacific coast) to Azuero (western Panamanian Pacific coast) clearly represent a major phase of accretion in the Paleocene to Early Eocene. Middle Eocene limestone is unconformably overlying the oldest hotspot track at Punta Blanca hence the old accretionary processes must have been concluded before Middle Eocene. Thereafter accretion was sporadic and appears to have occurred at a reduced rate. It however cannot be ruled out that large portions of younger accreted terranes are located offshore and thus were not sampled or that previously accreted portions of the paleo hotspot tracks were eroded after accretion [Hoernle *et al.*, 2002].

There are however two reasons why accretion may have been greater in the Paleocene and Early Eocene. The hotspot could have been more productive between 50-65 Ma, which represents the transition from the oceanic plateau (or LIP) stage to the less productive hotspot track stage. The wide belt of accreted terranes suggests that the 50-65 Ma hotspot track was wider than the present hotspot tracks, consistent with higher magma production between 50-65 Ma. Second the hotspot was closer to the subduction zone in the Paleocene and Early

Eocene. Therefore large island volcanoes on hot uplifted lithosphere, which could be more easily accreted, reached the trench [Duncan and Hargraves, 1984; Hauff *et al.*, 2000a]. As the subduction zone drifted away from the hotspot, the island volcanoes were heavily eroded and eventually subsided below sea level due to plate cooling. Guyot-type seamounts which are much less pronounced in morphology, reached the trench and were not as readily accreted, as is presently the case outboard of Costa Rica [von Huene *et al.*, 2000, Ranero and von Huene, 2002]. Therefore, accretion may have given way to tectonic erosion in the Middle to Late Eocene. At present tectonic erosion is the prominent process associated with subduction of the Cocos Ridge and its flanking seamounts along the Pacific coast of Costa Rica [von Huene *et al.*, 2000, Ranero and von Huene, 2002]. As proposed by Close [1993], the negative buoyancy of the subducting slab will increase as the subducting slab becomes older, causing a change from accretion to subduction erosion. Northward migration of the western Panamanian arc took place from Middle to Late Eocene [Lissinna *et al.*, 2002]. Since there is no evidence for a change in the angle (flattening) of the subducting slab in this time period nor in the geochemistry of the arc rocks, the northward migration is interpreted to result from tectonic erosion associated with a subducting Galápagos track (comparable to present Costa Rica). Therefore the northward migration of the western Panamanian arc provide additional evidence that there was a switch from predominately accretion to tectonic erosion in the Middle Eocene.

In conclusion, the magmatic productivity of the Galápagos hotspot appears to have decreased after ~50 Ma, representing the transition from oceanic plateau (plume head) to hotspot track (plume tail) stage in the evolution of the Galápagos hotspot. In addition there was also a transition from predominately subduction accretion to tectonic erosion at ~45-50 Ma, reflecting decreasing output of the hotspot and increasing distance of the hotspot from the subduction zone.

6 Conclusions

Investigated 109-16 Ma old rocks found in Panama are geochemically consistent with an origin from the Galápagos hotspot. The CLIP lavas show similar major and trace element concentrations and Sr-Nd-Pb isotope ratios as the accreted rocks with ocean island basalt-type signatures. Sr-Nd-Pb isotope signatures of the CLIP lavas are consistent with their derivation from Northern to Eastern Galápagos domain compositions. The Cretaceous Azuero lavas (94 - 115 Ma) probably represent part of the main CLIP phase formed at 89 ± 6 Ma and some of the oceanic crust on which the oceanic plateau was emplaced. Eastern Panamanian CLIP lavas (71–84 Ma) may represent the northern part of an igneous terrane (probably derived from the Galápagos hotspot) accreted to Central and South America. The Soná CLIP lavas (82.6 Ma) and the Campanian to Maastrichtian pillow lavas and sheet flows on western Azuero near Rio Torio probably belong to the last CLIP phase 76 ± 7 Ma and were accreted to Central America

as were the Eastern Panama and Western Columbia terranes of similar age. The Campanian to Maastrichtian Piedra Blanca CLIP lavas also must have been part of the youngest Clip phase, but appear to have erupted on the western margin of the 89 ± 6 Ma oceanic plateau.

Field and geochemical investigations of the 17-66 Ma igneous rocks along the western Panamanian Pacific coast and inshore islands are consistent with their being accreted pieces of the paleo-Galápagos hotspot tracks. Igneous complexes are composed of parts of ocean island volcanoes, seamounts and aseismic ridges. We infer that a Galápagos archipelago with subaerial ocean islands existed at least for the last 66 Ma. Igneous complexes of the early paleo-Galápagos hotspot track composed of at least 66-50 Ma old rocks extended from Quepos to southeastern Azuero. All four Galápagos geochemical domains were present at this time. The accreted terranes show the same unique zonation in enriched components as observed presently at the Galápagos archipelago, suggesting that the Galápagos hotspot has been zoned for at least the last 65 Ma. Magma production of the Galápagos hotspot was most-likely greater between 50–65 Ma than during the last 20 Ma. Associated with less positive buoyancy of the subducting hotspot track, a shift from subduction accretion to subduction erosion must have been occurred between 45–50 Ma.

7 Acknowledgements

We thank R. Werner, Juan de Dios Villa, Capitán de Fragata Jorge Rengifo and Sargento II, Pablo Arosemena (Servicio Marítimo Nacional) for field and logistical support. P. Denyer is thanked for providing samples. We thank S. Vetter, D. Rau, J. Sticklus, D. Garbe-Schönberg, H. Blaschek, S. Klauke and U. Westernströer for analytical assistance. The team of the reactor at the GKSS Research Center in Geesthacht (Germany) is thanked. This research was supported by Deutsche Forschungsgemeinschaft (projects HO 1833/6-1&2 and SFB574, subproject C2).

8 References

- Abratis, M., and G. Wörner, Ridge collision, slab window formation, and the flux of Pacific asthenosphere into the Caribbean realm, *Geological Society of America*, 29, 127-130, 2001.
- Adamek, S., C. Frohlich, and W.D. Pennington, Seismicity of the Caribbean-Nazca microplate boundary: Constraints on microplate tectonics of the Panama region, *Journal of Geophysical Research*, 93, 2053-2075, 1988.
- Alverado, G.E., P. Denyer, and C.W. Sinton, The 89 Ma Tortugal komatiitic suite, Costa Rica; implications for a common geological origin of the Caribbean and eastern Pacific region from a mantle plume, *Geology*, 25, 439-422, 1997.
- Bandy, O.L., and R.E. Casey, Reflector horizons and paleobathymetric history, eastern Panama, *Geological Society of America Bulletin*, 84, 3081-3086, 1973.

- Bourgeois, J., J. Azéma, J. Tournon, H. Bellon, B. Calle, E. Parra, J.-F. Toussaint, G. Glaçon, H. Feinberg, P. deWever, and I. Origlia, Ages et structures des complexes basiques et ultrabasique de la façade pacifique entre 3°N et 12°N (Colombie, Panama et Costa Rica), *Geological Society of France Bulletin*, 24, 545-554, 1982.
- Bowland, C. L., and E. Rosencrantz, Upper crustal structure of the western Colombian basin, Caribbean Sea, *Geological Society of America Bulletin*, 100, 534-546, 1988.
- Case, J.E., Oceanic Crust Forms Basement of Eastern Panama, *Geological Society of America Bulletin*, 85, 645-652, 1974.
- Christie, D.M., R.A. Duncan, A.R. McBirney, M.A. Richards, W.M. White, K. Harpp, and C.G. Fox, Drowned islands downstream from the Galápagos hotspot imply extended speciation times, *Nature*, 355, 246-248, 1992.
- Christie, D.M., R. Werner, F. Hauff, K. Hoernle, and B.B. Hanan, Morphological and geochemical variations along the eastern Galápagos Spreading Center, *Geochemistry, Geophysics, Geosystems*, DOI 10.1029/2004GC000714, 2005.
- Closs, M., Lithospheric buoyancy and collisional orogenesis: Subduction of oceanic plateaus, continental margins, island arcs, spreading ridges, and seamounts, *Geological Society of America Bulletin*, 105, 715-737, 1993.
- Collins, L.S., A.G. Coates, J.B.C. Jackson, and J.A. Obando, Timing and rates of emergence of the Limón and Bocas del Toro basins: Caribbean effects of Cocos Ridge subduction?, in *Geologic and Tectonic Development of the Caribbean Plate Boundary in Southern Central America*, , edited by P. Mann, , Geol Soc Am Spec Paper, 295, 263-289, 1995.
- Corrigan, J., P. Mann, and J.C. Ingle, Forearc response to subduction of the Cocos Ridge, Panama-Costa Rica, *Geological Society of America Bulletin*, 102, 628-652, 1990.
- Cowan, H., L. Sanchez, E. Camacho, J.-L. Palacios, A. Tapia, D. Irving, D. Esquivel, and C. Lindholm, Seismicity and Tectonics of Western Panama from new Portable Seismic Array Data, pp. 28, Instituto de Recursos Hidráulicos y Electrificación (IRHE), Panama, 1995.
- de Boer, J.Z., M.J. Defant, R.H. Stewart, and H. Bellon, Evidence for active subduction below western Panama, *Geology*, 19, 649-652, 1991.
- de Boer, J.Z., M.S. Drummond, M.J. Bordelon, M.J. Defant, H. Bellon, and R.C. Maury, Cenozoic magmatic phases of the Costa Rican island arc (Cordillera de Talamanca), *Geological Society of America Special Paper*, 295, 35-55, 1995.
- Defant, M.J., P.M. Richerson, J.Z. de Boer, R.H. Stewart, R.C. Maury, H. Bellon, M.S. Drummond, M.D. Feigenson, and T.E. Jackson, Dacite Genesis via both slab melting and differentiation: Petrogenesis of La Yeguada Volcanic Complex, Panama, *Journal of Petrology*, 1101-1142, 1991.
- Di Marco, G., P.O. Baumgartner, and J.E.T. Channell, Late Cretaceous-Early Tertiary paleomagnetic data and a revised tectonostratigraphic subdivision of Costa Rica and western Panama, *Geological Society of America, Special Paper 295*, 1995.

- Donnelly, T.W., D. Beets, M.J. Carr, T. Jackson, G. Klaver, J. Lewis, R. Maury, H. Schellenkens, A.L. Smith, G. Wadge, and D. Westercamp, History and tectonic setting of Caribbean magmatism, in *Geological Society of American*, vol. H., pp. 339-374, 1990.
- Duffield, W.A., and G.B. Dalrymple, The Taylor Creek Rhyolite of New Mexico; a rapidly emplaced field of lava domes and flows, *Bulletin of Volcanology*, 52, 475-487, 1990.
- Duncan, R.A., and R.B. Hargraves, Plate tectonic evolution of the Caribbean region in the mantle reference frame, *Geological Society of America Mem*, 162, 1984.
- Duque-Caro, H., The Choco block in the northwestern corner of South America: Structural, tectonostratigraphic, and paleogeographic implications, *Journal of South American Earth Science*, 3, 71-84, 1990.
- Elliot, T., T. Plank, A. Zindler, W. White, and B. Bourdon, Element transport from slab to volcanic front at the Marina arc, *Journal of Geophysical Research*, 102, 14991-15018, 1997.
- Fisher, S.P., and E.A. Pessagno, Upper Cretaceous Strata of Northwestern Panama, *Bulletin of the American Association of Petroleum Geologists*, 49, 433-444, 1965.
- Garbe-Schönberg, D., Simultaneous determination of thirty-seven trace elements in twenty-eight international rock standards by ICP-MS, *Geostandard Newsletter*, 17, 81-97, 1993.
- Geldmacher, J., B.B. Hanan, J. Blichert-Toft, K. Harpp, K. Hoernle, F. Hauff, R. Werner, and A.C. Kerr, Hafnium isotopic variations in volcanic rocks from the Caribbean Large Igneous Province and Galápagos hot spot tracks, *Geochemistry, Geophysics, Geosystems*, 4, 1062, doi.10.1029/2002GC000477, 2003.
- Handschuhmacher, D.W., Post-Eocene plate tectonics of the eastern Pacific, in *The Geophysics of the Pacific Ocean Basin and Its Margin*, *Geophysical Monographic Series*, vol. 19, edited by G.H. Sutton, M.H. Manghnani and R. Moberly, pp. 177-202, AGU, Washington, D.C., 1976.
- Harpp, K.S., and W.M. White, Tracing a mantle plume: Isotopic and trace element variations of Galápagos seamounts, *Geochemistry, Geophysics, Geosystems*, 2, 2000GC000137, 2001.
- Harpp, K.S., W. Wanless, R. Otto, K. Hoernle, R. Werner, The Cocos and Carnegie aseismic ridges: A trace element record of Long-term plume-spreading center interaction, *Journal of Petrology*, 46, 109-133, 2005.
- Hauff, F., K. Hoernle, H.-U. Schmincke, and R. Werner, A Mid Cretaceous origin for the Galápagos hotspot: volcanological, petrological and geochemical evidence from Costa Rican oceanic crustal segments, *Geologische Rundschau*, 86, 141-155, 1997.

- Hauff, F., K. Hoernle, P. van den Bogaard, G.E. Alvarado, and D. Garbe-Schönberg, Age and Geochemistry of Basaltic Complexes in Western Costa Rica: Contributions to the Geotectonic Evolution of Central America, *Geochemistry, Geophysics, Geosystems*, 1, 1999GC0000207, 2000b.
- Hauff, F., K. Hoernle, G. Tilton, D.W. Graham, and A.C. Kerr, Large volume recycling of oceanic lithosphere over short time scales: geochemical constraints from the Caribbean Large Igneous Province, *Earth and Planetary Science Letter*, 174, 247-263, 2000b.
- Hoernle, K., and G. Tilton, Sr-Nd-Pb isotopic data for Fuerteventura (Canary Islands) basal complex and subaerial volcanics: Applications to magma genesis and evolution, *Schweizerische Mineralogische Petrographische Mitteilung*, 71, 3-18, 1991.
- Hoernle, K., R. Werner, J.P. Morgan, D. Garbe-Schönberg, J. Bryce, and J. Mrazek, Existence of complex spatial zonation in the Galápagos plume for the at least 14 m. y., *Geology*, 28, 435-438, 2000.
- Hoernle, K., P.v.d. Bogaard, R. Werner, B. Lissinna, F. Hauf, G. Alverado, and D. Garbe-Schönberg, Missing history (16-71 Ma) of the Galápagos hotspot: Implications for the tectonic and biological evolution of the Americas, *Geology*, 30, 795-798, 2002.
- Hoernle, K., F. Hauff, and P.v.d. Bogaard, A70 m.y. history (139-69) for the Caribbean large igneous province, *Geology*, 32, 697-700, 2004.
- Hoernle K., and F. Hauff, Oceanic Igneous Complexes in Central America, in Bundschuh, J., and Avarado, G., eds., *Central America: Geology, Resources and Hazards*: Lisse, Swets & Zeitlinger Publishers, in press.
- Keigwin, L., Isotopic Paleoceanography of the Caribbean and East pacific: Role of Panama Uplift in Late Neogene Time, *Science*, 217, 350-353, 1982.
- Keller, G., C. Zenker, and S.M. Stone, Late Neogene history of the Pacific-Caribbean gateway, *Journal of South American Earth Sciences*, 2, 73-108, 1989.
- Kellog, J.N., V. Vaga, T.C. Stallings, and C.L.V. Aiken, Tectonic development of Panama, Costa Rica and the Colombian Andes: Constraints from Global Positioning System geodetic studies and gravity, *Geological Society of America Special Paper*, 295, 75-80, 1995.
- Kerr, A.C., G.F. Marriner, N.T. Arndt, J. Tarney, A. Nivia, A.D. Saunders, and R.A. Duncan, The petrogenesis of Gorgona komatiites, picrites and basalts: new field, petrographic and geochemical constraints, *Lithos*, 37, 245-260, 1996.
- Kerr, A.C., G.F. Marriner, J. Tarney, A. Nivia, A.D. Saunders, M.F. Thirlwall, and C.W. Sinton, Cretaceous basaltic terranes in western Columbia: elemental, geochronological and Sr-Nd constraints on petrogenesis, *Journal of Petrology*, 38, 667-702, 1997.

- Kerr, A.C., J. Tarney, P.D. Kempton, P. Spadea, A. Nivia, G.F. Marriner, and R.A. Duncan, Pervasive mantle plume head heterogeneity: Evidence from the Late Cretaceous Caribbean-Colombian oceanic plateau, *Journal of Geophysical Research*, 107, ECV 2 1-13, 2002.
- Kerr, R.C., and C. Mériaux, Structure and dynamics of sheared mantle plumes, *Geochemistry, Geophysics, Geosystems*, 5, doi: 10.1029/2004GC000749, 2004.
- Kesler, S.E., J.F. Sutter, M.J. Issigonis, L.M. Jones, and R.L. Walker, Evolution of Porphyry Copper Mineralization in an Oceanic Island Arc: Panama, *Economic Geology*, 72, 1142-1153, 1977.
- Kolarsky, R.A., P. Mann, and S. Monechi, Stratigraphic development of southwestern Panama as determined from integration of marine seismic data and onshore geology, *Geological Society of America Special Paper*, 295, 159-200, 1995.
- Kolarsky, R.A., and P. Mann, Structure and neotectonics of an oblique –subduction margin, southwestern Panama, *Geological Society of America Special Paper*, 295, 131-155, 1995.
- Krolikowska-Ciaglo, S., F. Hauff, and K. Hoernle, Sr-Nd isotope systematics in 14-28 Ma low-temperature altered mid-ocean ridge basalt from the Australian Antarctic Discordance, Ocean Drilling Program Leg 187, *Geochemistry, Geophysics, Geosystems*, doi: 10.1029/2004GC000802, 2005.
- Lapierre, H., D. Bosch, V. Dupuis, M. Polvé, R.C. Maury, J. Hernandez, P. Monié, D. Yeghicheyan, E. Jaillard, M. Tardy, B. Mercier de Lepinay, M. Mamberti, A. Desmet, F. Keller, and F. Sénebier, Multiple plume events in the genesis of the peri-Caribbean Cretaceous oceanic plateau province, *Journal of Geophysical Research*, 105, 8403-8421, 2000.
- Lissinna, B., K. Hoernle, and P. van den Bogaard, Northern migration of arc volcanism in western Panama: evidence for subduction erosion?, in *AGU*, vol. 83, *EOS Trans.*, pp. V11A-1368, 2002.
- Lissinna, B., K. Hoernle, P. van den Bogaard, F. Hauff, and D. Garbe-Schönberg, 70 Ma of arc magmatism in western Panama: A case study of the growth of the Central American landbridge, unpub.
- Lonsdale, P., and K.D. Klitgord, Structure and tectonic history of the eastern Panama Basin, *Geological Society of America Bulletin*, 89, 981-999, 1978.
- MacKay, M.E., and G.F. Moore, Variation in Deformation of the South Panama Accretionary Prism: Response to Oblique Subduction and Trench Sediment Variation, *Tectonics*, 9, 683-698, 1990.
- MacMillan, I., P.B. Gans, G. Alvarado, Middle Miocene to present plate tectonic history of the southern Central American Volcanic Arc, *Tectonophysics*, 392, 325-348, 2004.
- Moore, G.F., and K.L. Sender, Fracture zone collision along the South Panama margin, *Geological Society of America Special Paper*, 295, 1995.
- Okaya, D.A., and Z. Ben-Avraham, Structure of the continental margin of southwestern Panama, *Geological Society of America Bulletin*, 99, 792-802, 1987.

- Palmer, A.R., and J. Geissman, Geologic Time Scale, *Geological Society of America, product code CTS004*, 1999.
- Ranero, C.R., and R. von Huene, Subduction erosion along the Middle America convergent margin, *Nature*, *404*, 748-752, 2000.
- Réveillon, S., E. Hallot, N.T. Arndt, C. Chauvel, and R.A. Duncan, A complex history for the Caribbean plateau: Petrology, geochemistry, and geochronology of the Beata Ridge, south Hispaniola, *Journal of Geology*, *108*, 641-661, 2000.
- Silver, E.A., D.L. Reed, J.E. Tagudin, and D.J. Heil, Implications of the north and south Panama thrust belts for the origin of the Panama orocline, *Tectonics*, *9*, 261-281, 1990.
- Sinton, C.W., R.A. Duncan, and P. Denyer, A single suite of Caribbean oceanic plateau magmas, *Journal of Geophysical Research*, *102*, 15507-15520, 1997.
- Sinton, C.W., R.A. Duncan, M. Storey, J. Lewis, and J.J. Estrada, An oceanic flood basalt province within the Caribbean plate, *Earth and Planetary Science Letter*, *155*, 221-235, 1998.
- Sun, S.-S., and W.F. McDonough, Chemical and isotopic systematics of oceanic basalts: implications for mantle composition and processes, *Geological Society Special Publication*, *42*, 313-345, 1989.
- Todt, W., R.A. Cliff, A. Hanser, and A.W. Hofmann, Evaluation of a ^{202}Pb - ^{205}Pb double spike for high precision lead isotope analyses, in *Earth Processes: Reading of the Isotopic Code*, vol. 95, edited by A. Basu and S. Hart, pp. 429-437, AGU, Washington D.C., 1996.
- van Andel, T.H., et al., Initial Report Deep Sea Drilling Project, vol. 16, U.S. Printing Off., Washington D.C., 1973.
- von Huene, R., C.R. Ranero, W. Weinrebe, and K. Hinz, Quaternary convergent margin tectonics of Costa Rica, segmentation of the Cocos Plate, and Central American volcanism, *Tectonics*, *19*, 314-334, 2000.
- Vergara Muñoz, A.V., Tectonic patterns of the Panama Block deduced from seismicity, gravitational data and earthquake mechanisms: implications to the seismic hazard, *Tectonophysics*, *154*, 253-267, 1988.
- Werner, R., K. Hoernle, P. van den Bogaard, C. Ranero, R. von Huene, and D. Korich, Drowned 14-m.y.-Galápagos archipelago off the coast of Costa Rica: Implications for tectonic and evolutionary models, *Geology*, *27*, 499-501, 1999.
- Werner, R., K. Hoernle, U. Barckhausen, and F. Hauff, The geodynamic Evolution of the Galápagos Hotspot System (Central East Pacific) over the past 20 m.y.: Constraints from morphology, geochemistry, and magnetic Anomalies, *Geochemistry Geophysics Geosystems*, *2003/GC000576*, 2003.
- Westbrook, G.K., N.C. Hardy, and R.P. Heath, Structure and tectonics of the Panama-Nazca plate boundary, *Geological Society of America Bulletin, Special Paper 295*, 91-109, 1995.
- Weyl, R., *Geology of Central America*, 371 pp., Borntraeger, Berlin, 1980.
- White, W.M., and A.W. Hofmann, Geochemistry of the Galápagos Islands: Implications for mantle dynamics and evolution, *Year Book Carnegie Inst. Washington*, *77*, 596-606, 1978.

9 Tables

Table 1 A: Major and Trace Element Data from Panamanian Igneous Complexes

Sample	Major Elements, wt. %											Trace Elements, ppm										
	SiO ₂	Al ₂ O ₃	MnO	MgO	Na ₂ O	CaO	P ₂ O ₅	K ₂ O	TiO ₂	Fe ₂ O ₃	H ₂ O	CO ₂	TOTAL	Ba	Cr	Ni	Sr	Zr				
Azuero																						
G 22 *	47.42	13.92	0.28	7.65	2.27	12.33	0.11	0.24	1.25	12.00	1.33	0.03	98.83	117	243	94	119	64				
G 23	48.18	13.56	0.20	7.76	3.41	10.92	0.10	0.20	1.23	11.71	2.15	0.51	99.93	49	244	78	120	66				
G 25	48.30	13.53	0.19	7.62	2.97	10.96	0.09	0.20	1.20	11.94	2.86	0.03	99.93	21	210	99	152	65				
G 26	47.91	14.20	0.25	8.61	2.69	11.55	0.10	0.20	1.19	11.91	2.12	0.05	100.77	34	265	122	121	67				
G 30 *	47.55	13.55	0.17	6.61	3.18	9.00	0.27	0.20	2.88	13.84	1.64	0.03	99.97	249	72	81	254	173				
G 31	47.47	13.09	0.19	5.03	3.99	10.10	0.28	0.16	2.95	12.48	1.72	1.07	99.52	301	72	68	313	174				
G 33 *	46.52	13.31	0.23	6.38	3.45	9.33	0.28	0.60	2.93	13.85	1.91	0.05	98.85	238	57	60	253	177				
G 34	46.97	13.08	0.24	6.74	3.76	9.12	0.27	0.34	2.85	14.16	2.54	0.04	100.12	54	62	58	243	170				
G 36	48.99	13.66	0.21	8.34	2.97	11.46	0.10	0.12	1.20	12.03	1.83	0.08	100.99	37	250	94	131	68				
G 37	47.66	13.66	0.23	8.04	3.28	10.67	0.10	0.25	1.23	12.03	3.22	0.16	100.54	18	217	99	147	67				
G 38	48.11	13.51	0.18	7.99	2.43	12.02	0.10	0.14	1.25	11.56	1.88	0.04	99.20	67	290	107	132	68				
G 39	48.07	13.58	0.23	7.93	2.90	11.25	0.10	0.10	1.33	12.06	2.15	0.06	99.76	41	235	88	122	68				
G 40	47.25	13.63	0.21	6.03	4.38	8.81	0.29	0.52	3.00	13.77	2.65	0.04	100.58	125	61	64	286	179				
G 41	44.62	13.34	0.19	5.58	3.04	9.21	0.51	1.78	4.15	14.02	2.91	0.35	99.70	322	43	43	440	311				
G 42 *	46.41	14.25	0.17	6.16	2.70	11.01	0.32	1.12	2.90	11.57	2.76	0.37	99.75	187	97	72	465	211				
G 43	46.35	14.83	0.15	6.56	2.39	10.91	0.26	1.37	2.55	10.39	2.77	1.36	99.90	173	240	102	445	172				
G 44 *	47.45	15.62	0.17	4.16	3.53	9.59	0.44	1.29	3.99	12.20	1.58	0.14	100.06	254	31	36	517	294				
G 45	45.78	15.11	0.17	5.72	2.88	9.83	0.40	1.63	3.25	11.76	3.42	0.14	100.10	302	97	68	430	237				
G 46 *	47.70	13.65	0.18	7.18	2.68	11.62	0.26	0.45	2.68	11.99	1.22	0.03	99.64	99	171	99	412	169				
G 47	47.24	13.74	0.16	7.70	2.78	10.88	0.30	0.18	2.92	12.09	1.92	0.09	99.90	71	304	118	371	194				
G 48	46.69	13.49	0.16	7.66	2.78	10.78	0.29	0.13	2.87	12.04	2.10	0.09	99.08	43	296	132	385	187				
G 49	47.85	12.98	0.16	7.70	3.07	9.86	0.29	0.13	3.02	11.80	3.07	0.06	99.98	41	361	149	411	192				
G 50	48.32	13.51	0.19	7.88	2.72	11.35	0.11	0.12	1.28	12.21	2.30	0.08	100.06	38	221	84	141	68				
G 51	48.01	13.26	0.20	7.31	3.71	10.35	0.15	0.24	1.60	12.22	2.90	0.02	99.97	146	165	73	107	93				
AZ-36	46.76	14.81	0.21	5.55	2.86	10.57	0.25	0.23	2.70	13.94	2.62	0.15	100.65	98	125	67	305	174				
AZ-39-1 *	49.17	14.06	0.18	8.07	2.26	11.97	0.10	1.20	0.10	12.08	1.74	0.26	101.19									
AZ-55-1 *	47.42	12.64	0.20	5.92	2.17	10.09	0.48	0.58	4.05	15.76	1.27	0.03	100.61	132	144	81	287	311				
AZ-58-1	47.31	13.50	0.17	6.21	3.05	8.66	0.39	0.75	3.58	13.46	3.24	0.69	101.01	213	64	74	392	264				
AZ-58-3	48.05	14.69	0.21	7.91	1.81	12.68	0.11	0.08	1.30	11.82	2.00	0.17	100.83	41	227	98	122	72				
AZ-59-4 *	47.46	19.12	0.15	6.46	2.07	12.71	0.10	0.05	1.00	9.27	1.30	0.02	99.71	30	195	65	139	77				
AZ-66-1 *	48.50	13.51	0.18	5.73	2.14	10.80	0.34	0.40	3.45	14.46	1.27	0.04	100.82	88	196	86	266	233				
AZ-67 *	47.97	13.77	0.20	6.11	3.02	10.02	0.28	0.48	2.86	14.23	1.67	0.03	100.65	96	81	79	230	183				
AZ-69-1 *	48.12	14.19	0.19	4.84	3.29	10.53	0.59	0.46	4.11	13.76	2.04	0.14	100.51	264	55	48	528	396				
AZ-72-1 *	45.41	16.15	0.17	4.65	2.98	10.09	0.96	0.83	3.85	12.61	2.38	0.09	100.17	286	68	39	650	396				
AZ-74-4	47.97	14.32	0.16	6.64	3.39	9.84	0.37	0.57	3.07	11.26	2.15	0.45	100.19	175	213	86	297	231				
AZ-103-2 *	45.59	11.01	0.15	16.93	1.15	10.62	0.17	0.39	1.76	10.79	1.65	0.05	100.26	105	1124	541	278	96				
AZ-104-1 *	47.37	14.13	0.20	6.09	2.36	11.18	0.31	0.13	3.24	14.60	1.24	0.03	100.68	43	122	76	271	208				
M20KH	47.53	14.90	0.19	6.69	2.00	12.40	0.22	0.09	2.45	12.90	1.30	0.07	100.74	36	200	86	265	156				
M21KH	47.34	14.66	0.19	6.47	1.90	12.34	0.22	0.09	2.41	13.11	1.60	0.06	100.39	59	202	103	261	148				
M108b	45.66	15.66	0.17	5.16	3.19	11.10	0.54	1.12	4.79	12.61	1.78	3.49	103.41	458	335	24	202	279				
M109 b	46.35	14.80	0.22	5.48	2.70	10.83	0.53	0.81	3.89	13.02	2.12	0.06	100.81	239	78	79	481	360				
Azuero CLIP & basement																						
AZ-26-1	44.28	13.66	0.18	4.85	2.61	9.28	0.52	1.58	4.12	14.28	3.31	1.95	100.62	272	24	49	453	353				
AZ-27-1	48.82	14.43	0.19	7.61	2.60	10.59	0.11	0.13	1.24	12.10	2.77	0.08	100.67	105	228	106	207	69				
AZ-38-1	48.39	14.47	0.26	7.98	1.72	13.07	0.10	0.07	1.22	12.21	1.85	0.12	101.46	38	209	105	117	67				

* data published by Hoernle et al., 2002

Table 1 A: (continued)

Sample	Major Elements, wt. %										Trace Elements, ppm							
	SiO ₂	Al ₂ O ₃	MnO	MgO	Na ₂ O	CaO	P ₂ O ₅	K ₂ O	TiO ₂	Fe ₂ O ₃	H ₂ O	CO ₂	TOTAL	Ba	Cr	Ni	Sr	Zr
Sona																		
G 53	47.74	13.33	0.20	7.19	3.08	11.36	0.13	0.09	1.66	12.94	1.66	0.05	99.43	51	164	83	129	92
G 54 *	47.69	13.65	0.19	7.79	2.82	11.55	0.10	0.36	1.31	12.17	2.78	0.06	100.47	71	244	89	113	73
G 57a	48.17	13.73	0.20	8.41	2.36	12.04	0.10	0.17	1.26	11.69	1.67	0.05	99.85	50	341	109	116	70
G 57b	48.04	13.33	0.21	8.48	2.82	11.82	0.10	0.15	1.30	11.54	1.72	0.38	99.89	333	333	110	104	70
SO-99-4	48.53	13.78	0.20	8.52	1.77	12.54	0.10	0.16	1.26	11.96	1.70	0.07	100.59	43	300	106	117	71
Ladrones, Secas, Bolanos, Icazo, Coiba, Santa Catalina and Cebaco Island																		
7-14-4-03	48.45	14.01	0.20	8.18	2.82	11.23	0.12	0.06	1.34	12.27	1.71	0.09	100.62	32	258	94	107	75
5-16-4-03	47.52	14.36	0.19	6.58	2.37	12.46	0.22	0.10	2.43	13.47	0.99	0.03	100.90	46	268	107	244	144
2-17-4-03	47.58	14.52	0.19	6.50	2.44	12.03	0.24	0.10	2.64	13.76	0.99	0.01	101.19	51	204	96	253	162
3-17-4-03	47.52	14.42	0.20	6.92	2.43	11.90	0.25	0.12	2.64	13.07	1.11	0.07	100.84	66	183	101	255	159
2-21-4-03	48.63	13.75	0.21	8.06	2.65	11.25	0.12	0.32	1.25	12.14	1.98	0.07	100.58	159	240	100	130	68
10-21-4-0	48.47	13.92	0.23	8.21	2.23	12.18	0.12	0.05	1.19	12.42	1.57	0.02	100.76	29	265	111	116	70
9-16-4-03	46.00	10.68	0.18	15.26	1.60	10.11	0.14	0.23	1.69	12.87	1.40	0.01	100.44	14	790	439	179	89
G 58	48.28	13.54	0.20	9.04	2.89	10.58	0.07	0.28	0.92	11.88	2.24	0.07	100.00	95	175	79	77	44
G 59	48.59	13.60	0.19	8.52	3.22	10.67	0.08	0.25	0.92	12.15	2.15	0.10	100.43	178	174	85	86	46
G 61	54.01	16.17	0.14	4.64	6.37	4.54	0.17	1.89	0.84	8.21	2.95	0.04	99.98	622			257	168
G 62	47.10	13.70	0.20	7.93	3.06	10.94	0.10	0.18	1.34	12.21	3.41	0.04	100.21	70	250	93	188	71
G 63 *	48.04	13.93	0.20	7.93	2.79	11.65	0.10	0.12	1.27	12.07	2.74	0.03	100.87	38	293	104	191	71
CE-61-1	48.56	14.37	0.21	6.55	2.49	11.68	0.18	0.07	1.78	13.20	1.50	0.14	100.73	39	131	60	154	138
CE-63-1	49.47	13.70	0.19	8.15	2.69	11.05	0.08	0.18	1.02	11.50	2.10	0.12	100.25	41	276	122	335	60
CO-76-1	46.83	14.48	0.24	7.62	2.38	11.96	0.11	0.13	1.30	12.47	3.26	0.04	100.82	143	242	114	213	72
SC-100-3	48.55	13.65	0.20	7.32	2.53	11.39	0.12	0.08	1.45	13.13	2.53	0.02	100.97	63	98	69	95	79
Darien																		
M202 c	48.67	15.45	0.19	5.05	3.35	10.19	0.27	0.61	2.92	12.88	1.26	0.02	100.86	353	66	58	294	195
M202 b	48.19	13.26	0.33	6.24	2.61	10.72	0.27	0.24	2.98	14.42	1.59	0.02	100.87	80	79	80	223	187
M200 a	47.67	14.04	0.20	8.11	2.57	11.42	0.11	0.07	1.38	12.53	2.39	0.11	100.60	10	253	104	138	73
M200 b	47.73	14.38	0.24	8.13	2.34	11.82	0.11	0.09	1.37	12.59	2.30	0.08	101.18	47	248	106	124	77
TP29	48.66	13.06	0.21	4.29	3.62	8.54	0.24	0.33	2.42	16.54	2.29	0.11	100.48	515	515	13	45	151
TP34	48.05	13.62	0.21	7.81	2.89	9.83	0.07	0.49	0.86	12.83	3.34	0.04	100.25	197	360	7	573	52
Standards																		
JB-2 N=5	53.39	14.89	0.21	4.56	1.96	10.04	0.52	0.30	0.87	14.54			1.01	227	24	23	177	54
stand. dev	0.08	0.02	0.00	0.06	0.04	0.08	0.52	0.16	0.36	0.11			0.2	14.7	4.5	3.4	0.5	1.3
JB-3 N=5	50.92	17.40	0.17	5.10	2.54	9.85	0.74	0.58	1.15	11.91			100.52	254	60	44	408	98
stand. dev	0.06	0.05	0.00	0.04	0.07	0.05	0.55	0.23	0.31	0.09			0.18	15.1	5.0	2.9	1.7	1.9
JA-2 N=4	56.42	15.60	0.11	7.94	2.82	6.29	0.42	0.96	1.22	6.42			98.37	304	513	133	245	100
stand. dev	0.07	0.03	0.00	0.05	0.04	0.004	0.26	0.80	0.54	0.04			0.13	8.6	7.8	1.8	1.6	1.1

* data published by Hoernle et al., 2002

Table 1 B: Trace Element Data from Panamanian Igneous Complexes

Sample	Rb	Y	Nb	La	Ce	Pr	Nd	Sm	Eu	Gd	Tb	Dy	Ho	Er	Tm	Yb	Lu	Hf	Ta	Pb	Th	U
Trace Element, ppm																						
Azuero																						
G 22 *	3.02	21.72	3.60	3.29	8.94	1.45	7.55	2.52	0.96	3.41	0.62	4.05	0.86	2.33	0.36	2.32	0.35	1.82	0.22	0.26	0.23	0.08
G 30 *	13.99	29.02	15.36	12.04	30.65	4.55	21.31	5.98	2.07	6.62	1.05	6.15	1.17	2.96	0.43	2.62	0.36	4.65	0.94	0.88	1.05	0.22
G 33 *	6.43	32.06	15.70	12.98	32.22	4.73	22.17	6.04	2.10	6.85	1.08	6.44	1.25	3.15	0.45	2.77	0.39	4.66	0.94	0.88	1.06	0.38
G 34	6.15	29.68	15.05	12.16	30.64	4.56	21.41	5.96	1.98	6.57	1.05	6.20	1.19	2.99	0.43	2.59	0.37	4.56	0.93	0.76	1.05	0.48
G 37	1.34	21.03	3.37	3.09	8.43	1.39	7.20	2.37	0.90	3.26	0.59	3.85	0.82	2.25	0.35	2.25	0.33	1.79	0.21	0.26	0.23	0.08
G 39	1.55	21.44	3.48	3.15	8.69	1.43	7.32	2.50	0.97	3.32	0.59	4.01	0.85	2.31	0.36	2.31	0.34	1.85	0.22	0.27	0.24	0.08
G 40	32.06	28.20	28.23	21.36	49.02	6.74	29.72	7.32	2.43	7.55	1.13	6.32	1.15	2.73	0.36	2.11	0.27	2.21	1.78	1.35	1.14	0.26
G 41	44.77	31.60	39.23	30.24	68.41	9.19	39.76	9.45	3.00	9.24	1.36	7.30	1.29	3.05	0.41	2.33	0.31	5.61	2.39	1.40	2.01	0.59
G 42 *	24.08	22.31	27.82	21.44	48.33	6.55	28.43	6.81	2.21	6.55	0.96	5.15	0.91	2.13	0.27	1.56	0.20	2.84	1.63	0.76	0.90	0.33
G 44 *	24.99	31.50	42.10	30.11	67.07	8.81	37.43	8.77	2.79	8.48	1.27	7.04	1.27	3.00	0.40	2.30	0.30	2.15	2.51	1.10	2.56	0.54
G 47	2.62	27.35	25.79	18.63	45.00	6.23	27.28	6.72	2.21	6.84	1.03	5.80	1.08	2.69	0.38	2.30	0.32	5.08	1.50	0.69	1.71	0.53
G 50	1.34	22.12	3.68	3.21	9.10	1.49	7.72	2.62	0.99	3.42	0.63	4.12	0.87	2.39	0.37	2.39	0.36	1.97	0.23	0.16	0.25	0.09
AZ-36	3.27	29.05	13.43	11.03	28.89	4.17	19.84	5.56	1.94	6.21	1.02	6.13	1.19	3.12	0.44	2.76	0.38	4.33	0.68	0.67	1.02	0.36
AZ-39-1*	1.13	21.20	3.28	2.82	8.17	1.32	6.91	2.38	0.92	3.20	0.59	3.96	0.84	2.41	0.36	2.37	0.35	1.82	0.17	0.11	0.25	0.08
AZ-55-1*	12.25	48.19	27.13	22.52	55.15	8.25	37.50	9.90	3.24	10.50	1.67	9.60	1.79	4.62	0.64	4.01	0.56	7.34	1.69	1.45	2.07	0.64
AZ-56-2	1.11	26.29	23.29	17.32	43.78	5.85	25.69	6.40	2.08	6.41	0.98	5.65	1.06	2.71	0.36	2.22	0.31	5.08	1.16	0.50	1.82	0.54
AZ-58-1	0.72	21.76	3.51	2.91	8.71	1.42	7.39	2.57	0.98	3.36	0.62	4.12	0.87	2.47	0.36	2.42	0.36	1.98	0.18	0.10	0.25	0.08
AZ-58-3	15.21	23.78	3.15	4.83	12.89	2.32	12.11	3.80	1.38	4.37	0.72	4.54	0.90	2.44	0.35	2.32	0.33	1.85	0.19	1.41	0.39	0.15
AZ-59-4*	0.69	22.57	1.00	2.19	6.85	1.21	6.67	2.46	0.99	3.35	0.63	4.16	0.89	2.55	0.39	2.52	0.37	1.85	0.05	0.25	0.13	0.05
AZ-66-1*	6.83	39.97	19.16	15.92	40.21	6.15	28.32	7.59	2.57	8.24	1.33	7.81	1.48	3.89	0.54	3.40	0.48	5.52	1.21	1.12	1.39	0.44
AZ-67*	7.12	32.61	15.93	12.95	33.42	4.82	22.56	6.40	2.15	6.96	1.12	6.73	1.30	3.41	0.47	2.90	0.41	4.97	0.81	0.86	1.22	0.28
AZ-69-1*	2.29	29.73	14.58	11.84	30.61	4.39	20.62	5.78	1.98	6.34	1.03	6.14	1.18	3.12	0.43	2.66	0.37	4.57	0.73	0.77	1.12	0.34
AZ-72-1*	15.85	42.15	49.17	42.66	100.79	13.21	56.72	12.95	4.06	12.11	1.76	9.60	1.73	4.26	0.55	3.33	0.45	8.68	2.47	1.53	4.08	0.69
AZ-74-4	6.33	26.93	28.88	21.46	50.78	6.70	28.88	6.98	2.31	6.99	1.05	5.88	1.09	2.73	0.38	2.31	0.31	5.58	1.44	0.89	2.07	0.43
CO-76-1	1.89	22.55	3.74	3.40	9.43	1.49	7.62	2.59	1.00	3.48	0.63	4.19	0.88	2.52	0.38	2.45	0.36	1.94	0.18	0.18	0.28	0.09
AZ-103-2*	8.05	15.55	13.83	10.01	24.03	3.24	14.38	3.73	1.27	3.79	0.60	3.39	0.63	1.59	0.21	1.31	0.18	2.98	0.70	0.57	1.03	0.28
AZ-104-1*	0.64	33.14	16.93	13.72	35.46	5.10	23.89	6.63	2.24	7.26	1.18	7.00	1.35	3.51	0.49	3.05	0.43	5.24	0.85	0.93	1.28	0.39
M20KH	0.19	26.59	12.02	10.98	28.07	4.22	20.44	5.72	1.98	6.49	1.06	6.46	1.26	3.26	0.45	2.81	0.40	4.82	0.99	0.56	0.94	0.29
M21Kh	0.45	25.81	11.83	10.97	27.88	4.19	20.08	5.62	1.98	6.43	1.04	6.42	1.25	3.24	0.45	2.82	0.40	4.82	0.99	0.72	0.92	0.28

* data published by Hoernle et al., 2002

Table 1 B: Trace Element Data from Panamanian Igneous Complexes

Sample	Trace Element, ppm																					
	Rb	Y	Nb	La	Ce	Pr	Nd	Sm	Eu	Gd	Tb	Dy	Ho	Er	Tm	Yb	Lu	Hf	Ta	Pb	Th	U
Azuero CLIP & basement																						
AZ-26-1	38.90	34.25	43.32	31.90	72.91	10.11	42.92	9.81	3.15	9.46	1.39	7.44	1.29	3.14	0.40	2.39	0.31	5.72	2.76	1.70	2.23	0.73
AZ-27-1	1.57	20.72	3.64	3.78	10.30	1.60	8.10	2.64	0.98	3.39	0.60	3.94	0.82	2.34	0.34	2.24	0.33	1.90	0.19	0.10	0.36	0.12
AZ-38-1	0.68	20.11	3.45	3.12	8.79	1.38	7.07	2.42	0.91	3.20	0.58	3.80	0.80	2.27	0.35	2.25	0.33	1.81	0.17	0.31	0.24	0.08
Sona																						
G 54 *	0.63	28.41	6.40	5.81	14.30	2.17	10.75	3.53	1.28	4.57	0.81	5.34	1.11	3.07	0.47	3.01	0.44	2.56	0.39	0.29	0.49	0.16
G 57a	1.31	21.85	3.76	3.39	9.27	1.54	7.79	2.64	1.00	3.50	0.62	4.02	0.85	2.34	0.35	2.33	0.34	1.92	0.23	0.29	0.25	0.09
Ladrones, Secas, Bolanos, Icaico and Coiba Island																						
7-14-4-(0.51	24.73	3.68	3.29	9.63	1.64	8.41	2.83	1.12	3.64	0.66	4.40	0.92	2.58	0.39	2.56	0.38	1.96	0.24	0.33	0.28	0.09	0.09
2-21-4-(3.80	23.15	3.43	2.99	8.67	1.46	7.69	2.55	0.95	3.38	0.61	4.04	0.85	2.38	0.36	2.40	0.35	1.66	0.22	0.46	0.23	0.07	0.07
3-17-4-(0.60	31.86	11.83	10.34	26.70	4.21	20.04	5.60	2.02	6.22	1.02	6.15	1.19	3.14	0.44	2.82	0.40	3.96	0.76	0.76	0.79	0.25	0.25
9-16-4-(3.09	20.33	7.04	6.01	16.25	2.57	12.49	3.54	1.30	4.01	0.66	4.03	0.78	2.05	0.29	1.82	0.26	2.49	0.47	0.33	0.47	0.15	0.15
G 58	1.50	22.84	1.84	2.02	5.44	0.90	4.80	1.86	0.77	2.85	0.56	3.95	0.87	2.50	0.40	2.62	0.40	1.32	0.11	0.34	0.16	0.05
G 63 *	2.29	22.29	3.67	3.29	9.05	1.49	7.71	2.65	0.98	3.54	0.63	4.13	0.87	2.36	0.36	2.38	0.35	1.93	0.22	0.20	0.24	0.09
Darien																						
M200 b 0.75	22.93	3.49	3.76	10.32	1.69	9.00	3.06	1.17	4.10	0.76	5.16	1.11	3.11	0.46	3.10	0.46	2.61	0.30	0.09	0.29	0.10	0.10
M202 b 3.05	35.68	14.53	12.37	32.19	4.98	23.46	6.48	2.28	7.18	1.17	7.02	1.34	3.50	0.48	3.08	0.44	4.59	0.93	0.88	1.12	0.35	0.35
M202 c 5.99	22.90	9.37	9.00	23.63	3.52	16.85	4.72	1.63	5.17	0.87	5.15	1.00	2.62	0.36	2.27	0.33	3.61	0.71	0.50	0.76	0.23	0.23
Standards																						
JB-2	5.86	20.46	0.45	2.15	6.36	1.09	5.89	2.20	0.78	2.95	0.56	3.74	0.82	2.39	0.37	2.46	0.36	1.46	0.03	4.90	0.25	0.15
JA-1	72.07	16.29	8.46	15.95	33.25	3.81	14.71	3.20	0.91	3.34	0.52	3.20	0.64	1.83	0.27	1.77	0.27	3.27	0.68	18.89	4.98	2.26
BIR-1	10.25	15.36	0.53	0.66	2.00	0.39	2.44	1.14	0.55	1.86	0.38	2.68	0.59	1.74	0.26	1.74	0.26	0.63	0.04	3.14	0.03	0.01
stand. c0.09	0.27	0.04	0.07	0.09	0.01	0.06	0.05	0.05	0.02	0.09	0.02	0.13	0.03	0.08	0.02	0.10	0.01	0.06	0.003	0.18	0.003	0.001
BHVO- 9.19	24.99	16.72	15.47	38.30	5.54	25.22	6.32	2.14	6.36	0.98	5.51	1.01	2.58	0.34	2.06	0.29	4.71	1.13	1.99	1.27	0.44	0.44
stand. c0.29	0.64	0.87	0.57	1.33	0.19	1.05	0.31	0.10	0.45	0.06	0.40	0.08	0.18	0.03	0.14	0.02	0.50	0.08	0.06	0.06	0.06	0.02

* data published by Hoernle et al., 2002

Table 2. Sr Isotope Data of the Panamanian igneous complexes

sample #	AGE(Ma)	Rb [ppm]	Sr [ppm]	87/86 SR M	±2	TOT/86	AT. WT. SR	87Rb/86SR	87/86 SR IN	87/86 SR Mod
accreted OIB <30 Ma										
AZ72-1	20.8	15.8	623	0.703334	0.000003	10.1351	87.6172	0.074	0.703312	0.703298
accreted OIB samples from Azuero 50-65Ma										
CO76	38.0	1.9	206	0.703472	0.000003	10.1353	87.6172	0.027	0.703457	0.703431
AZ39-1	54.4	1.1	119	0.703374	0.000003	10.1352	87.6172	0.028	0.703352	0.703315
AZ55-1	63.2	12.3	294	0.703062	0.000003	10.1349	87.6172	0.121	0.702954	0.702910
AZ59-4	56.0	0.7	136	0.702757	0.000003	10.1345	87.6172	0.015	0.702745	0.702707
AZ66-1	61.7	6.8	266	0.703128	0.000003	10.1349	87.6172	0.074	0.703063	0.703021
AZ67	51.9	7.1	240	0.703128	0.000003	10.1349	87.6172	0.086	0.703065	0.703029
AZ69-1	66.0	2.3	253	0.703090	0.000003	10.1349	87.6172	0.026	0.703065	0.703020
AZ103-2	52.1	8.1	268	0.703584	0.000003	10.1354	87.6171	0.087	0.703520	0.703484
AZ104-1	60.0	0.6	261	0.703068	0.000003	10.1349	87.6172	0.007	0.703062	0.703021
M108bKH	49.7	8.0	202	0.703587	0.000002	10.1354	87.6171	0.115	0.703506	0.703472
M21KH	59.9	0.4	258	0.703081	0.000002	10.1349	87.6172	0.005	0.703076	0.703035
Rearshore islands western of Coiba										
10-21-4-03	60.0	0.4	116	0.703221	0.000005	10.1350	87.6172	0.010	0.703212	0.703171
2-21-4-03	60.0	0.5	132	0.703620	0.000005	10.1354	87.6171	0.010	0.703611	0.703570
3-17-4-03	60.0	0.8	253	0.702940	0.000005	10.1347	87.6172	0.009	0.702933	0.702892
7-14-4-03	60.0	0.3	105	0.703305	0.000005	10.1351	87.6172	0.009	0.703297	0.703256
9-16-4-03	60.0	0.3	178	0.702960	0.000005	10.1348	87.6172	0.005	0.702956	0.702915
CLIP 69-109 Ma										
AZ26-1	93.5	15.9	454	0.703431	0.000003	10.1352	87.6172	0.101	0.703297	0.703233
AZ38-1	110.0	0.7	111	0.703064	0.000003	10.1349	87.6172	0.018	0.703036	0.702960
M200bKH	68.8	0.1	111	0.703575	0.000005	10.1354	87.6171	0.002	0.703573	0.703522
M202b	84.1	0.9	223	0.703060	0.000003	10.1349	87.6172	0.011	0.703046	0.702988

For calculations of 87/86 SR Mod initial ratios were projected to present-day values by adding the radiogenic in-growth according to their age and assumed parent-daughter ratios. The following parent-daughter ratio representative for the Galápagos system were used, 87Rb/86Sr=0.048.

Table 2. Nd Isotope Data of the Panamanian igneous complexes

sample #	AGE(Ma)	Sm [ppm]	Nd [ppm]	$^{143}\text{Nd}/^{144}\text{Nd}$ M ± 2	$^{147}\text{Sm}/^{144}\text{Nd}$ E. 43/144ND II	Et ND	E0 ND	$^{143}/^{144}\text{Nd}$ Mod		
accreted OIB <30 Ma										
AZ72-1	20.80	12.9	56.7	0.512969	0.000002	0.137	0.512950	6.62	6.46	0.512971
accreted OIB samples from Azuero 50-65Ma										
CO76	38.00	2.6	7.6	0.513078	0.000003	0.204	0.513027	8.55	8.58	0.513064
AZ39-1	54.40	2.4	6.9	0.513084	0.000002	0.207	0.513011	8.64	8.71	0.513064
AZ55-1	63.20	9.9	37.5	0.512993	0.000002	0.159	0.512927	7.23	6.93	0.512989
AZ59-4	56.00	2.5	6.7	0.513152	0.000002	0.222	0.513070	9.84	10.02	0.513125
AZ66-1	61.70	7.6	28.3	0.513004	0.000003	0.161	0.512939	7.42	7.14	0.513000
AZ67	51.90	6.4	22.6	0.512997	0.000003	0.171	0.512939	7.17	7.00	0.512990
AZ69-1	66.00	5.8	20.6	0.512988	0.000003	0.169	0.512915	7.07	6.83	0.512980
AZ103-2	52.10	3.7	14.4	0.512961	0.000003	0.156	0.512908	6.57	6.30	0.512959
AZ104-1	60.00	6.6	23.9	0.513011	0.000003	0.167	0.512945	7.49	7.27	0.513004
M108bKH	49.70	13.0	57.0	0.512984	0.000002	0.137	0.512940	7.13	6.75	0.512988
M21KH	59.90	5.6	20.1	0.512986	0.000002	0.168	0.512920	7.01	6.80	0.512979
Rearshore islands western of Coiba										
10-21-4-03	60.00	2.7	8.0	0.513087	0.000003	0.201	0.513008	8.72	8.75	0.513067
2-21-4-03	60.00	2.5	7.7	0.513056	0.000003	0.199	0.512978	8.14	8.16	0.513037
3-17-4-03	60.00	5.6	20.0	0.513029	0.000003	0.168	0.512963	7.84	7.62	0.513022
7-14-4-03	60.00	2.8	8.4	0.513081	0.000003	0.202	0.513001	8.59	8.63	0.513060
9-16-4-03	60.00	3.5	12.5	0.513025	0.000003	0.171	0.512958	7.75	7.55	0.513017
CLIP 69-109 Ma										
AZ26-1	93.50	9.8	42.9	0.512950	0.000002	0.138	0.512866	6.80	6.09	0.512958
AZ38-1	110.00	2.4	7.1	0.513073	0.000003	0.206	0.512925	8.36	8.48	0.513033
M200bKH	68.80	3.1	9.0	0.513077	0.000003	0.204	0.512985	8.49	8.56	0.513050
M202b	84.10	6.5	23.5	0.513013	0.000003	0.166	0.512921	7.64	7.31	0.513004

Initial ratios were projected to present-day values by adding the radiogenic in-growth according to their age and assumed parent-daughter ratios. The following parent-daughter ratios representative for the Galápagos system were used, $^{147}\text{Sm}/^{144}\text{Nd}=0.15$.

Table 2. Pb Isotope Data of the Panamanian igneous complexes

sample #	AGE(Ma)	PB [ppm]	U [ppm]	TH [ppm]	206/204Pb M ±2	207/204Pb M ±2	208/204Pb M ±2	TOT/204	AT WT PB	238U/204PB	235U/204PB	232Th/204PB	232Th/238U	206/204PB IN			
										MU	MU	OMEGA	KAPPA				
accreted OIB <30 Ma																	
AZ72-1	20.80	1.53	0.69	3.93	19.313	0.002	15.585	0.001	39.175	0.003	75.07	207.20	29.35	0.21	172.55	5.88	19.22
accreted OIB samples from Azuero 50-65Ma																	
CO76	38.00	0.18	0.09	0.27	18.884	0.002	15.577	0.002	38.524	0.005	73.99	207.20	31.42	0.23	95.95	3.05	18.70
AZ39-1	54.40	0.11	0.08	0.24	19.111	0.002	15.574	0.002	38.690	0.004	74.37	207.20	47.46	0.34	141.70	2.99	18.71
AZ55-1	63.20	1.45	0.64	2.07	19.451	0.002	15.580	0.001	38.988	0.003	75.02	207.20	28.78	0.21	95.94	3.33	19.17
AZ59-4	56.00	0.25	0.05	0.13	18.557	0.004	15.502	0.003	38.030	0.007	73.09	207.20	11.77	0.09	34.31	2.92	18.45
AZ66-1	61.70	1.12	0.44	1.39	19.350	0.003	15.572	0.006	38.894	0.006	74.82	207.20	25.48	0.18	82.86	3.25	19.10
AZ67	51.90	0.86	0.28	1.22	19.259	0.001	15.569	0.001	38.869	0.003	74.70	207.20	20.93	0.15	94.97	4.54	19.09
AZ69-1	66.00	0.77	0.34	1.12	19.292	0.001	15.564	0.001	38.827	0.003	74.68	207.20	28.63	0.21	97.29	3.40	19.00
AZ103-2	52.10	0.57	0.28	0.95	19.361	0.001	15.580	0.001	39.060	0.003	75.00	207.20	31.73	0.23	112.14	3.53	19.10
AZ104-1	60.00	0.93	0.39	1.22	19.492	0.001	15.568	0.001	38.842	0.002	74.90	207.19	27.33	0.20	88.21	3.23	19.24
M108bKH	49.70	1.49	0.67	2.07	19.633	0.002	15.596	0.002	39.199	0.004	75.43	207.20	29.22	0.21	93.83	3.21	19.41
M21KH	59.90	0.72	0.28	0.92	19.341	0.002	15.575	0.002	38.873	0.004	74.79	207.20	25.51	0.19	85.07	3.33	19.10
Rearshore islands western of Coiba																	
10-21-4-03	60.00	0.39	0.08	0.26	19.103	0.003	15.552	0.003	38.682	0.006	74.34	207.20	13.77	0.10	43.61	3.17	18.97
2-21-4-03	60.00	0.46	0.07	0.23	19.019	0.002	15.543	0.002	38.572	0.005	74.13	207.20	10.44	0.08	34.10	3.26	18.92
3-17-4-03	60.00	0.76	0.25	0.79	19.058	0.001	15.530	0.001	38.553	0.002	74.14	207.20	21.03	0.15	68.88	3.28	18.86
7-14-4-03	60.00	0.33	0.09	0.28	19.116	0.004	15.554	0.003	38.688	0.008	74.36	207.20	18.35	0.13	56.69	3.09	18.94
9-16-4-03	60.00	0.33	0.15	0.47	19.220	0.003	15.551	0.003	38.778	0.007	74.55	207.20	29.13	0.21	93.80	3.22	18.95
CLIP 69-109 Ma																	
AZ26-1	93.50	1.70	0.73	2.23	19.323	0.001	15.570	0.001	38.974	0.002	74.87	207.20	27.88	0.20	88.05	3.16	18.92
AZ38-1	110.00	0.31	0.08	0.26	19.040	0.004	15.542	0.003	38.584	0.007	74.17	207.20	17.18	0.12	56.16	3.27	18.74
M200bKH	68.80	0.09	0.10	0.29	19.475	0.002	15.565	0.001	38.881	0.003	74.92	207.19	70.50	0.51	217.74	3.09	18.72
M202b	84.10	0.88	0.35	1.12	19.288	0.008	15.576	0.006	38.925	0.016	74.79	207.20	25.91	0.19	85.76	3.31	18.95

Initial ratios were projected to present-day values by adding the radiogenic in-growth according to their age and assumed parent-daughter ratios. The following parent-daughter ratios representative for the Galápagos system were used, 238U/204Pb=10, 235U/204Pb=0.07 and 232Th/204Pb=5.5.

Table 4: Sample locations from the Panamanian Igneous Complexes

Sample	Longitude	Latitude	Sample	Longitude	Latitude
Azuero			Azuero and Punta Piedra CLIP & basement		
G 22 *	-80.178	7.417	AZ-26-1	-80.618	7.377
G 23	-80.178	7.417	AZ-27-1	-80.517	7.375
G 25	-80.178	7.417	AZ-38-1	-80.293	7.575
G 26	-80.146	7.420	TP-69	-92.504	9.133
G 29	-80.568	7.238	TP-71	-92.504	9.133
G 30 *	-80.568	7.239	Sona		
G 31	-80.568	7.238	G 53	-81.198	7.651
G 33 *	-80.568	7.239	G 54 *	-81.216	7.652
G 34	-80.566	7.242	G 57a	-81.249	7.626
G 36	-80.425	7.261	G 57b	-81.249	7.626
G 37	-80.421	7.262	SO-99-4	-81.252	7.625
G 38	-80.421	7.262	Ladrones, Secas, Bolanos, Icaço,		
G 39	-80.536	7.241	Coiba, Santa Catalina and Cebaco Island		
G 40	-80.820	7.384	7-14-4-03	-82.442	7.855
G 41	-80.820	7.384	5-16-4-03	-82.268	8.087
G 42 *	-80.820	7.384	2-17-4-03	-82.290	8.072
G 43	-80.820	7.384	3-17-4-03	-82.290	8.072
G 44 *	-80.820	7.384	2-21-4-03	-82.065	7.985
G 45	-80.820	7.384	10-21-4-0	-82.065	7.985
G 46 *	-80.813	7.396	9-16-4-03	-82.268	8.087
G 47	-80.812	7.435	G 58	-81.856	7.258
G 48	-80.811	7.398	G 59	-81.856	7.258
G 49	-80.811	7.398	G 61	-81.857	7.532
G 50	-80.951	7.545	G 62	-81.778	7.621
G 51	-80.951	7.545	G 63 *	-81.776	7.622
AZ-36	-80.208	7.431	CE-61-1	-81.055	7.543
AZ-39-1 *	-80.146	7.420	CE-63-1	-81.221	7.489
AZ-55-1 *	-80.892	7.443	CO-76-1	-81.881	7.491
AZ-56-2	-80.842	7.408	SC-100-3	-81.321	7.623
AZ-58-1	-80.786	7.343	Darien		
AZ-58-3	-80.786	7.343	M200 a	-78.199	7.592
AZ-59-4 *	-80.893	7.233	M200 b	-78.199	7.592
AZ-66-1 *	-80.614	7.237	M202 c	-78.203	7.563
AZ-67 *	-80.559	7.239	M202 b	-78.203	7.563
AZ-69-1 *	-80.547	7.242	TP29	-78.163	8.419
AZ-71	-80.893	7.235	TP34	78.122	8.435
AZ-72-1 *	-80.893	7.235			
AZ-74-4	-80.893	7.235			
AZ-103-2 *	-80.803	7.207			
AZ-104-1 *	-80.614	7.230			
M20KH	-80.584	7.240			
M21Kh	-80.584	7.240			
M108b	-80.615	7.232			
M109 b	-80.893	7.235			

* data published by *Hoernle et al.*, 2002

Article (Chapter) 2: Subduction Output

65 Ma of Arc Magmatism in Western Panama: A Case Study of the Growth of the Central American Landbridge

Lissinna, B.¹, Hoernle, K.¹, van den Bogaard, P.¹, Hauff, F.¹, Garbe-Schönberg, D.²

¹ Leibniz-Institute for Marine Sciences IFM-GEOMAR, Wischhofstrasse 1-3, 24148 Kiel

² Institut für Geowissenschaften, Christian Albrechts Universität, Ludewig-Meyn-Str. 10, 24118 Kiel

Abstract

New ⁴⁰Ar/³⁹Ar age and geochemical data (major and trace elements, Sr-Nd-Pb isotope ratios) from igneous rocks throughout Panama are used to reconstruct the Cenozoic magmatic and tectonic evolution of the southern Central American landbridge. Tholeiitic to calc-alkaline island arc magmatism occurred throughout Panama from Paleocene to Miocene (60.9 ± 0.5 Ma to 7.4 ± 0.7 Ma). A paleo-Galápagos hotspot track subducted beneath central and southern Costa Rica and western Panama from about 60-45 Ma ago, leaving a belt of accreted ocean islands, seamount volcanoes and fragments of submarine aseismic ridges extending from Quepos (Costa Rica) to the Azuero Peninsula (Panama). Isotopic composition of Paleocene subduction-related rocks from the Azuero Peninsula confirm the nearby subduction of a hotspot track. Northern migration of the western Panamanian arc took place from the Early Eocene to Early Oligocene (~50-30 Ma) possibly resulting from tectonic erosion induced by the subduction of a paleo-Galápagos hotspot track. Tectonic erosion rates of 84-96 km³ Ma⁻¹ km⁻¹ for the Panamanian arc between 50-30 Ma were estimated. Elevated Pb isotope ratios (enriched Galápagos-type geochemical signature) in arc rocks on Azuero in the Middle Eocene (~45 Ma) and in eastern Panama in the Early Miocene (~20 Ma) suggest eastern migration of the subducting hotspot track. The Paleocene to late Eocene arc is offset to the north in eastern Panama relative to western Panama; however, the Miocene arc forms a continuous arc from western to eastern Panama, suggesting left-lateral displacement between the Late Eocene and Early Miocene (40-22 Ma) in the Panama canal region. We propose that the shift of the subducting hotspot track from Azuero to the east may have induced the left-lateral displacement. Volcanism in eastern Panama ceased around 12 Ma ago coeval to the collision of eastern Panama with South America. In the Pliocene through Holocene (4.5 ± 0.17 to 0.1 ± 0.08 Ma) volcanism was restricted to low volume eruptions of alkaline and adakitic magmatism in western Panama primarily in the forearc region of the Miocene arc (south of the Cordillera Central). The subduction of the Coiba and Cocos Ridges may have allowed a slab window to open inducing melting of the exposed slab edges and

subsequently to form adakites. Melting of Galápagos-type mantle upwelling through the slab window or metasomatism of the mantle wedge by adakitic melts and subsequent melting could have generated the alkali basalts. In conclusion, the interplay between the Galápagos hotspot track and the Panamanian subduction-zone can explain the variations in the geochemistry of arc rocks through time and has a significant impact in the tectonic evolution of Panama.

1 Introduction

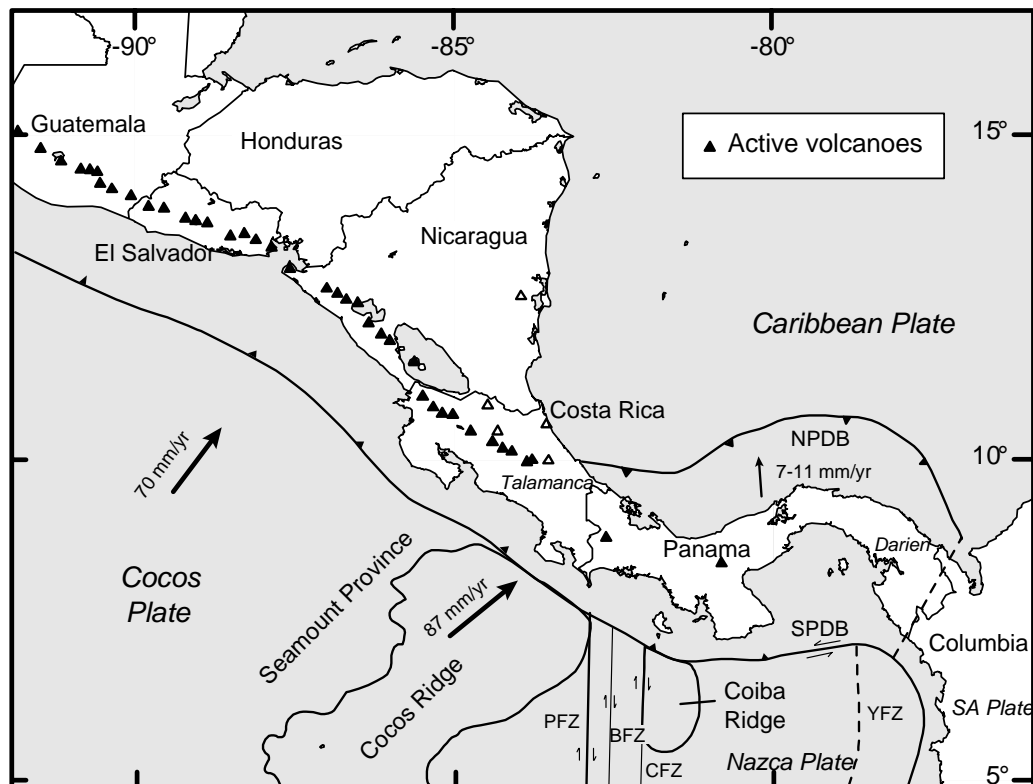


Fig.1: Overview map of Southern Central America. The South Panama Deformed Belt (SPDB) represents an active accretionary prism extending from at least 80°W to 83° W [Kolarsky and Mann, 1995]. The North Panama Deformed Belt (NPDB) is a broad belt of deformation north of the Panamanian Isthmus [Bowland and Rosencrantz, 1988]. The Panama Fracture Zone (PFZ), Balboa Fracture Zone (BFZ) and the Coiba Fracture Zone (CFZ) and Yaquina Fracture Zone (YFZ) are located south of Panama on the incoming Nazca Plate and its boundary with the Cocos Plate.

The magmatic evolution of Panama contains important clues for improving our understanding of the evolution of the southern Central American arc, the long-term evolution of the Galápagos hotspot and the formation of the Panamanian isthmus or landbridge. The arc

magmatism in Panama covering the entire Cenozoic also provides a unique opportunity to assess compositional changes in arc volcanism through time. The growth of the Panamanian arc on the western edge of the Cretaceous Caribbean oceanic plateau a large igneous province (LIP) ultimately led to the formation of the Central American landbridge in the Pliocene allowing the inter-American biotic exchange. Closure of the Caribbean-Pacific seaway is a prominent event in the late Neogene tectonic, biogeographic and paleo-oceanographic history of the Caribbean and the eastern Pacific region [e.g. *Burke*, 1988; *Duque Caro*, 1990], causing major changes in ocean circulation patterns and thus climate [*Haug and Tiedeman*, 1998]. We have carried out a regional geochronologic and geochemical study of arc volcanism in Panama since the inception of subduction at the western edge of the Caribbean large igneous province to the present, in order to constrain the tectonic evolution of the southern central American landbridge. Accreted igneous terranes in the west Panamanian forearc have been studied in a companion paper [*Lissinna et al.*, in prep.], that provides key information regarding the input into the subduction zone throughout the Cenozoic. We show that there is a clear link between the chemistry of the input and the output at the volcanic arc.

1.1 Geological Background

The earliest mapping of Panama was carried out by *Terry* [1956] and a team of geologists from the United Nations Development Program and the Dirección General de Recursos Minerales Panama [*del Giudice and Recchi*, 1969; *Metti and Recchi*, 1976]. The oldest reported suite of arc lavas outcrop in northwestern Panama near the town Changuinola [Fig.2]. Intercalated and overlying limestones sequences suggest that these igneous rocks are Upper Campanian to Lower Maastrichtian in age (~71 Ma) [*Fisher and Pessagno*, 1965]. Paleocene to Eocene subduction-related volcanism of Panama was described by *del Giudice and Recchi* [1969]; *Bandy and Casey* [1973], *Kesler et al.* [1977], *Weyl* [1980] and *Maury et al.* [1995]. Based on these studies, subduction of the Farallon plate beneath the Caribbean Large Igneous Province must have begun near the Cretaceous-Tertiary boundary [*Maury et al.*, 1995]. A continuous Paleocene arc from Nicaragua to South America was suggested by *Maury et al.* [1995]. *Kesler et al.* [1977] infers an early tholeiitic stage of arc volcanism between 60-70 Ma ago followed by calc-alkaline volcanism starting around 50 Ma ago. *Maury et al.* [1995] however found 55-61 Ma old igneous rocks at Rio Mortí (eastern Panama) with tholeiitic to calc-alkaline affinities. On the northern Azuero Peninsula, as is the case northeast of Panama City, erosion has exposed extensive parts of the intrusive core of the Paleocene arc. A K/Ar age of 69 Ma with a large uncertainty (± 10 Ma) was determined on a quartz-diorite from northwestern Azuero [*Weyl*, 1980]. Quartz diorite batholiths of the Loma Montuoso (western Azuero) and the Cerro Azul (eastern Panama) areas yielded Early Paleocene K/Ar ages of 64.9 ± 1.3 Ma [*Kesler et al.*, 1977] and 61.6 ± 0.7 Ma [*Weyl*, 1980].

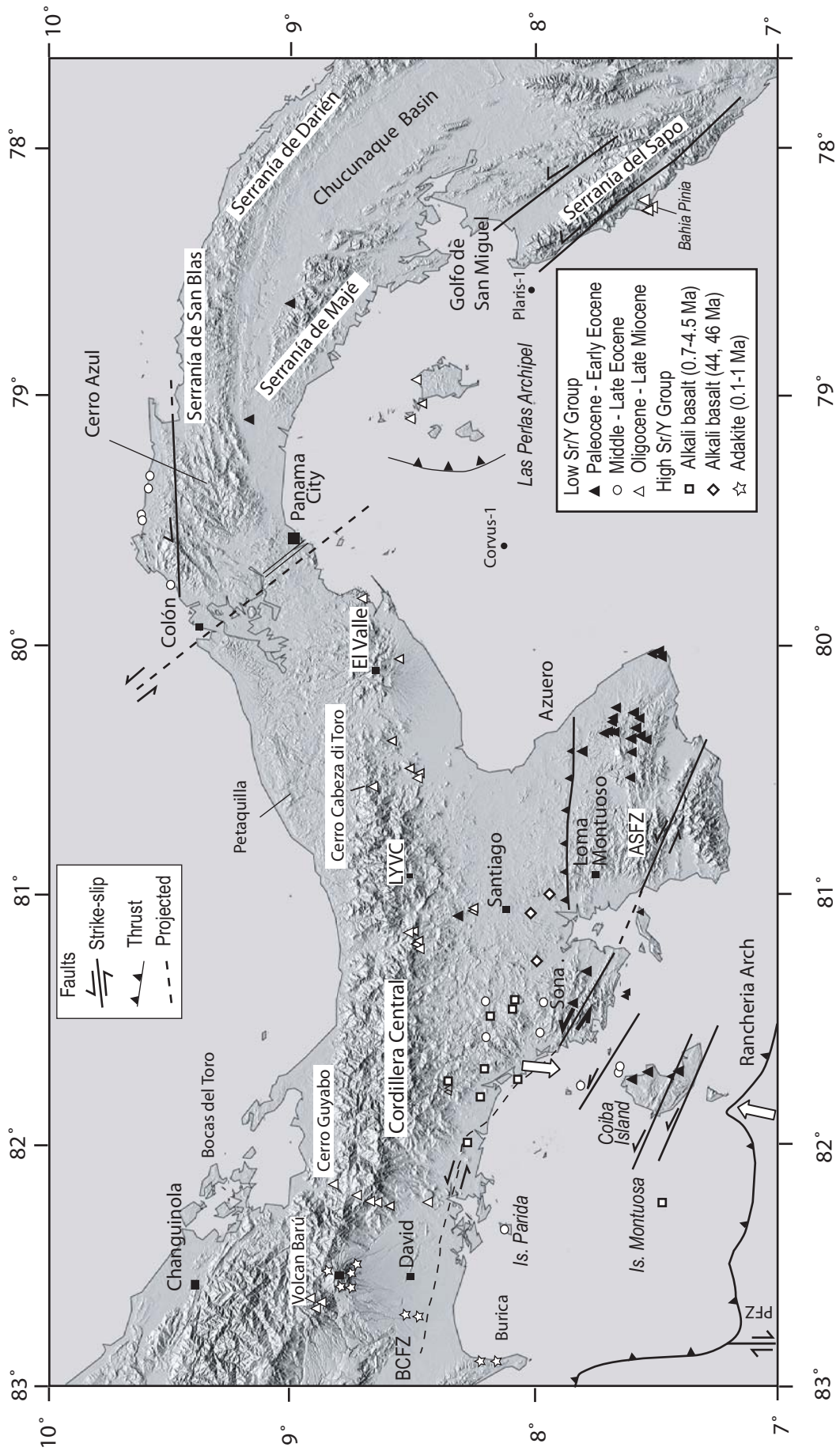


Fig. 2: Topographic map of Panama with sample locations and major tectonic features. Abbreviations: PFZ, Panama Fracture Zone; BCFZ, Ballena-Celmira Fault Zone; ASFZ, Azuero-Soná Fault Zone; LYVC, La Yeguada Volcanic Complex.

Both batholiths are intruded in bathyal limestone with a Late Campanian-Maastrichtian assemblage of planktonic foraminifera [*del Guidice and Recchi, 1969; Weyl, 1980*]. On southern Azuero, the lower Middle Eocene unit of the Tonosí Formation unconformably overlies basaltic rocks [*Kolarsky et al., 1995*], interpreted as accreted ocean island basaltic complexes derived from the Galápagos hotspot [*Hoernle et al., 2002*]. In western Panama on the Azuero and Soná Peninsulas, the Paleocene Arc is morphologically distinct from the Oligocene to Quaternary Cordillera Central, being deeply eroded so that the intrusive core of the former arc is exposed in low lying hills rarely reaching elevations above 500 m. The Paleocene arc in eastern Panama forms a pronounced morphological feature extending from the Serranía de San Blas to the Serranía de Darien reaching elevations of 1875 m at the Colombian border. The Cordillera Central in western Panama however forms the most dramatic mountain range in Panama reaching an elevation of 3475 m.

The western Panamanian Oligocene arc was dominated by a plutonic episode containing intrusive dioritic, granodioritic and granitic series [*de Boer et al., 1988; Drummond et al., 1995*]. An augite-hornblende-biotite diorite located on Volcan Barú yielded a K/Ar age of 31.2 ± 2.3 Ma [*de Boer et al., 1995*] and the Petaquilla batholith an age of 29.0 ± 0.4 Ma [*Kesler et al., 1977*]. This intrusive episode in western Panama is contemporary with the tholeiitic gabbro group of the Cordillera de Talamanca in Costa Rica (35-30 Ma) [*Drummond et al., 1995*].

According to the Geological map of Panama [1991], the Early Miocene San Pedrito group extends from western Panama north of the Azuero and Soná Peninsulas through Panama City to the western part of the Las Perlas Archipel. The San Pedrito group is characterized by basaltic to andesitic lavas, tuffs and conglomerates. During the Middle to Early Late Miocene ($14.8-7.1$ Ma), subduction-related volcanism was restricted to western Panama and is divided into three groups on the Geological map of Panama [1991]. The Cañazas group is the dominant group of the Miocene arc and is composed of basaltic to andesitic lavas and tuffs. *Kesler et al.* [1977] published a K/Ar age determination for a whole rock sample from the Cañazas group of 17.5 ± 0.6 Ma. The La Yeguada Formation in the center of the Cordillera Central is characterized by dacitic to rhyolitic volcanic rocks. The El Valle Formation consists primarily of dacitic lavas, breccias, ignimbrites and tuffs with subordinate basalts to andesites. *Defant et al.* [1991a,b] determined for calcalkaline volcanism of the La Yeguada Volcanic Complex an age range of 14 to 7 Ma and for El Valle of 10 to 7 Ma using the K/Ar technique. A new magmatic formation of middle Miocene age was defined by *Coates et al.* [2003] for the Bocas del Toro area. The Valiente Formation consists of columnar jointed basalts, flow breccias, pyroclastic deposits and coral-reef limestones, $^{40}\text{Ar}/^{39}\text{Ar}$ ages of the formation range from 12.0 ± 0.05 Ma to 12.1 ± 0.05 Ma. By 16 Ma, a submarine volcanic arc developed in the region of Bocas del Toro, which emerged above sea

level by ca. 12 Ma, forming an archipelago of volcanic islands [Coates *et al.*, 2003]. A dike that intruded in the Valiente Formation yielded $^{40}\text{Ar}/^{39}\text{Ar}$ plateau ages of 8.4 ± 0.05 and 8.5 ± 0.06 Ma [Coates *et al.*, 2003].

Geochemically distinct adakitic and high-Nb basaltic magmatism replaced calc-alkaline volcanism in the Pliocene (~5 Ma ago) [Defant *et al.*, 1991a,b]. The adakitic rocks have andesitic to rhyolitic but mainly dacitic compositions and are characterized by high Sr/Y, low Y and heavy rare earth element contents. The oldest dated adakitic rock from the La Yeguada volcanic complex (western Panama) produced a K/Ar age of 4.47 ± 0.23 Ma [Defant *et al.*, 1991b]. Between 4.5 ± 0.23 and 0.22 ± 0.07 Ma, adakites were erupted in the Central Cordillera of western Panama extending from El Barú to El Valle volcano and the eastern part of the Cordillera de Talamanca [Defant *et al.*, 1991a,b; de Boer *et al.*, 1995]. In comparison to the adakitic rocks, the alkali basalts have higher Nb and lower Sr/Y. High-Nb, alkali basalts in Panama yielded K/Ar ages of 0.52 ± 0.08 at the La Yeguada volcanic complex and 2.4 ± 0.1 Ma at Cerro Jesus [Defant *et al.*, 1991b; Defant *et al.*, 1992]. A high-Nb, alkali basaltic stage in Costa Rica started at least 5.8 ± 0.9 Ma ago and lasted at least until 1.2 ± 0.4 Ma [Abratis and Wörner, 2001; Tournon, 1984].

The subduction of the Cocos and Coiba ridges probably caused Pliocene uplift of the southern Central American Arc [de Boer *et al.*, 1995], which may have been responsible for the closure of the Panamanian Isthmus at ~3.6 Ma [Hoernle *et al.*, 2002]. Okaya and Ben-Avraham, [1987] and de Boer *et al.*, [1988] document active volcanism throughout western Panama during the Quaternary. Behling [2000] found evidence for at least three volcanic eruptions during the last 2000 years at Volcan Barú. Tephra layers of two minor eruptions dated at 1800 and 1000 yr BP and a 20 cm thick tephra layer of a major volcanic eruption dated at 1550 ± 10 yr (all ages determined with the ^{14}C method). Defant *et al.* [1991b] infers that a 360 ± 80 yr BP old peat layer in the La Yeguada volcanic complex dates the Media Luna lava flow. Thus the La Yeguada volcanic complex is presumed to be active.

1.2 Tectonic overview

Panama is situated at the junction of 5 plates: the North American, Caribbean, Cocos, Nazca and South American Plates. The Panama microplate overrides the Caribbean plate to the north at a rate of 7-11 mm/year [Kellog *et al.*, 1995], forming the North Panama Deformed Belt (NPDB). The Cocos plate subducts beneath southern Costa Rica and western Panama at rate of 72 mm/year [Kellog *et al.*, 1995]. Three seismically active N-S-trending, right-lateral strike-slip fracture zones (Panama, Balboa and Coiba) form a 70-km-wide, right-lateral transform boundary between the Cocos and Nazca plates [Adamek *et al.*, 1988; Kolarsky and Mann, 1995]. The fracture zones extend beneath the South Panama Deformed Belt (SPDB), an accretionary prism complex developed along the continental slope. Magnetic anomalies on

the Nazca Plate constrain a northwestward jump in the Cocos-Nazca Plate boundary at 11 to 8 Ma [Lonsdale and Klitgord, 1978].

In a seismic study of western Panama, Cowan *et al.* [1995] documented a decrease in seismicity to the east, reflecting a lateral change in stress associated with the geometry of the subducting Nazca plate beneath the region. Deep seismicity events (70-115 km) between the Gulf of Chiriquí and the Cordillera Central define a NE-dipping zone providing evidence for lithosphere subducting beneath Panama [Cowan *et al.*, 1995]. High heat flow along the isthmus (comparable with the Galápagos ridge system and 4 times higher than the Caribbean) [de Boer *et al.*, 1991] and recent volcanism at Barú and the LaYeguada volcanic complexes [Defant *et al.*, 1991b] support Holocene oblique subduction to the NE beneath western Panama [Moore and Sender, 1995; Westbrook *et al.*, 1995]. Active deformation along the SPDB extends eastward to at least longitude 80°30' W (SE Azuero) [Moore and Sender, 1995]. The dip of the subducting Nazca plate is inferred to be 3° to 6° to the northeast [MacKay and Moore, 1990; Kolarsky and Mann, 1995]. A broad 30-km-wide accretionary wedge overlies the subducting Nazca Plate. Sedimentary rocks of the subducting Nazca plate appear to underplate the overriding accretionary wedge [Kolarsky and Mann, 1995]. The Coiba ridge is presently subducting beneath western Panama. Reentrant structures form an about 15 km long deflection of the thrust front of the South Panama deformed belt [Silver *et al.*, 1990; Moore and Sender, 1995]. Arching of the forearc area along an extension of the Coiba Ridge in direction of subduction produced the Ranchería arch [see Fig.2; Kolarsky and Mann, 1995]. Upper Pliocene to Pleistocene sedimentary rocks overlying Eocene basement giving a maximum age of Upper Pliocene for the starting subduction of the Coiba Ridge at this location. Coiba Island, sampled within this study, represents an emergent part of the Ranchería arch, formed by the subduction of the Coiba Ridge.

Left-lateral strike-slip faulting occurs along WNW-ESE-trending faults extending from the Azuero Peninsula to southern Costa Rica [e.g. Okaya and Ben-Avraham, 1987; Kolarsky and Mann, 1995]. The Azuero-Soná fault system appears to be continuous with the Ballena-Celmira fault zone of southern Costa Rica, a strike slip fault or oblique-slip fault separating two distinct basement blocks of the Costa Rican forearc [Corrigan *et al.*, 1990]. Collision of the Coiba Ridge with western Panama and its northeast convergence may be responsible for the origin of these left-lateral strike-slip faults [Vergara Muñoz, 1988]. Major rifting and subsidence in the Gulf of Chiriquí in the Early Pliocene is associated with left-lateral, strike-slip faulting along the western Panamanian Pacific coast [Kolarsky and Mann, 1995].

2 Analytical Procedures

Major and trace element contents are reported in Table 1 and isotope data in Table 2 in section 9. Rock powders were produced by first crushing the samples to 0.5 - 1.0 cm chips. Then rock chips free of obvious signs of alteration and the presence of xenolithic material were picked under the binocular microscope. Chips were ground to a flour in an agate mill. Major and trace elements (SiO₂, Al₂O₃, MgO, Fe₂O₃, CaO, Na₂O, K₂O, TiO₂, MnO, P₂O₅ and Ba, Cr, Ni, Sr, Y, Zr) were analysed with a Phillips X'Unique PW1480 X-ray fluorescence spectrometer (XRF) at IFM-GEOMAR Leibniz Institute for Marine Sciences, Kiel (Germany). Volatile content was measured on a Fisher-Rosemount CWA 5003 infrared photometer. Major elements in all plots are normalized on a volatile free basis. Ca content was corrected assuming that CO₂ comes from CaCO₃. International reference standards JB-2, JB-3 (basalts), JA-2 (andesites), JR-1 (rhyolites) were measured with the samples and results are reported in Table 1 (section 9).

Additional trace elements (Rb, Nb, Hf, Ta, Pb, Th, U and REE) were analyzed by inductively-coupled-plasma mass spectrometer at the institute of Geosciences (University of Kiel), using a VG Plasmaquad PQ1 and a Agilent 7500c ORS quadrupole plasma mass spectrometer. Samples were cooked in a multi-stage acid pressure dissolution with HF-aqua regia-HClO₄. Details of the analytical procedures are reported in *Garbe-Schönberg* [1993]. Reproducibility estimated from duplicate sample preparation and replicate measurements was better than 1.5% RSD for all analyzed elements. International standards JB-2, BIR-1, BHVO-1 and blanks were analyzed with the samples in order to accuracy of the measurements [Tab 1B, section 9].

Sr-Nd-Pb isotopic analyses were carried out on whole rock powders (Sr and Nd) and chips (Pb) that were leached in hot (130°C, 1h) 6N HCl for Sr and 2N HCl (70°C, 1h) for Pb in order to minimize the effects of alteration and sample handling. Chemical separation procedures follow those described in *Hoernle and Tilton* [1991]. Sr and Nd isotopic ratios were analyzed on a TRITON thermal ionization mass spectrometer (TIMS) and Pb isotopic ratios were analyzed on a Finnigan MAT 262 RPQ²⁺ TIMS at IFM-GEOMAR. Both instruments operate in static multicollection mode. Sr and Nd isotopic ratios are normalized within run to $^{86}\text{Sr}/^{88}\text{Sr} = 0.1194$ and $^{146}\text{Nd}/^{144}\text{Nd} = 0.7219$ respectively and all errors throughout the manuscript are reported as 2 σ (95% confidence level). Over the course of the study, NBS987 gave $^{87}\text{Sr}/^{86}\text{Sr} = 0.710258 \pm 0.000008$ (N=51), La Jolla $^{143}\text{Nd}/^{144}\text{Nd} = 0.511846 \pm 0.000005$ (N=49) and our inhouse Nd-monitor SPEX $^{143}\text{Nd}/^{144}\text{Nd} = 0.511711 \pm 0.000006$ (N=39). Sr-Nd replicate analyses (separate digestions) were within the external errors of the standards. NBS981 (n=70) gave $^{206}\text{Pb}/^{204}\text{Pb} = 16.900 \pm 0.007$, $^{207}\text{Pb}/^{204}\text{Pb} = 15.438 \pm 0.009$ and $^{208}\text{Pb}/^{204}\text{Pb} = 36.528 \pm 0.030$ and are corrected to the NBS 981 values given in *Todt et al.* [1996]. Pb replicate analyses (separate digestions) of 14 samples were

within 0.021%/amu. Finally, Sr, Nd and Pb total chemistry blanks were <100 pg and thus considered negligible.

$^{40}\text{Ar}/^{39}\text{Ar}$ ages for 44 igneous rocks are reported in Table 3 and Fig. 3,4. Plagioclase, biotite, amphibole, and matrix were analyzed. Total fusion analyses of feldspar (fsp) single-crystals and matrix (mx) separates using a 25 W Spectraphysics Argon Ion laser connected to a MAP 216 noble gas mass spectrometer were carried out at the Geochronology Laboratory at the IFM-GEOMAR. All samples were irradiated for 144 hours in the 5-MW reactor at the GKSS Research Center in Geesthacht (Germany). For vertical and lateral control of the neutron flux gradient, Taylor Creek rhyolite (TCR) sanidine (Batch 85G003, 27.92 Ma [Duffield and Dalrymple, 1990]) was used as the monitor crystal. Isochron ages (ISA) and weighted mean apparent ages (WMA) were calculated from up to 12 particles of each sample analyzed separately. $^{40}\text{Ar}/^{39}\text{Ar}$ isochron ages are taken as the closing age, if the $^{40}\text{Ar}/^{36}\text{Ar}$ intercept lies outside 2σ standard deviation of the atmospheric value ($^{40}\text{Ar}/^{36}\text{Ar}=295.5$). If $^{40}\text{Ar}/^{36}\text{Ar}$ initial ratios are within the 2σ standard deviation of the atmospheric value, a mean apparent age is calculated assuming the atmospheric value for $^{40}\text{Ar}/^{36}\text{Ar}$. Laser step-heating analyses were primarily conducted using K-bearing matrix (mx), feldspar (fsp) and biotite (bt). Step-heating plateaus comprise three or more contiguous steps and $\gg 30\%$ of total ^{39}Ar released. Plateaus with $<50\%$ of the total ^{39}Ar released must be treated with caution. Probability-of-fit of the weighted-mean age of the steps is greater than 5%. Slope of the error-weighted line through the plateau ages is not different from zero at 5% confidence. Ages of outermost 2 steps on either side of the plateau are not significantly different (at 1.8σ) than the weighted-mean plateau age (6 or more steps only). Outermost 2 steps on either side of the plateau must not have non-zero slopes (at 1.8σ) with the same sign [Ludwig, 2001]. The geological timescale of Palmer and Geissman [1999] is used throughout the paper.

3 Results

3.1 Geochronological results

Paleocene-Early Eocene Arc (61-50 Ma)

The oldest dated rocks of this study are an olivine-rich basalt from the northeastern part of Azuero yielding an $^{40}\text{Ar}/^{39}\text{Ar}$ matrix stepheat age of 60.9 ± 0.47 Ma and an olivine-bearing gabbro from Granita D'Oro (little island onshore NW Coiba Island) with a matrix stepheat age of 59.3 ± 1.2 Ma [Tab.3; Fig.3A]. The latter is part of an intrusion into a pyroclastic breccia. Hence the breccia must at least belong to the Early Paleocene. The breccia consists of highly oxidized (reddish), highly vesicular basaltic clasts suggesting that land was present by the Early Paleocene. An Eocene conglomerate divides the island of Coiba from NW to SE and strikes parallel to two major transform faults. At the east end of the

southern transform fault, feldspar from a cobble in the conglomerate yielded a plateau age at 54.3 ± 1.6 Ma [Tab.3; Fig.3A]. Biotite from a diorite on the Soná Peninsula yielded a plateau age for biotite stepheat analyses of 50.1 ± 0.2 Ma and a plateau for a matrix stepheat analyses at 50.9 ± 0.2 Ma [Tab.3; Fig.3A]. Plagioclase from granodiorites from the intrusive complex of Valle Riquito (Azuelo) yielded $^{40}\text{Ar}/^{39}\text{Ar}$ ages of 49.5 ± 0.2 and 50.6 ± 0.3 Ma [Tab.3, Fig.3A].

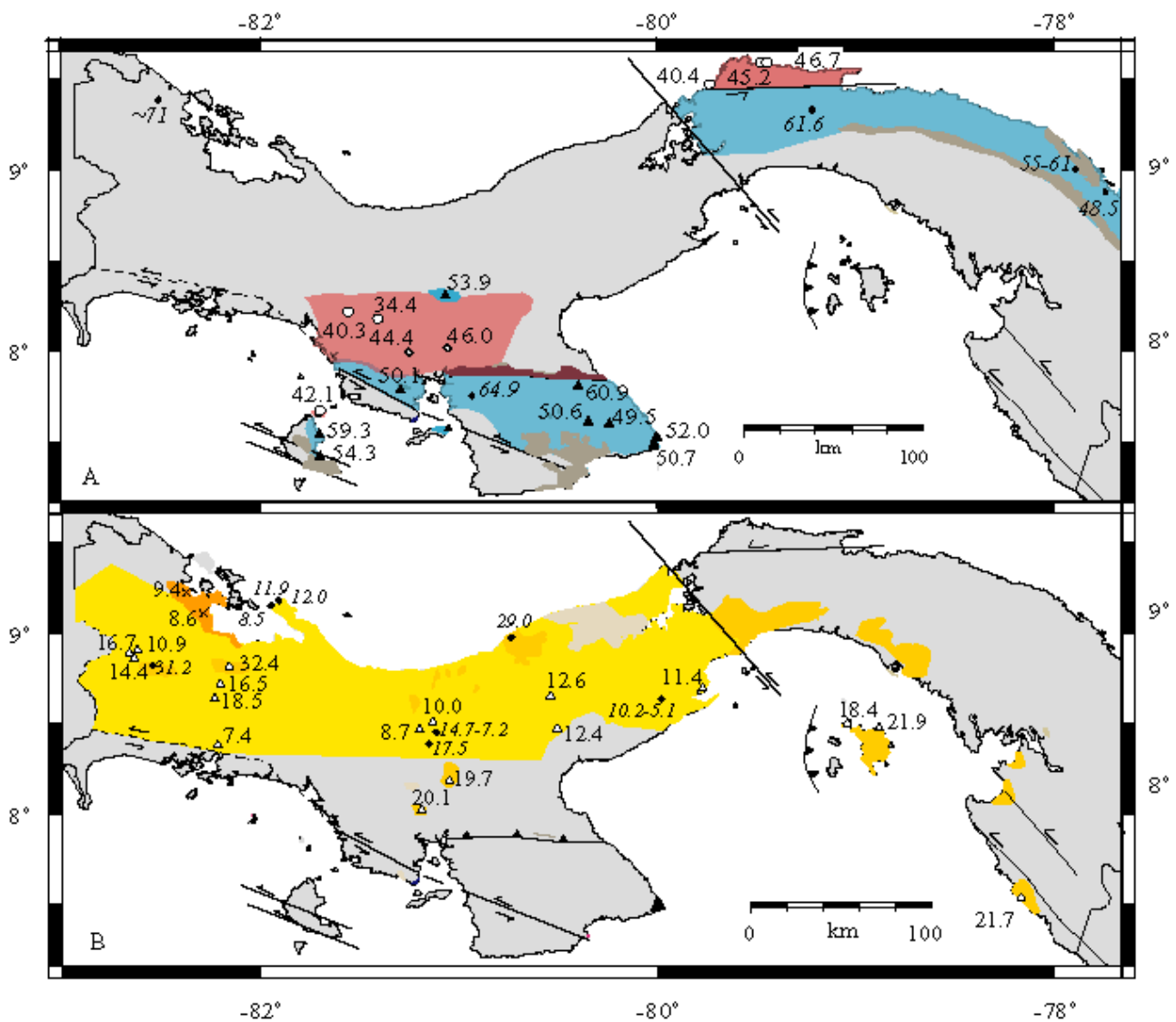


Fig. 3: A) $^{40}\text{Ar}/^{39}\text{Ar}$ ages in Ma for the Early Paleocene to Early Eocene arc (61-50 Ma) and Middle to Late Eocene arc (46-34 Ma). Published ages in italic are from Fisher and Pessagno [1965]; Kesler et al. [1977]; Weyl [1980]; Maury et al. [1995]; B) Oligocene-Miocene arc (32-7 Ma), published ages in italic from Kesler et al. [1977]; de Boer et al. [1995]; Coates et al. [2003]. Symbols are the same as in Fig.2.

A basalt from Punta Mala and a granite from the Represa di Mampostería from the southeastern edge of Azuero Peninsula yielded an weighted apparent mean age of 52.0 ± 0.2 Ma and plateau age of 50.7 ± 0.1 Ma [Tab.3; Fig.3A]. The northernmost Early Eocene sample was found south of the Cordillera Central but north of Santiago. A very fresh andesitic lava flow produced an apparent weighted mean age of 53.9 ± 1.3 Ma [Tab.3; Fig.3A].

The Middle to Late Eocene volcanic arc (47-34 Ma)

A basalt west of the town of Soná yields a feldspar stepheat plateau age of 44.4 ± 0.3 Ma [Tab.3; Fig.3A]. East of Soná, a basaltic andesite produced a plateau age of 46.0 ± 0.2 Ma. On the Island of Ranchería northeast of Coiba, an apparent weighted main age of 42.1 ± 3.0 Ma was determined for an aphyric, basaltic, andesite lava [Tab.3; Fig.3A]. Samples from north of the Soná Peninsula between Santiago and David produced feldspar and matrix stepheat plateau ages of 40.3 ± 0.3 and 34.4 ± 0.5 Ma respectively [Tab.3; Fig.3A]. In eastern Panama, along the Caribbean coast east of Colón, basaltic andesitic and andesitic clasts of a volcanic breccia at Playa Damas east of Nombre de Dios yielded matrix stepheat plateau ages of 45.2 ± 0.1 to 46.7 ± 0.3 Ma. At Playa María Chiquita, an andesite produced a matrix stepheat plateau age of 40.4 ± 0.06 Ma [Tab.3; Fig.3A]. In both west and east Panama, the Middle to Late Eocene magmatism primarily outcrops to the north of the Paleocene to Early Eocene volcanism.

The Oligocene to Late Miocene volcanic arc (32-7 Ma)

Only one extrusive Oligocene sample has been dated from the Cordillera Central. A 10 m thick basaltic lava flow from the eastern flank of Cerro Guyabo near Vulcan Barú yielded a matrix stepheat plateau age of 32.4 ± 2.4 Ma [Tab.3; Fig.3B]. Basaltic to andesitic lava flows of Barú, Cerro Pato de Macho and between Santiago and the Soná Peninsula yielded matrix stepheat plateau $^{40}\text{Ar}/^{39}\text{Ar}$ ages of 21.0 ± 0.8 to 16.5 ± 0.4 Ma (N=5) [Tab.3; Fig.3B]. Rocks with basaltic to dacitic composition from Isla del Rey (Las Perlas Archipel) and at Bahía Piña (Darién) in eastern Panama, yielded matrix and plagioclase plateau ages of 18.4 ± 0.3 to 21.9 ± 0.7 Ma [Tab.3; Fig.3B]. A basaltic lava flow from the western flank of Vulcan Barú produced a matrix plateau age of 14.4 ± 0.3 Ma and a basalt from the northeastern side of the volcano produced a stepheat plateau age of 10.9 ± 0.4 Ma [Tab.3; Fig.3B]. A matrix stepheat plateau age of 8.7 ± 0.7 Ma was measured for a plagioclase basalt from the eastern flank of the Cerro Cabeza de Toro (near Santa Fé). East of Santa Fé, a dacite yielded a feldspar stepheat plateau age of 10.0 ± 1.0 [Tab.3; Fig.3B]. Further to the east near Penonomé, a basaltic lava flow yielded a matrix plateau age of 12.4 ± 0.3 Ma [Tab.3; Fig.3B].

Tab. 3: New $^{40}\text{Ar}/^{39}\text{Ar}$ laser ages from the Panamanian arc.

Sample no.	Age [Ma] $\pm 1\sigma$	Rock typ	Location	Type of data	% ^{39}Ar in plateau/ No.of total fusion	MSWD
<i>Paleocene - Early Eocene arc</i>						
G20	52.0 \pm 0.2	basalt	Azuero	Matrix SXX MAA	/10	0.96
G21	49.5 \pm 0.2	granodiorite	Azuero	Plagioclase SXX MAA	/10	2.12
G52	50.1 \pm 0.2	diorite	Sona	Biotite STH PLA	73.0	2.69
	50.9 \pm 0.2	diorite	Sona	Matrix STH PLA	53.0	2.20
AZ-3-1	60.9 \pm 0.5	basalt	Azuero	Matrix STH PLA	99.9	1.4
AZ-17-1	50.7 \pm 0.1	granite	Azuero	Plagioclase STH PLA	39.3	1.4
AZ-51-2	50.6 \pm 0.3	granodiorite	Azuero	Plagioclase STH PLA	50.8	1.5
Co-87-2	54.3 \pm 1.6	bas. andesite	Isla de Coiba	Plagioclase STH PLA	54.5	1.5
Co-91-4	59.3 \pm 1.2	diorite	Isla de Coiba	Matrix STH PLA	67.3	
M132aKH	53.9 \pm 1.3	andesite	W. Panama	Plagioclase SXX MAA	/10	1
<i>Middle Eocene - Early Oligocene arc</i>						
CA-106-1	40.4 \pm 0.1	andesite	E. Panama	Matrix STH PLA	39.4	1.2
CA-111-1	45.2 \pm 0.1	andesite	E. Panama	Matrix STH PLA	90.9	1.16
CA-111-2	46.7 \pm 0.3	bas. andesite	E. Panama	Matrix STH PLA	57.2	3.4
CP-98-1	34.4 \pm 0.5	andesite	W. Panama	Plagioclase STH PLA	99.7	0.59
M35aKH	40.3 \pm 0.3	andesite	W. Panama	Matrix STH PLA	53.6	1.13
M117aKH	44.4 \pm 0.3	bas. andesite	W. Panama	Plagioclase STH PLA	67	0.68
M141KH	46.0 \pm 0.2	basalt	W. Panama	Matrix STH PLA	49	1.4
G64	42.1 \pm 3.0	bas. andesite	Isla de Coiba	Matrix SXX MAA	/7	2.60
<i>Late Oligocene - Late Miocene</i>						
M38KH	7.36 \pm 0.1	andesite	Chiriquí	Matrix STH PLA	39	1.0
M42aKH	10.9 \pm 0.4	basalt	Barú	Matrix STH PLA	50	2
M46aKH	16.7 \pm 0.4	basalt	Barú	Matrix STH PLA	46	1.6
M49aKH	14.4 \pm 0.3	basalt	Barú	Matrix STH PLA	48	1.12
M76aKH	32.4 \pm 2.4	basalt	W. Panama	Matrix STH PLA	99	1.2
M78KH	16.5 \pm 0.3	basalt	W. Panama	Matrix STH PLA	55.9	1.9
M84aKH	18.5 \pm 0.4	basalt	W. Panama	Matrix STH PLA	86	0.88
M124bKH	8.7 \pm 0.7	basalt	W. Panama	Matrix STH PLA	48	1.5
M125aKH	10.0 \pm 1	dacite	W. Panama	Plagioclase STH PLA	97	0.82
M137KH	21.0 \pm 0.8	basalt	W. Panama	Matrix STH PLA	86	0.54
M143KH	20.1 \pm 0.4	andesite	W. Panama	Matrix STH PLA	75	1.16
M155KH	12.6 \pm 0.3	andesite	W. Panama	Plagioclase STH PLA	49.9	1.4
M157KH	12.4 \pm 0.3	bas. andesite	W. Panama	Matrix STH PLA	87	0.76
M164KH	11.4 \pm 0.5	basalt	W. Panama	Matrix STH PLA	64.7	1.11
M210KH	21.7 \pm 0.3	bas. andesite	E. Panama/ Bahía Pina	Matrix STH PLA	67	1.05
M212KH	21.9 \pm 0.7	basalt	E. Panama/Is.del Rey	Matrix STH PLA	91	0.49
M219cKH	18.4 \pm 0.3	dacite	E. Panama/Las Perlas	Plagioclase STH PLA	47	0.74
<i>BVF</i>						
M73KH	9.4 \pm 0.18	bas.trachyandesite	Bocas del Toro	Matrix STH PLA	42	1.4
M69KH	8.6 \pm 0.3	bas.trachyandesite	Bocas del Toro	Plagioclase SXX MAA	/12	1.1
<i>Adakite</i>						
M63aKH	0.5 \pm 0.0	dacite	Burica	Biotite STH PLA	99.8	0.72
M64cKH	1.0 \pm 0.20	andesite	Burica	Amphibole STH PLA	79	0.78
M65aKH	0.1 \pm 0.08	bas. andesite	Chiriquí	Matrix STH PLA	93	0.75
<i>Arc-alkaline</i>						
So-96-1	1.3 \pm 0.1	basalt	Sona	Matrix STH PLA	95.7	1.3
CP-97-1	0.7 \pm 0.3	basalt	Chiriquí	Matrix STH PLA	99.99	0.35
M105aKH	1.4 \pm 0.12	basalt	Sona	Matrix STH PLA	100	0.92
M118bKH	1.2 \pm 0.1	basalt	Sona	Matrix STH PLA	97.2	1.06
M121aKH	4.5 \pm 0.17	basalt	Sona	Matrix STH PLA	73	0.93

SXX = Single-crystal total fusion
 STH = Laser step-heating analysis
 PLA = Plateau age

MAA = Mean apparent age (inverse-variance-weighted)
 ISA = Isochron age
 MSWD = Mean Square Weighted Deviates

An andesite from Cerro Peña Blanca, yielded a feldspar stepheat plateau age of 12.6 ± 0.3 Ma [Tab.3; Fig.3B]; whereas a basalt near the village of Majagual (11 km from Capira, near Panama City) generated a matrix stepheat plateau age of 11.4 ± 0.3 Ma [Tab.3; Fig.3B]. A basaltic trachyandesitic lava flow from the Caribbean coast of Bocas del Toro near Brazo Izquierdo across from Isla Pastores and a diorite near Chiriqui Grande were dated. The first yielded a matrix stepheat plateau age of 9.4 ± 0.18 Ma and the latter a mean apparent age of 8.6 ± 0.2 Ma [Tab.3; Fig.3B]. Finally a columnar jointed andesitic lava flow 24 km east of David (western Panama) generated an $^{40}\text{Ar}/^{39}\text{Ar}$ matrix stepheat plateau age of 7.36 ± 0.09 Ma [Tab.3; Fig.3B].

Late Miocene to Pleistocene volcanism (4.5-0.1 Ma)

On the western side of the Burica Peninsula, andesitic to dacitic lavas yielded $^{40}\text{Ar}/^{39}\text{Ar}$ amphibole and biotite stepheat plateau ages of 0.5 ± 0.02 Ma and 1.0 ± 0.20 Ma [Tab.3, Fig.4]. About 40 km west of David a basaltic andesite produced a matrix plateau age of 0.1 ± 0.08 Ma. A basalt lava flow 63 km west of Santiago overlying an altered scoria cone and phreatomagmatic deposits yielded a matrix plateau age of 4.5 ± 0.17 Ma [Tab.3, Fig.4].

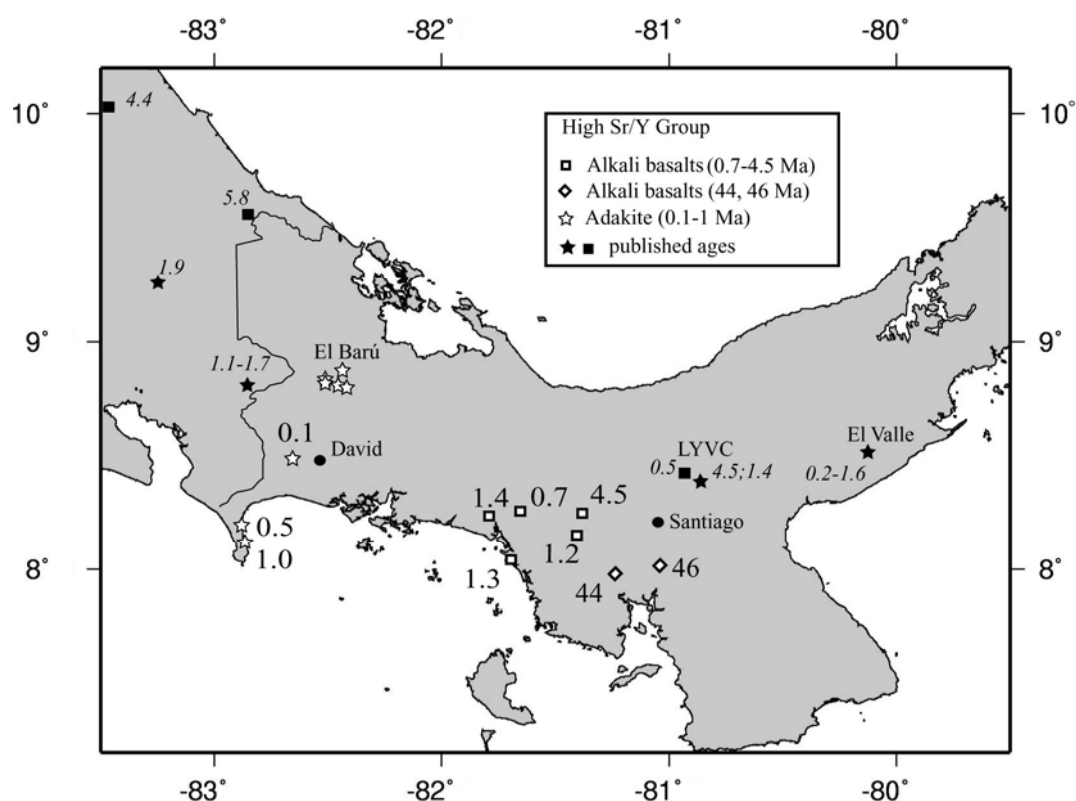


Fig. 4: $^{40}\text{Ar}/^{39}\text{Ar}$ ages in Ma for the Pliocene to Quaternary arc in western Panama and southern Costa Rica. Published ages in italic are from *Defant et al.* [1991a,b], *de Boer et al.* [1995]; *Drummond et al.* [1995], *Abratis and Wörner* [2001]; *MacMillan et al.* [2004].

Younger partly columnar jointed lava flows north of Soná and near Tolé are associated with cinder cones. They produced matrix stepheat plateau ages of 1.4 ± 0.09 Ma to 0.7 ± 0.30 [N=4] [Tab.3, Fig.4].

3.2 Petrography

The Paleocene arc rocks on Azuero Peninsula are characterized by clinopyroxene, olivine and plagioclase bearing basalts and gabbros with accessory Fe-Ti oxides. Early Eocene (49.5-50.6 Ma) intrusive rocks from Coiba Island and Soná and southern Azuero Peninsulas range from dioritic to granitic in composition. Constituent minerals are plagioclase, clinopyroxene, amphibole, biotite, titanomagnetite, quartz and potash feldspar. Secondary minerals are carbonate, serpentine, chlorite and epidote. Clinopyroxene and plagioclase with subordinated magnetite are the dominant phenocrysts of the extrusive rocks from the Early Eocene. East of Panama City, river cobbles of the Serranía de Majé and Serranía de San Blas contain hornblende cumulates partly with hornblende megacrysts (>1cm) and plagioclase. Middle to Late Eocene igneous rocks are basaltic andesitic to andesitic in composition, constituent minerals are plagioclase, clinopyroxene, olivine, amphibole and titanomagnetite, secondary carbonate and chlorite are also present.

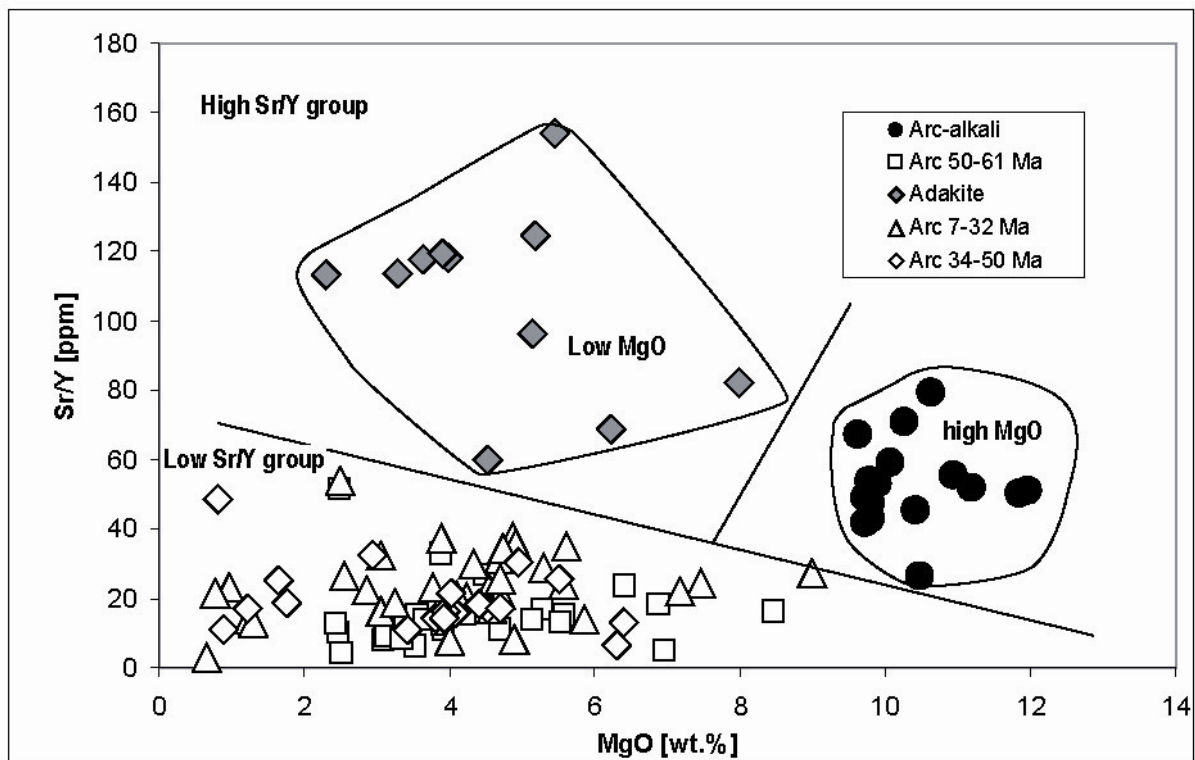


Fig.5: MgO versus Sr/Y diagram divides samples in two major groups: low Sr/Y and high Sr/Y groups. The high Sr/Y group can be subdivided in a low MgO group having adakitic affinities and a high MgO group with alkali basalt affinities.

Oligocene rocks and Miocene rocks west of La Yeguada volcanic complex are basaltic except one basaltic andesite. Olivine, plagioclase and clinopyroxene phenocrysts are present in most of these samples. East of La Yeguada volcanic complex Miocene volcanic rocks range from basaltic andesites to dacites. Plagioclase, clinopyroxene, amphibole with subordinate biotite, orthopyroxene and titanomagnetite represent their characteristic phenocryst assemblage. Intrusive rocks of this period outcrop at Bahia Piña, a gabbro sill with large (>1cm) plagioclase phenocrysts and a hornblende-plagioclase diorite of Isla Viveros (Las Perlas Islands).

Rocks younger than 5 Ma can be divided into two groups. 1) Alkali basalts (4.5–0.7 Ma) have olivine and clinopyroxene phenocrysts and subordinate plagioclase. One sample was found with quartz phenocrysts, which are interpreted as crustal xenocrysts. 2) Basaltic andesites to dacites (1-0.1 Ma) contain olivine, clino- and orthopyroxene, amphibole and biotite phenocrysts.

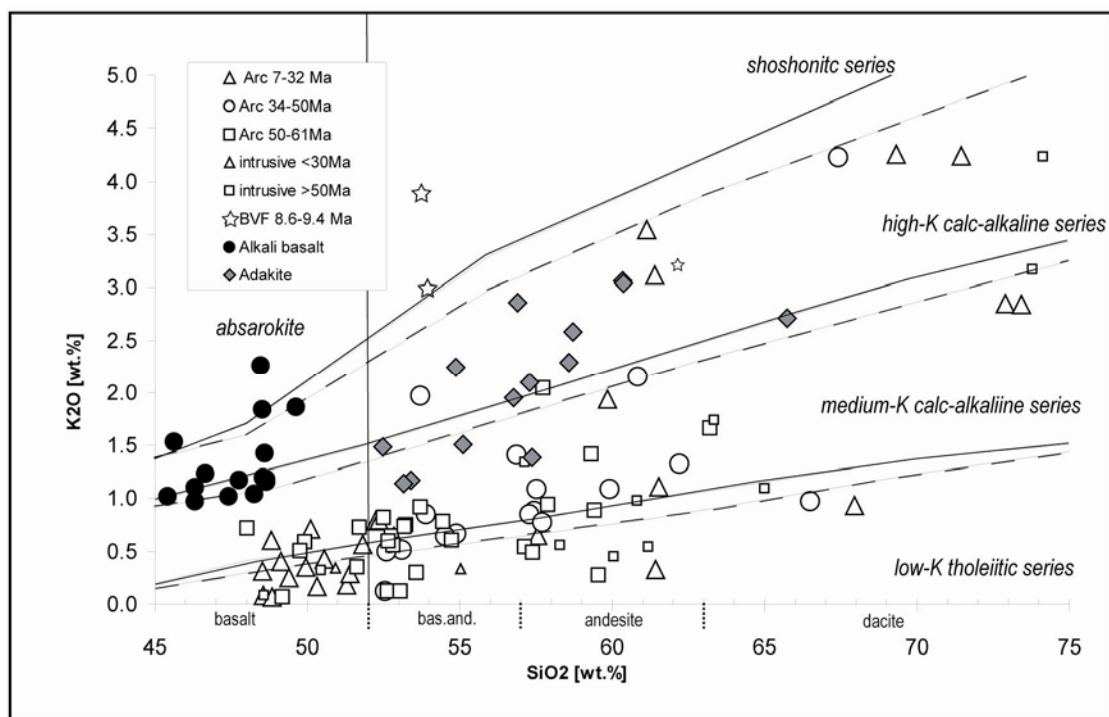


Fig.6: Silica versus K_2O diagram shows that there is a systematic progression with time in the low Sr/Y group from the low-K tholeiitic to the high-K calc-alkaline series. An exception are the Oligocene and western Miocene arc samples which are mainly basaltic belonging to the Low-K tholeiitic series. Late Miocene behind volcanic front (BVF) samples are shoshonitic in composition. The high Sr/Y group is more enriched in K_2O . The alkaline rocks range from high-K calc-alkaline to absarokitic whereas the adakitic rocks range from medium to high-K calc-alkaline. Separation lines after *Le Maître et al.* [1989] and *Rickwood* [1989].

3.3 Classification

The investigated rocks have been divided into a high Sr/Y and low Sr/Y group using the MgO versus Sr/Y diagram [Fig.5]. The low Sr/Y group represents the Paleocene through Miocene rocks, whereas the high Sr/Y group defines the Pliocene through Holocene rocks. The high Sr/Y group can be further subdivided into a low MgO group with chemical compositions similar to adakite and a high MgO group with compositions similar to alkali basalts. On the total silica diagram ($\text{Na}_2\text{O} + \text{K}_2\text{O}$ versus SiO_2 , not shown) the high MgO, high Sr/Y group plots within the alkali basalt field. Therefore they are referred henceforth as alkali basalts. On the Silica versus K_2O diagram, the adakites range from medium-K calc-alkaline to high-K calc-alkaline, whereas the alkali basalts range from high-K calc-alkaline, to absarokitic compositions [Fig.6].

The oldest low Sr/Y arc group (50-61 Ma) ranges primarily from low-K tholeiitic to medium-K calc-alkaline, whereas the intermediate arc group (34-50 Ma) is primarily medium-K calc-alkaline [Fig.6]. The youngest low Sr/Y arc group (7-32 Ma) ranges from low-K tholeiitic to the high-K calc-alkaline series. Oligocene and Miocene arc samples of the youngest low Sr/Y group west of La Yeguada Volcanic Complex are however mainly basaltic belonging to the Low-K tholeiitic series. The Miocene behind the volcanic front volcanism (BVF) is represented by two extrusive shoshonitic, alkaline, samples and one intrusive high-K calcalkaline subalkaline diorite [Fig.6].

3.4 Major and trace elements

3.4.1 Low Sr/Y group

With decreasing MgO the low Sr/Y group displays decreasing FeO, CaO, TiO_2 , Ni and Cr but increasing SiO_2 , K_2O , Na_2O , Rb, Nb, Ba, Y and Zr. Al_2O_3 and P_2O_5 initially increase and then decrease [Fig.7]. These trends are consistent with fractionation of olivine, clinopyroxene, Fe-Ti oxides and plagioclase beginning at MgO ~5 wt.%. All age groups of the low Sr/Y suite display overlapping trends on the MgO variation diagrams. Behind the volcanic front basaltic trachyandesitic and dioritic samples of the Caribbean coast of western Panama (Bocas del Toro) demonstrate lower SiO_2 content at the same MgO compared to the coeval rocks of the volcanic front and elevated incompatible element abundances (i.e. Ba >1300 ppm, K >36200 ppm, Sr >824 ppm, Nb >11.8 ppm, Ta >0.73 ppm, Zr >178 ppm). Relative enrichment of Nb ($(\text{Nb}/\text{Ti})_{\text{N}}=3.77 \pm 0.24$, N=3; young arc: $(\text{Nb}/\text{Ti})_{\text{N}}=1.00 \pm 0.49$, N=6) to other incompatible elements proves its evolved character compared to the coeval rocks of the volcanic front.

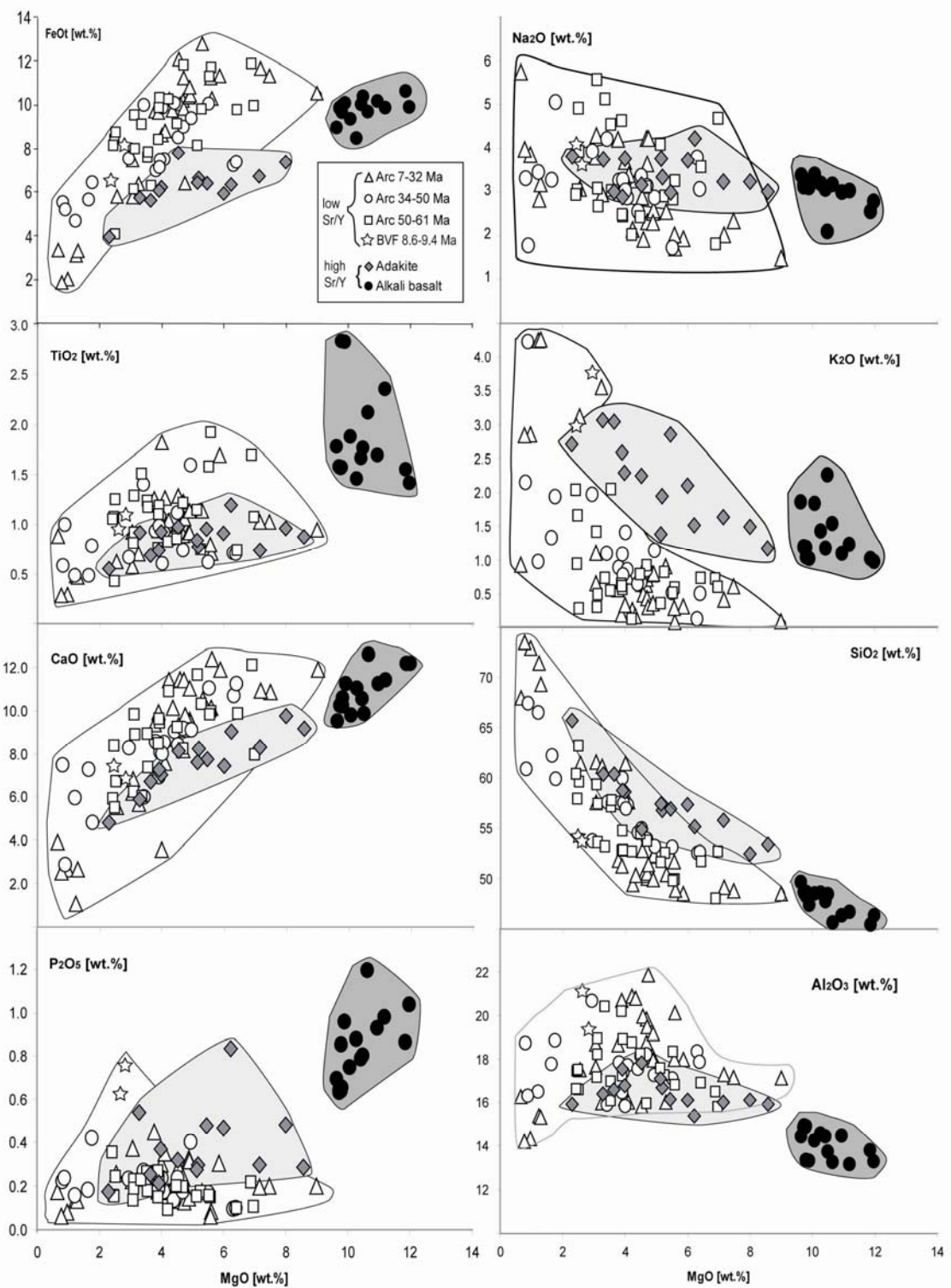


Fig. 7 A: Harker variation diagrams for MgO versus major elements.

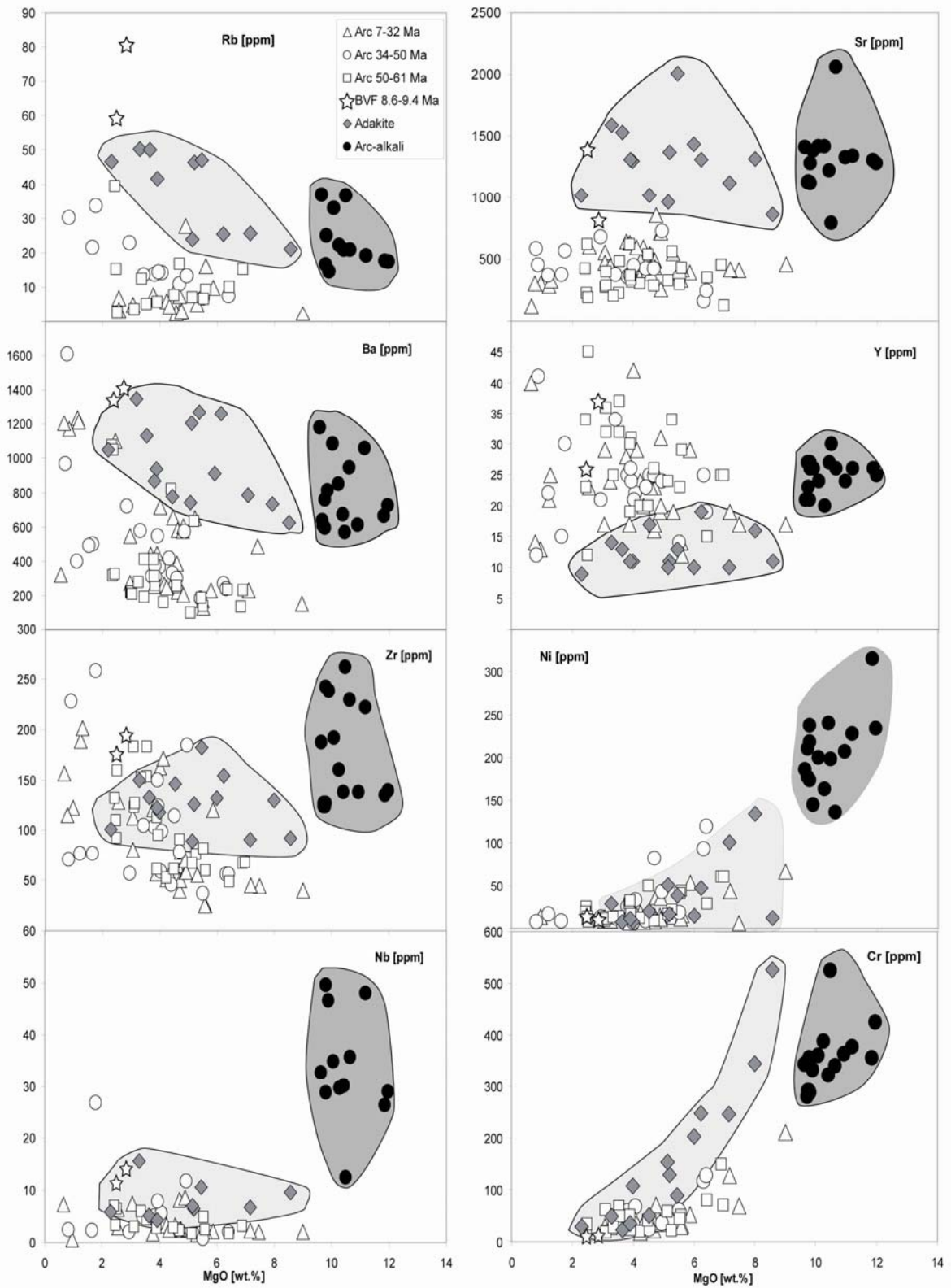


Fig. 7 B: Harker variation diagrams for MgO versus trace elements

The 7-61 Ma low Sr/Y arc samples display typical arc-like characteristics on the multi-element diagram, such as peaks at mobile elements (i.e. large-ion lithophile elements LILE: Rb, Ba, K, Sr) and troughs at immobile high-field strength elements (HFSE e.g. Nb, Ta, Zr, Ti) [Fig.8]. High ratios of large-ion lithophile elements to high-field strength elements can be e.g. shown by $(\text{Ba/Nb})_{\text{N primitive mantle}}=12.1 \pm 8.5$, $N=50$, where subscript N denotes normalized to primitive mantle. Relative depletion of Nb and Ta (e.g. $(\text{Nb/La})_{\text{N}}=0.43 \pm 0.18$, $N=48$) to other incompatible elements is also characteristic for subduction-related rocks. Trace element characteristics (e.g. multi-element diagram patterns) are very similar for each age group. Whereas behind the volcanic front samples show enrichment in highly to moderately incompatible elements regardless if fluid mobile or not. Behind the volcanic front samples have higher Th/Yb values ($(\text{Th/Yb})_{\text{N}}=10.5 \pm 2.6$, $N=3$) than the arc samples $(\text{Th/Yb})_{\text{N}}=1.54 \pm 0.71$, $N=35$. Ratios of large-ion lithophile elements to high-field strength elements are comparable to the volcanic front rocks (7-61 Ma). $(\text{Ba/Nb})_{\text{N}}$ in the behind the volcanic front is 10.5 ± 1.4 , ($N=3$), for example. Low $(\text{Sm/Yb})_{\text{N}}$ of 1.5 ± 0.28 , ($N=35$) suggests melting in equilibrium with spinel peridotite [Fig.8].

3.4.2 High Sr/Y group

The high Sr/Y group has lower FeO, CaO, Y but higher SiO₂, K₂O, Sr, Ba and Rb at a given MgO than the low Sr/Y group. The high Sr/Y group has higher concentrations of moderately to highly incompatible elements compared to the low Sr/Y group.

High MgO, high Sr/Y group - alkali basalts

The alkali basalts are characterized by high FeO, CaO, TiO₂, P₂O₅, Nb, Ni, Ba, Sr, Zr and Cr and low SiO₂, Na₂O, and Al₂O₃. Alkali basalts have high MgO (9.6-12.0 wt.%), Ni (136-315 ppm) and Cr (280-524 ppm) indicating their primitive nature. Nb concentrations of the alkali basalts (Nb=12.4-49.6 ppm) range from ocean island basalts (OIB)-like (*Sun and McDonough*, 1989; Nb=48 ppm) to adakitic concentrations (4.3-10.7 ppm). The alkali basalts appear to have only undergone minor fractionation of olivine and clinopyroxene, consistent with the observed phenocryst phases.

Typical arc-like characteristics, such as peaks at mobile elements (i.e. large-ion lithophile elements LILE, e.g. Rb, Ba, K, Sr) and troughs for nearly all samples at the immobile high-field-strength elements (HFSE, e.g. Nb, Ta, Zr, Ti) are displayed by the high MgO high Sr/Y group on the multi-element diagram [Fig.8]. Low ratios of large-ion lithophile elements to high-field strength elements is illustrated by $(\text{Ba/Nb})_{\text{N primitive mantle}}=2.72 \pm 0.88$, $N=13$. Steep HREE patterns are similar to OIB but the concentrations of most HREE's are

lower than in OIB [Fig.8]. The steep HREE patterns and high $(\text{Sm}/\text{Yb})_{\text{N primitive mantle}}=5.59 \pm 0.64$ (N=13) indicate residual garnet in the source.

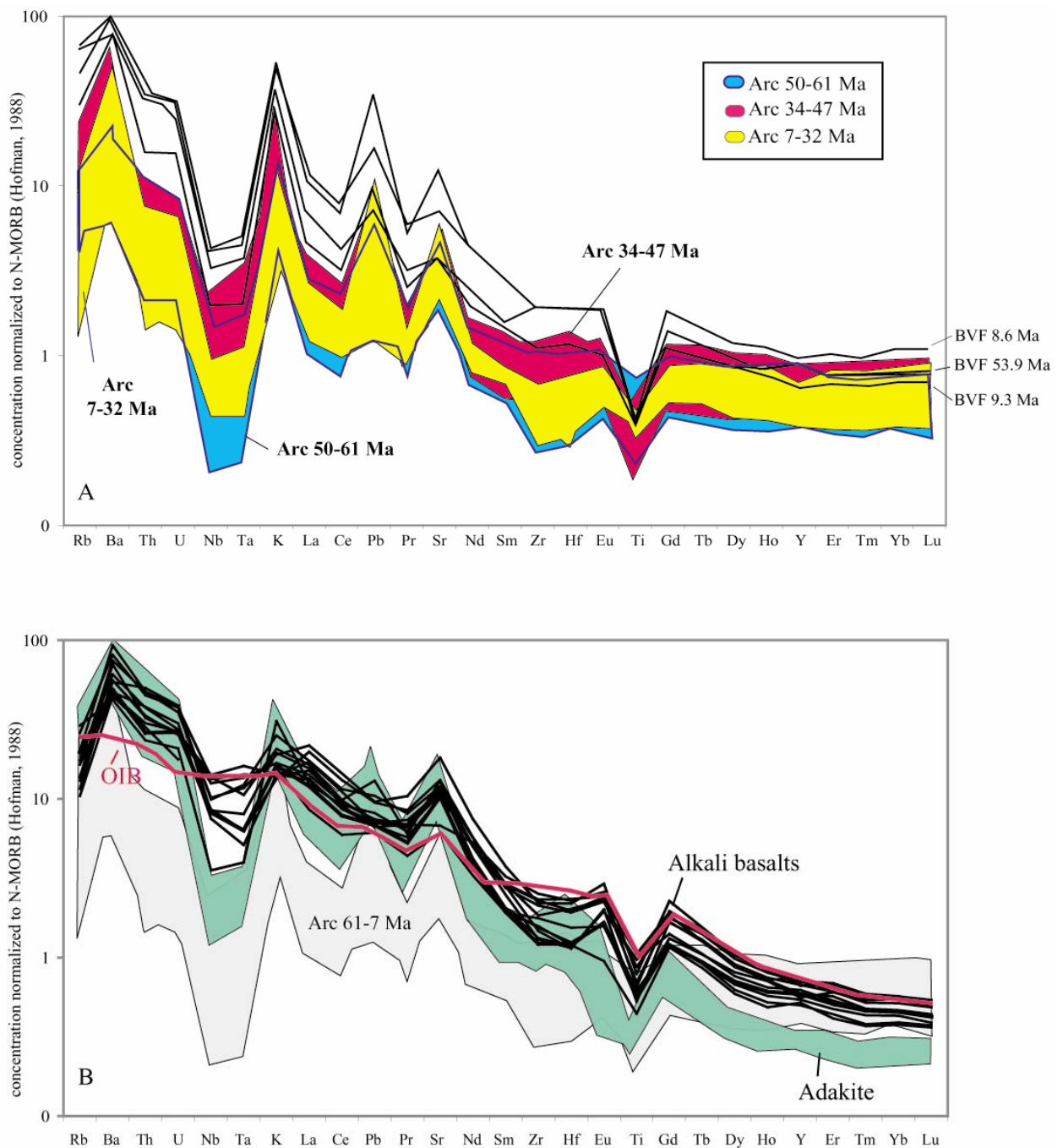


Fig. 8 A: Multi element variation diagrams for the 61-7 Ma arc rocks of Panama. Behind the volcanic front (BVF) samples of the Paleocene and the Late Miocene arc displays higher concentrations for all trace elements
 B: Multi element variations diagrams for the <7 Ma arc rocks of Panama. High Sr/Y group with adakite and alkali basalt subgroups. The 61-7 Ma old arc rocks (shaded field) and average OIB [Sun and McDonough, 1989] are shown for reference.

Low MgO, high Sr/Y group - adakites

Adakitic rocks have similar major element content as the low Sr/Y group but show a flatter positive correlation for FeO_t and higher values for Ba, Nb, Sr and are more depleted for Al₂O₃ and Y compared to most arc rocks [Fig.7]. The adakites have MgO contents of 2.3-8.6 wt.%, SiO₂ is mostly higher than 56 wt.%, and they are characterized by high Sr (861-2006 ppm), Nb (4.3-10.7 ppm), and Cr (23-526 ppm) and low Al₂O₃ (15.4-17.8 wt.%). With decreasing MgO, low-MgO adakites display decreasing FeO_t, CaO, TiO₂, P₂O₅, Ni and Cr but increasing SiO₂, K₂O, Na₂O, Al₂O₃, Nb, Ba and Zr [Fig.7].

On the multi-element diagram adakites demonstrate typical arc-like characteristics, such as peaks at mobile elements (e.g. LILE) and troughs at immobile elements (e.g. HFSE) [Fig.8]. They however show steeper HREE patterns than the low Sr/Y group and $(\text{Sm}/\text{Yb})_{\text{N primitive mantle}} = 4.75 \pm 1.18$ (N=10). Normalized ratios of highly incompatible to less incompatible elements are higher in the adakites $((\text{La}/\text{Yb})_{\text{N primitive mantle}} = 26.8 \pm 14.5, \text{N}=10)$ than for the arc-related rocks $((\text{La}/\text{Yb})_{\text{Arc}} \sim 1)$.

Comparison of high and low MgO high Sr/Y subgroups

On several diagrams, for example MgO versus Cr, Nb, Ba, Zr and possibly TiO₂, the two high Sr/Y groups form distinct subparallel trends, suggesting that they are derived from distinct parents. The trends with decreasing MgO of each group probably reflect minor differentiation.

The contents of mobile elements overlap in the adakites and alkali basalts, but the adakites show a more pronounced relative depletion in Nb and Ta typical for island-arc-related rocks. The adakitic rocks are more depleted in the HFSE and HREE than the alkali basalts [Fig.8].

3.5 Isotopes

3.5.1 Sr-Nd-Pb isotope data

The Sr-Nd-Pb isotope data are summarized in Table 2. The western Panamanian arc rocks (7-61 Ma) form a crude negative correlation on the ⁸⁷Sr/⁸⁶Sr versus ¹⁴³Nd/¹⁴⁴Nd isotopic correlation diagram [Fig.9] with ⁸⁷Sr/⁸⁶Sr ratios ranging from 0.703360 – 0.703968 and ¹⁴³Nd/¹⁴⁴Nd ranging from 0.512946 – 0.513021. Adakitic and alkali basalt samples extend to lower ¹⁴³Nd/¹⁴⁴Nd ranging from 0.512689 to 0.513005. Arc rocks form general positive correlations on the ²⁰⁶Pb/²⁰⁴Pb versus ²⁰⁷Pb/²⁰⁴Pb and ²⁰⁸Pb/²⁰⁴Pb isotope diagrams [Fig.9,10].

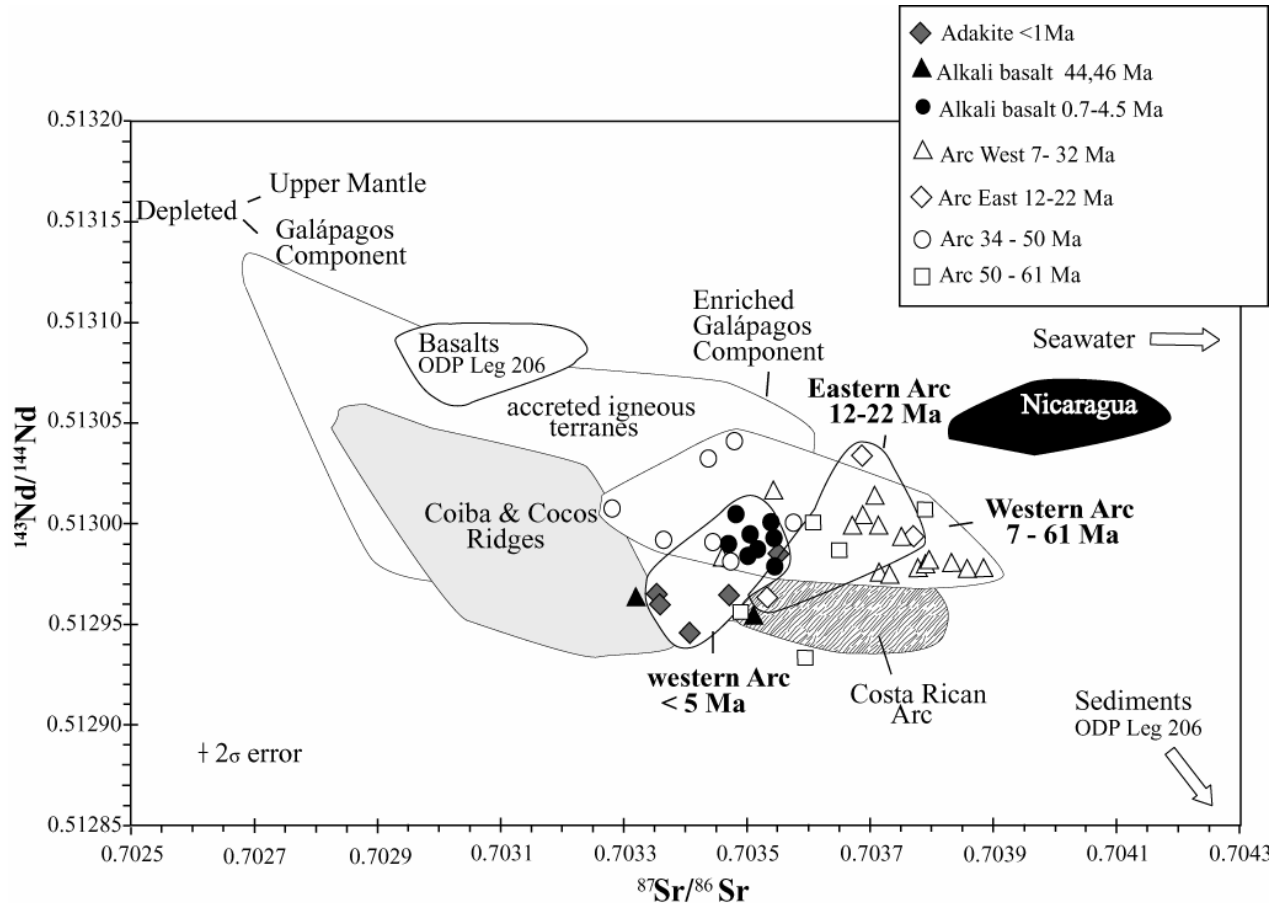


Fig. 9: Temporal variations of $^{87}\text{Sr}/^{86}\text{Sr}$ vs. $^{143}\text{Nd}/^{144}\text{Nd}$; fields of the recent Galápagos hotspot track (Coiba and Cocos Ridges) [Hauff *et al.*, 2000a, Hoernle *et al.*, 2000, Werner *et al.*, 2003], Galápagos hotspot accreted igneous complexes [Hoernle *et al.*, 2002; Lissinna *et al.*, in prep.], central Nicaragua [Hoernle *et al.*, unpub. data], central Costa Rica (VF) <2 Ma [Hoernle *et al.*, unpub. data] and sediments from ODP Leg 206 [Hoernle *et al.*, unpub. data] are shown for reference.

For the Panamanian arc rocks a fairly large range in $^{206}\text{Pb}/^{204}\text{Pb} = 18.730 - 19.324$, $^{207}\text{Pb}/^{204}\text{Pb} = 15.535 - 15.594$, $^{208}\text{Pb}/^{204}\text{Pb} = 38.418 - 39.046$ was measured [Tab.2]. On the $^{206}\text{Pb}/^{204}\text{Pb}$ versus $^{143}\text{Nd}/^{144}\text{Nd}$ isotopic correlation diagram the data form a crude inverse correlation. The Sr-Nd-Pb isotope data for the Panamanian arc rocks require at least three endmembers. 1) An enriched endmember with isotope ratios of $^{206}\text{Pb}/^{204}\text{Pb} \geq 19.3$, $^{207}\text{Pb}/^{204}\text{Pb} \geq 15.55$, $^{208}\text{Pb}/^{204}\text{Pb} \geq 38.6$, $^{87}\text{Sr}/^{86}\text{Sr} \geq 0.7032$, $^{143}\text{Nd}/^{144}\text{Nd} \leq 0.51295$, having affinities to the HIMU mantle endmember. 2) A depleted endmember with isotope ratios of $^{206}\text{Pb}/^{204}\text{Pb} \leq 18.7$, $^{207}\text{Pb}/^{204}\text{Pb} \leq 15.52$, $^{208}\text{Pb}/^{204}\text{Pb} \leq 38.2$, $^{87}\text{Sr}/^{86}\text{Sr} \leq 0.7032$, $^{143}\text{Nd}/^{144}\text{Nd} \geq 0.51305$, having affinities to MORB. 3) An enriched component with of $^{206}\text{Pb}/^{204}\text{Pb} \leq 18.7$, $^{207}\text{Pb}/^{204}\text{Pb} \leq 15.52$, $^{208}\text{Pb}/^{204}\text{Pb} \leq 38.2$, $^{87}\text{Sr}/^{86}\text{Sr} \geq 0.7038$, $^{143}\text{Nd}/^{144}\text{Nd} \leq 0.51295$, possibly reflecting sediments.

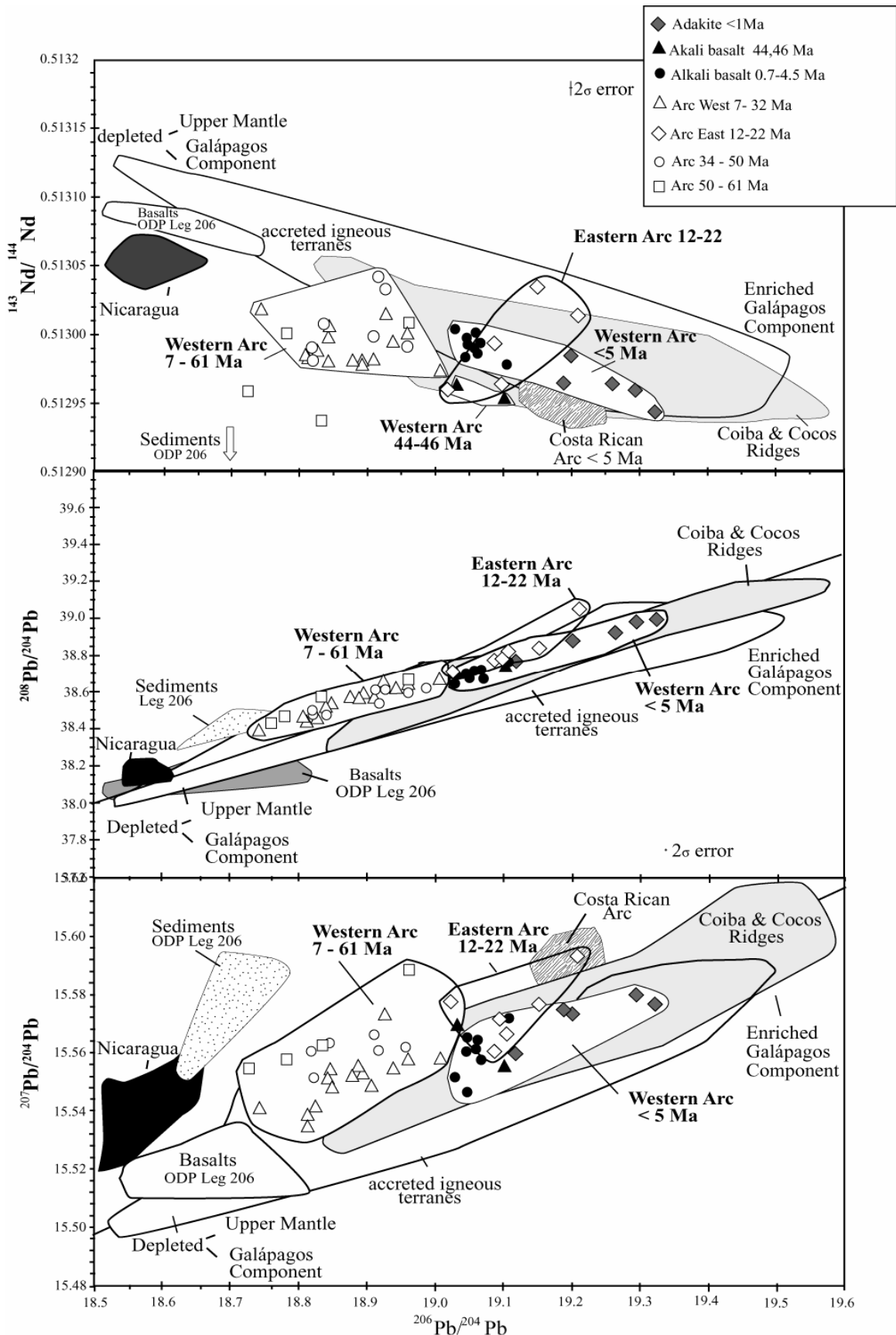


Fig. 10: Temporal variations of $^{206}\text{Pb}/^{204}\text{Pb}$ vs. $^{208}\text{Pb}/^{204}\text{Pb}$ and $^{206}\text{Pb}/^{204}\text{Pb}$ vs. $^{207}\text{Pb}/^{204}\text{Pb}$ vs. $^{143}\text{Nd}/^{144}\text{Nd}$; fields of the recent Galapagos hotspot track (Coiba and Cocos Ridges) [Hauff et al., 2000a, Hoernle et al., 2000, Werner et al., 2003], Galapagos hotspot accreted igneous complexes [Hoernle et al., 2002; Lissinna et al., in prep.], central Nicaragua [Hoernle et al., unpub. data], central Costa Rica (VF) <2 Ma [Hoernle et al., unpub. data] and sediments from ODP Leg 206 [Hoernle et al., unpub. data] are shown for reference.

Despite the large age range in the Panamanian samples (0.1-61 Ma), these data fall in the same trend as data from central Nicaragua to central Costa Rica within the last 2 Ma, although the Panamanian samples do not reach compositions as depleted in Pb isotopic composition as occur in central Nicaragua.

The Panamanian data can be divided into three groups based on age and geographic distribution. 1) The western Panamanian arc samples (7-61 Ma) extending from the boarder with Costa Rica to the Serranía de San Blas, 2) the Miocene eastern arc from La Yeguada volcanic complex to the Colombian border, and 3) the adakitic and alkali basalt group (0–5 Ma). In the western arc group, there are no systematic variations of isotopic composition with age except that the oldest (50-61 Ma) arc group extends to lower $^{143}\text{Nd}/^{144}\text{Nd}$ and higher $^{207}\text{Pb}/^{204}\text{Pb}$ isotope ratios. These samples have compositions similar to samples from the < 2 Ma volcanic front in western Costa Rica and eastern Nicaragua. The Miocene eastern arc is shifted to more enriched compositions than the western arc displaying more radiogenic Pb and slightly less radiogenic Nd isotopic compositions. The isotopic composition of the eastern arc overlaps with those of samples from central Costa Rica < 2 Ma. The adakitic and alkali basalt group has enriched compositions similar to those from the eastern Miocene arc and central Costa Rica < 2 Ma.

3.5.2 Age Correction on isotope data of subduction-related samples

Fractional crystallization may affect the parent/daughter ratios of the different isotope systems ($^{87}\text{Rb}/^{86}\text{Sr}$, $^{147}\text{Sm}/^{144}\text{Nd}$, $^{238}\text{U}/^{204}\text{Pb}$, $^{235}\text{U}/^{204}\text{Pb}$, $^{232}\text{Th}/^{204}\text{Pb}$). The studied subduction-related samples range from basalts to andesites and may be influenced by differentiation processes e.g. fractional crystallization. Variations for the parent/daughter ratios of the $^{87}\text{Rb}/^{86}\text{Sr}$ and $^{147}\text{Sm}/^{144}\text{Nd}$ systems as a function of SiO_2 are negligible ($^{87}\text{Rb}/^{86}\text{Sr}$ mean \pm standard deviation = 0.08 ± 0.066 , $N=50$ and $^{147}\text{Sm}/^{144}\text{Nd} = 0.14 \pm 0.037$, $N=50$). Only one sample (M155) has elevated $^{87}\text{Rb}/^{86}\text{Sr}$ parent/daughter ratios, probably due to low temperature alteration. $^{238}\text{U}/^{204}\text{Pb}$, $^{235}\text{U}/^{204}\text{Pb}$ and $^{232}\text{Th}/^{204}\text{Pb}$ parent/daughter ratios as a function of SiO_2 for the alkali basalts and the adakite group are elevated compared to the tholeiitic to calc-alkaline samples ($^{238}\text{U}/^{204}\text{Pb}_{\text{adakite}} = 20.67 \pm 4.06$ $N=8$, $^{238}\text{U}/^{204}\text{Pb}_{\text{alkali basalt}} = 33.39 \pm 3.31$; $^{235}\text{U}/^{204}\text{Pb}_{\text{adakite}} = 0.15 \pm 0.03$, $^{238}\text{U}/^{204}\text{Pb}_{\text{alkali basalt}} = 0.24 \pm 0.024$; $^{232}\text{Th}/^{204}\text{Pb}_{\text{adakite}} = 74.19 \pm 16.6$, $^{232}\text{Th}/^{204}\text{Pb}_{\text{alkali basalt}} = 111.9 \pm 13.8$). Higher concentrations of U and Th within the alkali basalt and the adakite samples is the reason for their enriched character. The tholeiitic to calc-alkaline samples have lower $^{238}\text{U}/^{204}\text{Pb}$, $^{235}\text{U}/^{204}\text{Pb}$ and $^{232}\text{Th}/^{204}\text{Pb}$ ratios ($^{238}\text{U}/^{204}\text{Pb} = 10.2 \pm 5.6$, $^{235}\text{U}/^{204}\text{Pb} = 0.08 \pm 0.04$, $^{232}\text{Th}/^{204}\text{Pb} = 29.5 \pm 16.6$ $N=30$). The $^{238}\text{U}/^{204}\text{Pb}$, $^{235}\text{U}/^{204}\text{Pb}$ and $^{232}\text{Th}/^{204}\text{Pb}$ parent/daughter ratios are large enough that an age correction over 60 Ma will be

significant. Therefore the samples were age corrected and then projected to the future using the same parent/daughter ratios as for the accreted terranes.

3.5.3 Age Correction on isotope data of accreted terranes

To compare isotopic signatures of the paleo-Galápagos hotspot track to the subduction related samples, initial values were calculated using their parent-daughter trace element concentrations and age data. Initial ratios were then projected to present-day values by adding the radiogenic in-growth according to their age and assumed parent-daughter ratios. The following parent-daughter ratios representative for the Galápagos system were used, $^{87}\text{Rb}/^{86}\text{Sr}=0.048$, $^{147}\text{Sm}/^{144}\text{Nd}=0.15$, $^{238}\text{U}/^{204}\text{Pb}=10$, $^{235}\text{U}/^{204}\text{Pb}=0.07$ and $^{232}\text{Th}/^{204}\text{Pb}=57.5$.

4 Discussion

4.1 Forming of an island arc

At least four major volcanic phases can be distinguished for the Panamanian arc: 1) Early Paleocene to Early Eocene, 2) Middle to Late Eocene, 3) Early Oligocene to Late Miocene and 4) Pliocene to Holocene volcanic phase. Late Cretaceous volcanic rocks, occur along the Changuinola river north of Volcan Barú [*Fisher and Pessagno, 1965*]. Intercalations of volcanic tuffs and flows with paleontologically dated bathyal limestone of the Campanian to Lower Maastrichtian (84-65 Ma) form part of the Changuinola Formation. Based primarily on phenocryst assemblage *Fisher and Pessagno [1965]* interpreted these rocks to be the oldest arc-related volcanic rocks in Panama. Our geochemical analyses of samples from this unit show ocean island tholeiitic character, consistent with these rocks belonging to the Caribbean basement [*Lissinna et al., in prep.*]. Therefore the oldest Panamanian arc rocks appear Paleocene in age.

4.1.1 Early Paleocene to Early Eocene volcanic arc

Remnants of the Early Paleocene to Early Eocene arc (65-49 Ma) can be documented in western Panama at Coiba Island, Central Soná to Azuero and along the Caribbean coast of eastern Panama from Cerro Azul along the Serranía de San Blas to the Colombian border (age data from *Kesler et al. [1977]*; *Maury et al. [1995]* and this study). An Early Paleocene low-K tholeiitic to low-K calc-alkaline stage of arc volcanism is represented by olivine-rich arc tholeiites from east Azuero. Low-K tholeiitic to low-K calc-alkaline volcanic rocks were erupted during the Late Paleocene on the eastern and northern part of Coiba Island. A volcanic breccia of Granita d'Oro (Coiba Island) consists of Late Paleocene (59.3 Ma) reddish, vesicular-rich basaltic clasts. The reddish oxidation and high vesicularity are consistent with subaerial activity during this early stage of arc evolution, reflecting the growth

of this arc on the shallow western flank of the Caribbean oceanic plateau. Early Eocene (49.5-52.0 Ma) intrusive activity has been dated on Azuero and Soná. An Early Eocene andesite (M132KH) with an age of 53.9 Ma outcropping at the southern flank of the Cordillera Central north of Azuero shows similar geochemical characteristics to the Miocene behind the volcanic front rocks and is thus interpreted as an Early Eocene behind the volcanic front sample, consistent with the main volcanic front being located in southern Azuero in the Early Eocene to Paleocene. Sr-Nd-Pb isotope compositions are similar to western Costa Rica and eastern Nicaragua which may indicate the nearby presence of a subducting Galápagos hotspot track [Hoernle *et al.*, 2003].

Late Eocene calcalkaline volcanism was also active in easternmost Panama near to the Colombian border as demonstrated by a quartz porphyry from Rio Pito which yielded a K/Ar age of 49.0 ± 0.6 [Kesler *et al.*, 1977]. The Eocene Rio Pito intrusions have the same age and composition as intrusions along the north coast of Colombia [Tschanz *et al.*, 1974].

4.1.2 Middle to Late Eocene volcanic arc

Middle Eocene to Late Eocene (46-34.4 Ma) subduction-related rocks outcrop between northern Soná and Azuero Peninsulas and south of the Cordillera Central. The younger samples (34-40 Ma) have calc-alkaline affinities, but the samples near Soná (44-46 Ma) have alkali basalt geochemical affinities. They are characterized by enrichment of highly incompatible elements to less incompatible elements such as the HREE (e.g. $(La/Yb)_N^{alkali\ basalt} = 12.69 \pm 2.96$, N=2; $(La/Yb)_N^{calc-alkaline} = 3.00 \pm 0.21$, N=2).

The Middle Eocene arc continuous east of Azuero confirmed by a Middle Eocene section, which were drilled in the Gulf of Panama at the El Paso Corvus-1 well, east of the Azuero Peninsula [Fig.2]. This section consists of sandstone and shale with interbedded basaltic volcanic rocks and associated pyroclastics [Mann and Kolarsky, 1995]. The top of the El Paso Corvus-1 Middle Eocene section is separated from the overlying Plio-Pleistocene section by a major unconformity.

Middle Eocene low-K tholeiites, basaltic andesites and andesites also occur east of the Panama Canal zone along the Caribbean coast. This area is interpreted on the geological map to belong to the Cretaceous Changuinola group. Basaltic andesitic and andesitic clasts of a volcanic breccia at Playa Damas east of Nombre de Dios and a basalt lava flow at Playa Maria Chiquita however yielded ages of 45.2 ± 0.1 to 46.7 ± 0.3 Ma and 40.4 ± 0.06 Ma [Tab.3]. As noted previously, the volcanic rocks in the Changuinola group near Changuinola have compositions similar to the Caribbean basement (CLIP). In contrast to the Middle Eocene alkali basalts from Azuero (44.4-46.0 Ma), the east Panamanian rocks are not alkali basalts. In addition Sr and Pb isotope ratios are more radiogenic in the western Panamanian alkali basalts than in the eastern Panamanian Middle Eocene rocks.

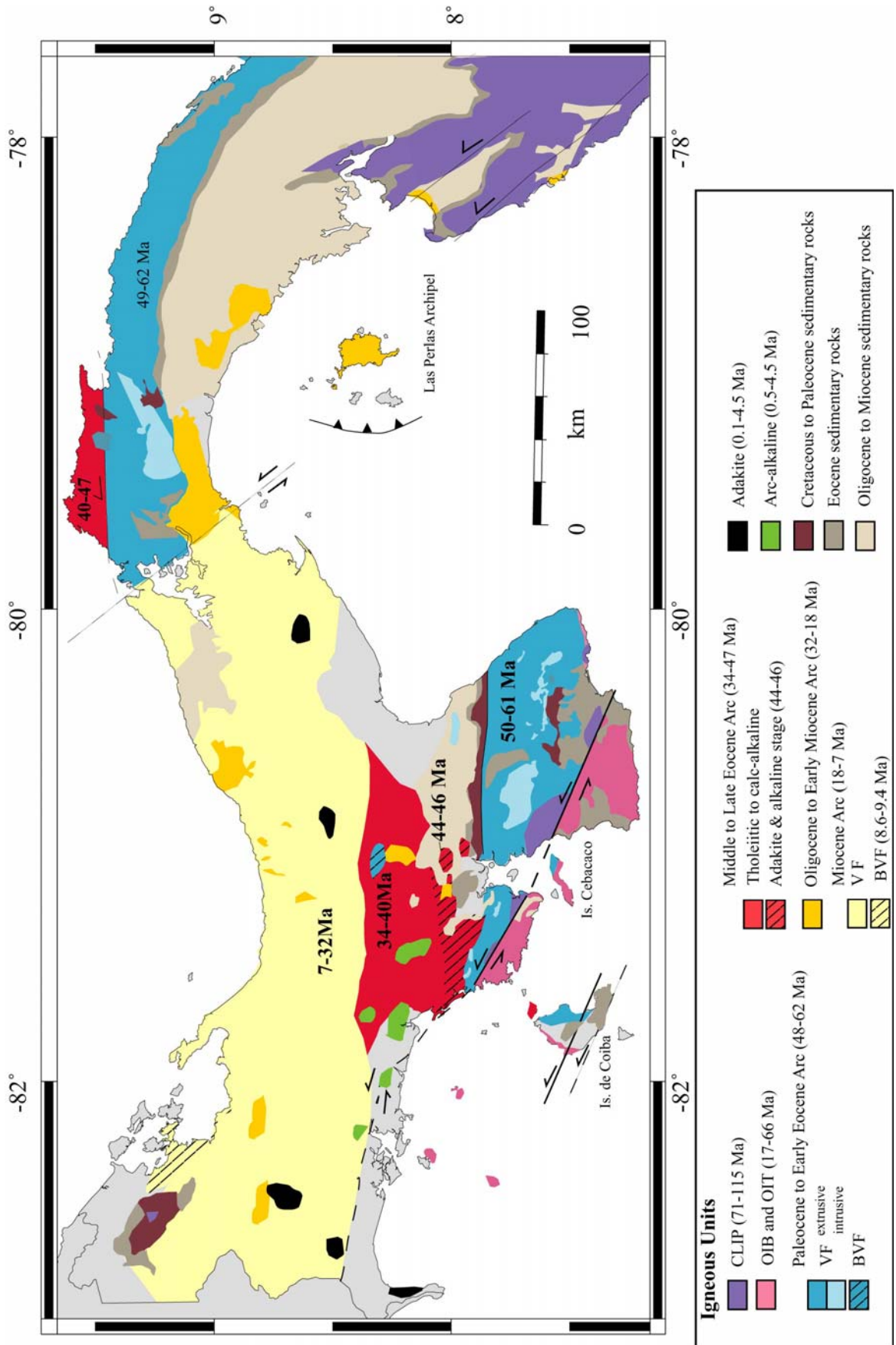


Fig. 11: Geological summary map of Panama based on age dating and composition of volcanic rocks.

Based on gravity data, *Terry* [1956] and *Case* [1974] discussed that parallel to the canal and to the eastern coast of Azuero two major wrench faults with possible left-lateral displacement trend from the Gulf of Panama north-northwest into or across the isthmus. *Case* [1974] and *Recchi* [1975] infer that the gravity data may reflect a concealed fault zone of early Cenozoic age. Based on the Late Eocene (40.4 Ma) old rocks at the northern coast of central eastern Panama near Colon and the formation of the Early Miocene (from 21.9 Ma) arc extending from Costa Rica to Colombia as shown below, displacement of the arc has to be accomplished between 40 and 22 Ma. According to *Woodring* [1955], a northwest-trending fault west of the canal zone does not cut the Oligocene and younger sequence. *Recchi* [1975] believed that all strike slip motions were most likely accomplished during the Late-Middle Eocene. *Maury et al.* [1995] assumed that the offset of the arc was most probably accomplished during the Late Oligocene. Based on our new ages from the Caribbean coast of eastern Panama, we propose that the eastern and western Panamanian Paleocene to Late Eocene arc was a continuous zone until the Early-Late Eocene (~40 Ma). During the Late Eocene to Oligocene ~40-24 Ma, a left-lateral displacement shifted eastern Panama to the north relative to western Panama.

4.1.3 The Oligocene Miocene arc

Oligocene volcanism is rare in western Panama. A mafic Oligocene stage of arc volcanism is represented by a tholeiitic basalt at the eastern flank of the Cerro Guyabo near Volcano Barú (MgO= 9 wt. %, 32.4 Ma), suggesting that Oligocene volcanism may have been buried by voluminous Miocene volcanism in the same area. This Oligocene and Miocene phase of volcanism outcrops further northward compared to the Paleocene-Eocene arc volcanism indicating that the northward migration of arc volcanism occurred over at least 20 Ma from ~50 to ~30 Ma.

From Panama City to the east, Oligocene volcanism forming the Majé and Panama group has been suggested based on stratigraphic relationships [*Geological map of Panama*, 1991]. The Panama group crops out mainly around Panama City and the Majé group flanks the Chucunaque basin to the north and partly to the south suggesting a syncline. These groups consist of basaltic to andesitic lavas, pyroclastic rocks and agglomerates.

Passage of a transform fault over the Galápagos hotspot caused breakup of the Farallon plate at 23 Ma into the Cocos and Nazca Plates and spreading at the former transform fault [*Handschuhmacher et al.*, 1976]. Early Miocene volcanism (22-14 Ma), extending from Barú to Bahia Piña (Darien), followed formation of the Galápagos or Cocos-Nazca spreading center. *de Boer et al.* [1995] infers that subduction was directed northeast and the subduction angle appears to have decreased during the Oligocene. A shallowing of the dip of the subducting slab is consistent with a widening of the volcanic front in the Oligocene

and Miocene and a cessation of the northward migration of the arc, presumably reflecting decreased tectonic erosion associated with a more shallow subduction angle. Early to middle Miocene (~22-12 Ma) arc volcanism shows differences in chemistry between western and eastern Panama. The eastern Panamanian rocks have more radiogenic Pb isotopic compositions than the coeval western Panamanian rocks and Pb-Nd-Sr isotopic compositions similar to seawater-altered portions of the subducting Cocos and Coiba Ridges and to Late Eocene to Miocene accreted Galápagos hotspot terranes. Therefore we interpret the more Galápagos-type geochemical composition to reflect migration of the subducting Galápagos hotspot track to the east relative to the island arc.

A second Miocene volcanic phase ranging from tholeiitic to high-K calcalkaline in composition took place between 13-7 Ma but has thus far only been found in western Panama west of the canal zone and in eastern Costa Rica [i.e. *Defant et al.*, 1992; *Drummond et al.*, 1995; *Abratis*, 1998]. Two Middle Miocene (14.4 Ma, 10.9 Ma) lavas were dated on Vulcan Barú. Their stratigraphic position indicates that much of the base of this volcano is Miocene.

Late Miocene (8.6-9.3 Ma) volcanism in the Bocas del Toro area has higher moderately to highly incompatible element contents, typical for behind the volcanic front volcanism (BVF). A dike within the Valiente Formation with an age of 9.5 Ma [*Coates et al.*, 2003] may belong to the behind the volcanic front volcanism.

Calcalkaline volcanism in the Cordillera Central ceased in the Late Miocene at ≤ 7 Ma and in Costa Rica at 3.5 Ma ago [*Defant et al.*, 1991a; *Gans et al.*, 2003].

4.1.4 Pliocene-Holocene adakitic and alkaline volcanism in western Panama

During the late Miocene-Early Pliocene the slab dip of the Cocos plate decreased and underplating begun at the thickened crust of the Chorotega block below western Panama and southern Costa Rica [*de Boer et al.*, 1995]. Initial subduction of the Cocos ridge has been proposed around 1 Ma [*Lonsdale and Klitgord*, 1978], 2-3 Ma [*MacMillan et al.*, 2004], 3.5 Ma [*Collins et al.*, 1995; *Gans et al.*, 2003], or 5 Ma ago [*de Boer et al.*, 1995; *Hoernle et al.*, 2002], and 8 Ma [*Abratis and Wörner*, 2001].

Between ca. 7 and 4.5 Ma, there was a dramatic shift in the composition of volcanism in western Panama from tholeiitic and calc-alkaline to adakitic (4.5-0.22 Ma) and alkaline (4.5-0.7 Ma) volcanism. Adakitic rocks were sampled on and north of the Burica Peninsula. These basaltic andesitic to dacitic samples from Panama yielded ages of 0.1 ± 0.08 Ma to 1.0 ± 0.20 Ma (N=3) [Tab.3]. Adakites with similar compositions have been reported from the Talamanca Mountains and further south in southern Costa Rica [*Drummond et al.*, 1995; *de Boer et al.*, 1995; *Abratis and Wörner*, 2001; *MacMillan et al.*, 2004] and range in age from 2.8 to 0.95 Ma. Alkali basalts were erupted in the Central Cordillera of western Panama from El Barú to El Valle Volcanoes and the eastern part of the Cordillera de Talamanca over the

last 5.8 Ma [Defant *et al.*, 1992; de Boer *et al.*, 1995; Abratis and Wörner, 2001]. The alkali basalts sampled in this study outcrop between the Soná Peninsula and the Cordillera Central. The majority of Panamanian alkali basalts (4.5-0.7 Ma) crop out around the landward extension of the subducting Coiba Ridge and Rancheria arch formed by the subduction of the Coiba Ridge. The Plio-Pleistocene Panamanian volcanism was mainly active coeval to the peaks in Costa Rican volcanic activity between 4-6 Ma, 1-2 Ma, 0.4-0.6 Ma and <0.1 Ma [Gans *et al.*, 2003].

Geochemical composition of adakites and alkali basalts is characterized by higher ratios of fluid mobile/ fluid immobile (LILE/HFSE) ratios and enriched Galápagos-like isotopic compositions. They also have higher SiO₂ but lower FeO, CaO and CaO/Al₂O₃ at a given MgO content. Adakites can be produced by melting of hydrous basalts in the mantle wedge or by direct melting of the subducting slab [i.e. Defant *et al.*, 1990; Grove *et al.*, 2002]. Compared to other adakites globally, the Panamanian adakites have the highest La/Yb ratios, consistent with an origin of the adakites through melting of the subducting Galápagos hotspot track characterized by high La/Yb ratios [Bindeman *et al.*, 2005]. $\delta^{18}\text{O}_{\text{olivine}}$ values of the Panamanian adakitic rocks are very similar to N-MORB [Bindeman *et al.*, 2005]. Therefore in agreement with Defant *et al.*, [1990] and Bindeman *et al.* [2005] we favor the generation of the Panamanian adakites through partial melting of the subducting slab. Alternatively they could be formed through melting of accreted Galápagos terranes, subsequently eroded into the mantle through the subduction process.

Although both the Pliocene to Holocene adakites and alkali basalts have more enriched (Galápagos-like) isotopic compositions than the Paleocene to Miocene tholeiitic and calc-alkaline arc basalts, there are also differences in isotopic composition between the adakites and alkali basalts. The alkali basalts have less radiogenic Pb and more radiogenic Nd than the adakites. There are two possible ways of explaining the origin of the alkali basalts and these differences in isotopic composition. Following the hypothesis of Dickson and Snyder [1979], and Johnson and Thorkelson [1997] and Abratis and Wörner [2001], a slab window could have formed after the subduction of the Galápagos spreading center. Mantle material from the Pacific could upwell through the window entering the Caribbean mantle wedge [Abratis and Wörner, 2001]. Decompression melting of a mixture of upwelling Galápagos-type source mantle and more depleted MORB-type mantle could produce the alkali basalts. Alternatively, Kepezhinskas *et al.*, [1997] suggested that the Kamchatkan alkali basalts could be formed by the melting of sub-arc mantle metasomatized by adakitic melts. In this case, the isotopic compositions of the alkali basalts represent a hybrid between more depleted mantle in the wedge and the adakites with enriched (Galápagos-type) isotopic compositions.

4.2 Northern migration of the arc

Subduction-type igneous activity in western Panama shows a northward migration from the Late Eocene to the Oligocene. Subduction-related volcanic and plutonic rocks from southern Azuero, Soná and Coiba Islands range in age from 61-50 Ma. Further north, between the Sona and Azuero Peninsulas and the Cordillera Central, igneous rocks with subduction-related geochemical signatures range in age from 47-34 Ma. Still further north, subduction-related volcanism in the Cordillera Central ranges in age from 32-7 Ma. In eastern Panama, there also appears to be a northward progression in igneous activity from Early to Late Eocene [Fig.3, 11; Tab.3]. An important question is the cause of this apparent northward migration in igneous activity.

To begin with, the question of whether the Azuero complex is an accreted arc terrane or formed in situ needs to be addressed. Based on paleomagnetic data, the Azuero Peninsula is interpreted to be derived from an equatorial Late Cretaceous paleolatitude and to have undergone a counterclockwise rotation of about 60° relative to the Chorotega block, leading Di Marco et al (1995) to propose that the Azuero Peninsula is an accreted terrane. Cretaceous volcanic rocks, with Galápagos-type geochemistry, form the basement of the Azuero Peninsula. Assuming a hotspot that hasn't wandered significantly since the Late Cretaceous, the equatorial latitude is consistent with the generation of these Cretaceous volcanic rocks above the Galápagos hotspot [*Lissinna et al.*, in prep.] The uniformity in isotopic and trace element geochemistry of the volcanic fronts of the Paleocene through Miocene arcs is consistent with the Paleocene to Early Eocene arc rocks being derived from the same arc as the middle Eocene to Miocene arc rocks. The presence of Early Eocene volcanic rocks in the southernmost part of the Oligocene-Miocene arc, which have trace element compositions consistent with their being from BVF, suggest that the later arcs were formed on the remnants of the Paleocene-Early Eocene arc. Finally, the continuation of the Paleocene to Early Eocene arc in eastern Panama with middle to Late Eocene rocks to the north suggests that there was once a continuous Paleocene through Eocene arc extending through Panama that was most likely offset in the Oligocene. Based on the above arguments, we believe that the apparent northward progression in igneous activity does not represent accretion of older arcs against younger arcs but instead northward migration of the same arc. We note that the 60° counterclockwise rotation could be related to the collision of parts of the Galápagos hotspot tracks, for example Cocos and Coiba Ridges, with the subduction zone [e.g. *Hauff et al.*, 2000a].

The age data show that the volcanic arc migrated ~120 km northwards (away from the trench) from ca 50 to ca 30 Ma, yielding a rate of ~ 6 mm/yr. This migration could either reflect: (1) Subduction erosion resulting from the subduction of the Galápagos hotspot track, as has been recently proposed off the coast of Costa Rica [*Ranero and von Huene*, 2000], or

(2) a shallowing of the angle of the subducting slab, possibly resulting from the subduction of progressively younger and more buoyant oceanic lithosphere through time. A change in the dip of the subducting slab should also cause changes in the geochemistry of the arc rocks [e.g. *Patino et al.*, 2000; *Rüpke et al.*, 2002]. When the subduction angle is steep, fluids/melts from the subducting slab will be concentrated in a narrow zone producing arc melts with a contribution from a large depth range of the subducting slab. When the subduction angle is shallow, fluids/melts will be distributed over a much larger region perpendicular to the strike of the arc, forming a broader volcanic zone. In the case of a steeply subducting slab, all fluids will be concentrated into a narrow zone so that the associated arc melts will be enriched in fluid mobile elements (e.g. LILE) compared to fluid immobile elements (e.g. HFSE and HREE). Ratios of LILE/HFSE or LILE/HREE however do not show any systematic variations with age. For example, the Paleocene to Early Eocene arc has Ba/Nb = 29-264, U/Nb = 2.0-6.2, K/Nb = 1469-3458, Pb/Nd = 0.05-0.39, and Sr/Y = 6-32; the Middle to Late Eocene arc, excluding the alkali basalts, has Ba/Nb = 42-287, U/Nb = 1.4-4.7, K/Nb = 1187-4462, Pb/Nd = 0.11-0.25, and Sr/Y = 12-23; and the Oligocene to Miocene Arc has Ba/Nb = 45-300, U/Nb = 1.8-7.5, K/Nb = 502-4399, Pb/Nd = 0.10-0.35, and Sr/Y = 10-40. Considering the roughly constant composition in fluid mobile to fluid immobile element ratios, we conclude that the northern migration in arc volcanism reflects tectonic erosion of the forearc.

The SW corner of Azuero, southernmost Azuero and Coiba Island have been interpreted as forearc accretionary complex(es) containing accreted paleo-Galápagos terranes. Most of these accreted terranes range in age from 50-65 Ma and were most likely accreted between ~ 45-60 Ma [*Lissinna et al.*, in prep.]. Younger accreted paleo-Galápagos terranes are rare and range in age from 16-38 Ma and were accreted between ~0-30 Ma. Therefore the gap in accretion ~30-45 Ma agrees reasonably well with the period in which tectonic erosion is likely to have dominated. We note however that the accretionary complex(es) have been transported eastwards along the Pliocene left-lateral Azuero-Sona Fault Zone and therefore may not be directly associated with the region in which northward migration of the arc occurred between ~30-50 Ma. Due to the abundance and wide distribution (from Quepos in Costa Rica to Azuero) of Galápagos terranes with ages between 50-65 Ma and the rarity of accreted Galápagos terranes with ages <50 Ma, *Lissinna et al.* [in prep.] proposed: 1) that between 50-65 Ma the paleo-hotspot track was much larger due to greater productivity of the hotspot and accretion of the paleo-hotspot track was the dominant process, and 2) that as the trench moved eastwards away from the hotspot, more time for erosion of the ocean island volcanoes and for cooling and subsidence of the lithosphere resulted in a change from predominantly accretion to predominantly tectonic erosion.

In summary, we conclude that the ~120 km of northward migration of subduction-related igneous activity away from the trench between ~50-30 Ma resulted from tectonic

erosion of the forearc. Assuming a constant rate of erosion and a thickness of the overriding plate at the coastline of 14-16 km [Sallares *et al.*, 2001; Christeson *et al.*, 1990; Vannucchi *et al.*, 2003], we calculate a rate of subduction erosion for the Panamanian arc between 50-30 Ma of $84\text{-}96 \text{ km}^3 \text{ Ma}^{-1} \text{ km}^{-1}$. The rate of tectonic erosion for the Panamanian arc between 50-30 Ma is higher than the global average rate of erosion of $\sim 40 \text{ km}^3 \text{ Ma}^{-1} \text{ km}^{-1}$ from Scholl and von Huene [2001]. The values for Panama are nearly as high as erosional rates calculated for Costa Rica of $107\text{-}123 \text{ km}^3 \text{ Ma}^{-1} \text{ km}^{-1}$ since the subduction of the Cocos ridge. An average rate of erosion for the last 16.5 Ma in front of Nicoya yielded a value of $\sim 45 \text{ km}^3 \text{ Ma}^{-1} \text{ km}^{-1}$ and for Guatemala of $\sim 12 \text{ km}^3 \text{ Ma}^{-1} \text{ km}^{-1}$ [Vannucchi *et al.*, 2003; Vannucchi *et al.*, 2004]. The elevated rates of subduction erosion are consistent with the subduction of a paleo-Galápagos hotspot in central Panama between 50-30 Ma as is presently the case in southern Costa Rica.

5 Evolution of the Central American Landbridge at Panama: Interaction of the Galápagos hotspot with the Panamanian subduction zone

Several observations point to an important role for the Galápagos hotspot in the development of the Central American landbridge in Panama: 1) Cretaceous basaltic basement with Galápagos-type geochemistry, 2) accreted portions of Galápagos paleo-hotspot tracks in western Panama ranging in age from 65-50 Ma and 38-17 Ma [Hoernle *et al.*, 2002; Hoernle and Hauff, 2005; Lissinna *et al.*, in prep.], and 3) the Galápagos-signature in the geochemistry of Paleocene to Holocene arc volcanism in Panama. The Cretaceous basaltic basement in Panama consists of oceanic crust formed at a mid-ocean ridge spreading center at ~ 115 Ma and intraplate lavas belonging to two large volcanic events at ~ 89 Ma and ~ 75 Ma, possibly associated with a more productive, pulsating early Galápagos hotspot [Hoernle *et al.*, 2002, 2004; Hoernle and Hauff, 2005; Lissinna *et al.*, in prep.]. At ~ 89 Ma, an oceanic plateau formed on mid Cretaceous (~ 115 Ma) oceanic crust. At ~ 75 Ma, a second plateau phase of volcanism erupted in part on the western margin of the ~ 89 Ma oceanic plateau and west of this margin. Possibly as a result of the ~ 75 Ma phase of volcanism occurring at the western margin of the plateau, this margin was thermally weakened, resulting in the initiation of subduction along this margin at ~ 70 Ma.

The oldest dated subduction-related volcanism in Panama is 60-65 Ma old. Arc volcanism has continued until the present with at least the Barú and La Yeguada volcanic complexes still being active. An important question concerns the origin of the enriched Galápagos-type signature (radiogenic Pb and relatively unradiogenic Nd) in the geochemistry of the arc volcanism. The radiogenic Pb isotopic compositions cannot be explained through generation from a MORB-type source or through a mixture of subducted sediments and MORB-type mantle wedge [Fig. 10]. One possible explanation for the radiogenic Pb isotopic

composition is that the mantle wedge contained early Galápagos plume mantle. This mantle could be residual plume (or fossil plume head) mantle from which the 89 Ma oceanic plateau was generated or associated with the ~75 Ma magmatic phase. Detailed variations in Pb isotopic composition through time [Fig. 12] can help us to evaluate further this hypotheses.

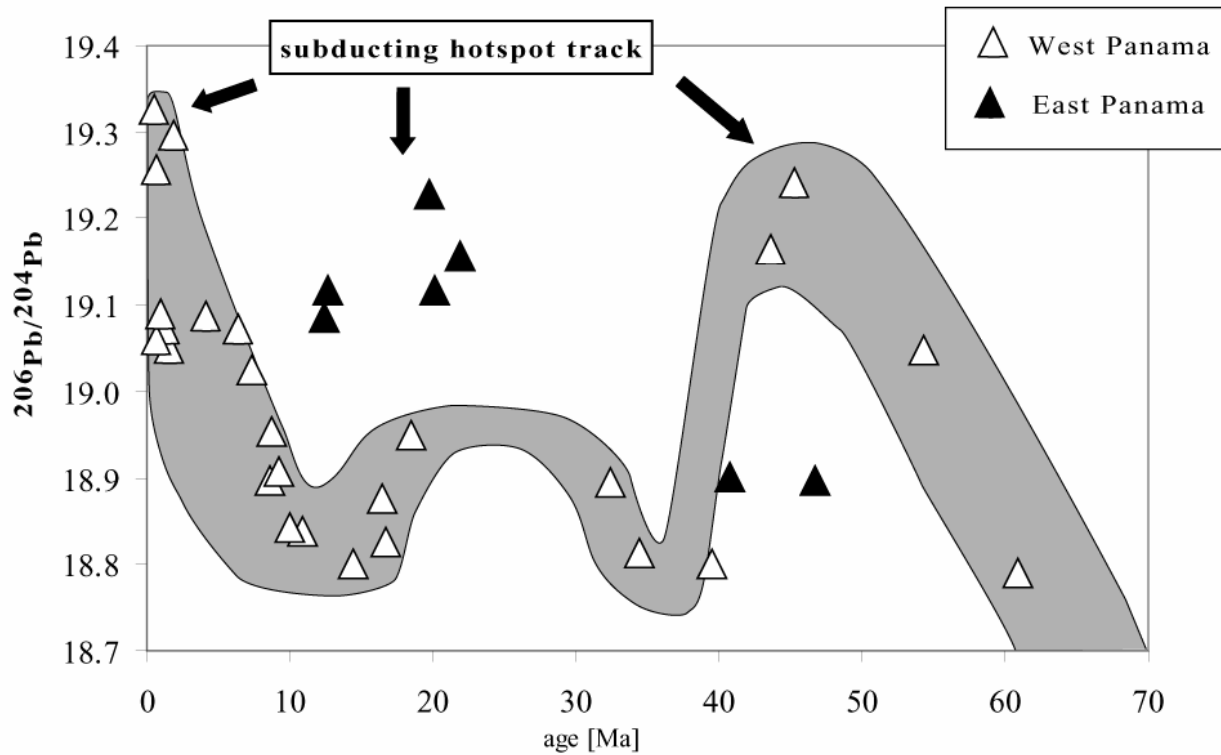


Fig. 12: $^{206}\text{Pb}/^{204}\text{Pb}$ versus age diagram shows enriched $^{206}\text{Pb}/^{204}\text{Pb}$ ratios for the Panamanian island arc lavas in relationship to a subducting Galápagos hotspot track. Subduction of a paleo-Galápagos hotspot track in western Panamá occurred from around 40-50 Ma and since 5 Ma and in eastern Panama from around 23-12 Ma.

If the mantle wedge contained residual Galápagos plume-type mantle at the beginning of subduction, we would expect the intensity of the Galápagos signal to decrease through time, which however is not the case. To the contrary, the intensity of the Galápagos-type signal (radiogenic Pb isotopic composition) increases twice in the history of arc volcanism in western Panama: at 44-46 Ma and within the last 5 Ma. Therefore the enriched composition of the arc lavas is likely to have another origin.

The presence of accreted paleo-Galápagos hotspot tracks in western Panama ranging in age from 17-65 Ma indicate that the Galápagos paleo-hotspot tracks subducted beneath Panama during much of the last ca 60 Ma [Fig. 13]. Looking at variations in arc chemistry along the present volcanic front in Nicaragua and Costa Rica, we see that the most radiogenic Pb isotopic compositions occur in Costa Rica [Feigenson *et al.*, 2004], exactly where the Galápagos hotspot track (Cocos Ridge and associated seamounts) is presently subducting

[Hoernle *et al.*, 2003]. Considering that Pb is a highly fluid-mobile element primarily derived from the subducting slab, the radiogenic Pb isotopic composition in the arc volcanic rocks in central and southern Costa Rica are likely to reflect subduction of the Galápagos hotspot track [Hoernle *et al.*, 2003].

The less enriched (intermediate Pb and Nd) isotopic compositions of Paleocene to Middle Eocene arc lavas are similar to present-day western Costa Rica and eastern Nicaragua volcanic front rocks that receive some of the signal from the subducting Galápagos hotspot track [Fig.9,10]. It should be noted that western Costa Rica and eastern Nicaragua overlie part of the Cocos Plate affected by hotspot volcanism (such as intrusive dike/sill activity) which is not represented at the surface but is observed for example in sills drilled at ODP Site 170. In analogy, we explain the geochemical composition of the Paleocene to Middle Eocene (ca 65-50 Ma) Panamanian arc rocks to result from proximity to the subducting Galápagos hotspot. Galápagos hotspot track terranes on southern Azuero, accreted between ca 60-45 Ma, represent terranes on the margin of the subducting hotspot track. We note that these accreted complexes moved eastwards along left-lateral faults such as the Azuero-Sona Fault System and therefore do not directly reflect the input into the subduction zone beneath Azuero.

In the middle Eocene at ca 45 Ma, there is a peak in the Pb isotopic composition of volcanic rocks in western Panama at the Azuero Peninsula whereas volcanic rocks in eastern Panama have intermediate Pb isotope ratios, reflecting subduction of the southern end of the hotspot track beneath Azuero [Fig. 12]. Between ~45-23 Ma, the hotspot track subduction shifted from southern Costa Rica and western Panama to eastern Panama, as is indicated by a shift in the most radiogenic Pb isotopic compositions from arc volcanics at Azuero to arc volcanic rocks east of the Panama canal zone [Fig. 12,13]. Between ca 50-30 Ma, the arc migrated northwards. Between 45-30 Ma, there is no evidence for accretion of Galápagos hotspot terranes in western Panama, indicating that subduction erosion has replaced accretion as the dominant process affecting the forearc. Between 22-12 Ma, the eastern Panama arc rocks have more radiogenic Pb isotope ratios and the western Panama arc rocks have intermediate Pb isotope ratios, which we interpret to reflect subduction of the main part of the hotspot track beneath eastern Panama [Fig. 12,13]. It is interesting to note that offset of the Paleocene to Late Eocene arc which occurred between 40-23 Ma. A shift in the subduction of the hotspot track to the east, possibly reflecting a right-lateral offset in the subducting hotspot track, may have played a role in causing the left-lateral offset along faults in the Panama canal zone region.

Isotopic compositions of eastern Panama in the Oligocene and Miocene were similar to Central Costa Rica < 2 Ma, where the Cocos Ridge is presently subducting.

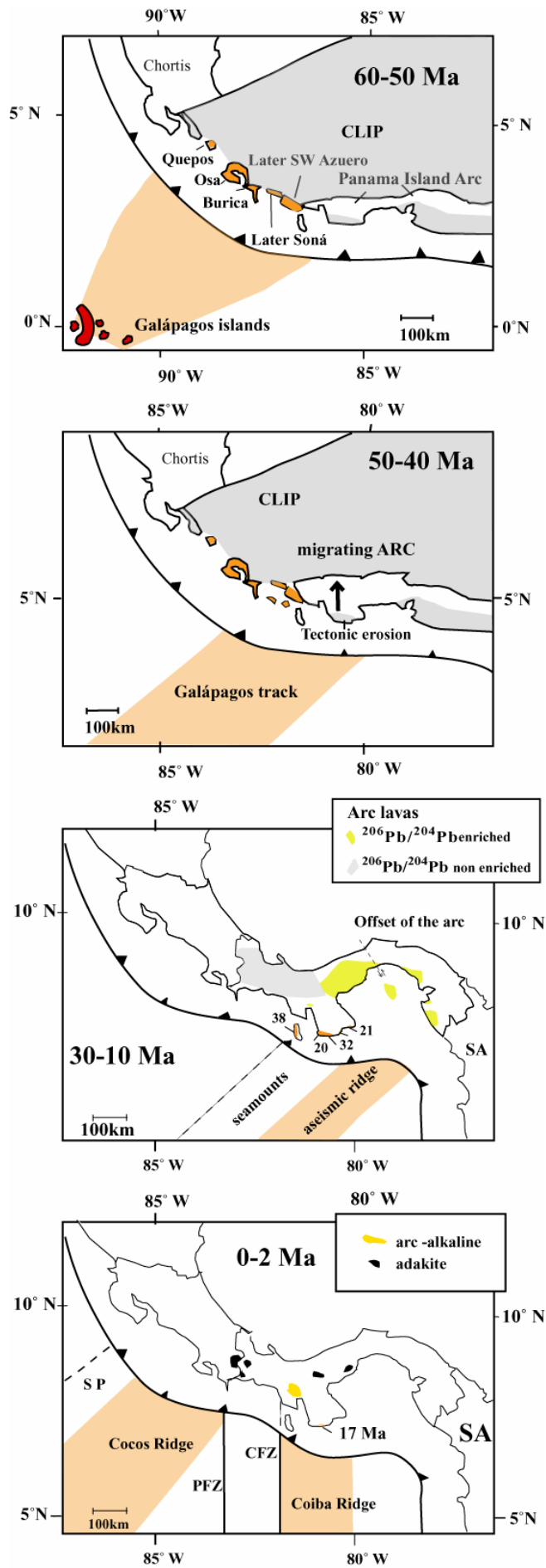


Fig. 13: Tectonic model for the interaction of the Galápagos hotspot track with the southern Central American subduction zone over the last 60 Ma.

We deduce that the difference between isotopic compositions of arc lavas between eastern and western Panama implies that the main hotspot track was subducting beneath eastern Panama between at least 23-12 Ma [Fig. 13]. Western Panama Oligocene and Miocene arc lavas show isotopic compositions similar to present-day western Costa Rica and eastern Nicaragua, possibly reflecting subduction of the margin of the hotspot track.

During the Miocene and Early Pliocene significant compressive tectonic activity in Panama resulted in folding, faulting and rotation [IHRE, 1985]. The position of the Costa Rican volcanic front has been rotated counterclockwise 30° since the Middle Miocene to the present. Deformation of the overriding plate caused the rotation, leading to shortening in the south, coeval extension in the NW, accompanied by trench retreat in the north. Rotation of the volcanic front in Costa Rica took place between 15 and 8 Ma, since 8 Ma the Costa Rican volcanic front has migrated progressively to the NE [Gans *et al.*, 2003]. Wadge and Burke [1983] presented qualitative reconstructions of Panama based mainly on a rigid body rotation of Central America along the strike-slip faults of the Cayman trough and the Motagua-Pelochic fault system of northern Central America, inferring that the Panamanian arc may originally may have been east-trending and have been internally deformed and bent into its present-day reclined s-shape as a result of collision with South America about 10 Ma ago. Mann and Corrigan [1995] however infer that the dominant elements of the Late Neogene deformation are two northwest-striking, 60-70km-wide strike-slip fault systems in Eastern Panama (east of the Golfo de San Miguel) and along the Azuero-Soná fault zone (AZFZ). They concluded that active strike-slip segmentation of the arc accommodated collision-related bending of the isthmus of Panama [Mann and Corrigan, 1990]. If Panama is affected by the Costa Rican rotation, extension would be provoked in the eastern part. Accordingly extension in the Gulf of Panama has been described by Mann and Kolarsky [1995]. A foredeep basin was filled with more than 2000m of Miocene sediments which were drilled at the El Paso Plaris-1 well in the eastern part of the Gulf of Panama [Mann and Kolarsky, 1995]. The El Paso Corvus-1 drill hole in the western part of the Gulf of Panama however show a hiatus from the Pleistocene to the Middle Eocene [Mann and Kolarsky, 1995]. We suggest that the interplay of the subduction of a Paleo-hotspot track in eastern Panama and the collision with South America resulted in the before mentioned folding, faulting and rotation. After the collision the subducting track was forced to shift back to the west. Presently the Cocos Ridge needs about 15 Ma from the formation at the Galápagos archipelago to reach the central American subduction zone [Werner *et al.*, 1999, Hoernle *et al.*, 2000]. The Presence of several young accreted terranes 16-22 Ma, and the more isotopically enriched composition of the adakites and alkali basalts (4.5-0.1 Ma) in western Panama may reflect a shift in the subduction of the hotspot track from eastern to western Panama and probably Costa Rica between 12-5 Ma ago. In agreement with the Middle to late Miocene (16-5 Ma) collision of

the Central American Arc with South America [*Wadge and Burke, 1983; Silver et al., 1990; Duque-Caro, 1990*] and coeval to ceasing subduction in eastern Panama. *Mac Millan et al. [2004]* suggests for the Early Pliocene the subduction of a hotspot track or a Coiba-like ridge along the Yaquina Fracture Zone (YFZ) in front of Soná and Azuero and the Coiba Ridge subducted beneath southeastern Costa Rica. This Yaquina ridge may have produced the 4.5 Ma old alkali basalt in northern Azuero and the 4.5 Ma old adakite at La Yeguada volcanic complex. Shifting further to the east inducing the generation of adakitic rocks at El Valle from 1.6-0.2 Ma. Holocene adakitic lavas in the Barú area were probably induced through the subduction of the Cocos Ridge [*Abratis and Wörner, 2001*].

6 Conclusions/Summary

Paleocene to Early Eocene tholeiitic to calc-alkaline arc volcanism was primarily tholeiitic and extended from the Azuero Peninsula to the Colombian border. BVF volcanism (54 Ma) of this Paleocene to Eocene arc outcrops to the north on the southernmost flank of the Cordillera Central. Isotopic composition of the Paleocene arc lavas are consistent with the subduction of a paleo-Galápagos hotspot track beneath Costa Rica and westernmost Panama. A replacement of tholeiitic to calc-alkaline volcanism during the Middle Eocene (49-41 Ma) in western Panama by isotopically enriched alkali basalts and adakites suggests the subduction of the Galápagos hotspot track beneath Soná and Azuero. During this time, the volcanic front also migrated to the north, which we interpret to result from tectonic erosion. Contemporaneous Middle Eocene (40.4-46.7 Ma) calc-alkaline lavas of eastern Panama (Costa Arriba) have more radiogenic Pb isotopic compositions, consistent with the subduction of the center of a paleo-Galápagos hotspot track beneath Azuero. The Paleocene to Late Eocene arc was offset along a left lateral transform fault running through the Panama Canal Zone area between Late Eocene (40-22 Ma) to Early Miocene. The offset was possibly caused by the eastern shift of the subducting paleo-Galápagos hotspot track. From at least Early Miocene (22-12 Ma) to Middle Miocene, east Panamanian lavas have enriched isotope compositions similar to Central Costa Rica, where the Cocos Ridge is presently subducting. Volcanism and probably subduction in eastern Panama ceased in the Middle Miocene, possibly induced by the collision of the Central American landbridge with South America. BVF volcanism in the Bocas del Torro has been identified at ca 9 Ma. For the last ca. 5 Ma, only adakitic and alkaline rocks have been identified in western Panama. During this same time interval, 17-22 Ma old terranes from the paleo-Galápagos hotspot track were accreted in southern Azuero, confirming the subduction of a hotspot track during the last 5 Ma. All Pliocene to Holocene rocks are characterized by highly enriched Galápagos-like isotopes. We favor derivation of the adakites through slab melting and of the alkali basalts through metasomatism of Galápagos-type mantle upwelling through a slab window.

7 Acknowledgements

We thank R. Werner, Juan de Dios Villa for field support. For providing samples P. Denye is thanked. Capitán de Fragata Jorge Rengifo and Sargento II, Pablo Arosemena (Servicio Marítimo Nacional) and the staff of the Tropic Star Lodge is thanked for logistic support and allowing us to stay there on short notice. The Panamanian Special Forces we thank for help and protection while sampling on Coiba Island and along the Colombian border. S. Hauff, D. Rau, J. Sticklus, H. Blaschek, S. Klauke and U. Westernströer we thank for analytical assistance. Additionally we thank the team of the reactor at the GKSS Research Center in Geesthacht (Germany). This research was supported by Deutsche Forschungsgemeinschaft (projects HO 1833/6-1and2 and SFB574, subproject C2).

8 References

- Abratis, M., Geochemical variations in magmatic rocks from southern Costa Rica as a consequence of Cocos Ridge subduction and uplift of the Cordillera de Talamanca, pp. 126, 1998.
- Abratis, M., and G. Wörner, Ridge collision, slab window formation, and the flux of Pacific asthenosphere into the Caribbean realm, *Geol. Soc. Am.*, 29, 127 - 130, 2001.
- Adamek, S., C. Frohlich, and W.D. Pennington, Seismicity of the Caribbean-Nazca microplate boundary: Constraints on microplate tectonics of the Panama region, *J. Geophys. Res.*, 93, 2053-2075, 1988.
- Bandy, O.L., and R.E. Casey, Reflector horizons and paleobathymetric history, eastern Panama, *Geol. Soc. Am. Bull.*, 84, 3081-3086, 1973.
- Behling, H., A 2860-year high resolution pollen and charcoal record from the Cordillera de Talamanca in Panama: a history of human and volcanic forest disturbance, *Holocene*, 10, 387-393, 2000.
- Bindeman, I.N., J.M. Eiler, G.M. Yogodzinski, Y. Tatsumi, C.R. Stern, T.L. Grove, M. Portnyagin, K. Hoernle, and L.V. Danyushevsky, Oxygen isotope evidence for slab melting in modern and ancient subduction zones, *Earth Planet. Sci. Lett.*, in press.
- Bourgeois, J., J. Azéma, J. Tournon, H. Bellon, B. Calle, E. Parra, J.-F. Toussaint, G. Glaçon, H. Feinberg, P. deWever, and I. Origlia, Ages et structures des complexes basiques et ultrabasique de la façade pacifique entre 3°N et 12°N (Colombie, Panama et Costa Rica), *Geol. Soc. Fr. Bull*, 24, 545-554, 1982.
- Bowland, C. L, and E. Rosencrantz, Upper crustal structure of the western Colombian basin, Caribbean Sea, *Geol. Soc. Am. Bull.*, 100, 534-546, 1988.
- Bowland, C. L, Depositional history of the western Colombian basin, Caribbean Sea, revealed by seismic stratigraphy, *Geol. Soc. Am. Bull.*, 105, 1321-1345, 1993.
- Burke, K., Tectonic Evolution of the Caribbean, *Earth Planet. Sci. Lett.*, 16, 201-230, 1988.

- Case, J.E., Oceanic Crust Forms Basement of Eastern Panama, *Geol. Soc. Am. Bull.*, 85, 645-652, 1974.
- Christeson, G.L., K.D. McIntosh, T.H. Shipley, R.E. Flueh, and H. Goede, Structure of the Costa Rica convergent margin, offshore Nicoya Peninsula, *J. Geophys. Res.*, 104, 25,443-25,468, 1999.
- Coates, A.G., M.P. Aubry, W.A. Berggren, L.S. Collins, and M. Kunk, Early Neogene history of the Central American arc from Bocas del Toro, western Panama, *Geol. Soc. Am. Bull.*, 115, 271-287, 2003.
- Corrigan, J., P. Mann, and J.C. Ingle, Forearc response to subduction of the Cocos Ridge, Panama-Costa Rica, *Geol. Soc. Am. Bull.*, 102, 628-652, 1990.
- Cowan, H., L. Sanchez, E. Camacho, J.-L. Palacios, A. Tapia, D. Irving, D. Esquivel, and C. Lindholm, Seismicity and Tectonics of Western Panama from new Portable Seismic Array Data, 1995.
- de Boer, J.Z., M.J. Defant, R.H. Stewart, J.F. Restrepo, L.F. Clark, and A.H. Ramirez, Quaternary calc-alkaline volcanism in western Panama: regional variations and implication for the plate tectonic framework, *J. South. Amer. Earth Sci.*, 1, 275-293, 1988.
- de Boer, J.Z., M.S. Drummond, M.J. Bordelon, M.J. Defant, H. Bellon, and R.C. Maury, Cenozoic magmatic phases of the Costa Rican island arc (Cordillera de Talamanca), *Geol. Soc. Am. Spec. Paper*, 295, 35-55, 1995.
- Defant, M.J., L.F. Clark, R.H. Stewart, M.S. Drummond, J.Z. de Boer, R.C. Maury, T.E. Jackson, and J.F. Restrepo, The geology and geochemistry of El Valle volcano, Panama: andesite and dacite genesis via contrasting processes, *Contrib. Mineral. Petrol*, 106, 309-324, 1991a.
- Defant, M.J., P.M. Richerson, J.Z. de Boer, R.H. Stewart, R.C. Maury, H. Bellon, M.S. Drummond, M.D. Feigenson, and T.E. Jackson, Dacite Genesis via both slab melting and differentiation: Petrogenesis of La Yeguada Volcanic Complex, Panama, *J. Petrol*, 1101-1142, 1991b.
- Defant, M.J., T.E. Jackson, M.S. Drummond, J.Z. de Boer, H. Bellon, M.D. Feigenson, R.C. Maury, and R.H. Stewart, The geochemistry of young volcanism throughout western Panama and southeastern Costa Rica: an overview, *Geol. Soc.*, 149, 569-579, 1992.
- del Guidice, D., and G. Recchi, Geologia del area del proyecto minero de Azuero: Proyecto Minero Panama, Fase I, pp. 48, United Naciones, Panama, 1969.
- Dickinson, W.R., and W.S. Snyder, Geometry of subducted slabs related to San Andreas transforms, *J. Geol.*, 87, 609-627, 1979.

- Di Marco, G., P.O. Baumgartner, and J.E.T. Channell, Late Cretaceous-early Tertiary paleomagnetic data and a revised tectonostratigraphic subdivision of Costa Rica and western Panama, *Geol. Soc. Am. Spec. Paper*, 295, 1-29, 1995.
- Drummond, M.S., M.J. Bordelon, J.Z. de Boer, M.J. Defant, H. Bellon, and M.D. Feigenson, Igneous petrogenesis and tectonic setting of plutonic and volcanic rocks of the Cordillera de Talamanca, Costa Rica-Panama, Central American Arc, *Am. J. Sci.*, 295, 875-919, 1995.
- Duffield, W.A., and G.B. Dalrymple, The Taylor Creek Rhyolite of New Mexico; a rapidly emplaced field of lava domes and flows, *Bull. Volcanol.*, 52, 475-487, 1990.
- Duncan, R.A., and R.B. Hargaves, Plate tectonic evolution of the Caribbean region in the mantle reference frame, *Geol. Soc. Am. Mem.*, 162, 89-121, 1984.
- Duque-Caro, H., The Choco block in the northwestern corner of South America: Structural, tectonostratigraphic, and pleogeographic implications, *J. South. Amer. Earth Sci.*, 3, 71-84, 1990.
- Feigenson, M.D., S.V. Maharaj, S. Juliano, L.L. Bolge, Lead isotope composition of Central American volcanoes: Influence of the Galapagos plume, *Geochem. Geophys. Geosyst.*, 5, 2003GC0000621, 2004.
- Fisher, S.P., and E.A. Pessagno, Upper Cretaceous Strata of Northwestern Panama, *Amer. Ass. Petrol. Geol. Bull.*, 49, 433-444, 1965.
- Garbe-Schönberg, D., Simultaneous determination of thirty-seven trace elements in twenty-eight international rock standards by ICP-MS, *Geostandard Newsletter*, 17, 81-97, 1993.
- Gans, P.B., G. Alvarado-Induni, W. Perez, I. Macmillan, and A. Calvert, Neogene evolution of the Costa Rican arc and development of the Cordillera Central, in *Cordilleran Section-99th Annual Meeting Proceedings*, edited by GSA, Puerto Vallarta, Jalisco, 2003.
- Geological map of Panama, Ministerio de Comercio e Industrias de Panamá, Dirección General de Recursos Minerales, Instituto Tommy Guardia, 1991.
- Grove, T.L., S.W. Parman, S.A. Bowring, R.C. Price, and M.B. Baker, The role of an H₂O-rich fluid component in the generation of primitive basaltic andesites and andesites from the Mt. Shasta region, N California, *Contrib. Mineral. Petrol.*, 142, 375-396, 2002.
- Handschuhmacher, D.W., Post-Eocene plate tectonics of the eastern Pacific, in *The Geophysics of the Pacific Ocean Basin and Its Margin*, *Geophys. Monogr. Ser.*, vol. 19, edited by G.H. Sutton, M.H. Manghnani and R. Moberly, pp. 177-202, AGU, Washington, D.C., 1976.

- Haug, G.H., and R. Tiedemann, Effect of the formation of the Isthmus of Panama on Atlantic Ocean thermohaline circulation, *Nature*, 393, 673-676, 1998.
- Hauff, F., K. Hoernle, H.-U. Schmincke, and R. Werner, A Mid Cretaceous origin for the Galápagos hotspot: volcanological, petrological and geochemical evidence from Costa Rican oceanic crustal segments, *Geologische Rundschau*, 86, 141-155, 1997.
- Hauff, F., K. Hoernle, P. van den Bogaard, G.E. Alvarado, and D. Garbe-Schönberg, Age and Geochemistry of Basaltic Complexes in Western Costa Rica: Contributions to the Geotectonic Evolution of Central America, *Geochem. Geophys. Geosyst.*, 1, 1999GC0000207, 2000b.
- Hauff, F., K. Hoernle, G. Tilton, D.W. Graham, and A.C. Kerr, Large volume recycling of oceanic lithosphere over short time scales: geochemical constraints from the Caribbean Large Igneous Province, *Earth Planet. Sci. Lett.*, 174, 247-263, 2000b.
- Hellmann, W., Struktur und Kinematik eines Forearc-Komplexes im Westpanamá-Segment (Azüero-Soná-Komplex), südliches Mittelamerika, PhD thesis, 178 pp., Universität Stuttgart, Germany, 1998.
- Hoernle, K., and G. Tilton, Sr-Nd-Pb isotopic data for Fuerteventura (Canary Islands) basal complex and subaerial volcanics: Applications to magma genesis and evolution, *Schweiz. Mineral. Petrogr. Mitt.*, 71, 3-18, 1991.
- Hoernle, K., P.v.d. Bogaard, R. Werner, B. Lissinna, F. Hauf, G. Alverado, and D. Garbe-Schönberg, Missing history (16-71 Ma) of the Galápagos hotspot: Implications for the tectonic and biological evolution of the Americas, *Geology*, 30, 795-798, 2002.
- Hoernle, K., S. Sadofsky, H. Nichols, M. Portnyagin, P. van den Bogaard and G. Alvarado, Volatile, trace element and isotopic variations of mafic arc volcanic rocks from Nicaragua and Costa Rica. *Eos, Trans. AGU*, V. 84, Fall Meet. Suppl., Abstract V32H-08, 2003.
- IRHE, F.I., Estudio de Prefactibilidad Avanzada de la Region del Valle de Anton y Tonosí, Instituto de Recursos Hydráulicos y Electrificación, *Informe del Convenio IHRE-BID-OBLADE*, Panama City, pp. 36, 1985.
- Johnston, S.T., and D.J. Thorkelson, Cocos-Nazca slab window beneath Central America, *Earth Planet. Sci. Lett.*, 146, 465-474, 1997.
- Kellog, J.N., V. Vaga, T.C. Stallings, and C.L.V. Aiken, Tectonic development of Panama, Costa Rica and the Colombian Andes: Constraints from Global Positioning System geodetic studies and gravity, *Geol. Soc. Am. Spec. Paper*, 295, 75-80, 1995.

- Kepezhinskas, P., M.J. Defant, and M.S. Drummond, Progressive enrichment of island arc mantle by melt-peridotite interaction inferred from Kamchatka xenoliths, *Geochim. Cosmochim. Acta*, 60, 1217 - 1229, 1996.
- Kesler, S.E., J.F. Sutter, M.J. Issigonis, L.M. Jones, and R.L. Walker, Evolution of Porphyry Copper Mineralization in an Oceanic Island Arc: Panama, *Econom. Geol.*, 72, 1142-1153, 1977.
- Kolarsky, R.A., P. Mann, and S. Monechi, Stratigraphic development of southwestern Panama as determined from integration of marine seismic data and onshore geology, *Geol. Soc. Am. Spec. Paper*, 295, 195, 1995.
- Kolarsky, R.A., and P. Mann, Structure and neotectonics of an oblique –subduction margin, southwestern Panama, *Geol. Soc. Am. Spec. Paper*, 295, 131-155, 1995.
- Le Maitre, R.W., A classification of igneous rocks and glossary of terms. Recommendations of the International Union of Geological Sciences, subcommission of the systematics of igneous rocks, *Blackwell Scientific Publications*, Oxford, 1989.
- Lissinna, B., K. Hoernle, F. Hauff and P. van den Bogaard, Ocean island basalt-type volcanic rocks in Panama (17 - 115 Ma): Long-term evolution of the Galápagos hotspot and input into the Panamanian subduction zone, unpub.
- Lonsdale, P., and K.D. Klitgord, Structure and tectonic history of the eastern Panama Basin, *Geol. Soc. Am. Bull.*, 89, 981-999, 1978.
- Ludwig, K.Ý., Isoplot/Ex, rev. 2.49. A geochronological toolkit for Microsoft Excel, Barkley Geochronology Center, *Spec. Publ. 1a*, 2001.
- MacKay, M.E., and G.F. Moore, Variation in deformation of the south Panama accretionary prism: Response to oblique subduction and trench sediment variation, *Tectonics*, 9, 683-698, 1990.
- MacMillan, I., P.B. Gans, G. Alvarado, Middle Miocene to present plate tectonic history of the southern Central American Volcanic Arc, *Tectonophysics*, 392, 325-348, 2004.
- Mann, P., and J. Corrigan, Model for late Neogene deformation in Panama, *Geology*, 18, 558-562, 1990.
- Mann, P., and R.A. Kolarsky, East Panama deformed belt: Structure, age, and neotectonic significance, *Geol. Soc. Am. Spec. Paper*, 295, 111-130, 1995.
- Maurý, R.C., M.J. Defant, H. Bellon, J.Z. de Boer, R.H. Stewart, and J. Cotten, Early Tertiary arc volcanics from eastern Panama, *Geol. Soc. Am. Spec. Paper*, 295, 1995.
- Metti, A., and G. Recchi, Geología de la península de Soná e Isla de Coiba, in *Segundo Congreso Latinoamericano de Geología*, vol. 2, pp. 541-553, 1976.
- Moore, G.F., and K.L. Sender, Fracture zone collision along the South Panama margin, *Geol. Soc. Am. Spec. Paper*, 295, 1995.
- Okaya, D.A., and Z. Ben-Avraham, Structure of the continental margin of southwestern Panama, *Geological Society of America Bulletin*, 99, 792-802, 1987.

- Palmer, A.R., and J. Geissman, Geologic Time Scale *Geol. Soc. Amer.*, product code CTS004, 1999.
- Patino, L.C., M.J. Carr, and M.D. Feigenson, Local and regional variations in Central American arc lavas controlled by variations in subducted sediment input, *Contrib. Mineral. Petrol.*, 138, 265-283, 2000.
- Ranero, C.R., and R. von Huene, Subduction erosion along the Middle America convergent margin, *Nature*, 404, 748-752, 2000.
- Recchi, J., Paleografia Atlas Nacional de Panama: Instituto Geografico Nacional, Tommy Guardia, Panama City, 1975.
- Rickwood, P.C., Boundary lines within petrologic diagrams which use oxides of major and minor elements, *Lithos*, 22, 247-263, 1989.
- Rüpke, L.H., J.P. Morgan, M. Hort, and J.A.D. Connolly, Are the regional variations in Central American arc lavas due to differing basaltic versus peridotitic slab sources of fluids?, *Geol. Soc. Amer.*, 30, 1035-1038, 2002.
- Sallares, V., J.J. Donobeitia, and E.R. Flueh, Lithospheric structure of the Costa Rican isthmus: Effects of subduction zone magmatism on a oceanic plateau. *J. Geophys. Res.*, 106, 621-643, 2001
- Silver, E.A., D.L. Reed, J.E. Tagudin, and D.J. Heil, Implications of the north and south Panama thrust belts for the origin of the Panama orocline, *Tectonics*, 9, 261-281, 1990.
- Sinton, C.W., R.A. Duncan, M. Storey, J. Lewis, and J.J. Estrada, An oceanic flood basalt province within the Caribbean plate, *Earth Planet. Sci. Lett.*, 155, 221-235, 1998.
- Sun, S.-S., and W.F. McDonough, Chemical and isotopic systematics of oceanic basalts: implications for mantle composition and processes, *Geol. Soc. Spec. Publ*, 42, 313-345, 1989.
- Terry, R.A., A geological reconnaissance of Panama, *Calif. Acad. Sci. Occasional Papers*, 23, 1-91, 1956.
- Tschanz, C.M., R.F. Marvin, B.J. Cruz, H.H. Mehnert, and G.T. Cebula, Geologic evolution of the Sierra Nevada de Santa Maria, northeastern Colombia, *Geol. Soc. Am. Bull.*, 85, 273-284, 1974.
- Todt, W., R.A. Cliff, A. Hanser, and A.W. Hofmann, Evaluation of a ^{202}Pb - ^{205}Pb double spike for high precision lead isotope analyses, in *Earth Processes: Reading of the Isotopic Code*, vol. 95, edited by A. Basu and S. Hart, pp. 429-437, AGU, Washington D.C., 1996.
- Tournon, J., Magmatismes du mésozoïque à l'actuel en Amérique Centrale. L'exemple de Costa Rica, des ophiolites aux andesites, Ph.D. thesis, 335 pp., Université Pierre et Marie Curie, 1984.
- Vannucchi, P., S. Galeoti, P.D. Clift, C.R. Ranero, and R. von Huene, Long-term subduction-erosion along the Guatemalan margin of the Middle America Trench, *Geol. Soc. Am.*,

32, 617-620, 2004.

- Vannucchi, P., C.R. Ranero, S. Galeoti, S.M. Straub, D.W. Scholl, and K. MacDougall-Ried, Long-term subduction-erosion along the Guatemalan margin of the Middle America Trench, *Geol. Soc. Am.*, 32, 617-620, 2004.
- Vergara Munoz, A., Tectonic patterns of the Panama Block deduced from seismicity, gravitational data and earthquake mechanisms: implications to the seismic hazard, *Tectonophysics*, 154, 253-267, 1988.
- von Huene, R., and D.W. Scholl. Observation at convergent margins concerning sediment subduction, subduction erosion, and the growth of continental crust, *Rev. Geophys.*, 29, 279-316, 1991.
- Wadge, G., and K. Burke, Neogene Caribbean plate rotation and associated Central American tectonic evolution, *Tectonics*, 2, 633-643, 1983.
- Westbrook, G.K., N.C. Hardy, and R.P. Heath, Structure and tectonics of the Panama-Nazca plate boundary, *Geol. Soc. Am. Spec. Paper*, 295, 91-109, 1995.
- Werner, R., K. Hoernle, P. van den Bogaard, C. Ranero, R. von Huene, and D. Korich, Drowned 14-m.y.-Galápagos archipelago off the coast of Costa Rica: Implications for tectonic and evolutionary models, *Geology*, 27, 499-501, 1999.
- Weyl, R., *Geology of Central America*, Gebrüder Borntraeger, Berlin, 1980.
- Withmore, F.C., and R.H. Stewart, Miocene mammals and Central American seaways, *Science*, 148, 180-185, 1965.
- Woodring, W.P., Geologic map of the Canal Zone and adjoining parts, Geol. survey Misc. geol. Inv. Map I-1, 1955.

Table 1 A: Major and Trace Element Data from Panamanian Igneous Complexes

Sample	SiO ₂	Major Elements, wt.%											Trace Elements, ppm										
		Al ₂ O ₃	MnO	MgO	Na ₂ O	CaO	P ₂ O ₅	K ₂ O	TiO ₂	Fe ₂ O ₃	H ₂ O	CO ₂	TOTAL	Ba	Cr	Ni	Sr	Y	Zr				
Adakites 0.1-1 Ma																							
M44KH	basaltic and.	54.91	15.77	0.11	7.04	3.19	8.20	0.29	1.61	0.73	7.35	0.23	0.03	99.46	787	246	101	1120	10	91			
M57a KH	basaltic and.	52.40	15.62	0.13	8.41	2.95	8.98	0.28	1.15	0.86	8.18	0.44	0.00	99.40	626	526	12	861	11	92			
M91a KH	andesite	56.49	15.88	0.09	5.91	3.68	7.38	0.46	2.07	0.90	6.43	0.47	0.05	99.81	909	203	15	1437	10	132			
M38KH	andesite	58.52	15.90	0.09	3.19	3.63	5.74	0.52	2.97	0.89	6.19	1.31	0.03	98.98	1347	50	29	1591	14	150			
M53a KH	andesite	59.83	16.43	0.10	3.61	2.97	6.65	0.25	3.01	0.68	6.19	0.14	0.00	99.86	1130	23	5	1528	13	133			
M55KH	basaltic and.	55.91	16.44	0.12	5.11	3.29	8.10	0.29	1.92	0.76	7.28	0.34	0.01	99.57	1204	130	17	1370	11	126			
M61a KH	basaltic and.	57.26	16.39	0.09	3.89	3.68	6.89	0.36	2.24	0.90	6.75	0.59	0.02	99.06	939	108	8	1298	11	118			
M63aKH	dacite	64.34	15.58	0.06	2.25	3.74	4.80	0.17	2.65	0.54	4.28	0.48	0.09	99.25	1050	30	20	1019	9	101			
M64 b KH	basaltic and.	53.61	17.41	0.17	4.42	3.09	8.27	0.31	2.19	0.95	8.47	0.47	0.34	99.98	776	51	20	1015	17	146			
M64c KH	andesite	58.18	17.38	0.10	3.87	2.85	7.20	0.21	2.56	0.73	6.68	0.23	0.01	100.32	867	36	11	1312	11	122			
M64 f KH	basaltic and.	51.48	15.80	0.11	7.84	3.18	9.59	0.47	1.46	0.94	8.06	0.4	0.02	99.70	733	344	134	1314	16	130			
M65a KH	basaltic and.	55.96	15.86	0.10	5.36	2.93	7.66	0.47	2.81	0.94	6.99	0.41	0.03	99.97	1270	90	38	2006	13	182			
M66a KH	andesite	56.82	16.92	0.11	5.09	3.73	7.53	0.27	1.37	0.83	7.08	0.24	0.01	100.28	742	154	51	964	10	89			
M99a KH	basaltic and.	53.67	14.99	0.12	6.06	4.12	8.84	0.81	1.47	1.16	6.88	1.2	0.04	99.36	1262	247	47	1307	19	154			
Arct alkaline 0.7-4.5 Ma																							
SO-96-1	basalt	47.74	14.62	0.15	9.62	3.15	10.09	0.64	1.16	1.54	10.54	0.51	0.05	99.81	595	288	237	1118	26	127			
So-96-III	basalt	47.80	14.59	0.15	9.55	3.11	10.07	0.63	1.16	1.55	10.76	0.48	0.03	99.88	636	280	210	1125	27	127			
SO-96-2	basalt	46.81	14.13	0.15	10.21	2.99	10.36	0.77	1.15	1.63	10.92	0.46	0.04	99.62	673	322	240	1222	27	138			
SO-96-3	basalt	48.00	14.64	0.15	9.65	3.14	10.09	0.63	1.14	1.54	10.78	0.3	0.02	100.08	599	291	174	1127	21	124			
SO-96-4	basalt	47.63	14.64	0.15	9.55	3.05	10.09	0.62	1.17	1.54	10.77	0.96	0.03	100.20	608	291	177	1130	23	124			
SO-96-5	basalt	45.50	14.21	0.15	10.75	2.94	11.06	0.91	1.08	1.66	11.11	0.32	0.01	99.70	611	363	207	1326	24	138			
CP-97-1	basalt	44.20	13.41	0.17	11.54	2.47	11.86	0.84	0.99	1.51	11.51	1.07	0.02	99.59	663	356	315	1304	26	135			
M36KH	basalt	47.13	13.03	0.15	9.57	3.10	10.35	0.83	1.02	2.77	10.82	1.18	0.02	99.97	760	356	218	1282	27	242			
M37a KH	basalt	45.83	12.91	0.16	10.99	2.97	11.25	0.96	1.21	2.31	10.76	0.54	0.05	100.37	1058	377	228	1342	26	222			
M98a KH	basalt	46.10	12.93	0.15	9.62	3.01	10.96	0.93	0.99	2.75	10.9	1.59	0.05	99.98	812	333	145	1382	26	238			
M105aKH	basalt	47.67	14.26	0.15	10.07	3.12	10.91	0.86	1.40	1.43	9.24	0.59	0.11	99.81	852	387	163	1415	20	160			
M118aKH	basalt	47.49	13.94	0.16	9.86	3.33	9.68	0.73	1.80	1.84	10.17	0.57	0.09	99.66	1085	360	200	1417	24	192			
M118bKH	basalt	48.62	14.14	0.15	9.44	3.30	9.41	0.68	1.82	1.74	9.74	0.59	0.11	99.74	1180	343	186	1408	21	187			
M121 a KH	basalt	44.35	12.88	0.16	10.34	3.08	12.32	1.16	1.49	2.06	10.46	0.65	0.08	99.03	946	340	136	2061	26	229			
3-12-4-03	basalt	45.11	12.92	0.17	11.66	2.70	11.87	1.01	0.95	1.38	10.7	0.39	0.01	99.26	724	425	234	1278	25	139			
BVF 8.6-9.3 Ma																							
M69KH	basaltic trachyte	52.04	18.44	0.21	2.77	3.43	6.53	0.74	3.77	1.09	8.7	1.93	0.07	99.72	1412		13	824	37	197			
M73KH	basaltic trachyte	52.38	20.29	0.15	2.42	3.94	7.29	0.56	2.92	0.95	7.03	2.06	0.06	100.05	1344		15	1404	26	178			

Table 1 A: (continued)

Sample	SiO ₂	Major Elements, wt.%											Trace Elements, ppm							
		Al ₂ O ₃	MnO	MgO	Na ₂ O	CaO	P ₂ O ₅	K ₂ O	TiO ₂	Fe ₂ O ₃	H ₂ O	CO ₂	TOTAL	Ba	Cr	Ni	Sr	Y	Zr	
<i>Cordillera Central 7-32Ma</i>																				
M38KH	andesite	58.52	15.90	0.09	3.19	3.63	5.74	0.52	2.97	0.89	6.19	1.31	0.03	98.98	1347	50	29	1591	14	150
M161aKH	andesite	60.94	17.46	0.13	3.03	3.76	6.17	0.22	1.10	0.57	6.35	0.58	0.03	100.34	545	30	10	553	17	80
M164KH	basalt	55.98	18.17	0.17	2.98	4.18	6.70	0.36	0.63	0.90	8.08	0.74	0.07	98.96	274	39	13	468	29	113
M42a KH	basalt	51.00	18.36	0.17	3.71	4.14	9.25	0.44	0.56	1.24	10.62	0.59	0.02	100.10	440	39	14	641	28	121
M45a KH	basaltic and.	51.78	15.52	0.26	4.45	2.82	9.19	0.28	0.63	1.26	13.17	0.93	0.03	100.32	656	23	5	539	24	57
M46a KH	basalt	48.15	18.83	0.26	4.45	4.02	8.50	0.20	0.60	1.01	10.76	2.74	0.74	100.26	384	23	5	496	16	40
M49a KH	basalt	48.47	18.15	0.22	4.54	3.53	8.92	0.23	0.69	1.19	12.09	2.29	0.08	100.40	583	70	6	486	23	60
M50a KH	basalt	46.76	16.45	0.21	7.16	2.23	10.51	0.19	0.58	0.98	12.05	3.19	0.11	100.42	484	53	53	395	29	120
M67KH	basalt	46.52	17.23	0.18	5.62	1.84	11.95	0.29	0.30	1.62	12.07	2.51	0.55	100.68	230	53	53	395	29	120
M76a KH	basalt	46.60	16.45	0.19	8.64	1.42	11.60	0.19	0.08	0.91	11.25	0.39	0.20	98.11	153	211	66	459	17	40
M78a KH	basalt	49.23	15.62	0.22	5.18	2.49	10.32	0.17	0.88	1.11	13.86	1.53	0.06	100.91	652	19	14	546	19	55
M80KH	basalt	48.58	20.52	0.22	4.16	2.11	11.25	0.17	0.25	1.02	11.22	1.31	0.04	100.85	263	19	18	488	24	51
M81a KH	basalt	48.11	16.92	0.20	7.02	1.97	10.76	0.19	0.40	1.00	12.69	1.33	0.05	100.83	228	128	44	416	19	45
M84aKH	basalt	49.20	19.49	0.18	4.47	1.86	11.23	0.13	0.48	0.89	10.93	1.23	0.05	100.14	292	34	16	387	23	56
M122a KH	basalt	48.05	19.86	0.14	4.14	3.13	9.81	0.18	0.16	0.84	10.36	3.95	0.15	100.94	246	38	8	596	20	57
M123a KH	basalt	49.66	20.03	0.17	3.76	2.96	9.72	0.17	0.18	0.91	10.4	2.44	0.11	100.70	255	35	7	632	17	57
M124b KH	basalt	49.57	19.11	0.19	4.61	2.27	11.21	0.19	0.42	0.87	10.72	1.25	0.04	100.60	223	35	4	435	17	50
M125a KH	dacite	71.93	14.15	0.05	0.95	3.80	2.67	0.08	2.81	0.29	2.24	0.64	0.06	99.88	1172	35	4	301	13	122
M128 b KH	dacite	72.83	14.08	0.05	0.77	3.94	2.52	0.06	2.82	0.28	2.06	0.54	0.01	99.96	1204	35	4	302	14	115
M133a KH	basaltic and.	53.41	17.17	0.24	4.32	2.50	8.90	0.13	0.63	0.84	10.98	1.2	0.07	100.39	417	33	9	422	23	46
M136a KH	basalt	47.53	19.58	0.18	5.45	1.66	12.15	0.08	0.07	0.69	11.12	1.01	0.10	99.62	131	33	16	416	12	25
M143a KH	andesite	55.96	15.56	0.16	3.99	3.29	7.39	0.34	0.73	1.23	9.5	1.87	0.02	100.04	715	28	16	598	29	171
<i>Cordillera Central 34-40Ma</i>																				
CP-98	andesite	55.90	17.27	0.15	3.98	2.79	8.37	0.17	0.83	0.89	8.13	1.22	0.07	99.77	364	68	33	349	22	99
G 64	basaltic and.	51.06	17.83	0.15	6.13	3.68	10.46	0.09	0.12	0.69	7.82	2.028	0.08	100.14	267	117	93	162	25	56
M35a KH	andesite	56.06	17.39	0.15	3.72	3.17	8.42	0.18	0.86	0.91	7.57	1.75	0.09	100.43	311	58	25	355	25	103
M102aKH	andesite	55.91	15.45	0.21	3.33	4.09	5.90	0.26	1.06	1.36	10.78	2.19	0.10	100.64	578	39	12	377	34	105
M106a KH	andesite	56.20	16.93	0.15	3.84	3.14	7.94	0.20	0.75	1.05	8.1	1.42	0.09	99.81	307	39	13	384	24	124
M107a KH	andesite	58.57	16.10	0.13	3.83	3.19	6.85	0.18	1.06	0.96	7.75	1.96	0.08	100.66	375	46	13	371	26	150
M119a KH	basaltic and.	53.68	17.70	0.20	4.42	3.29	8.25	0.23	0.65	1.09	9.24	1.39	0.05	100.19	330	24	11	421	25	114
<i>Cordillera Central 44-46 Ma</i>																				
M117a KH	basaltic and.	51.71	16.78	0.17	4.81	2.79	9.05	0.39	1.11	1.55	10.13	1.67	0.19	100.35	571	35	43	726	24	184
M141 a KH	basalt	46.54	13.18	0.16	10.07	2.00	9.62	0.77	2.17	1.69	11.08	2.52	0.15	99.95	570	524	198	791	30	262
M148a KH	andesite	57.21	18.02	0.12	1.69	4.83	4.61	0.40	1.85	0.75	6.83	1.56	0.03	98.09	500	500	563	30	258	

Table 1 A: (continued)

Sample	SiO ₂	Major Elements, wt.%										Trace Elements, ppm								
		Al ₂ O ₃	MnO	MgO	Na ₂ O	CaO	P ₂ O ₅	K ₂ O	TiO ₂	Fe ₂ O ₃	H ₂ O	CO ₂	TOTAL	Ba	Cr	Ni	Sr	Y	Zr	
Eastern Panama 12-22Ma																				
M137a KH	basalt	50.23	17.48	0.19	5.41	1.96	9.91	0.06	0.28	0.77	12.12	2.09	0.06	100.56	173	30	11	336	14	25
M155a KH	andesite	59.82	15.65	0.13	3.18	2.88	5.60	0.23	3.47	0.69	6.92	1.29	0.04	99.90	1072	29	7	449	24	161
M157a KH	basaltic and.	49.86	17.32	0.24	4.66	2.42	10.05	0.31	0.75	0.88	10.98	1.03	0.92	99.42	576	39	15	712	19	58
M158a KH	dacite	66.69	14.36	0.06	1.15	2.64	2.93	0.13	3.96	0.45	3.24	1.67	1.93	99.21	1234			285	21	189
M159a KH	andesite	59.63	17.02	0.14	2.48	2.98	5.55	0.25	3.03	0.61	6.26	1.84	0.19	99.98	1100			601	23	128
M160a KH	dacite	67.59	14.92	0.08	1.26	3.11	2.89	0.13	4.15	0.46	3.59	1.42	0.30	99.90	1213			325	25	201
M204d KH	basalt	48.88	20.81	0.09	4.51	4.01	9.42	0.12	0.28	1.01	6.78	3.41	0.13	99.45	262	71	37	859	25	78
M205a KH	andesite	55.63	14.65	0.09	3.62	3.34	5.32	0.27	0.30	1.65	8.68	3.66	2.09	99.30	443	31	22	331	42	162
M212KH	basalt	48.39	18.56	0.23	4.74	2.23	10.73	0.14	0.34	1.10	11.63	1.29	0.06	99.44	204	39	36	257	31	70
M219c KH	dacite	67.15	16.09	0.14	0.65	5.67	3.96	0.17	0.92	0.87	3.68	0.4	0.10	99.80	321			121	40	156
Eastern Panama 40-50Ma																				
CA-106	andesit	57.76	17.77	0.34	0.78	3.14	8.91	0.21	2.04	0.55	5.82	0.5	1.81	99.63	966		5	583	12	71
CA-111-1	andesit	64.87	16.09	0.12	1.19	3.37	5.83	0.15	0.95	0.47	5.06	0.52	0.03	98.65	397		17	370	22	77
CA-111-2	basaltic and.	52.61	17.79	0.19	4.58	3.05	9.06	0.17	0.83	0.72	9.74	0.82	0.13	99.69	299	216	82	423	25	78
CA-111-5	andesit	58.83	16.81	0.21	1.56	3.09	8.54	0.17	1.25	0.46	5.94	0.84	1.68	99.38	488		6	374	15	77
CA-112-1	basaltic and.	51.40	19.77	0.13	2.82	3.75	8.05	0.22	1.88	0.64	8.01	3.31	0.15	100.13	720		13	676	21	57
M165c KH	dacite	62.34	17.28	0.07	2.46	4.85	5.45	0.15	1.64	0.42	4.45	0.3	0.03	99.44	1051	34	2	618	12	92
M167b KH	basalt	48.42	18.70	0.16	8.34	1.25	15.33	0.03	0.07	0.31	6.55	1	0.04	100.20	37	354	103	177	11	18
Azuero, Sona Peninsula and Coiba Island 50-61 Ma																				
G 16	basaltic and.	51.81	15.40	0.19	4.54	2.96	8.36	0.20	0.88	1.17	12.67	2.44	0.40	101.02						
G 17	basalt	50.21	17.02	0.12	5.04	3.85	11.46	0.16	0.34	1.11	8.79	2.7294	0.10	100.93	97	54	22	326	19	69
G 18	andesite	58.76	17.00	0.17	3.06	5.52	6.22	0.13	1.40	0.80	6.74	0.7458	0.05	100.60	218	62	9	272	36	183
G 19	andesite	56.49	15.91	0.14	3.50	4.49	8.88	0.26	0.54	1.22	8.33	0.5646	0.06	100.38	193	67	13	228	37	153
G 20	basalt	50.27	16.45	0.18	6.25	3.47	9.60	0.10	0.71	0.72	10.56	1.0832	0.03	99.42	235	80	29	353	15	49
Az-1-1	basaltic and.	50.26	17.98	0.14	3.51	4.56	8.28	0.16	0.71	0.79	9.12	4.36	0.21	100.08	261	49	23	649	20	64
AZ-1-3	basaltic and.	49.95	19.10	0.12	3.68	4.38	8.14	0.14	0.61	0.72	8.84	3.73	0.11	99.52	410	49	29	622	19	61
AZ-3-1	basalt	47.33	15.94	0.13	5.30	3.08	9.54	0.14	0.56	1.82	12.33	3.86	0.10	100.13	139	51	44	431	29	60
AZ-4-3	basalt	46.92	16.11	0.19	6.73	1.77	11.87	0.21	0.70	1.65	12.88	1.33	0.05	100.41	133	149	60	452	25	67
AZ-8-1	andesit	55.58	16.33	0.13	3.42	2.91	7.19	0.17	1.97	1.13	8.37	2.69	0.11	100.00	412	50	14	481	32	183
AZ-15	basaltic and.	51.57	18.36	0.19	4.13	1.97	10.69	0.09	0.12	0.81	11.18	0.85	0.03	99.99	159	20	12	304	20	52
AZ-33	basaltic and.	51.06	18.29	0.16	3.80	2.35	9.19	0.23	0.54	1.15	11.08	1.98	0.07	99.90	261	23	17	336	31	95
AZ-44-1	basalt	48.24	17.77	0.18	5.36	2.74	9.56	0.15	0.49	1.53	12.18	2.37	0.05	100.62	185	44	41	23	23	82
AZ-46-1	basaltic and.	53.56	16.85	0.23	3.82	2.43	9.43	0.26	0.59	1.08	10.72	1.6	0.04	100.61	311	51	32	30	30	113
AZ-48	basaltic and.	52.02	18.38	0.16	3.02	2.99	9.55	0.22	0.29	1.25	10.28	2.15	0.03	100.34	223	20	13	36	36	123

Table 1 A: (continued)

Sample	SiO ₂	Major Elements, wt. %										Trace Elements, ppm								
		Al ₂ O ₃	MnO	MgO	Na ₂ O	CaO	P ₂ O ₅	K ₂ O	TiO ₂	Fe ₂ O ₃	H ₂ O	CO ₂	TOTAL	Ba	Cr	Ni	Sr	Y	Zr	
AZ-49-1	andesit	54.93	17.42	0.14	2.99	2.56	8.55	0.18	0.47	0.88	8.49	3.6	0.06	100.27	207	19	11	286	32	127
CE-60-2	basaltic and.	52.18	17.48	0.19	4.30	2.32	9.69	0.19	0.75	0.82	9.74	2.18	0.83	100.67	820	42	50	534	20	61
Co-78-2	basaltic and.	50.16	15.05	0.20	6.64	4.46	7.61	0.10	0.57	1.02	10.55	3.73	0.04	100.13	230	71	60	123	25	68
Co-87-2	basaltic and.	51.52	19.76	0.33	3.25	4.97	6.02	0.22	0.71	1.46	9.82	1.88	0.19	100.13	276	27	13	204	25	152
Co-88-4	andesit	56.56	17.03	0.23	2.41	2.97	8.21	0.15	0.92	1.05	9.12	1.13	0.03	99.81	316	21	25	228	23	110
CO-91-4	diorite	56.35	16.34	0.16	3.47	3.10	8.32	0.17	0.84	0.77	6.61	1.48	0.65	98.26	450	122	46	264	19	105
CO-93-1	andesit	58.88	16.39	0.22	2.49	3.88	6.65	0.24	0.27	1.24	9.61	1.53	0.03	101.43	325	8	189	45	159	
SC-100-1F	basaltic and.	51.32	16.87	0.19	5.15	2.84	10.11	0.17	0.80	0.73	10.65	0.95	0.03	99.81	634	22	22	559	34	76
M113 KH	basaltic and.	51.75	16.67	0.19	5.37	1.67	10.75	0.16	0.50	0.60	10.89	0.82	0.02	99.53	182	60	18	355	14	37
M132a KH	andesite	58.05	16.00	0.18	2.34	2.83	6.81	0.34	1.96	1.01	8.71	0.79	1.12	100.14	1076	19	19	420	34	132
Standards																				
JB-2 N=5		53.39	14.89	0.21	4.56	1.96	10.04	0.52	0.30	0.87	14.54			101	227	24	23	177	54	
stand. devi.		0.08	0.02	0.00	0.06	0.04	0.08	0.52	0.16	0.36	0.11			0.2	14.7	4.5	3.4	0.5	1.3	
JB-3 N=5		50.92	17.40	0.17	5.10	2.54	9.85	0.74	0.58	1.15	11.91			100.52	254	60	44	408	98	
stand. devi.		0.06	0.05	0.00	0.04	0.07	0.05	0.55	0.23	0.31	0.09			0.18	15.1	5.0	2.9	1.7	1.9	
JA-2 N=4		56.42	15.60	0.11	7.94	2.82	6.29	0.42	0.96	1.22	6.42			98.37	304	513	133	245	100	
stand. devi.		0.07	0.03	0.00	0.05	0.04	0.004	0.26	0.80	0.54	0.04			0.13	8.6	7.8	1.8	1.6	1.1	

Table 1 B: Trace Element Data from the Panamanian Island Arc

Sample	Rb	Nb	La	Ce	Pr	Nd	Sm	Eu	Gd	Tb	Dy	Ho	Er	Tm	Yb	Lu	Hf	Ta	Pb	Th	U
<i>Adakites 0.1-1 Ma</i>																					
M44KH	25.57	6.78	23.50	43.82	5.35	19.85	3.55	0.65	2.99	0.39	2.00	0.36	0.98	0.13	0.90	0.13	2.53	0.36	5.68	4.15	1.35
M57a KH	21.01	9.65	23.56	45.24	5.57	20.78	3.75	0.81	3.24	0.45	2.37	0.44	1.18	0.17	1.11	0.16	2.45	0.52	3.85	3.54	1.07
M53a KH	50.02	5.19	30.33	59.82	7.05	26.59	4.63	1.33	3.53	0.47	2.18	0.40	1.03	0.13	0.90	0.13	4.51	0.37	10.14	11.41	2.94
M55KH	46.35	6.51	33.02	62.87	7.63	27.90	4.45	0.44	3.49	0.44	2.20	0.40	1.11	0.15	1.03	0.15	3.91	0.34	6.34	7.70	2.23
M63aKH	46.67	5.90	20.85	37.74	4.55	16.50	2.90	0.14	2.34	0.30	1.46	0.26	0.69	0.09	0.61	0.09	2.08	0.39	7.46	6.51	2.12
M64cKH	41.72	4.30	23.05	45.63	5.55	21.61	3.96	1.19	3.50	0.46	2.49	0.48	1.28	0.18	1.17	0.17	4.76	0.30	7.81	7.11	2.07
M65a KH	47.03	10.66	66.56	127.81	14.69	52.55	7.72	2.07	6.08	0.67	3.12	0.54	1.40	0.18	1.15	0.17	7.04	0.70	8.64	12.64	3.06
M66a KH	23.94	7.06	24.30	45.85	5.50	21.08	3.82	1.14	3.39	0.44	2.42	0.46	1.23	0.17	1.15	0.17	3.20	0.49	3.74	3.59	1.22
M99a KH	25.46	48.03	63.94	118.19	12.41	44.15	7.19	1.27	5.88	0.76	3.72	0.65	1.71	0.23	1.46	0.21	3.57	2.04	6.36	8.88	2.67
<i>Arc alkaline 0.7-4.5 Ma</i>																					
SO-96-1	24.95	28.79	46.81	94.14	10.98	41.19	7.27	2.20	6.08	0.83	4.45	0.82	2.11	0.29	1.77	0.25	3.63	1.21	3.34	4.88	1.88
SO-96-2	20.92	30.06	52.27	103.68	11.85	43.95	7.60	2.24	6.05	0.81	4.26	0.77	1.96	0.27	1.67	0.23	3.50	1.21	3.33	5.61	1.89
CP-97-1	17.59	26.36	66.67	133.13	15.26	55.98	9.30	2.61	7.14	0.93	4.81	0.87	2.21	0.29	1.81	0.25	3.41	0.98	3.43	7.13	2.13
M36KH	16.44	49.57	51.28	106.08	13.65	55.97	10.91	3.23	9.76	1.27	6.57	1.15	2.85	0.37	2.22	0.31	6.96	3.09	3.47	6.13	1.86
M37a KH	19.08	48.00	56.34	115.75	14.73	58.52	10.83	3.13	9.47	1.19	6.14	1.08	2.75	0.36	2.17	0.31	6.37	2.90	3.76	6.47	1.95
M98a KH	14.59	46.53	58.66	117.48	14.37	57.22	10.75	3.20	9.01	1.25	6.19	1.08	2.68	0.34	2.11	0.29	5.87	2.74	3.51	6.27	1.79
M105aKH	22.12	29.65	60.54	109.61	12.90	47.07	7.68	2.17	6.09	0.81	3.94	0.70	1.82	0.24	1.52	0.22	3.71	1.54	3.99	7.03	1.95
M118aKH	32.90	34.80	67.66	138.25	16.77	63.63	10.88	3.07	9.32	1.13	5.53	0.96	2.35	0.29	1.81	0.26	6.04	2.35	5.11	8.42	2.68
M118bKH	36.76	32.68	66.33	134.72	16.38	62.03	10.64	2.99	8.98	1.11	5.42	0.94	2.34	0.30	1.85	0.25	5.87	2.22	5.07	8.38	2.72
M121 a KH	20.80	35.65	84.58	173.47	21.60	83.46	14.06	3.90	11.51	1.37	6.61	1.13	2.79	0.35	2.20	0.30	6.50	2.25	4.69	8.85	2.50
3-12-4-03	17.29	28.91	77.22	157.72	17.57	64.12	10.55	2.68	8.51	1.12	5.49	0.97	2.50	0.33	2.13	0.30	3.38	1.21	4.63	9.36	2.76
<i>BVF 8.6-9.3 Ma</i>																					
M69KH	80.81	14.45	46.00	91.70	12.05	48.18	9.79	2.56	9.14	1.28	7.46	1.49	4.16	0.61	4.15	0.64	5.47	0.86	8.20	6.19	2.14
M73KH	59.39	11.82	41.11	81.10	10.45	41.27	7.87	2.23	7.07	0.94	5.21	1.02	2.78	0.40	2.69	0.41	5.03	0.73	17.00	6.49	2.28
<i>Cordillera Central 7-32Ma</i>																					
M38KH	50.21	15.68	50.47	93.43	11.14	41.44	6.73	1.79	5.38	0.63	3.03	0.54	1.40	0.18	1.21	0.17	4.61	1.09	7.30	8.41	2.79
M42a KH	4.80	7.46	19.24	39.28	5.29	22.69	5.31	1.65	5.26	0.83	4.94	0.99	2.73	0.39	2.57	0.38	0.41	0.46	4.41	1.74	0.36
M46a KH	7.54	1.77	6.36	13.09	1.93	9.09	2.53	0.93	2.76	0.47	2.85	0.58	1.62	0.23	1.56	0.23	0.90	0.10	5.35	0.76	0.27
M49a KH	9.56	3.34	7.21	16.09	2.60	12.44	3.40	0.89	3.85	0.63	3.92	0.80	2.23	0.33	2.18	0.32	1.28	0.17	2.52	0.56	0.20
M50a KH	7.34	2.45	5.93	13.08	2.07	9.86	2.72	0.67	3.02	0.49	3.08	0.62	1.74	0.25	1.68	0.25	1.01	0.13	3.40	0.55	0.20
M67KH	2.14	8.14	13.28	30.03	4.55	20.90	5.58	1.79	5.94	0.95	5.81	1.16	3.17	0.45	2.97	0.44	3.68	0.60	1.51	1.37	0.48
M76a KH	0.31	2.00	8.39	16.74	2.34	10.56	2.73	0.99	2.87	0.47	2.81	0.57	1.55	0.23	1.48	0.22	1.05	0.12	1.63	1.05	0.27
M78a KH	9.75	2.16	8.54	16.73	2.36	10.62	2.86	1.00	3.12	0.53	3.27	0.68	1.90	0.28	1.89	0.28	1.34	0.13	3.58	1.43	0.47
M80KH	0.86	1.97	5.07	12.04	2.03	10.45	3.14	1.15	3.78	0.65	4.27	0.91	2.57	0.38	2.55	0.39	1.39	0.11	1.58	0.30	0.11
M81a KH	4.97	1.53	4.93	11.54	1.89	9.46	2.75	1.00	3.08	0.53	3.31	0.68	1.93	0.28	1.89	0.28	1.10	0.08	1.66	0.27	0.14
M84a KH	5.87	3.24	6.61	14.22	2.08	9.60	2.75	0.97	3.24	0.55	3.60	0.77	2.13	0.32	2.12	0.32	1.73	0.22	1.52	0.88	0.30
M122a KH	1.07	2.33	3.55	8.33	1.29	6.27	1.94	0.68	2.49	0.47	2.99	0.62	1.67	0.23	1.44	0.18	0.53	0.15	0.97	0.24	0.10
M123a KH	1.20	2.45	5.76	13.54	2.03	9.74	2.75	1.00	3.11	0.55	3.43	0.72	2.04	0.30	2.02	0.31	1.52	0.16	1.11	0.36	0.14
M124b KH	4.33	2.41	6.00	13.81	2.09	9.87	2.77	1.00	3.11	0.55	3.35	0.69	1.92	0.28	1.84	0.27	1.21	0.15	1.18	0.34	0.10
M136a KH	0.37	0.55	2.41	5.45	0.88	4.54	1.48	0.63	1.79	0.34	2.14	0.45	1.30	0.19	1.31	0.20	0.55	0.03	0.94	0.14	0.06
M143a KH	27.65	8.58	24.98	52.06	6.67	27.83	6.20	1.65	6.02	0.95	5.54	1.10	3.09	0.45	3.01	0.46	4.92	0.60	5.54	4.36	1.31

Table 1 B: continued Trace Element, ppm

Sample	Rb	Nb	La	Ce	Pr	Nd	Sm	Eu	Gd	Tb	Dy	Ho	Er	Tm	Yb	Lu	Hf	Ta	Pb	Th	U
Cordillera Central 34-40Ma																					
G 65	7.46	2.02	2.54	6.88	1.13	5.54	1.87	0.72	2.57	0.46	3.11	0.68	1.90	0.30	1.97	0.29	1.56	0.12	1.18	0.37	0.16
CP-98	14.12	5.64	10.17	22.37	3.13	13.54	3.42	1.08	3.84	0.61	3.80	0.77	2.18	0.33	2.18	0.33	2.56	0.34	2.64	1.02	0.37
M35a KH	13.59	5.03	10.40	23.23	3.28	14.56	3.69	1.16	3.98	0.69	4.22	0.87	2.45	0.36	2.46	0.37	2.83	0.36	3.62	1.02	0.37
M102aKH	13.37	4.93	10.17	23.67	3.68	17.98	5.08	1.61	5.88	1.00	6.37	1.34	3.73	0.55	3.70	0.56	3.22	0.33	2.49	1.06	0.41
M106a KH	14.38	7.81	14.23	30.77	4.19	18.06	4.30	1.35	4.64	0.74	4.61	0.94	2.62	0.39	2.60	0.39	4.01	0.62	2.41	1.71	0.55
Cordillera Central 44-46 Ma																					
M117a KH	13.17	11.81	33.33	71.17	9.07	36.77	7.19	2.10	6.69	0.92	5.09	0.95	2.49	0.34	2.12	0.30	4.58	0.87	3.00	5.29	1.26
M141 a KH	36.57	12.41	48.52	108.69	14.26	59.39	12.17	3.45	9.95	1.33	6.51	1.11	2.76	0.36	2.22	0.32	6.76	0.76	3.25	4.38	1.48
M148a KH	33.58	26.80	32.21	64.40	8.00	30.79	6.32	1.86	6.03	0.94	5.42	1.05	2.91	0.43	2.89	0.44	6.16	1.63	4.29	5.13	1.42
Eastern Panama 12-22Ma																					
M155 a	82.05	7.27	20.43	39.75	4.95	19.89	4.33	1.15	4.25	0.69	4.05	0.83	2.38	0.36	2.43	0.37	4.04	0.52	6.21	3.81	1.49
M157 a	15.96	2.15	10.52	21.66	3.00	13.50	3.41	1.16	3.46	0.56	3.39	0.70	1.98	0.29	1.94	0.30	1.43	0.13	2.82	0.89	0.41
M164KH	6.72	6.40	12.94	27.79	3.91	17.29	4.35	1.51	4.85	0.80	5.08	1.04	2.95	0.44	2.94	0.45	3.61	0.46	1.76	1.08	0.41
M204d KH	3.36	2.82	5.38	12.86	1.94	9.47	2.93	1.17	3.78	0.67	4.49	0.94	2.60	0.38	2.46	0.36	2.44	0.21	0.42	0.55	0.15
M212KH	2.34	2.64	5.92	13.58	2.13	10.76	3.29	1.15	4.35	0.78	5.34	1.17	3.42	0.51	3.38	0.53	2.25	0.20	1.17	0.75	0.20
Eastern Panama 40-50Ma																					
CA-106	30.05	2.43	6.19	12.47	1.75	7.73	2.09	0.72	2.38	0.41	2.64	0.55	1.62	0.25	1.70	0.25	1.63	0.12	3.33	0.95	0.45
CA-111-2	10.92	2.30	7.46	16.92	2.56	11.70	3.08	1.01	3.38	0.55	3.46	0.74	2.12	0.33	2.20	0.33	2.08	0.11	1.33	1.02	0.37
CA-111-5	21.46	2.24	7.71	15.82	2.21	9.44	2.32	0.75	2.38	0.40	2.54	0.55	1.64	0.27	1.84	0.29	1.76	0.11	1.52	1.17	0.44
CA-112-1	22.83	2.01	6.40	13.17	1.81	8.18	2.25	0.76	2.56	0.44	2.83	0.61	1.76	0.28	1.86	0.28	1.49	0.09	3.82	1.02	0.49
M167b KH	0.50	0.17	1.50	3.86	0.70	3.78	1.34	0.57	1.81	0.35	2.32	0.51	1.45	0.22	1.47	0.22	0.58	0.06	0.39	0.04	0.01
Azuero, Sona Peninsula and Coiba Island 50-61 Ma																					
G 16	16.65	2.25	8.77	21.57	3.17	14.08	3.66	1.16	4.14	0.66	4.19	0.88	2.41	0.37	2.44	0.36	2.36	0.13	1.84	1.34	0.42
G 17	6.91	1.74	4.88	12.58	1.94	9.49	2.79	0.98	3.40	0.60	3.89	0.84	2.26	0.34	2.18	0.32	1.88	0.10	0.91	0.52	0.16
G 19	5.02	4.43	10.91	27.55	4.15	18.95	5.09	1.57	5.59	0.91	5.55	1.13	2.99	0.44	2.73	0.37	1.29	0.25	2.53	1.31	0.65
G 20	10.01	1.76	3.89	9.98	1.54	7.35	2.10	0.74	2.48	0.41	2.57	0.53	1.43	0.22	1.41	0.20	0.40	0.10	2.87	0.50	0.17
AZ-3-1	9.21	2.37	4.40	11.99	2.22	11.99	3.85	1.36	4.40	0.74	4.52	0.90	2.43	0.34	2.18	0.31	1.68	0.12	0.59	0.39	0.15
AZ-4-3	15.11	3.16	4.84	12.83	2.34	12.13	3.76	1.38	4.40	0.72	4.50	0.89	2.46	0.35	2.29	0.33	1.87	0.19	1.07	0.51	0.17
AZ-44-1	6.59	4.91	5.27	13.95	2.18	10.60	3.21	1.20	3.78	0.64	4.11	0.83	2.28	0.33	2.18	0.33	2.16	0.30	1.07	0.51	0.17
AZ-46-1	5.66	2.73	11.44	25.42	3.62	16.09	4.21	1.32	4.90	0.81	5.33	1.11	3.16	0.47	3.18	0.48	2.88	0.15	2.18	2.07	0.58
AZ-48	3.49	2.95	10.48	24.57	3.66	16.70	4.67	1.46	5.56	0.94	6.19	1.29	3.69	0.55	3.73	0.57	3.34	0.17	2.44	1.99	0.63
CE-60-2	7.65	2.80	9.61	19.19	2.59	11.30	2.85	0.99	3.05	0.48	2.96	0.60	1.66	0.24	1.60	0.24	1.29	0.12	1.88	0.99	0.41
Co-87-2	12.26	6.01	8.23	18.58	2.78	13.02	3.93	1.41	4.94	0.88	5.62	1.20	3.45	0.52	3.48	0.52	3.87	0.29	1.13	1.07	0.36
Co-88-4	15.09	3.28	5.79	13.16	2.01	9.63	2.88	1.04	3.60	0.64	4.18	0.89	2.57	0.40	2.65	0.39	2.65	0.16	2.08	0.82	0.35
CO-93-1	2.58	6.47	9.35	20.57	3.17	15.12	4.74	1.55	6.25	1.15	7.61	1.65	4.83	0.73	4.86	0.73	4.16	0.32	2.01	1.05	0.39
M113 KH	6.77	0.71	3.87	8.88	1.50	7.21	1.99	0.61	2.19	0.36	2.31	0.49	1.41	0.21	1.46	0.22	0.89	0.05	1.23	0.42	0.17
M132a KH	39.37	7.00	17.88	37.92	5.23	22.15	5.39	1.34	5.71	0.89	5.57	1.13	3.21	0.48	3.23	0.49	3.44	0.38	4.45	2.94	1.12
Standards																					
JB-2	5.86	0.45	2.15	6.36	1.09	5.89	2.20	0.78	2.95	0.56	3.74	0.82	2.39	0.37	2.46	0.36	1.46	0.03	4.90	0.25	0.15
JA-1	72.07	8.46	15.95	33.25	3.81	14.71	3.20	0.91	3.34	0.52	3.20	0.64	1.83	0.27	1.77	0.27	3.27	0.68	18.89	4.98	2.26
BIR-1 N=5	0.25	0.53	0.66	2.00	0.39	2.44	1.14	0.55	1.86	0.38	2.68	0.59	1.74	0.26	1.74	0.26	0.63	0.04	3.14	0.03	0.01
stand. devi.	0.09	0.04	0.07	0.09	0.01	0.06	0.05	0.02	0.09	0.02	0.13	0.03	0.08	0.02	0.10	0.01	0.06	0.00	0.18	0.00	0.00
BHVO-1 N=3	9.19	16.72	15.47	38.30	5.54	25.22	6.32	2.14	6.36	0.98	5.51	1.01	2.58	0.34	2.06	0.29	4.71	1.13	1.99	1.27	0.44
stand. devi.	0.29	0.87	0.57	1.33	0.19	1.05	0.31	0.10	0.45	0.06	0.40	0.08	0.18	0.03	0.14	0.02	0.50	0.08	0.06	0.06	0.02

Table 2. Sr Isotope Data from the Panamanian Arc

sample	Age (Ma)	Rb [ppm]	Sr [ppm]	87/86 Sr measured	$\pm 2\sigma$	87Rb/86Sr	87/86 Sr inital	87/86 Sr modeled
<i>Adakites 0.1-1 Ma</i>								
M53KH	<i>1.0</i>	50.02	1532	0.703411	3	0.094	0.703411	0.703410
M44KH	<i>1.0</i>	25.57	1196	0.703553	5	0.062	0.703552	0.703551
M55KH	<i>1.0</i>	46.35	1562	0.703473	5	0.086	0.703472	0.703472
M57aKH	<i>1.0</i>	21.01	898	0.703575	3	0.068	0.703574	0.703573
M64c KH	<i>1.0</i>	41.72	1251	0.703361	4	0.096	0.703360	0.703359
M65a KH	<i>0.1</i>	47.03	1911	0.703360	3	0.071	0.703360	0.703360
M99a KH	<i>1.0</i>	25.46	1477	0.703541	3	0.050	0.703541	0.703540
<i>Arc alkaline 0.7-4.5 Ma</i>								
3-12-4-03	<i>1.0</i>	17.29	1488	0.703547	5	0.034	0.703547	0.703546
CP97-1	<i>0.7</i>	17.59	1257	0.703546	3	0.040	0.703545	0.703545
SO96-1	<i>1.3</i>	24.95	1170	0.703502	3	0.062	0.703501	0.703500
M36KH	<i>4.5</i>	16.44	1207	0.703488	2	0.039	0.703484	
M37KH	<i>4.5</i>	19.08	1310	0.703493	2	0.042	0.703489	0.703485
M105 KH	<i>1.4</i>	22.12	1345	0.703475	3	0.048	0.703474	0.703473
M118a KH	<i>1.4</i>	32.90	1346	0.703506	3	0.071	0.703505	0.703504
M121aKH	<i>4.5</i>	20.80	1937	0.703523	3	0.031	0.703521	0.703518
<i>BVF 8.6-9.3 Ma</i>								
M73KH	<i>9.3</i>	59.39	1288	0.703857	3	0.133	0.703840	0.703833
M69 KH	<i>8.6</i>	80.81	814	0.703898	3	0.287	0.703863	0.703857
<i>Cordillera Central 7-32Ma</i>								
M38 KH	<i>7.4</i>	50.21	1476	0.703747	3	0.098	0.703736	0.703731
M42KH	<i>10.9</i>	4.80	605	0.703726	2	0.023	0.703722	0.703715
M46KH	<i>16.7</i>	7.54	483	0.703799	2	0.045	0.703788	0.703776
M49aKH	<i>14.4</i>	9.56	497	0.703817	3	0.056	0.703806	0.703796
M50aKH	<i>14.5</i>	7.34	426	0.703812	3	0.050	0.703801	0.703791
M67KH	<i>10.0</i>	2.14	386	0.703483	3	0.016	0.703480	0.703474
M76aKH	<i>32.4</i>	0.31	450	0.703741	3	0.002	0.703740	0.703718
M78aKH	<i>16.5</i>	9.75	542	0.703909	3	0.052	0.703897	0.703885
M81aKH	<i>17.0</i>	4.97	418	0.703565	3	0.034	0.703556	0.703545
M84aKH	<i>18.5</i>	5.87	382	0.703776	3	0.045	0.703765	0.703752
M122aKH	<i>9.0</i>	1.07	547	0.703696	3	0.006	0.703695	0.703689
M124b KH	<i>8.7</i>	4.33	417	0.703684	3	0.030	0.703680	0.703674
M136 KH	<i>20.0</i>	0.37	416	0.703719	3	0.003	0.703718	0.703704
M143aKH	<i>20.1</i>	27.65	559	0.703586	3	0.143	0.703545	0.703531
<i>Cordillera Central 34-40Ma</i>								
CP98KH	<i>34.4</i>	14.12	366	0.703556	3	0.112	0.703502	0.703478
M35KH	<i>40.3</i>	13.59	336	0.703541	5	0.117	0.703474	0.703446
M106KH	<i>40.0</i>	14.38	367	0.703462	5	0.113	0.703397	0.703367
<i>Cordillera Central 44-46 Ma</i>								
M117aKH	<i>44.4</i>	13.17	695	0.703389	2	0.055	0.703354	0.703324
M141KH	<i>46.0</i>	36.57	769	0.703637	3	0.138	0.703547	0.703515
<i>Eastern Panama 12-22Ma</i>								
M137aKH	<i>21.0</i>	29.09	466	0.703768	2	0.181	0.703714	0.703699
M155aKH	<i>12.6</i>	82.05	433	0.703940	3	0.548	0.703842	0.703834
M157aKH	<i>12.4</i>	15.96	700	0.703787	3	0.066	0.703776	0.703767
M210KH	<i>21.7</i>	17.46	387	0.704399	2	0.130	0.704358	0.704343
M212KH	<i>21.9</i>	2.34	249	0.703712	3	0.027	0.703704	0.703689
<i>Eastern Panama 40-50Ma</i>								
CA-106-1	<i>40.4</i>	30.05	538	0.703691	2	0.162	0.703599	0.703571
CA-111-2	<i>46.7</i>	10.92	394	0.703365	2	0.080	0.703312	0.703280
CA-112-1	<i>46.0</i>	22.83	627	0.703577	3	0.105	0.703508	0.703477
M167bKH	<i>50.0</i>	0.39	167	0.703474	3	0.007	0.703469	0.703435
<i>Azuero & Sona 50-61 Ma</i>								
AZ3-1	<i>60.9</i>	9.21	403	0.703593	3	0.066	0.703536	0.703494
AZ34-2	<i>52.3</i>	27.07	313	0.703821	3	0.250	0.703635	0.703609
CO-87-2	<i>54.3</i>	12.26	196	0.703968	2	0.181	0.703828	0.703599
M113KH	<i>40.0</i>	6.77	363	0.703675	5	0.054	0.703644	0.703791
M132aKH	<i>53.9</i>	39.37	430	0.703894	3	0.265	0.703692	0.703655

ages in italic are estimated

Table 2. Nd Isotope Data from the Panamanian Arc

sample	Age (Ma)	Sm [ppm]	Nd [ppm]	143/144Nd measured	$\pm 2\sigma$	147Sm/144Nd	143/144Nd initial	Et ND	E0 ND	143/144Nd modeled
<i>Adakites 0.1-1 Ma</i>										
M53KH	<i>1.00</i>	4.63	26.6	0.512946	3	0.105	0.512946	6.01	6.01	0.512946
M44KH	<i>1.00</i>	3.55	19.8	0.512986	3	0.108	0.512985	6.79	6.78	0.512986
M55KH	<i>1.00</i>	4.45	27.9	0.512964	3	0.096	0.512964	6.38	6.37	0.512965
M57aKH	<i>1.00</i>	3.75	20.8	0.512989	2	0.109	0.512688	1.00	0.99	0.512689
M64c KH	<i>0.97</i>	3.96	21.6	0.512961	2	0.110	0.512960	6.30	6.29	0.512961
M65a KH	<i>0.13</i>	7.72	52.5	0.512965	2	0.088	0.512965	6.38	6.38	0.512965
M99a KH	<i>1.00</i>	7.19	44.2	0.513002	2	0.098	0.513001	7.10	7.09	0.513002
<i>Arc alkaline 0.7-4.5 Ma</i>										
3-12-4-03	<i>1.00</i>	10.55	64.1	0.512990	3	0.099	0.512978	6.66	6.65	0.512979
M36KH	<i>0.70</i>	10.91	56.0	0.512997	3	0.117	0.512993	6.94	6.93	0.512993
SO96-1	<i>1.30</i>	7.27	41.2	0.512987	3	0.106	0.512994	6.98	6.96	0.512995
M37KH	<i>6.00</i>	10.83	58.5	0.513003	3	0.111	0.512992	7.06	7.00	0.512998
M141KH	<i>6.00</i>	12.17	59.4	0.512979	2	0.123	0.512999	7.19	7.12	0.513005
M105 KH	<i>1.40</i>	7.68	47.1	0.512984	2	0.098	0.512989	6.88	6.86	0.512990
M118a KH	<i>1.43</i>	10.88	63.6	0.512995	2	0.103	0.512983	6.77	6.75	0.512985
M121aKH	<i>4.50</i>	14.06	83.5	0.512993	5	0.101	0.512984	6.85	6.80	0.512988
<i>BVF 8.6-9.3 Ma</i>										
M73KH	<i>9.30</i>	7.87	41.3	0.512978	3	0.115	0.512972	6.74	6.64	0.512981
M69 KH	<i>8.60</i>	9.79	48.2	0.512977	3	0.122	0.512970	6.69	6.61	0.512978
<i>Cordillera Central 7-32Ma</i>										
M38 KH	<i>7.36</i>	6.73	41.4	0.512972	3	0.098	0.512968	6.61	6.52	0.512975
M42KH	<i>10.90</i>	5.31	22.7	0.512998	3	0.141	0.512988	7.10	7.02	0.512999
M46KH	<i>16.70</i>	5.35	9.1	0.513001	2	0.354	0.512962	6.74	7.07	0.512978
M49aKH	<i>14.40</i>	3.40	12.4	0.512984	2	0.164	0.512969	6.82	6.76	0.512983
M50aKH	<i>14.50</i>	2.72	9.9	0.512981	2	0.166	0.512966	6.75	6.70	0.512980
M67KH	<i>10.00</i>	5.58	20.9	0.512988	2	0.161	0.512977	6.87	6.82	0.512987
M76aKH	<i>32.40</i>	2.73	10.6	0.512977	2	0.156	0.512944	6.78	6.61	0.512976
M78aKH	<i>16.46</i>	2.86	10.6	0.512980	3	0.162	0.512963	6.75	6.68	0.512979
M81aKH	<i>17.00</i>	2.75	9.5	0.513020	2	0.175	0.513000	7.50	7.45	0.513017
M84aKH	<i>18.50</i>	2.75	9.6	0.512998	2	0.173	0.512977	7.07	7.02	0.512995
M122aKH	<i>9.00</i>	1.94	6.3	0.513008	5	0.186	0.512997	7.23	7.21	0.513006
M124b KH	<i>8.70</i>	2.77	9.9	0.513002	3	0.169	0.512992	7.13	7.10	0.513001
M136 KH	<i>35.00</i>	1.48	4.5	0.513021	3	0.196	0.512995	7.47	7.47	0.513015
M143aKH	<i>20.10</i>	6.20	27.8	0.512962	2	0.134	0.512944	6.47	6.31	0.512964
<i>Cordillera Central 34-40Ma</i>										
CP98KH	<i>34.40</i>	3.42	13.5	0.512983	3	0.152	0.512949	6.93	6.73	0.512983
M35KH	<i>40.30</i>	3.69	14.6	0.512991	3	0.153	0.512951	7.12	6.90	0.512991
M106KH	<i>40.00</i>	2.09	18.1	0.512973	3	0.070	0.512955	7.18	6.54	0.512994
<i>Cordillera Central 44-46 Ma</i>										
CP97-1	<i>44.40</i>	9.30	56.0	0.512954	2	0.100	0.512920	6.62	6.17	0.512964
M117aKH	<i>46.00</i>	7.19	36.8	0.512946	2	0.118	0.512909	6.44	6.01	0.512954
<i>Eastern Panama 12-22Ma</i>										
M137aKH	<i>21.00</i>	4.09	17.1	0.513013	3	0.144	0.512994	7.46	7.32	0.513014
M155aKH	<i>12.60</i>	4.33	19.9							
M157aKH	<i>12.40</i>	3.41	13.5	0.512994	3	0.152	0.512982	7.01	6.94	0.512994
M210KH	<i>21.70</i>	3.24	13.5	0.512960	3	0.144	0.512940	6.43	6.28	0.512961
M212KH	<i>21.90</i>	3.29	10.8	0.513039	3	0.184	0.513013	7.87	7.83	0.513035
<i>Eastern Panama 40-50Ma</i>										
CA-106-1	<i>40.40</i>	2.09	7.7	0.513004	3	0.163	0.512961	7.32	7.15	0.513001
CA-111-2	<i>46.70</i>	3.08	22.7	0.512970	3	0.082	0.512963	7.51	6.82	0.513009
CA-112-1	<i>46.00</i>	2.25	22.7	0.513016	2	0.060	0.512998	8.17	7.37	0.513043
M167bKH	<i>50.00</i>	1.34	3.8	0.513057	3	0.213	0.512986	8.07	8.18	0.513035
<i>Azuero & Sona 50-61 Ma</i>										
AZ3-1	<i>60.89</i>	3.85	12.0	0.512974	2	0.193	0.512897	6.57	6.54	0.512956
AZ34-2	<i>52.30</i>	3.65	15.6	0.512930	3	0.141	0.512882	6.07	5.70	0.513001
CO-87-2	<i>54.30</i>	3.93	13.0	0.513020	2	0.182	0.512955	7.55	7.44	0.512933
M113KH	<i>40.00</i>	1.99	7.2	0.512994	10	0.166	0.512951	7.11	6.95	0.513008
M132aKH	<i>53.90</i>	5.39	22.2	0.512986	3	0.146	0.512934	7.14	6.79	0.512987

ages in italic are estimated

Table 2. Pb Isotope Data from the Panamanian Arc

sample #	Age (Ma)	Pb [ppm]	U [ppm]	Th [ppm]	206/204Pb measured	±2σ	207/204Pb measured	±2σ	208/204Pb measured	±2σ
<i>Adakites 0.1-1 Ma</i>										
M53KH	<i>1.00</i>	10.14	2.94	11.41	19.324	1	15.577	1	38.991	2
M44KH	<i>1.00</i>	5.68	1.35	4.15	19.202	1	15.574	1	38.875	1
M55KH	<i>1.00</i>	6.34	2.23	7.70	19.191	1	15.575	1	38.869	2
M57aKH	<i>1.00</i>	3.85	1.07	3.54	19.119	1	15.561	1	38.770	3
M64c KH	<i>0.97</i>	7.81	2.07	7.11	19.296	1	15.580	1	38.980	2
M65a KH	<i>0.13</i>	8.64	3.06	12.64	19.263	1	15.572	1	38.925	3
M99a KH	<i>1.00</i>	6.36	2.67	8.88	19.069	1	15.557	1	38.697	2
<i>Arc alkaline 0.7-4.5 Ma</i>										
3-12-4-03	<i>1.00</i>	4.63	2.76	9.36	19.110	1	15.572	1	38.776	2
M36KH	<i>0.70</i>	3.47	1.86	6.13	19.070	6	15.567	5	38.715	13
SO96-1	<i>1.30</i>	3.34	1.88	4.88	19.073	1	15.559	1	38.698	2
M37KH	<i>6.00</i>	3.76	1.95	6.47	19.052	1	15.553	1	38.665	3
M141KH	<i>6.00</i>	3.25	1.48	4.38	19.242	2	15.562	2	38.849	5
M105 KH	<i>1.40</i>	3.99	1.95	7.03	19.063	1	15.562	1	38.705	3
M118a KH	<i>1.43</i>	5.11	2.68	8.42	19.051	2	15.561	2	38.697	4
M121aKH	<i>4.50</i>	4.69	2.50	8.85	19.079	1	15.565	1	38.731	2
<i>BVF 8.6-9.3 Ma</i>										
M73KH	<i>9.30</i>	17.00	2.28	6.49	18.907	1	15.549	1	38.559	1
M69 KH	<i>8.60</i>	8.20	2.14	6.19	18.896	1	15.556	1	38.564	2
<i>Cordillera Central 7-32Ma</i>										
M38 KH	<i>7.36</i>	7.30	2.79	8.41	19.024	1	15.559	1	38.677	2
M42KH	<i>10.90</i>	4.41	0.36	1.74	18.838	1	15.549	1	38.512	0
M46KH	<i>16.70</i>	5.35	0.27	0.76	18.825	1	15.550	1	38.492	2
M49aKH	<i>14.40</i>	2.52	0.20	0.56	18.801	1	15.535	1	38.435	2
M50aKH	<i>14.50</i>	3.40	0.20	0.55	18.801	1	15.539	1	38.446	2
M67KH	<i>10.00</i>	1.51	0.48	1.37	18.842	1	15.543	1	38.465	2
M76aKH	<i>32.40</i>	1.63	0.27	1.05	18.896	1	15.554	1	38.586	1
M78aKH	<i>16.46</i>	3.58	0.47	1.43	18.876	1	15.553	1	38.563	2
M81aKH	<i>17.00</i>	1.66	0.14	0.27	18.730	1	15.540	1	38.360	1
M84aKH	<i>18.50</i>	1.52	0.30	0.88	18.949	2	15.556	2	38.615	4
M122aKH	<i>9.00</i>	0.97	0.10	0.24	18.841	2	15.555	2	38.518	5
M124b KH	<i>8.70</i>	1.18	0.10	0.34	18.954	1	15.558	1	38.619	2
M136 KH	<i>35.00</i>	0.94	0.06	0.14	18.909	1	15.572	1	38.616	3
M143aKH	<i>20.10</i>	5.54	1.31	4.36	19.116	1	15.573	1	38.770	2
<i>Cordillera Central 34-40Ma</i>										
CP98KH	<i>34.40</i>	2.64	0.37	1.10	18.814	1	15.560	1	38.468	3
M35KH	<i>40.30</i>	3.62	0.37	1.02	18.800	1	15.551	1	38.440	3
M106KH	<i>40.00</i>	2.41	0.55	1.71	18.990	1	15.564	1	38.629	2
<i>Cordillera Central 44-46 Ma</i>										
CP97-1	<i>44.40</i>	3.34	1.88	4.88	19.052	1	15.547	1	38.678	3
M117aKH	<i>46.00</i>	3.00	1.26	5.29	19.152	2	15.575	2	38.880	5
<i>Eastern Panama 12-22Ma</i>										
M137aKH	<i>21.00</i>	3.71	0.88	2.30	19.228	1	15.594	1	39.046	3
M155aKH	<i>12.60</i>	6.21	1.49	3.81	19.116	2	15.567	1	38.796	4
M157aKH	<i>12.40</i>	2.82	0.41	0.89	19.086	1	15.561	0	38.758	1
M210KH	<i>21.70</i>	2.79	0.98	1.67	19.067	2	15.580	1	38.711	3
M212KH	<i>21.90</i>	1.17	0.20	0.75	19.156	1	15.576	1	38.839	3
<i>Eastern Panama 40-50Ma</i>										
CA-106-1	<i>40.40</i>	3.33	0.45	0.95	18.902	0	15.565	0	38.506	1
CA-111-2	<i>46.70</i>	1.33	0.37	1.02	18.897	2	15.567	1	38.506	3
CA-112-1	<i>46.00</i>	3.82	0.49	1.02	18.905	3	15.561	3	38.498	7
M167bKH	<i>50.00</i>	0.39	0.01	0.04	18.868	5	15.570	4	38.542	11
<i>Azuero & Sona 50-61 Ma</i>										
AZ3-1	<i>60.89</i>	0.59	0.15	0.42	18.790	2	15.558	2	38.418	4
AZ34-2	<i>52.30</i>	4.08	0.67	2.24	18.839	2	15.563	1	38.567	3
CO-87-2	<i>54.30</i>	1.13	0.36	1.07	19.049	2	15.593	2	38.730	4
M113KH	<i>40.00</i>	1.23	0.17	0.42	18.776	3	15.558	2	38.424	6
M132aKH	<i>53.90</i>	4.45	1.12	2.94						

ages in italic are estimated

Table 2. Pb Isotope Data from the Panamanian Arc, continued

sample #	²³⁸ U/ ²⁰⁴ Pt Mu	²⁰⁶ / ²⁰⁴ Pb initial	²⁰⁷ / ²⁰⁴ Pb initial	²⁰⁸ / ²⁰⁴ Pb initial	²⁰⁶ / ²⁰⁴ Pb modeled	²⁰⁷ / ²⁰⁴ Pb modeled	²⁰⁸ / ²⁰⁴ Pb modeled
M53KH	18.75	19.32	15.58	38.99	19.32	15.58	38.99
M44KH	15.34	19.20	15.57	38.87	19.20	15.57	38.87
M55KH	22.68	19.19	15.58	38.86	19.19	15.58	38.87
M57aKH	17.83	19.12	15.56	38.77	19.12	15.56	38.77
M64c KH	17.16	19.29	15.58	38.98	19.30	15.58	38.98
M65a KH	22.83	19.26	15.57	38.92	19.26	15.57	38.92
M99a KH	26.92	19.07	15.56	38.69	19.07	15.56	38.70
3-12-4-03	38.29	19.10	15.57	38.77	19.11	15.57	38.77
M36KH	34.44	19.04	15.57	38.68	19.05	15.55	38.68
SO96-1	36.03	19.07	15.56	38.69	19.07	15.56	38.69
M37KH	33.35	19.02	15.55	38.63	19.05	15.57	38.69
M141KH	29.38	19.03	15.55	38.64	19.03	15.55	38.64
M105 KH	31.41	19.06	15.56	38.70	19.06	15.56	38.70
M118a KH	33.59	19.04	15.56	38.69	19.05	15.56	38.69
M121aKH	34.22	19.06	15.56	38.70	19.06	15.56	38.71
M73KH	8.58	18.89	15.55	38.55	18.91	15.55	38.57
M69 KH	16.68	18.87	15.55	38.54	18.89	15.56	38.56
M38 KH	24.54	19.00	15.56	38.65	19.01	15.56	38.66
M42KH	5.26	18.83	15.55	38.50	18.85	15.55	38.52
M46KH	3.22	18.82	15.55	38.48	18.84	15.55	38.52
M49aKH	5.03	18.79	15.53	38.42	18.81	15.54	38.45
M50aKH	3.69	18.79	15.54	38.44	18.82	15.54	38.47
M67KH	20.30	18.81	15.54	38.44	18.83	15.54	38.46
M76aKH	10.76	18.84	15.55	38.52	18.89	15.55	38.58
M78aKH	8.48	18.85	15.55	38.54	18.88	15.55	38.57
M81aKH	5.31	18.72	15.54	38.35	18.74	15.54	38.39
M84aKH	12.69	18.91	15.55	38.58	18.94	15.56	38.62
M122aKH	6.60	18.83	15.55	38.51	18.85	15.55	38.53
M124b KH	5.46	18.95	15.56	38.61	18.96	15.56	38.63
M136 KH	4.00	18.90	15.57	38.61	18.93	15.57	38.65
M143aKH	15.20	19.07	15.57	38.72	19.10	15.57	38.76
CP98KH	9.01	18.77	15.56	38.42	18.82	15.56	38.49
M35KH	6.59	18.76	15.55	38.40	18.82	15.55	38.48
M106KH	14.67	18.90	15.56	38.54	18.96	15.56	38.62
CP97-1	36.00	19.05	15.55	38.67	19.03	15.57	38.71
M117aKH	27.15	18.96	15.57	38.62	19.10	15.56	38.73
M137aKH	15.34	19.18	15.59	39.00	19.21	15.59	39.04
M155aKH	15.40	19.09	15.57	38.77	19.11	15.57	38.80
M157aKH	9.46	19.07	15.56	38.75	19.09	15.56	38.77
M210KH	22.58	18.99	15.58	38.67	19.02	15.58	38.71
M212KH	11.10	19.12	15.57	38.79	19.15	15.58	38.84
CA-106-1	8.63	18.85	15.56	38.47	18.91	15.57	38.55
CA-111-2	17.65	18.77	15.56	38.39	18.84	15.56	38.48
CA-112-1	8.27	18.85	15.56	38.46	18.92	15.56	38.55
M167bKH	2.35	18.85	15.57	38.526	18.93	15.57	38.63
AZ3-1	16.60	18.63	15.55	38.28	18.73	15.56	38.40
AZ34-2	10.54	18.75	15.56	38.47	18.79	15.56	38.47
CO-87-2	20.26	18.88	15.59	38.56	18.83	15.56	38.58
M113KH	8.81	18.72	15.56	38.38	18.96	15.59	38.67
M132aKH							

ages in *italic* are estimated

Table 4: Sample locations from the Panamanian Arc

Sample	Longitude	Latitude	Sample	Longitude	Latitude
<i>Adakites 0.1-1 Ma</i>			<i>Cordillera Central 34-40Ma</i>		
M44KH	-82.621	9.669	CP-98	-81.593	8.207
M57a KH	-82.474	8.796	G 64	-81.705	7.637
M91a KH	-82.486	8.829	M35a KH	-81.593	8.207
M53a KH	-82.585	8.794	M102aKH	-81.343	8.326
M55KH	-82.474	8.796	M106a KH	-81.640	8.055
M61a KH	-82.730	8.824	M107a KH	-81.487	8.025
M63aKH	-82.874	8.140	M119a KH	-81.486	8.163
M64 b KH	-82.877	8.184	<i>Cordillera Central 44-46 Ma</i>		
M64c KH	-82.877	8.184	M117a KH	-81.385	8.023
M64 f KH	-82.877	8.184	M141 a KH	-81.169	8.049
M65a KH	-82.710	8.470	M148a KH	-80.927	8.000
M66a KH	-82.694	8.529	<i>Eastern Panama 12-22Ma</i>		
M99a KH	-81.826	8.340	M137a KH	-81.016	8.153
<i>Arc alkaline 0.7-4.5 Ma</i>			M155a KH	-80.583	8.626
SO-96-1	-81.732	8.073	M157a KH	-80.530	8.530
SO-96-2	-81.732	8.073	M158a KH	-80.506	8.463
S0-96-3	-81.732	8.073	M159a KH	-80.434	8.558
S0-96-4	-81.732	8.073	M160a KH	-80.275	8.581
SO-96-5	-81.732	8.073	M204d KH	-78.173	7.570
CP-97-1	-81.587	8.217	M205a KH	-78.173	7.570
M36KH	-82.038	8.274	M212KH	-78.938	8.459
M37a KH	-82.038	8.274	M219c KH	-79.033	8.549
M98a KH	-82.047	8.280	<i>Eastern Panama 40-50Ma</i>		
M105aKH	-81.791	8.241	CA-106	-79.743	9.450
M118aKH	-81.447	8.129	CA-111-1	-79.468	9.593
M118bKH	-81.447	8.129	CA-111-2	-79.468	9.593
M121 a KH	-81.488	8.188	CA-111-5	-79.468	9.593
3-12-4-03	-82.238	7.470	CA-112-1	-79.652	9.551
<i>BVF 8.6-9.3 Ma</i>			M165c KH	-78.514	8.982
M69KH	-82.282	9.085	M167b KH	-79.076	9.191
M73KH	-82.353	9.205	<i>Azuero, Sona Peninsula and Coiba Island 50-</i>		
<i>Cordillera Central 7-32Ma</i>			G 16	-79.993	7.514
M38KH	-82.129	8.239	G 17	-79.993	7.514
M161aKH	-80.079	8.587	G 18	-79.999	7.472
M164KH	-79.804	8.744	G 19	-79.999	7.472
M42a KH	-82.621	9.669	G 20	-79.999	7.472
M45a KH	-82.621	9.669	Az-1-1	-80.256	7.679
M46a KH	-82.621	9.669	AZ-1-3	-80.256	7.679
M49a KH	-82.621	9.669	AZ-3-1	-80.402	7.810
M50a KH	-82.621	9.669	AZ-4-3	-80.386	7.818
M67KH	-82.197	8.953	AZ-8-1	-80.213	7.710
M76a KH	-82.189	8.789	AZ-15	-80.238	7.594
M78a KH	-82.253	8.744	AZ-33	-80.408	7.654
M80KH	-82.247	8.578	AZ-44-1	-80.290	7.722
M81a KH	-82.225	8.608	AZ-46-1	-80.309	7.705
M84aKH	-82.221	8.686	AZ-48	-80.305	7.693
M122a KH	-81.115	8.502	AZ-49-1	-80.335	7.658
M123a KH	-81.114	8.515	CE-60-2	-81.041	7.572
M124b KH	-81.085	8.513	Co-78-2	-81.870	7.517
M125a KH	-81.073	8.520	Co-87-2	-81.775	7.435
M128 b KH	-81.068	8.527	Co-88-4	-81.700	7.418
M133a KH	-81.007	8.300	CO-91-4	-81.710	7.590
M136a KH	-80.970	8.255	CO-93-1	-81.728	7.625
M143a KH	-81.297	8.001	SC-100-1F	-81.321	7.623
			M113 KH	-81.384	7.881
			M132a KH	-81.035	8.355

Lebenslauf

Persönliche Daten

Britta Lissinna

Möwenstr. 13
24113 Molfsee

Telefon 04347-908586
email: b.lissinna@kielnet.net

21.03.1972 geboren in Metzingen

Promotion

2000-2005

Leibniz Institute for Marine Sciences IFM-GEOMAR, Kiel

Geochemikerin

Die magmatische Evolution Panamás

Studium

1993-1999

CHRISTIAN ALBRECHTS UNIVERSITÄT ZU KIEL

Abschluß: Diplom Geologin

Schwerpunkte: Erdölgeologie, Petrologie, Meeresgeologie/Paläoozeanographie

1998-1999

Diplomarbeit: „Geochemical charge modeling of the Northern Euphrates Graben (Syrien)“ bei Deminex, Essen in Kooperation mit Shell/Amsterdam
Diplomkartierung auf Sizilien (Italien): „Die Messinanische Salinitätskrise“

1997

Intensivkurs „Applied Hydrogeology“ Erasmus Projekt-ICP-96-B-1183 Granada (Spanien)

1995-1996

Auslandsstudium, Mercator Erasmus Programm Bologna (Italien)
Speologie, Vulkanologie, Geländearbeit Apennin

Berufspraxis

1995

INTERNATIONALE FORSCHUNGSFAHRT „PAGANINI“
Wissenschaftliche Mitarbeiterin

1997-1998

DEMINEX, Essen
Assistentin der Abteilungsleitung Exploration

Besondere Fortbildung

„Basin Anlysis“ Prof. Cloetingh, (Amsterdam)
„Pyroclastic Rocks“ Prof. H.U. Schmincke, (Kiel, IFM-GEOMAR)

Schulische Bildung

1982 - 91

Gymnasium Insel Föhr
Abitur

Hiermit erkläre ich an Eides statt, daß ich die Vorliegende Abhandlung, abgesehen von der Beratung durch meinen akademischen Lehrer, nach Inhalt und Form meine eigene Arbeit darstellt.

Kiel, den 14.04.05

Britta Lissinna